ERDC/CHL TR-20-X

Coastal and Hydraulics Laboratory

US Army Corps of Engineers®
Engineer Research and Development Center

Coastal Texas Protection and Restoration Feasibility Study

Coastal Texas Flood Risk Assessment: Hydrodynamic Response and Beach Morphology

Jeffrey A. Melby, Thomas C. Massey, Fatima Diop, Himangshu Das, Norberto Nadal-Caraballo, Victor Gonzalez, Mary Bryant, Amanda Tritinger, Leigh Provost, Margaret Owensby, and Abigail Stehno

July 2020

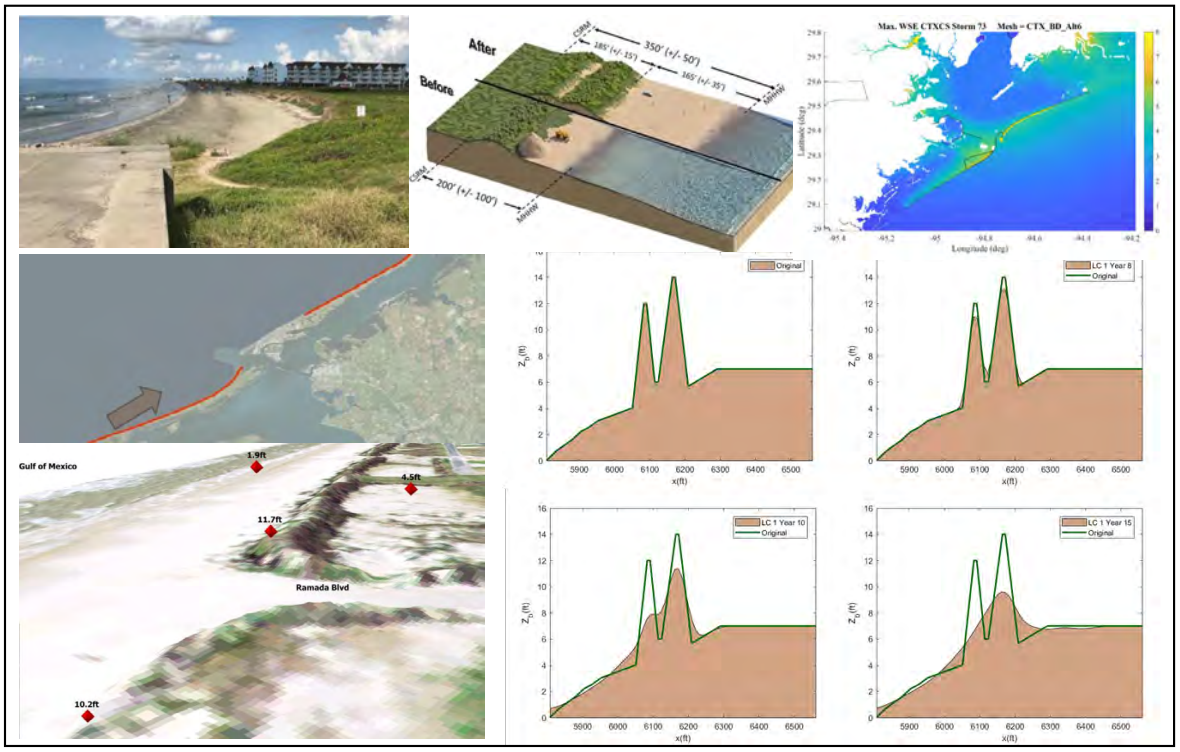

Draft.

ERDC/CHL TR-20-X
July 2020

Coastal Texas Protection and Restoration Feasibility Study

Coastal Texas Flood Risk Assessment: Hydrodynamic Response and Beach Morphology

Jeffrey A. Melby, Thomas C. Massey, Norberto Nadal-Caraballo, Victor Gonzalez, Mary Bryant, Amanda Tritinger, Leigh Provost, Margaret Owensby and Abigail Stehno

Coastal and Hydraulics Laboratory
U.S. Army Engineer Research and Development Center
3909 Halls Ferry Road
Vicksburg, MS 39180-6199

Fatima Diop

Noble Consultants, Inc.
201 Alameda Del Prado
Novato, CA 94949-6698

Himangshu Das

U.S. Army Engineer District, Galveston
CESWG-EC-H
2000 Fort Point Road, Galveston, TX 77550

Draft report

Prepared for U.S. Army Engineer District, Galveston
Galveston, TX

Washington, DC 20314-1000

Executive Summary

The U.S. Army Corps of Engineers Galveston District (SWG) is executing the Coastal Texas Protection and Restoration Feasibility Study (CTXCS) coastal storm risk management (CSRM) project for the region. The project is currently in the feasibility phase. The primary goal is to develop CSRM measures that maximize net national economic development (NED) benefits. This project is one component of the larger regional Coastal Texas Protection and Restoration Feasibility Study that includes a variety of measures and alternatives.

The study reported herein evaluated impacts from the following alternatives:

- Roughly 19 miles of beach, berm and dune along Galveston Island and 26 miles of beach, berm and dune along Bolivar Peninsula
- Ring levee around Galveston
- Surge barrier at Bolivar Roads
- Smaller navigation gates at Clear Creek and Dickinson Bayou

As part of the ongoing feasibility phase of the project, this report documents the coastal storm water level (surge, tide, relative sea level rise) and wave hazard and beach morphology modeling.

Climatology

A joint probabilistic model of historical tropical cyclone (TC) parameters was developed that spans the full range of tropical storm hazards from frequent, low-intensity storms to very rare, very intense storms. The probabilistic model describes the continuous spatial and temporal hazard. This probabilistic model was sampled efficiently to develop a suite of 660 TCs that characterize the coastal storm flood hazard for Texas. This suite was further subsampled to efficiently to develop a suite of 170 synthetic tropical storms that effectively capture the flood hazard for the Galveston and Galveston Bay region. Wind and pressure fields were developed for the 660 TCs using the Planetary Boundary Layer (PBL) model.

Regional Hydrodynamics

The CSTORM coupled surge and wave modeling system was used to accurately quantify surge and wave hazards. New model meshes were developed from very high-resolution land and sub-aqueous surveys for with- and without-project scenarios. With-project meshes include the measures listed above. The new meshes provide the highest resolution regional surge and wave modelling done to-date for the region. The CSTORM model was validated against historical storms and then used to model the 170 synthetic TCs. The storms were run on 2 relative sea level change (RSLC) scenarios for with- and without-project meshes. These RSLC scenarios are: 1. SLC0 corresponding to historical sea level change rate, and 2. SLC1 corresponding to a high rate. A third intermediate rate was applied within the morphological modeling.

Flood hazard exposure of the project features was quantified by computing hazard curves for the CSTORM TC output over the region. Annual exceedance probabilities (AEP) were computed for the range of 1 to 0.0001 for peak TC water level (SWL) and wave height (H_{m0}). Wave period (T_p) and mean wave direction associated with H_{m0} were also computed. Both mean values and confidence limits (CL) were computed for the case of no project, with the ring levee and Surge Barrier closed and for the case with the ring levee, Surge Barrier closed and the beach-dune system.

Morphology

Historical morphological performance of Galveston Island and Bolivar Peninsula was relevant to the present study. In particular, net alongshore sediment transport rates and shoreline recession/accretion were applicable to the morphological modeling. Prior recent USACE studies covered this topic in detail so the results of those studies were summarized herein.

A suite of historical non-tropical storms was developed using a peaks-over-threshold sampling technique with measured water levels and historical hindcast waves offshore. These storms produced relatively minor responses compared to the tropical storms that did not impact the extremal statistics of SWL but were required for the morphological modeling because frequent minor events can erode the beach.

The CSHORE beach morphology model was used to model cross-shore sediment transport during significant storm events. Results from recent geomorphological, geologic and beach morphology studies were used as a basis for defining the modeling configurations and constraints. These include the sand and clay layer thicknesses, longshore sediment transport, longterm erosion, and beach sediment gradation. Four reaches were defined spanning the length of the beach-dune alternative, two each for Galveston Island and Bolivar Peninsula. Two dune configurations were modeled, each consisting of single and dual dune configurations. So four total profiles were modeled. All 170 TC storms and all non-tropical storms were modeled individually.

For stochastic assessment of the beach morphology, the CSHORE model was embedded in a time-dependent Monte Carlo sampling scheme within the larger StormSim stochastic modeling system. The climatology consisted of tropical storms and non-tropical storms. The number of storms per year was Poisson distributed which were defined according to the non-tropical and TC historical storm rates. Individual TC storms were sampled according to their probability masses. Each storm was modeled as a time series of wave and water level conditions. A convergence test was conducted and it was determined that 30 life cycles at 50 years each produced a stable statistical response. The waves and water levels for each storm were combined with a random tidal time series and each RSLC scenario. The simulations progressed from time step to time step with CSHORE computing the morphology change for each storm. During the simulations, the damaged profile from a given storm was used as the starting profile for the next event. Beach profile and hydrodynamic parameters, including water levels and overtopping, were recorded throughout the life cycle. The profiles were tracked at key locations. The beach was rebuilt to its original profile if the dune height reduction exceeded 50%.

Non-tropical storms were shown to produce only slight profile responses but were frequent so the total impact on profile evolution was significant. TCs had dramatic effect on the dune with near complete destruction if the dune crest was submerged. The berm did not show significant erosion throughout the life cycles. However, the dune did degrade with time. Degradation of the dune caused sediment to be transported from the dune to the berm and then to the swash area of the beach so the dune acted as a somewhat inefficient renourishment source for the berm and beach.

A primary goal of the stochastic simulation was to define the number of rebuilds during a life cycle. A basic renourishment criterion of loss of half of the as-built dune height provided a heuristic optimized CSRM that limited the condition where there was little to no flood protection while requiring a renourishment rate roughly consistent with national average rates. The mean and mean+1 standard deviation of the number of rebuilds from 30 life cycles is reported. It was found that a single dune on Bolivar Peninsula with an initial elevation of 14 ft, NAVD88, yielded renourishment rates of 10.2 and 13.9 rebuilds per 50 years for RSLC scenarios low and high, respectively, at the mean+1SD quantile. That is, in a given 50-year period, at the low RSLC scenario, the beach was rebuilt to the as-constructed condition an average of 10.2 times. These rates are the average across the two reaches. Similarly, a dual dune configuration for Bolivar yielded renourishment rates of 6.8 and 8.1 rebuilds per 50 years. For Galveston Island single dune, the simulation yielded renourishment rates of 8.6 and 12.1 rebuilds per 50 years for RSLC scenarios low and high, respectively. For Galveston Island dual dune, the simulation yielded renourishment rates of 4.6 and 6.4 rebuilds per 50 years for RSLC scenarios low and high, respectively.

Total wave and overflow overtopping for each storm was computed. Probability distributions for each life cycle were computed and then an average and 90% confidence limit were computed across all life cycles. These statistics correspond to overtopping criteria used for levees. In general, the total overtopping at 1% AEP is governed by TCs that inundate the dune. The total overtopping at the 1% AEP is roughly 10^6 ft^3/ft. Interestingly, a counter-intuitive outcome was that the dual dune configurations on both Bolivar Peninsula and Galveston Island had higher overtopping than the single dune because the dual dune is not rebuilt as often so the average dune elevation is lower. A potential mitigation of this issue is to stretch out the major rehabilitation rebuilds and add periodic minor maintenance to maintain the height of the dune. These sediment management decisions require economic optimization that could be done with iterative application of the StormSim morphology model described herein.

Contents

Figures and Tables

Figures

Tables

Preface

The study summarized in this report was conducted at the request of the Galveston District (SWG), U.S. Army Corps of Engineers (USACE). Dr. Himangshu Das was the primary engineering point of contact at SWG. The portion of the study reported herein was funded by SWG and primarily conducted at the Engineering Research and Development Center (ERDC), Coastal and Hydraulics Laboratory (CHL), Vicksburg, MS, during the period October 2018–April 2020.

SWG project leadership included Kelly Burkes-Copes, SWG Project Manager and Dr. Himangshu Das, SWG project technical lead. At the time of this study, Robert Thomas was Chief, Engineering and Construction, SWG. At the time of this study, James Gutshall was Chief of HES Branch which was within Navigation Division, led by Dr. Jackie Pettway, Chief. Ms. Ashley Frey was Chief of Coastal Processes Branch which was within Flood and Storm Protection Division, led by Dr. Cary Talbot. Ty Wamsley was Director, CHL, and Jeff Eckstein was Deputy Director, CHL. At the time of publication, Col. Teresa Schlosser was Commander and Dr. David Pittman was Director of ERDC.

Acknowledgment

This report went through the USACE review process. Internal SWG review (DQC) included independent review by 4 individuals from Planning and Engineering. In addition, ATR and IEPR reviews were thorough. All reviewers are gratefully acknowledged for improving this report.

Table of Report Review

	Date	Changes
First Draft	02/28/2020	N/A
Post-DQC Revision	04/28/2020	Extensive changes and updates based on DQC comments
Post-ATR Revision	7/7/2020	Minor edits to report
Post-IEPR Final		

DQC, ATR and IEPR comments, responses, back-checks and DQC certification are available from the Galveston District and in ProjNet.

Unit Conversion Factors

A sponsor requirement for this study was the use of English Customary units of measurement. Most measurements and calculations were done in International System (SI) units and then converted to English Customary. The following table can be used to convert back to SI units.

Multiply	By	To Obtain
feet	0.3048	meters
cubic feet	0.02831685	cubic meters
pounds (force)	4.448222	Newtons
square feet	0.09290304	square meters

1 Introduction

Background

The U.S. Army Corps of Engineers Galveston District (SWG) is executing the Coastal Texas Protection and Restoration Feasibility Study (CTXCS) Coastal Storm Risk Management (CSRM) project. The CTXCS, also known as the Coastal Texas Study, involves engineering, economic and environmental analyses on large-scale civil works projects. The purpose of the Coastal Texas Study is to identify coastal storm risk management and ecosystem restoration measures that would reduce the coastal storm threats to the health and safety of Texas coastal communities, reduce the risk of storm damage to industries and businesses critical to the Nation's economy, and address critical coastal ecosystems in need of restoration.

A "multiple lines of defense" strategy is utilized in the formulation of the measures and alternatives in the Coastal Texas Study. Employing four primary goals – prepare, adapt, withstand, and recover – coastal communities are considering a system of comprehensive, resilient and sustainable coastal storm risk management and ecosystem restoration solutions.

The system includes a combination of measures (structural, natural and nature-based features, and nonstructural) to form resilient, redundant, robust and adaptable strategies that promote life and safety based on local site conditions and societal values. The features along the Recommended Plan alignment consist of beach and dune, levee, floodwall, combi-wall, seawall, roadway gates, railroad gates, navigation gates, and vertical and sluice gates to serve navigation needs or for tidal exchange, drainage closure structures and pump stations.

The study area for the Coastal Texas Study consists of the entire Texas Gulf coast from the mouth of the Sabine River to the mouth of the Rio Grande, and includes the Gulf and tidal waters, barrier islands, estuaries, coastal wetlands, rivers and streams, and adjacent areas that make up the interrelated ecosystems along the coast of Texas. The study area encompasses 18 coastal counties along the Gulf coast and bayfronts that are in the Texas Coastal Zone Boundary from the Texas Coastal Management Program. The study area has been divided into four Texas

coastal sections: upper coast, mid to upper coast, mid coast, and lower coast. The upper Texas coast encompasses the Sabine Pass to Galveston Bay area and includes Orange, Jefferson, Chambers, Harris, Galveston, and Brazoria counties. The mid to upper Texas coast is comprised of the Matagorda Bay area and includes Matagorda, Jackson, Victoria, and Calhoun counties. The mid Texas coast covers the Corpus Christi Bay area and includes Aransas, Refugio, San Patricio, Nueces, and Kleberg counties. The lower Texas coast encompasses the South Padre Island area and includes Kenedy, Willacy, and Cameron counties. This particular study focuses on the upper coast Houston-Galveston area.

Objective

The objective of the current study is to evaluate the effectiveness and performance of CTXCS CSRM system components against storm water levels, waves, sea level rise and background erosion to provide quantitative guidelines to help the project sponsors choose optimal alternatives. USACE (2017) identified measures for reducing risks of tropical storm inundation impacts. This report evaluates impacts from the following alternatives:

- Roughly 19 miles of beach, berm and dune along Galveston Island and 26 miles of beach, berm and dune along Bolivar Peninsula
- Ring levee around Galveston
- Surge Barrier at Bolivar Roads
- Smaller navigation gates at Clear Creek and Dickinson Bayou

As part of the ongoing feasibility phase of the project, this report documents the methodology to analyze coastal storm hydrodynamics and beach morphology related to the response of the above measures. The coastal storm hydrodynamics include regional and local circulation, surge, tide, local wave and wind setup, relative sea level rise and seasonal water level variations as well as wave response. Storm hydrodynamics in the Gulf of Mexico basin, local nearshore, bay and inland waterway were modeled in high fidelity for without-project and with-project alternatives. Beach, berm and dune response are quantified for life cycles of coastal storms. Conceptual sketches of the alternatives evaluated herein are shown in Figure 1 through Figure 3. Wave and water level modeling described herein included the alternative of a closed surge barrier/navigation gate at Bolivar Roads (Galveston Entrance Channel) or the combination of the closed surge barrier and the beach/dune system as with-project

alternatives. Figure 4 and Figure 5 show photographs looking southwest along Galveston Island. Figure 6 shows a view looking southwest of Galveston Island along the surface of a color shaded LiDAR elevation map. Figure 7 shows a similar view but along Bolivar Peninsula.

Figure 1. Conceptual sketch of berm and beach single dune alternative

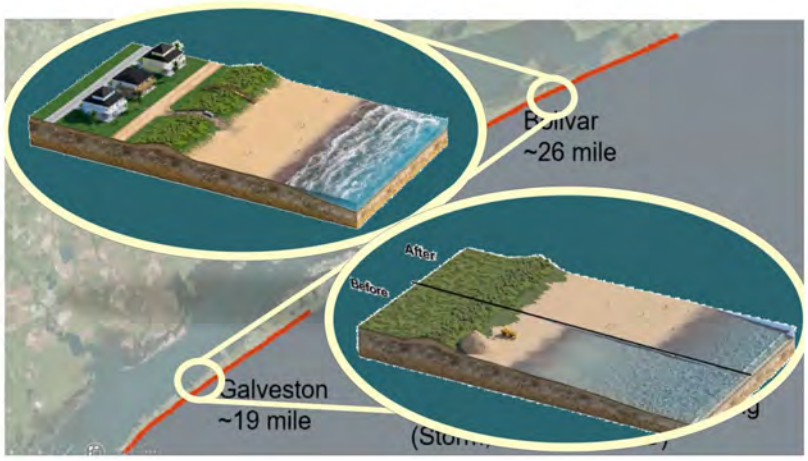

Figure 2. Conceptual sketch of berm and beach dual dune alternative

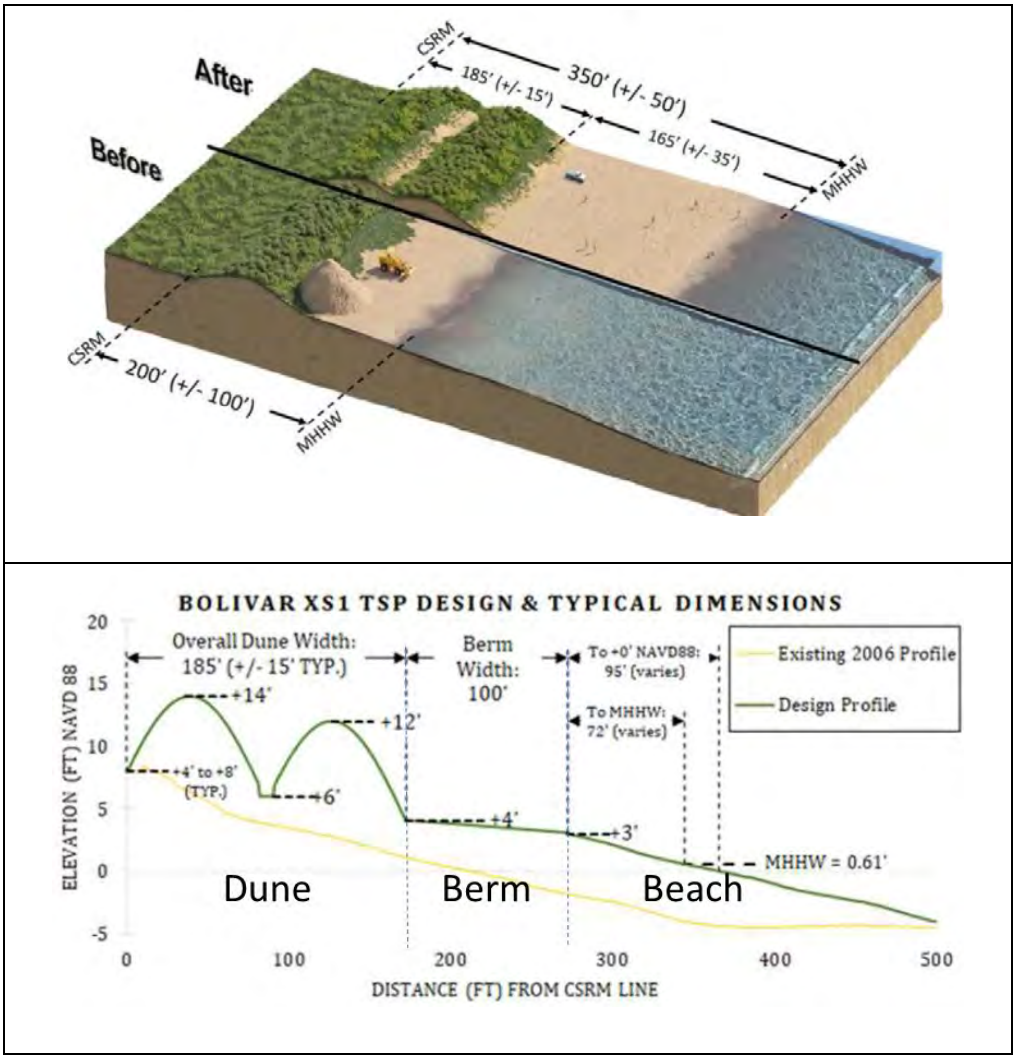

Figure 3. Layout of Alternative with surge barrier (gate) at Bolivar Roads, ring levee, and beach, berm and dune segments along Galveston Island to south east of Galveston inlet and Bolivar Peninsula to northeast.

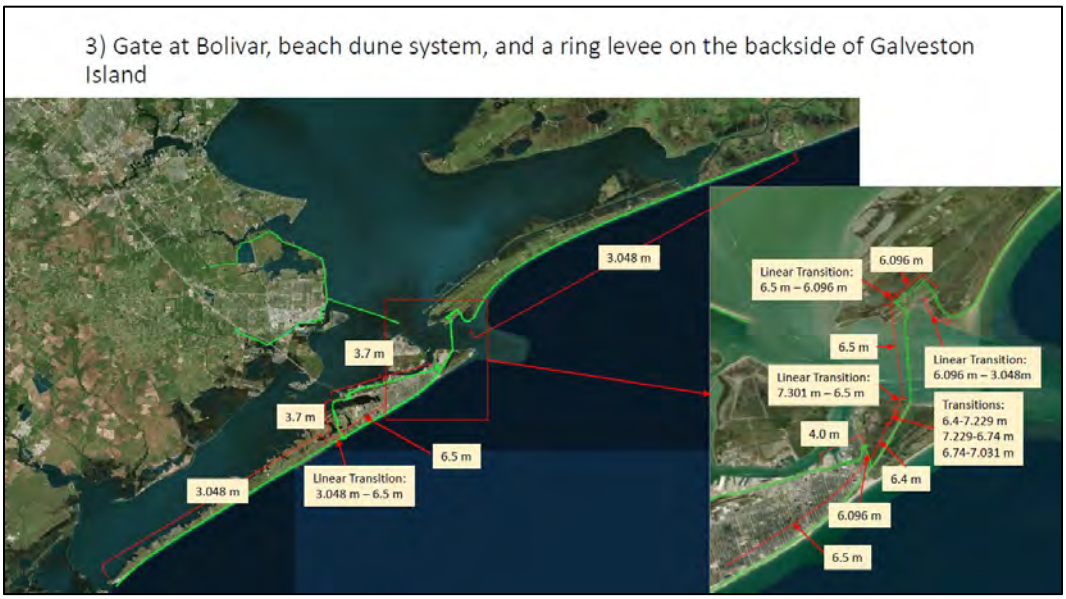

Figure 4. View looking southwest along Galveston Island from end of seawall

Figure 5. View looking southwest along Galveston Island. Dune crest elevation is 5 – 12 ft, NAVD88.

Figure 6. Topography view southwest along Galveston Island with elevations at select locations.

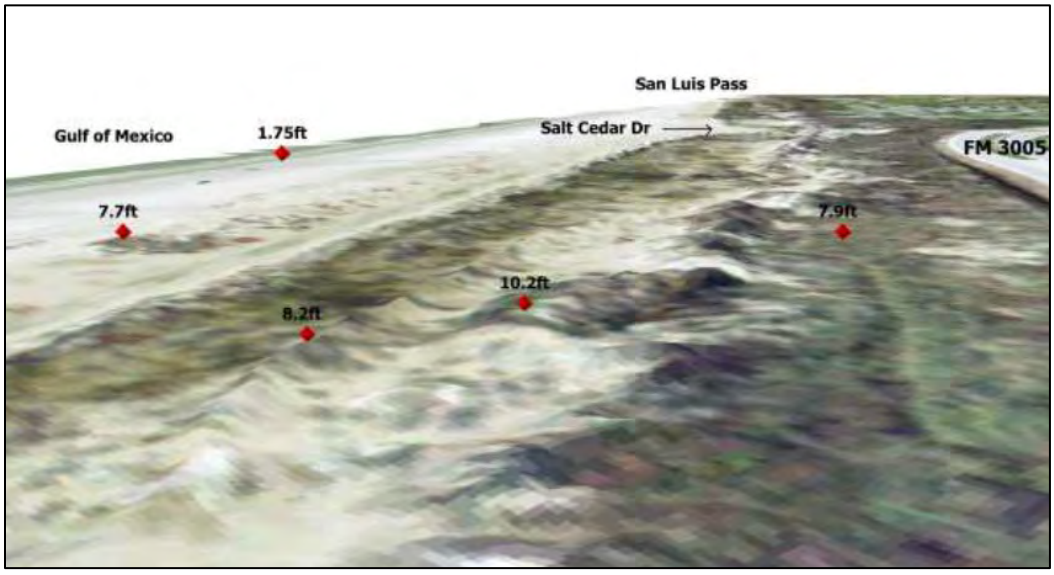

Figure 7. Topography view southwest along Bolivar Peninsula with elevations at select locations

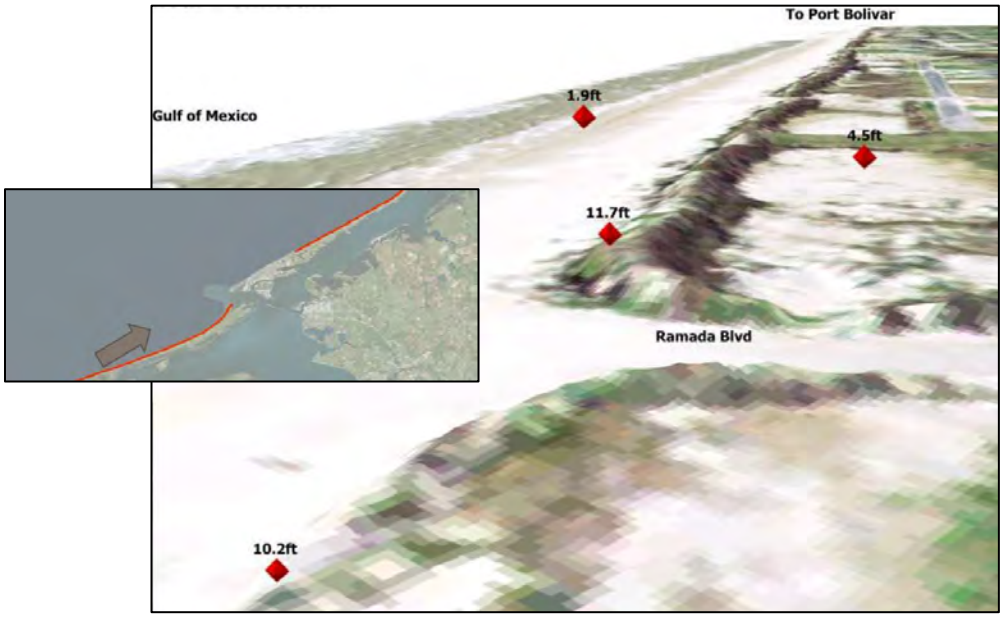

Approach

The analysis approach summarized herein took advantage of previous regional modeling completed under the FEMA FIS study that followed Hurricane Ike (FEMA 2011), S2G Feasibility Study (USACE 2017, Melby et al. 2015a) and prior modeling within the CTXCS (Nadal-Caraballo et al. 2018a, Massey et al., 2018) (See Appendix A for description of prior modeling and analysis studies). However, all of the storm wave and water level forcing used herein for morphology evaluation was based on new modeling done specifically for this portion of the CTXCS. The analysis includes regional hurricane surge and wave hydrodynamic modeling, nearshore wave modeling, and stochastic simulation of beach morphology modeling. The extremal statistics were computed for the storm responses. The process used in the present analysis was as follows:

1. Assessed local geology and historical morphological and shoreline change.
2. Developed a joint probability model of tropical cyclone (TC) storm parameters.
    - Methodology defined in Nadal-Caraballo et al. (2018a)

- The process yielded 660 synthetic TCs that spanned practical probability space for typical coastal storm responses such as storm surge and waves. Storm recurrence rates and probability masses were defined for the storms in order to quantify the probabilistic storm hazards. In addition, epistemic uncertainty was defined.
- These storms had a frequency range based on storm water levels of roughly 1 in 1 years to 1 in 2000 years.

3. Applied an optimization scheme based on a genetic algorithm error minimization of the TC water level hazard to determine an optimal suite of the 170 TCs from the base set of 660 synthetic storms.
    - The suite of 660 CTXCS TCs spanned the entire Texas coast and neighboring region and spanned the practical probability space.
    - The subset of 170 storms optimally characterized the TC response hazard for the coastal region of Bolivar Peninsula, Galveston Island and Galveston Bay.
4. Adopted the wind and pressure fields for all storms developed for the base 660 TC storms using Planetary Boundary Layer (PBL) TC96 Model. Associated TROP files, which contain time series of hurricane meteorological parameters such as central pressure, wind speed, location, radius to maximum winds and heading at 1-hour intervals, were used to define TC meteorological parameters.
5. The TCs were modeled using CSTORM coupled ADCIRC circulation model and STWAVE wave transformation model. Revised without-project and with-project ADCIRC and STWAVE grids by refining the base mesh and adding new bathymetry and topography, as well as higher spatial resolution in the areas of the surge barrier and the beach/berm/dune system. With-project grids incorporated tentative alternative selection options that include the Galveston Entrance Channel surge barrier system, Galveston ring barrier system and the dune-berm-beach system.
6. Revalidated CSTORM TC response against observations using historical hurricanes Carla (1961), Bret (1999), Rita (2005), Katrina (2005), Ike (2008), Gustav (2008) and Isaac (2012).

7. Used CSTORM to compute wave and water level responses for all synthetic TCs for with- and without-project conditions and two relative sea level change (RSLC) scenarios.
    - CSTORM modeling save locations corresponded to high density coverage of Texas coast.
8. Computed relative sea level change curves for use in simulations. Low (historical) and high RSLC rates were used to compute fixed RSLC values at specific times: start of project in 2035 and end of project in 2085. These were used, along with a steric (seasonal) offset and datum offset to create total geoid offsets for regional hydrodynamic modeling. The rates were also used in morphology modeling to compute continuous RSLC during each life cycle.
9. Using regional hydrodynamic modelling output but without morphology modeling, computed extremal statistics and confidence limits for TC waves and water levels using StormSim (Nadal-Caraballo et al. 2015, Melby et al. 2015b, Melby et al. 2017) and the joint probability method. Response statistics were for 2 RSLC conditions and with- and without-project alternatives for years 2035 and 2085.
    - Peak storm water level (SWL) and peak significant wave height (H_{m0}) probability distributions were computed and discrete probabilities were tabulated for the full range from frequent to extreme rare events. Associated statistical peak wave period and mean wave direction corresponding to peak SWL and H_{m0} values were also tabulated. Output spanned the Texas coast.
    - The resulting probabilistic model of TC responses was conditionally joint with JPM-OS storm parameters.
    - TC hazard output was at 50% confidence limit as well as 90% and 10% confidence limits.
10. Developed a peaks-over-threshold sample of extreme non-tropical high water level events using the NOAA water level Gage in Galveston Pier 21 and Wave Information Study wave conditions just offshore of the site. Tropical storms were excluded from this data set. Time series of waves and detrended water levels for these historical non-tropical storms were saved for use in the time-dependent morphology life cycle simulations.

11. Assembled time series of wave and storm water level conditions at locations offshore of Galveston Island and Bolivar Peninsula in a depth of roughly 40 ft for use as input to life cycle simulation of coastal morphological response. Storm water level was constructed by linearly superimposing tide, storm water level and relative sea level rise. Storm water level included surge and steric offset. Tide time series for each storm was randomly sampled from predicted tide associated with the local NOAA water level gage.
12. Conducted Monte Carlo simulations to determine the stochastic beach response for individual storms and for the stochastic response over 50-year life cycles.
    - The response simulation was conducted with StormSim stochastic simulation software which randomly samples from the 170 tropical cyclones and non-tropical events. Each event is run with CSHORE, a time averaged wave transformation and beach morphology model that included intra-storm time-dependent morphological evolution and wave and steady flow overtopping of dune.
    - Life cycle simulations of 50 years each were run including major rehabilitation if dune elevation limit state was exceeded. Roughly 30 unique life cycles with random storm sampling were run per scenario in order to assure statistical convergence.
13. Reported statistical results from the above analysis including:
    - Wave and water level results for both with- and without-project alternatives and confidence limits (CL) across for the three RSLC scenarios;
    - Morphology response as statistical variation of the elevations of key locations along the transect;
    - Number of major rehabilitation rebuilds of beach;
    - Wave and steady flow overtopping extremal distributions.

This report is organized around the process described above in the following sections:

2 Historical Trends in Morphologic Behavior

Geographic setting for morphology study

The morphology study area extends from High Island on the east end of Bolivar Peninsula to San Luis Pass on the west end of Galveston Island as shown in Figure 8 and Figure 9. To the east of High Island is a mostly muddy shoreline to Sabine Pass. Bolivar Peninsula is 26 miles long and extends to the east-northeast from Galveston Entrance Channel. Galveston Island is 29 miles long and extends to the west of the entrance along a long axis in the west-southwest direction. Both landforms consist of a sandy veneer overlying a muddy substrate. Galveston Entrance Channel is the jettied deep-draft channel and entrance to Galveston Bay. It is one of the most economically important and busiest entrance channels in the country. The eastern third of Galveston Island is the most populated with the densely populated commercial and residential city of Galveston. This section is includes a stepped seawall and raised land and a broad fronting beach is periodically renourished. The center and western portions of the island consist of relatively sparse residential neighborhoods, condominiums, and marinas. Bolivar Peninsula includes some residential neighborhoods but is relatively sparsely populated.

A large fillet exists on the west end of Bolivar Peninsula next to the north jetty of the inlet. Beach face corings near Caplen show 6-10 ft of sand overlying a clay substrate (Figure 10, from White et al. 1985) and this sand thickness increases towards the inlet. Sand thicknesses are similar on Galveston Island but somewhat more uniform away from the inlet as shown in Figure 10. In the inner shelf region in the offshore area, the sea bottom is mostly mud but there are significant quantities of beach quality sand in scattered pockets. King et al. (2007) reported median grain sizes between Sabine Pass and Galveston Inlet from 0.0854 to 0.230 mm with an average value of 0.167 mm and median grain sizes ranging from 0.104 to 0.154 mm, with an average value of 0.129 mm on Galveston Island.

Figure 8. Regional map from King (2007)

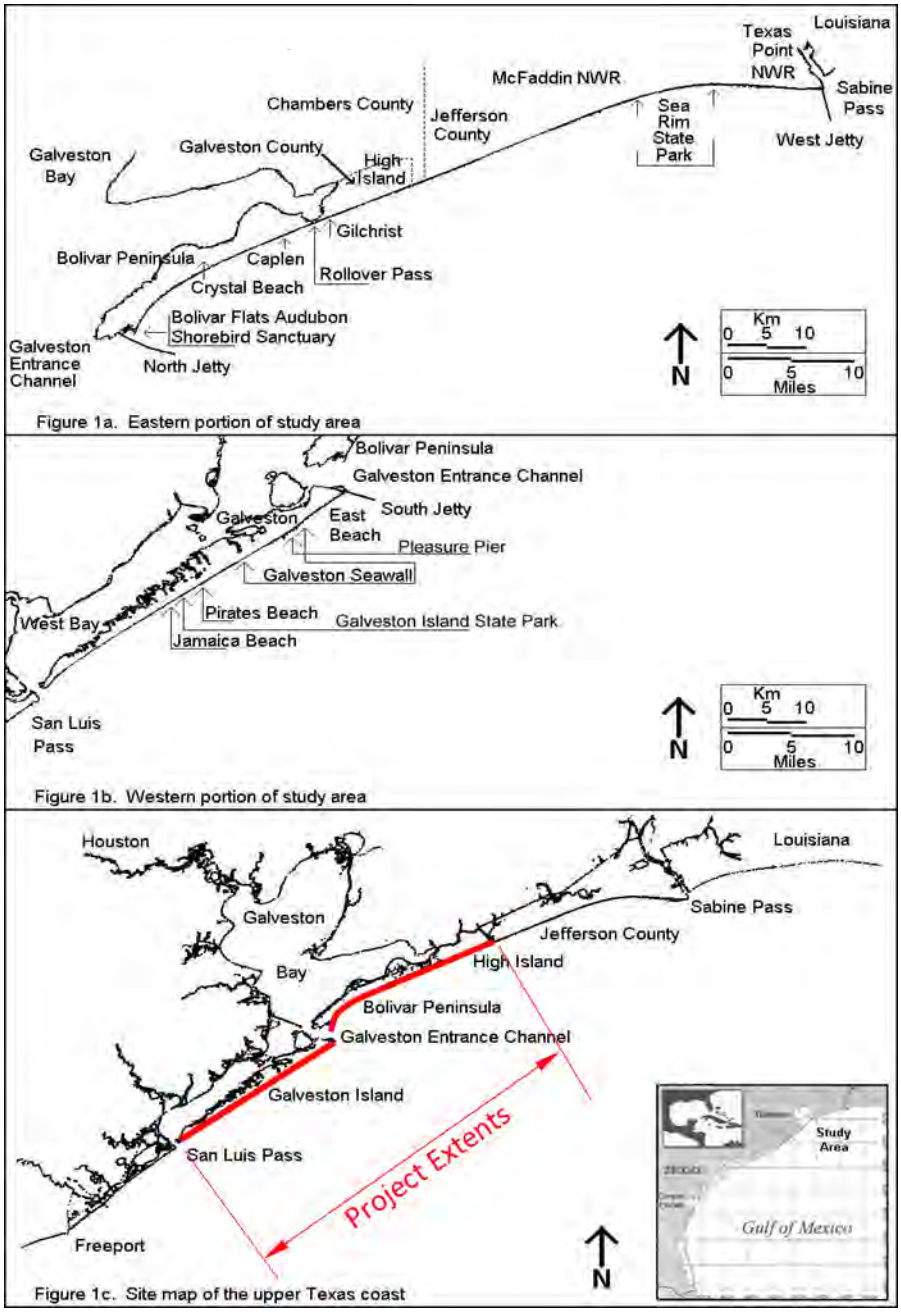

Figure 9. Study area, Galveston Island and Bolivar Peninsula (From Frey et al. 2013).

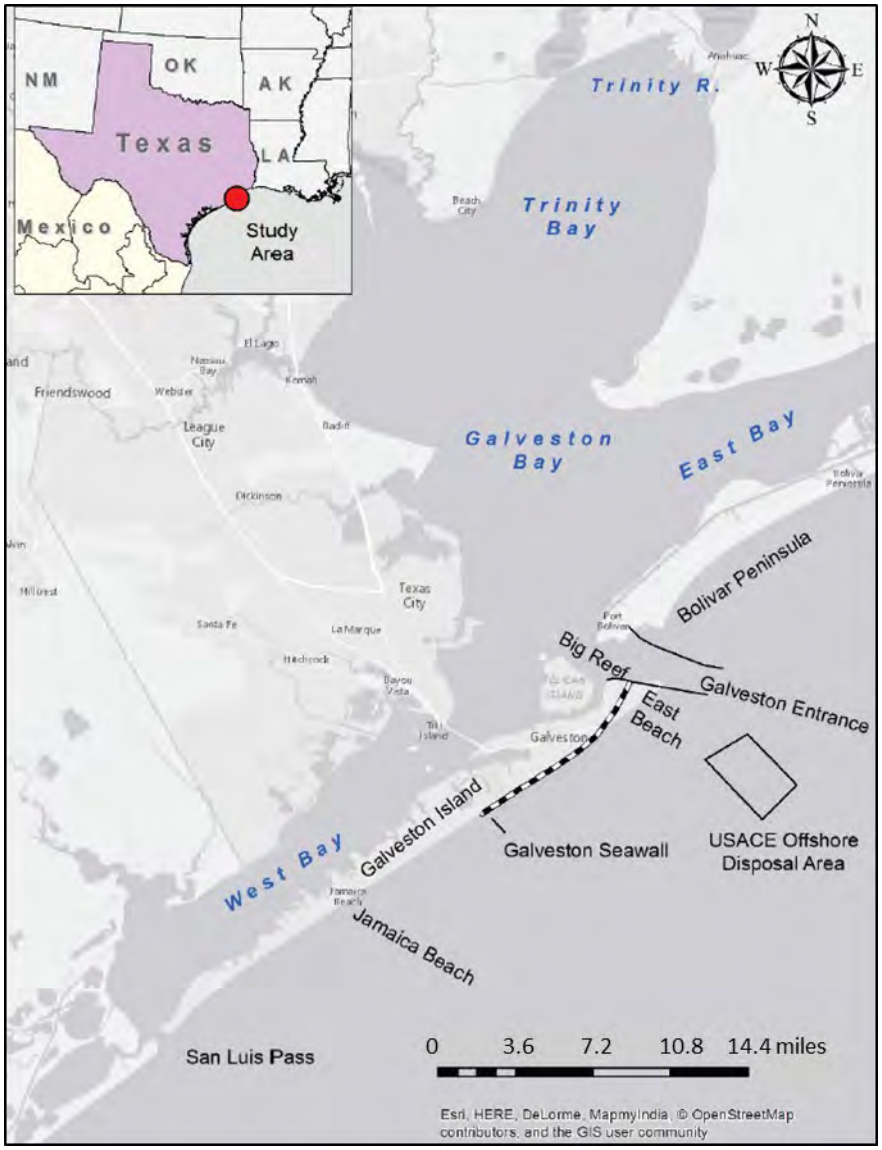

Figure 10. Isopach map of Holocene sediments (top) and strike section of Holocene sediments and subsea depth of the Holocene-Pleistocene unconformity from White et al. (1985)

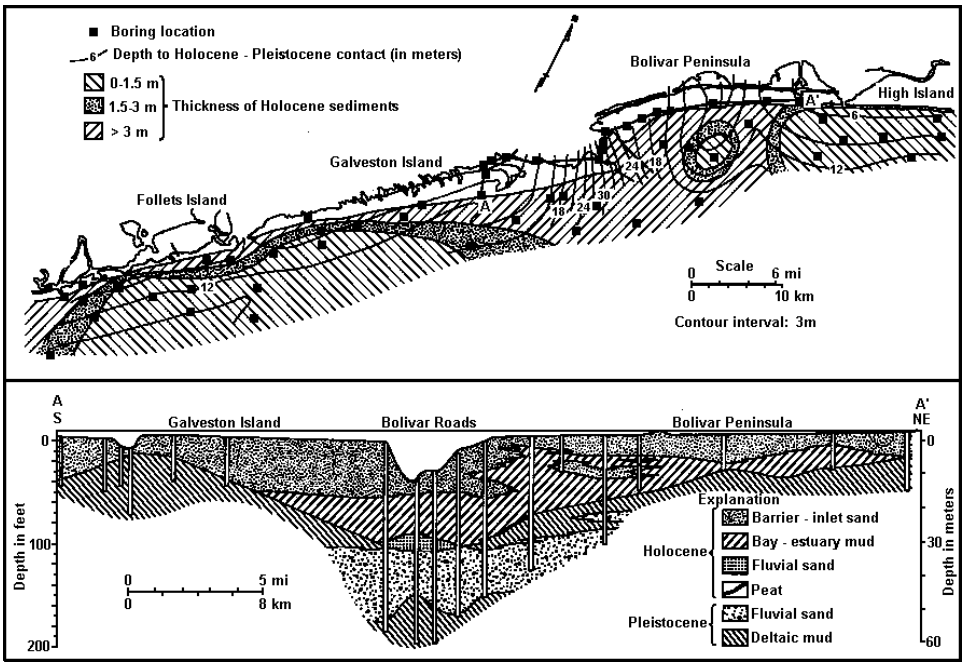

Sediment transport

The following is a summary of material from Frey et al. (2013) and King (2007). For Galveston Island, the net sediment transport is to the southwest although along the Galveston seawall there is a reversal with net transport on the eastern end towards the entrance. While most of the island has relatively low levels of erosion, the ends at San Luis pass and the entrance are accreting as shown in Figure 11 and updated from a study by Frey et al. in Figure 12. In addition, the area near the west end of the seawall has significant erosion. Most of the sandy material is fine grained with median diameter of 0.15 mm (Frey et al. 2013). The area is sand limited and there is very little coarse grained material being delivered to the beaches in modern times. King (2007) stated that net longshore transport is to the southwest for the region. He summarized the transport rates as shown in Table 1.

Figure 11. Aerial map of study area with overlay of sediment transport rates (Paine et al. 2011).

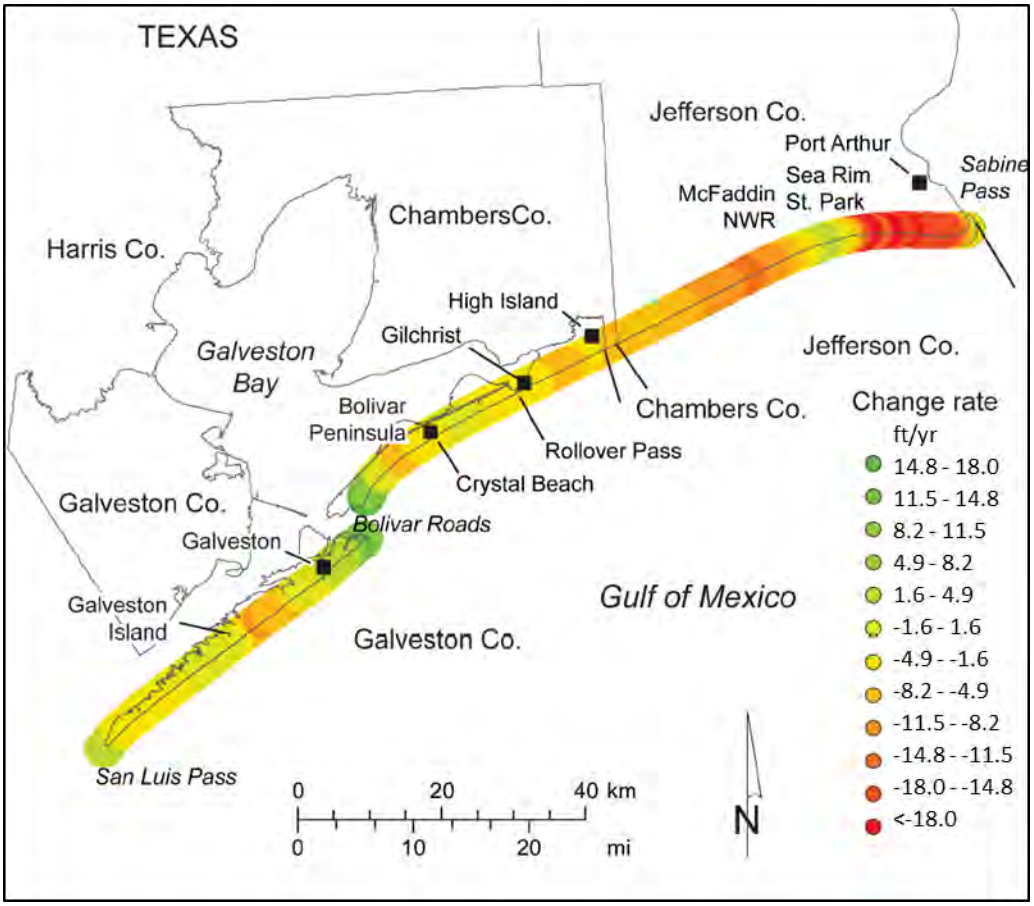

Figure 12. Aerial map of study area with overlay of sediment transport rates (From Frey et al. 2013).

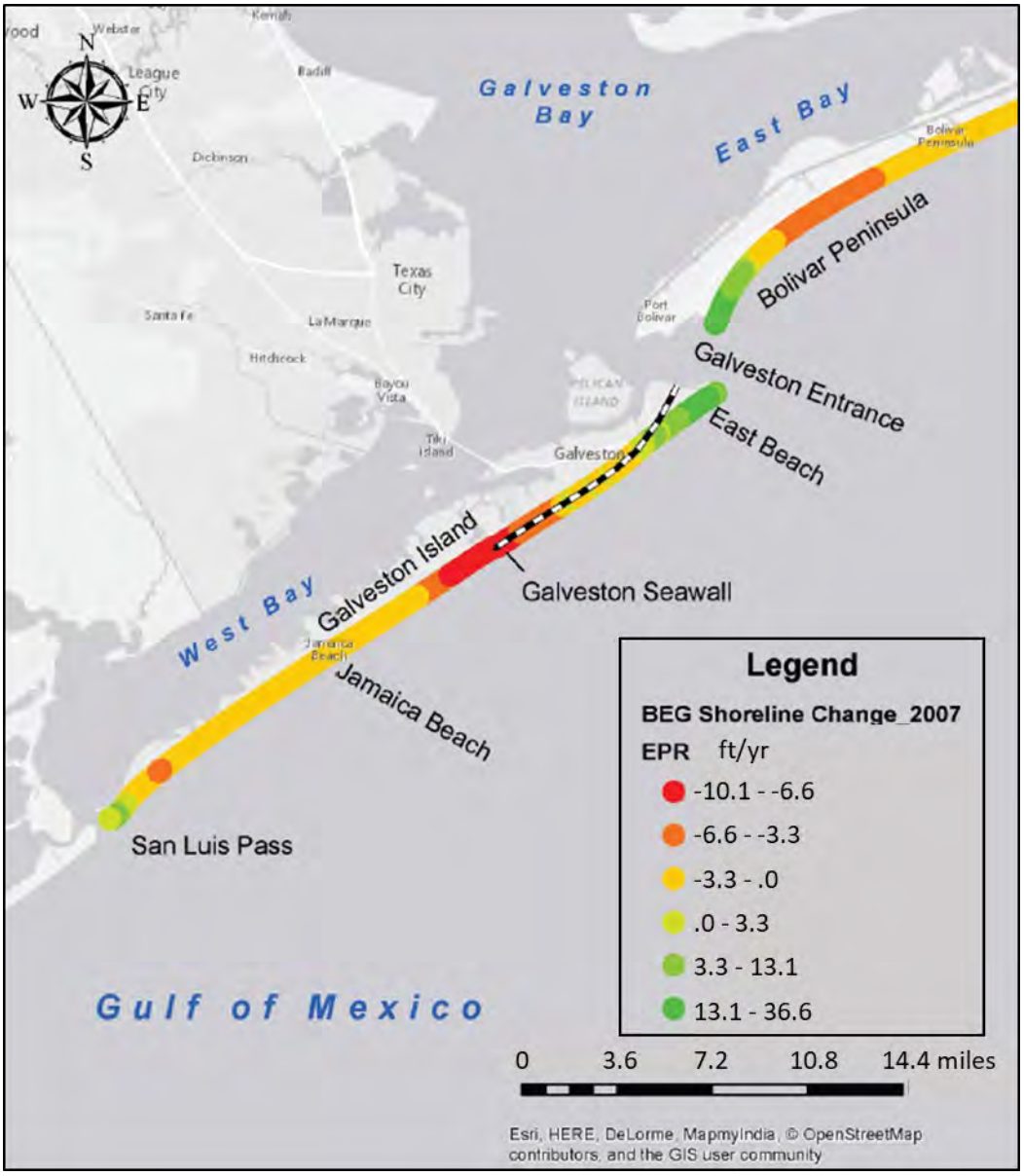

Table 1. Sediment Transport Rates Reported in the Literature

Author	Transport Rate cy/yr Net	Net Dir	Data Yrs
Sea Rim State Beach			
Mason (1981)	35,315	NE	75,77
USACE (1983)	70,629	SW	10 yr
High Island			
USACE (1983)	102,020	SW	10 yr
Gilchrist / Rollover Pass			
USACE (1959)	200,116		
Prather and Sorensen (1972)	75,861	SW	
Hall (1976)	53,626	SW	1975
Mason (1981)	57,550	SW	75,77
Bales and Holley (1989)	241,971- 289,057	SW	56-84
Crystal Beach			
USACE (1983)	98,096	SW	10 yr
Galveston Entrance Channel			
Mason (1981)	77,169	SW	75,77
USACE (1983)	47,086	SW	10 yr
12th St., Galveston			
USACE (1983)	30,083	SW	10 yr
Bermuda Beach			
Hall (1976)	151,722	SW	1975
Mason (1981)	396,309	SW	1975
USACE (1983)	57,550	SW	10 yr
Galveston Island State Beach			
Hall (1976)	86,325	SW	1975
Sea Isle			
Hall (1976)	134,719	SW	1975
Mason (1981)	232,815	SW	1975
USACE (1983)	20,927	SW	10 yr
East Side of San Luis Pass			
USACE (1983)	26,159	SW	10 yr

Historical shoreline change rates for the area from Sabine Pass to Galveston Entrance Channel from King (2007) are shown in Figure 13. As stated by King, "*…the M 1882 1974, P&M 1974-1982, and M 1974-1996 bar graph labels refer to average annual shoreline change rates over the listed intervals using data from Morton (1975), Paine and Morton (1989), and Morton (1997), respectively*." "*The 1974 and 1982 photographs were digitally scanned and ortho-rectified typically using 30-60 ground control points per image. Shoreline change rates, established at 50-meter intervals (rather than the earlier 5000 ft intervals), were calculated using a linear regression analysis involving all four shorelines. These rates are shown as the black line, labeled G 1974-2000,…*". In the figure, positive numbers indicate accretion while negative indicate erosion. The relatively recent solid black line on the figure is the most pertinent for the present study. The shoreline change rates from High Island to the Galveston Entrance Channel can be seen as being

relatively small compared to the area northeast of High Island except at the Galveston Entrance Channel north jetty fillet where accretion rates are high. Based on this figure, the project area along Bolivar Peninsula has both accretion and erosion areas with the central portion near Caplan being slightly erosive and the populated areas of the peninsula being slightly erosive to slightly accretive from east to west. King noted that this central area of Bolivar Peninsula is neutral with respect to shoreline recession.

Similarly, historical change rates for Galveston Island are shown in Figure 14. For this Figure, King notes that "*…data sources are the same except that M 1882-1974 refers to Morton (1974).*" For this area, there is strong accretion near the east end next to the Galveston Entrance Channel where the net rate is northeastward. Over about the eastern two-thirds of the seawall, the area is accreting. The net rate direction reversal location is clear in the figure and it is about a distance of one-third the wall length going east from the west end of the seawall. Near the west end of the Galveston seawall, the shoreline change rate transitions from near zero to clearly erosive (roughly 6-9 feet per year) due to the net southwesterly sediment transport rate and sediment mobility constraining effects of the seawall. Since the 1960's, the shoreline has retreated 200-300 feet just west of the seawall. Erosion decreases going west, with the net rate increasing again near San Luis Pass and dramatically transitioning to accretion at the inlet fillet. Overall, net shoreline change rates are greater on Galveston Island than on Bolivar Peninsula with Bolivar having a net rate that is -5 to 5 ft/yr over the majority of the length with a mean that is near zero while Galveston Island has a mostly erosive rate of 0 - 10 ft/yr.

Coastal shoreline sediment transport in the region is primarily a result of day-to-day wave and current action, storm waves and currents, and aeolian forcing. Additionally, some of the sediment is transported into the inlets and then dredged and transported. The day-to-day wave and current forcing is mostly accretionary. Mild frequent storms are influential in long term sediment movement. The predominant wave direction is to the southwest so sediment tends to move in this direction in the area. This moves the sediment towards the Galveston Entrance Channel on Bolivar and towards San Luis Pass on Galveston Island which explains the large fillets on the updrift sides of the inlets. However, most of this sediment movement from these frequent events stays within the system composed of these two landforms. Intense hurricanes, on the other hand, can

permanently move sediment either offshore into relatively deep water or well inshore and out of the beach-dune system where it is lost to the beach system. This permanent erosion is the focus of the erosion study herein.

Figure 13. Historical shoreline change rates for region from Sabine Pass (on left) to Galveston Entrance Chanel (on right).

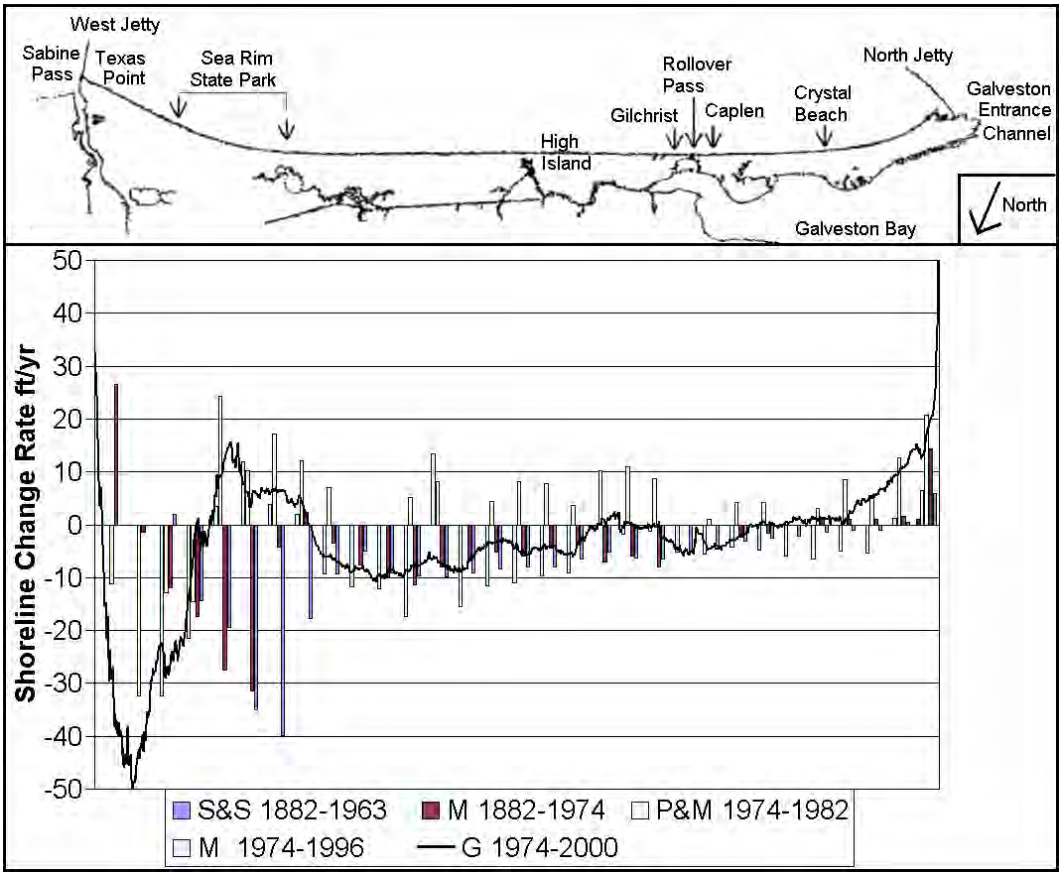

Figure 14. Historical shoreline change rates for region from Galveston Entrance Chanel (on right) to San Luis Pass (on right).

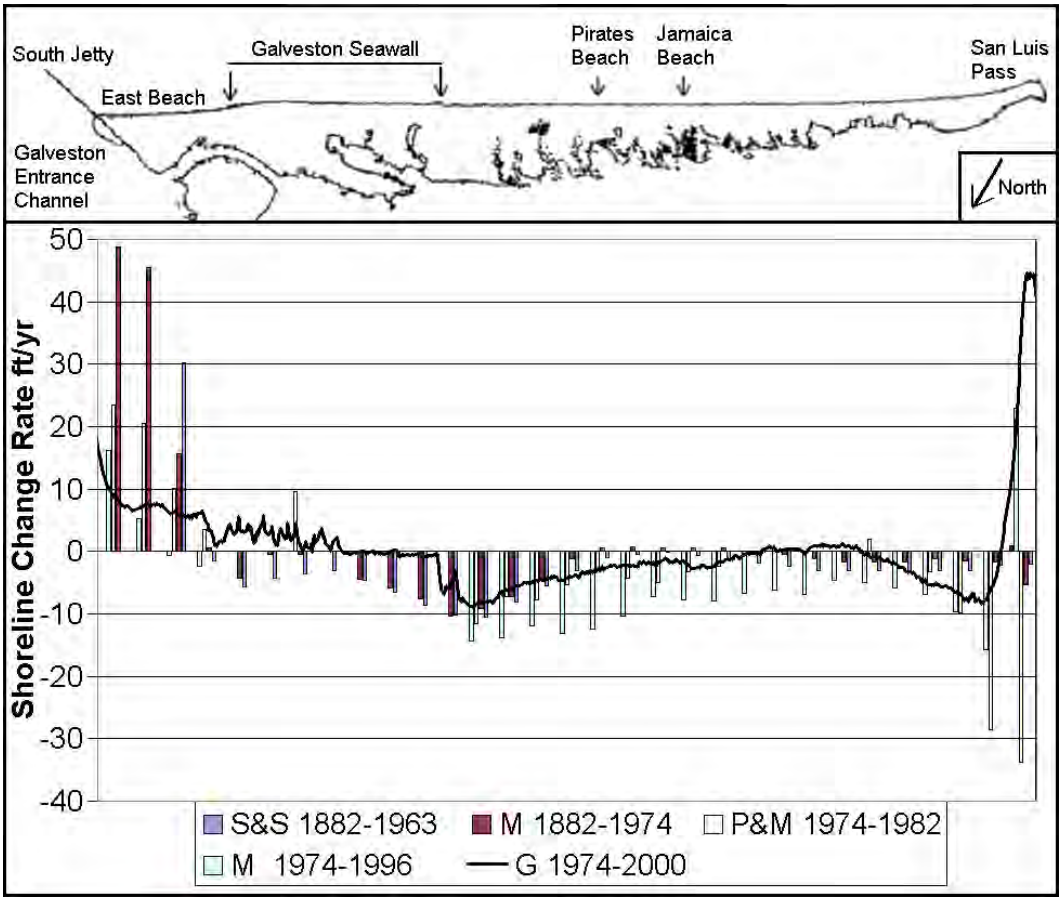

3 Regional Storm Hazard

JPM

Tropical cyclone storm occurrences are relatively sparse in hurricane-prone areas in both time and space. In addition, there are few water level and wave gages along the Gulf of Mexico Texas coastline. This is similar to other regions of the U.S. coastline. The combination of sparse occurrences and sparse measurements results in large uncertainties in extreme predictions based on point gage water level measurement. This is a well known vulnerability in risk estimates of coastal flood control systems exposed to TC storms.

Following Hurricane Katrina, the USACE initiated a program to dramatically improve the statistical estimates of extreme storm responses. This led to development of the probabilistic synthetic storm modeling approach outlined herein (Resio et al. 2007, Nadal Caraballo et al. 2018a). Since then, the joint probability method (JPM) has become the dominant probabilistic approach used to assess the coastal storm hazard in hurricane-prone areas of the United States. Although the JPM approach has been in development since the 1970s, recent advancements in technology have made it possible to reduce the necessary number of synthetic storms resulting in improved sampling techniques. This approach is termed JPM with Optimal Sampling (JPM-OS). While the methods have improved considerably, JPM studies have considerable uncertainty stemming from the probabilistic model, the meteorological and hydrodynamic numerical models, and the climatological and oceanic observations. The employment of the JPM-OS approach attempts to quantify these uncertainties and reflect these uncertainties in the resulting hazard statistical output as confidence limits. The developmental progression of the JPM-OS methodology for Texas, including storm selection and uncertainty quantification, culminating in the approach taken during the CTXCS study, is described in Appendix A.

The JPM approach used herein is described in Nadal Caraballo et al. (2018a) and follows that shown in Figure 15. The methodology generally followed the steps listed below:

- Characterization of historical storm climatology;

- Computation of historical spatially varying TC storm recurrence rate (SRR);
- Storm parameterization and development of probability distributions of historical TC parameters;
- Discretization of probability distributions of TC parameters;
- Development of synthetic TC set;
- Meteorological and hydrodynamic simulation of synthetic TC;
- Peaks-over-threshold screening of water level and wave measurements to define non-tropical (extratropical in figure) storm events;
- Estimation of epistemic uncertainty and other secondary terms;
- Integration of joint probability of storm responses.

Figure 15. JPM methodology as employed in this study (from Nadal Caraballo et al. 2018a).

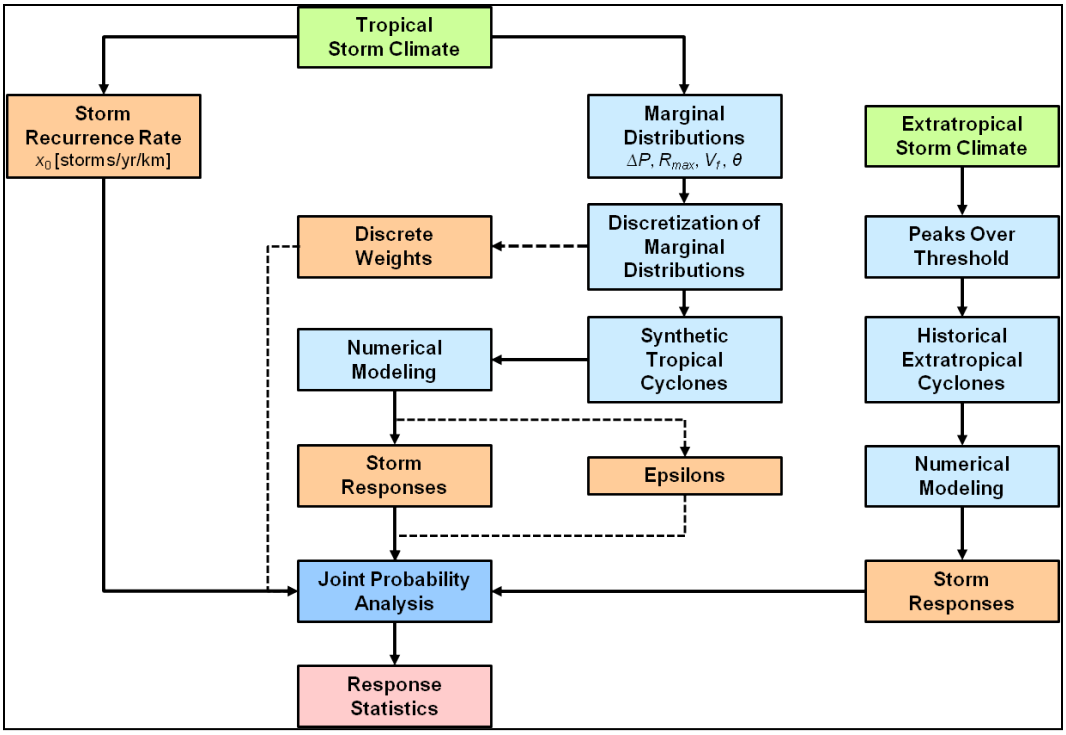

Historical TC climatology was defined based on the National Oceanographic and Atmospheric Administration (NOAA) National Hurricane Center HURDAT2 (HURricane DATa 2nd generation) database. This database extends back over 150 years but the analysis of TCs for this study was confined to the period 1938–2017, corresponding to a few years before the initiation of hurricane hunter aircraft reconnaissance missions.

This period is considered to correspond to the period of reasonably high accuracy in climatological data concerning TCs. Figure 16 shows storm tracks for the historical landfalling TCs that occurred in the Gulf of Mexico region during this period.

Figure 16. Tracks of historical TCs in region within modern period of hurricane hunter aircraft reconnaissance (from Nadal Caraballo et al. 2018a).

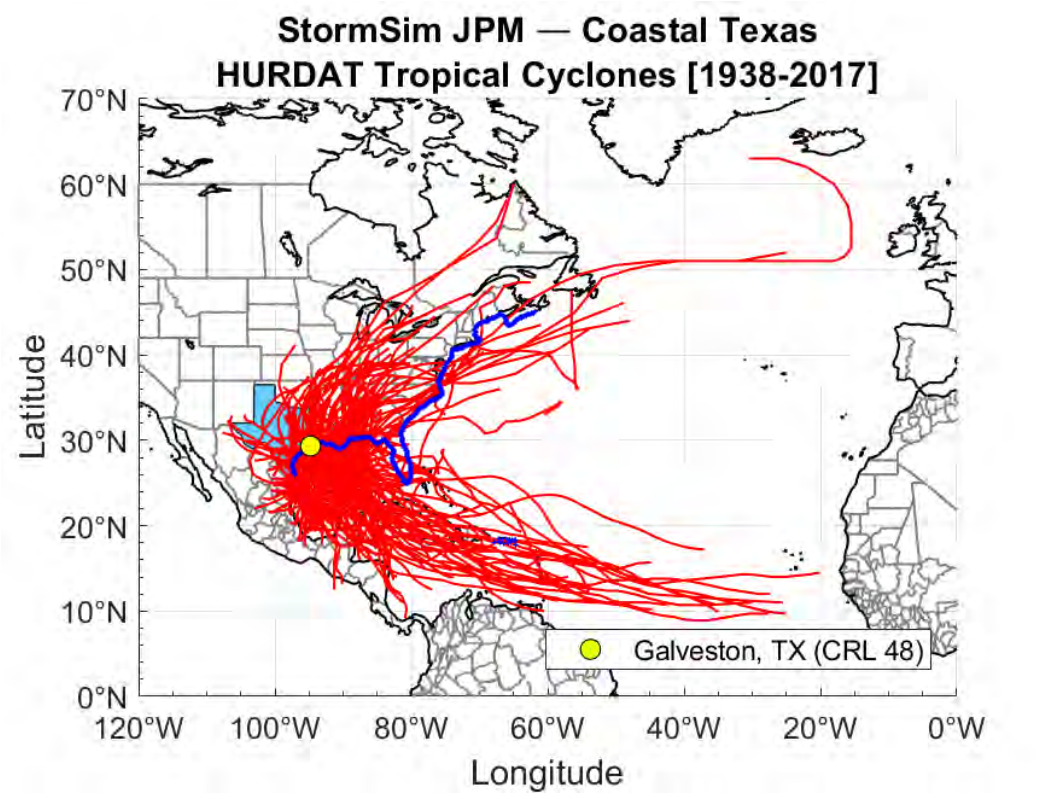

The HURDAT2 database quantifies TC storm characteristics using the following parameters:

1. track location (x_o)
2. heading direction (θ)
3. central pressure deficit (δp)
4. radius of maximum winds (r_{max})
5. translational speed (v_t).

Nadal-Caraballo et al. (2018a) provides a summary of how these parameters are used to define the synthetic TCs. "*In order to develop the set of synthetic storms, each parameter is treated as a correlated random variable and either a marginal or a conditional probability distribution*

is sought for each parameter based on the TCs observed in the historical record. The probability distributions are then discretized, and the corresponding weights are assigned to the range of discrete values. Synthetic storms are developed as possible combinations of samples from the marginal or conditional distributions. Each synthetic storm must consist of a physically and meteorologically realistic combination of the aforementioned parameters. The parameterized TCs are used as inputs to the PBL model. This model is used as part of the JPM methodology to estimate the time histories of the wind and pressure fields that drive high-fidelity storm surge and wave numerical hydrodynamic models such as ADCIRC and STWAVE."

A suite of 660 storms was developed using the JPM-OS approach. The storm tracks align with idealized master tracks shown in Figure 17 and Figure 18. The storms are listed in Appendix C.

Figure 17. Map of TC tracks for JPM storms

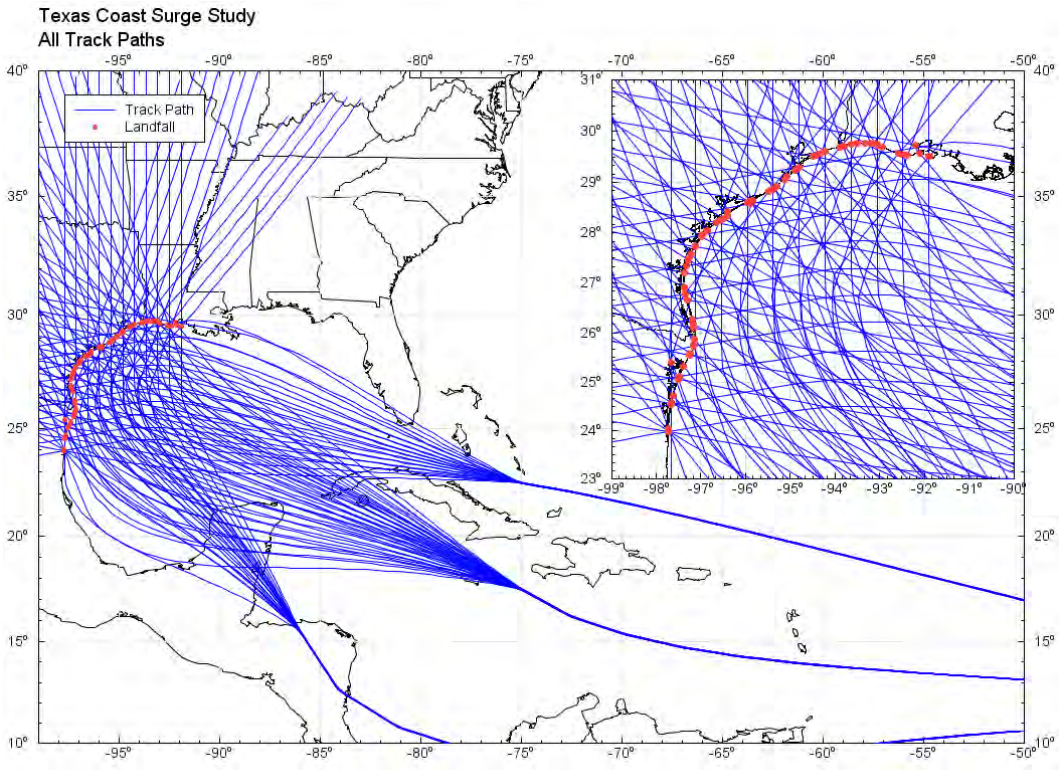

Figure 18. Zoomed in map of TC master tracks for entire region (left) and TCs that significantly influence project (right)

Storm selection beach morphology investigation

A Matlab® genetic algorithm toolbox function was used to select an optimal subsample of the 660 CTXCS TCs. The method is based on the design of experiments approach as described in detail in Appendix E. Storm Selection and sought to select the optimal 170 TCs from the initial base set of 660 TCs that minimizes the difference in SWL hazard curves. The genetic algorithm method is described on the Matlab website as "*The genetic algorithm is a method for solving both constrained and unconstrained optimization problems that is based on natural selection, the process that drives biological evolution. The genetic algorithm repeatedly modifies a population of individual solutions. At each step, the genetic algorithm selects individuals at random from the current population to be parents and uses them to produce the children for the next generation. Over successive generations, the population "evolves" toward an optimal solution.*"

Peak SWL response for the full suite of 660 storms run using CSTORM had been output at points throughout Texas and extending offshore. The SWL peaks from the 660 were used as input for the subsampling. In this approach, an initial subsample of storms is obtained and tested against the full suite of storms. The SWL hazard curves are computed for each of the save locations and the reduced sample hazard curve is compared against the full sample. The best storm sample set is determined by minimizing the fitness function which, in this case, is the difference in hazard curves. The optimal set of events that minimizes the fitness function is selected. Figure 19 shows the results of the process where the Genetic Algorithm penalty value is the error of the fitness function defined by the normalized

hazard curve difference. The horizontal axis shows the number of generations or groups of storms as the algorithm progresses, approaching the optimal. On the right are the water level hazard curves for both the full storm set and the reduced optimized storm set of 170 storms following optimization. The figures illustrate that the sample of 170 storms converged and the ultimate hazard curve error is very close to zero. Here, convergence describes the fact that the error reduces to nearly zero as the sample size approaches 170. Note that the error between sample and original is small even for small samples. However, a larger sample was required in order to span the large region. The set of 170 storms and the original 660 storms are summarized in Appendix C. The final set of 170 storms includes virtually all of the master tracks shown in Figure 17 and includes all of the headings.

Figure 19. Genetic Algorithm penalty value plotted as a function of generation (left) and water level hazard curve for CTXCS save point 17396.

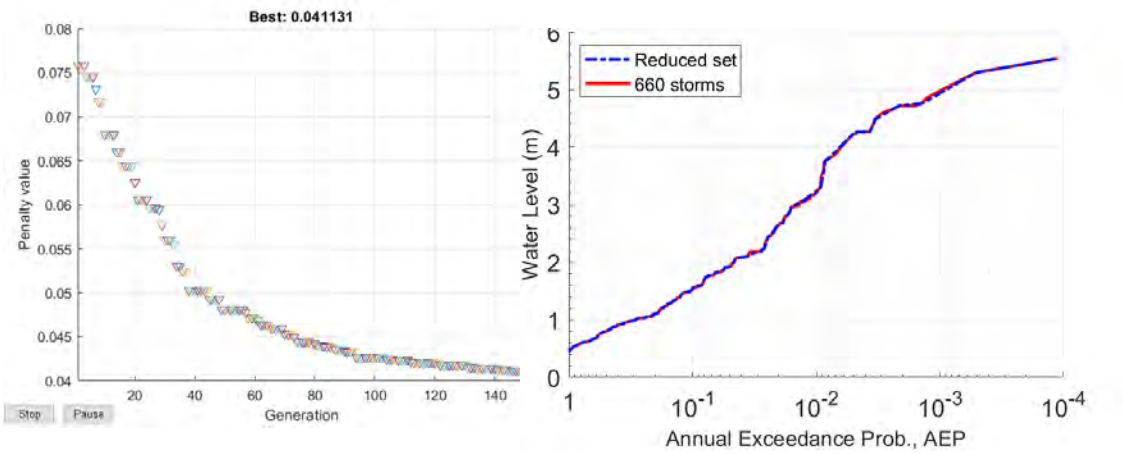

Non-tropical wave and water level event selection

While tropical storms can produce dramatic erosion in the beach and dune areas, they are relatively infrequent. On the other hand, non-tropical storm events are fairly frequent but produce fairly small responses compared to tropical storms. However, the cumulative effect of frequent low-intensity events can result in significant erosion and therefore impact beach management approaches.

The non-tropical water level events were identified through a peaks-over threshold (POT) analysis of NOAA water level station Galveston Pier 21 8771450. This station was selected based on the criteria of central

proximity to the site and hourly measurement record length of at least 30 years. The measured time series was detrended with a nonlinear polynomial in order to remove long-term sea level rise. The detrended time series was pivoted about the center of the epoch in 1992. The screening of the NOAA station measurements excluded tropical storm water level events by comparing storm dates to those in the HURDAT2 database. POT application resulted in a set of 35 water level events for the study area. It is likely that all of the identified events were associated with coastal storms of some sort that were either frontal systems or extratropical. However, the nature of the climatology was not critical for the lesser events which have relatively much milder responses than tropical storms. The corresponding wave conditions (H_{m0}, T_p, mean wave direction) were selected from Wave Information Study (WIS) hindcast for stations 73067 and 73077 offshore of the area. Figure 20 shows the locations of WIS stations 73067 and 73077 along with NOAA water level station 8771450. Table 2 lists the historical non-tropical events with their respective responses. The smallest value in Table 2 has an average return interval of about 1 year.

Figure 20. Location map of WIS station and NOAA water level gages

Table 2. Peak parameter values for non-tropical storms ranked by water level

Date of Peak SWL	MWD (deg, Az)	T_p (s)	H_{m0} (ft)	SWL (ft, NAVD88)
16-Oct-2006 09:00:00	152	8.39	8.30	3.75
25-Oct-2015 18:00:00	26	6.30	9.71	3.43
31-Oct-2015 09:00:00	152	8.39	8.07	3.42

03-Dec-2016 09:00:00	101	7.63	8.33	3.36
02-May-2016 07:00:00	122	5.73	4.10	3.22
18-Apr-2016 07:00:00	109	7.63	6.96	3.19
21-Nov-2009 08:00:00	99	6.93	6.53	3.09
28-Dec-2015 01:00:00	168	10.15	8.01	3.09
05-Apr-1997 08:00:00	163	8.39	9.09	3.07
18-Nov-2003 07:00:00	165	6.93	6.66	2.99
22-Oct-2009 10:00:00	143	6.93	5.87	2.91
21-Oct-2017 00:00:00	113	6.93	4.40	2.91
18-Apr-2009 22:00:00	129	6.93	4.69	2.87
29-Apr-2017 23:00:00	144	9.23	8.66	2.86
16-Nov-2004 09:00:00	102	6.30	5.18	2.84
02-Dec-2009 01:00:00	70	5.73	4.23	2.76
26-Apr-1997 02:00:00	116	6.93	6.96	2.74
02-Nov-2004 12:00:00	177	7.63	5.35	2.73
15-Jan-1991 06:00:00	157	7.63	8.50	2.72
12-Oct-1997 07:00:00	126	6.93	5.84	2.72
12-Dec-2009 06:00:00	93	6.93	7.35	2.71
22-May-2017 18:00:00	130	6.93	4.66	2.70
07-Nov-2016 08:00:00	107	5.21	3.31	2.69
09-May-2016 20:00:00	161	6.30	6.30	2.67
01-Nov-1992 14:00:00	165	6.30	6.23	2.65
17-Nov-2015 20:00:00	159	7.63	6.79	2.65
09-Mar-2016 20:00:00	146	9.23	8.17	2.64
27-Apr-2016 13:00:00	150	6.30	3.58	2.62
28-Nov-2015 01:00:00	123	10.15	3.94	2.61
21-Sep-2003 10:00:00	113	5.73	4.23	2.61
24-Nov-2007 23:00:00	84	6.93	6.20	2.59
27-Apr-1990 12:00:00	146	7.63	4.53	2.58
05-Nov-2013 07:00:00	120	6.30	5.64	2.58
23-Dec-1986 05:00:00	109	6.93	3.15	2.57
10-Nov-2016 09:00:00	56	5.21	4.79	2.57

4 Regional Surge and Wave Modeling

CSTORM model domain, topography, bathymetry and mesh

Regional wind and surface pressure fields were produced for three wind/pressure field grids for each storm (see Figure 21). The Level 1 (also referred to as WNAT, or Western Northern Atlantic) grid boundaries extended from 5.0° to 47.2° north latitude and from 99.0° to 54.8° west longitude and used a 0.20° by 0.20° grid spacing. The Level 2 (referred to as the GOM for Gulf of Mexico) grid boundaries centered on the Gulf of Mexico and extended from 18.0° to 31.04° north latitude and 98.0° to 79.92° west longitude and used a 0.08° by 0.08° grid spacing. The third set of wind/pressure files had grid boundaries centered on the landfall location of the storm (as such the grid was referred to as the Landfall domain). Since landfall locations changed by storm, this domain was not fixed in any one location as the other two domains were, but the spatial grid resolution and domain size were fixed for every storm. A grid spacing of 0.02° by 0.02° was used for the landfall domains and each domain covered a 3.0° by 3.0° square.

Wave Model (WAM)

The wave modeling technology used to generate the offshore wave estimates for CTXCS is the 3rd generation wave model WAM (Komen et al., 1994). WAM is similar to other 3rd generation wave models like WaveWatch III (Tolman, 2014) or SWAN (The SWAN Team, 2017). WAM makes no *a priori* assumptions governing the spectral shape of the waves and the source term solution is formulated to the wave model's frequency/directional resolution. WAM was selected based on its use for previous tropical cyclone simulations as part of the Interagency Performance Evaluation Task Force (USACE, 2009), the Louisiana Coastal Protection and Restoration Project (USACE, 2006), and Hurricane Katrina and Rita simulations (Bunya et al, 2010; Dietrich et al, 2010).

Figure 21. Map showing the three grid boundary extents for the regional wind and pressure fields in (red) and the ADCIRC model domain shown in black. Note, the Landfall domain is track dependent and not fixed in one location.

Accurately estimating the offshore wave conditions for the entire coastal area of Texas required developing the wave field grid for the entire Gulf of Mexico and extending into the Caribbean Sea and a small part of the western basin of the Atlantic Ocean. However, all synthetic TCs for this study are confined to the area west of 75° West longitude. The bounding box defining the bathymetry used for the offshore wave generation is displayed in Figure 22. Open water gaps occur between the Straits of Florida and Cuba, and between the western tip of Cuba and the Yucatan Peninsula of Mexico. Portions of the synthetic storm tracks population reside in these areas. So wind-waves will initially develop outside the gulf and the resulting energy penetrates into the Gulf of Mexico.

The color contoured bathymetry shown in Figure 22 was derived from the General Bathymetric Chart of the Oceans (GEBCO) (Becker et al. 2009). The WAM grid boundary extents were from 18.0° to 31.0° north latitude and from 98.0° to 75.0° west longitude. A grid spacing of 0.05° by 0.05° was used for discretizing the domain. Defining the wave model grid at this resolution provides accuracy levels for the Caribbean Islands and shoreline features.

Figure 22. Offshore wave generation domain. Water depth color contours are given in meters.

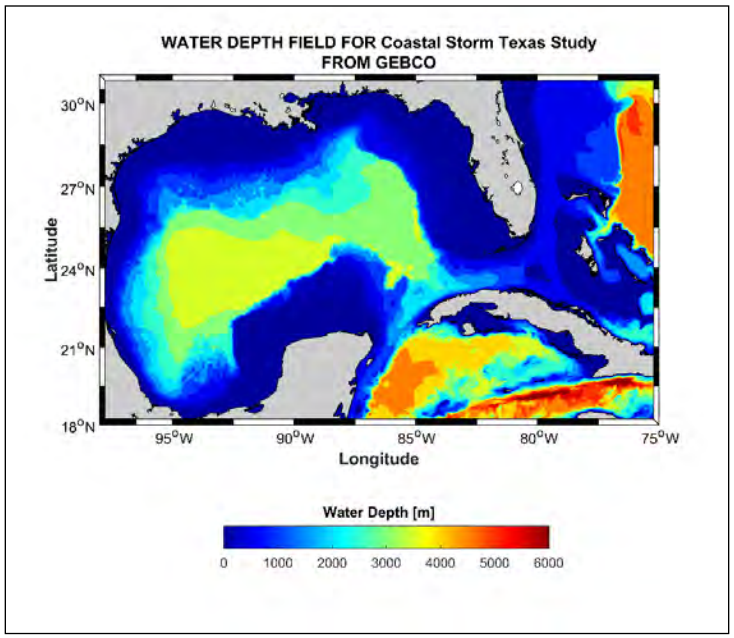

Nearshore waves: The Steady State WAVE (STWAVE) Model

Like the WAM model, STWAVE is a finite-difference model that is formulated on a Cartesian grid. STWAVE grids have the x-axis oriented in the cross-shore direction (I) and the y-axis oriented alongshore (J). Wave angles are measured counterclockwise from the x-axis. As a starting point, three STWAVE grids originally developed based on those of the 2011 Flood Insurance Study (FEMA, 2011) were analyzed for use: TX-S, TX-C, and TX-N. A fourth grid was added to better bridge the Texas-Louisiana border: TX-LA (Figure 23). The STWAVE grids span two State Plane coordinate systems, Louisiana Offshore (FIPS 1703) and Texas South Central (FIPS 4204). The bathymetry, topography, and Manning's n bottom friction values were interpolated from the ADCIRC mesh. A grid resolution of 656 ft was selected for the TX-S and the TX-C grid as its domain did not intersect directly with any project areas. The TX-N grid, which encompasses Freeport, Galveston Bay, and Port Arthur, used a 492 ft resolution and output from this grid was used for the morphology inputs. The TX-LA grid, which overlaps the TX-N grid and encompasses parts of Port Arthur and Orange County, used a 656 ft resolution grid spacing. Previous studies of Hurricanes Katrina, Rita, Gustav, and Ike in the Gulf of Mexico as well as the North Atlantic Coast Comprehensive Study used similar resolutions (656 ft in coastal areas, 328 - 656 ft in nested bays) and demonstrated good agreements with measurements

(Dietrich et al. 2011; Hope et al. 2013; Bunya et al. 2010; Dietrich et al. 2010; Bender et al. 2013, Cialone et al. 2015). These past studies showed that a 656 resolution sufficiently resolved the surf zone to capture the wave breaking processes that drive wave radiation stresses and wave setup. The TX-N grid used a 492 ft resolution to better resolve with- and without-project configurations and other local topographic features near the project areas.

Figure 23 shows the location of STWAVE grids with respect to the WAM grid and the ADCIRC mesh along with a close-up view of the STWAVE grids with color contours of bathymetry/topography. The specifics about the grid geometries are presented in Table 3. The full names of the grids are based on their relative regional location within Texas, moving from north to south. The grids' offshore boundaries were extended into depths of at least 131 ft, which is considered deep by STWAVE criteria. Wave interactions with the bottom at this offshore extent are relatively small, particularly in comparison to the importance of wave generation.

STWAVE has two modes available, half-plane and full-plane. Half-plane mode allows wave energy to propagate only from the offshore towards the nearshore (± 87.5o from the x-axis of the grid). STWAVE half-plane grids are typically aligned with the dominant wave direction, since all waves traveling in the negative x-direction, such as those generated by offshore-blowing winds, are neglected in half-plane simulations. Full-plane mode allows wave generation and transformation in all directions. Due to the large number of storm simulations and possible variations in the dominant wave direction, all simulations used the full-plane mode of STWAVE.

Figure 23. Maps showing the STWAVE grid boundaries in relation to the WAM boundary (a) and a close-up view along the Texas/Louisiana coastline with color contours of bathymetry/topography in (b).

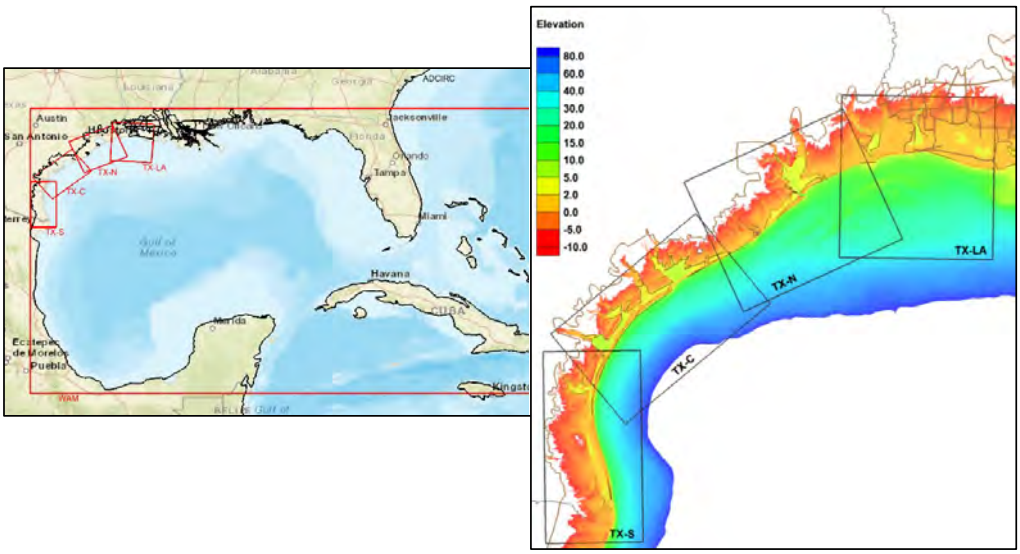

(a) (b)

Table 3. Grid properties for the STWAVE domains.

Grid	Projection	Grid Origin (x,y) (m)	Azimuth (deg)	Resolution (ft)	Number of Cells	
					I	J
Texas-Louisiana (TX-LA)	Louisiana Offshore (FIPS 1703)	(891818.0, 339821.0)	85.8	656	979	926
Texas-North (TX-N)	Texas South Central (FIPS 4204)	(1132495.0, 4123323.0)	115.0	492	1147	1407
Texas-Central (TX-C)	Texas South Central (FIPS 4204)	(973560.0, 4044100.0)	130.0	656	705	1137
Texas-South (TX-S)	Texas South (FIPS 4205)	(467740.0, 5226000.0)	180.8	656	588	1156

Circulation and water levels: The ADvanced CIRCulation (ADCIRC) model

The computational domain for storm-surge modeling by ADCIRC contains the western North Atlantic, the Gulf of Mexico, and the Caribbean Sea

(Figure 24). It covers an approximately 38° by 38° square area in longitudinal (from 98° W to 60° W) and latitudinal (from 8.0° N to 46° N) directions. The mesh consists of approximately 4.6 million computational nodes and 9.2 million unstructured triangular elements with an open ocean boundary specified along the eastern edge (60° W longitude). The largest elements are in the deep waters of the Atlantic Ocean and Caribbean Sea, with element sizes of about 36 miles, as measured by the longest triangular edge length. The smallest elements resolve detailed geographic features such as tributaries and control structures like levees and roadways. Color contour maps of the ADCIRC mesh resolution are shown in Figure 25 and Figure 26. Water depths range from roughly 26,000 ft in the deep Atlantic to over 328.1 ft of land elevation (above mean sea level).

Figure 24. Map showing the computation domain for the ADCIRC model.

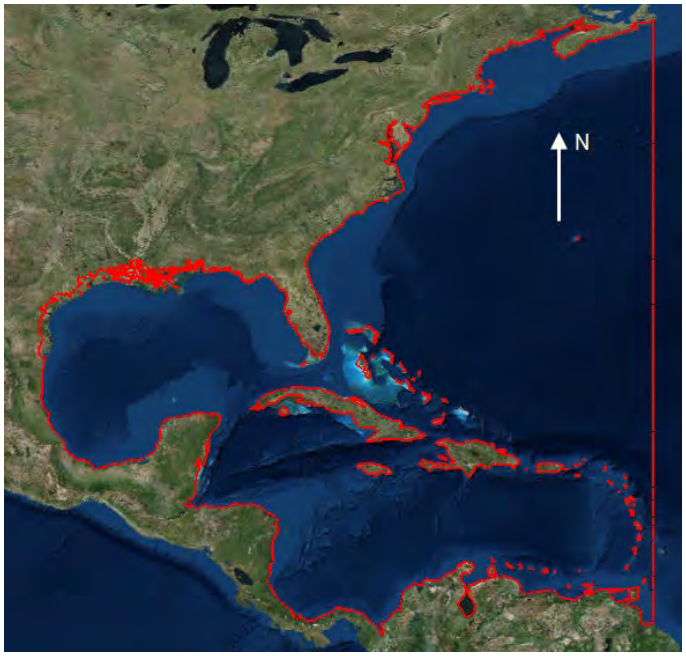

Figure 25. Map showing the ADCIRC mesh with color contours representing the element resolution.

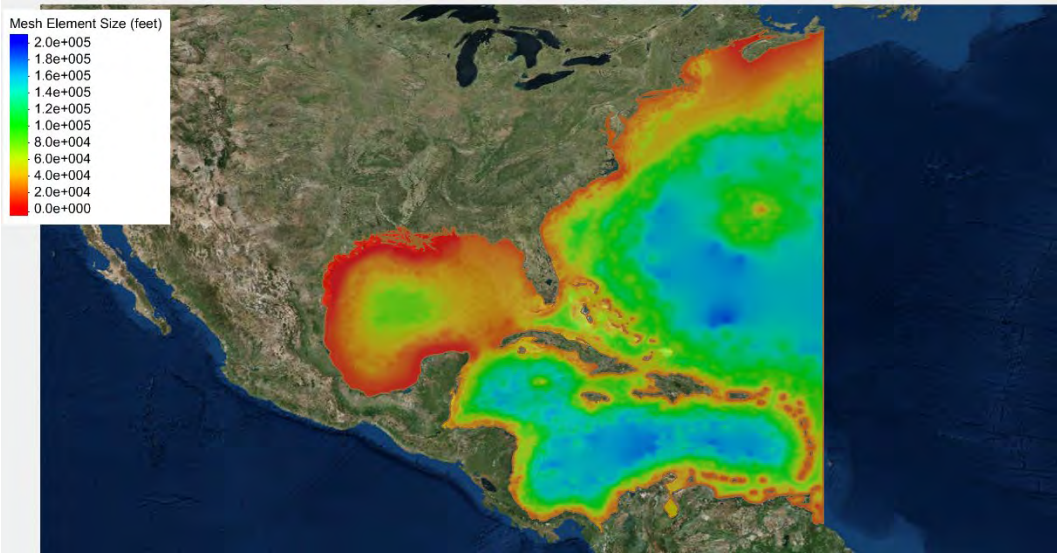

Figure 26. A close-up view of the ADCIRC mesh in the northern Gulf of Mexico showing element sizes as color contours.

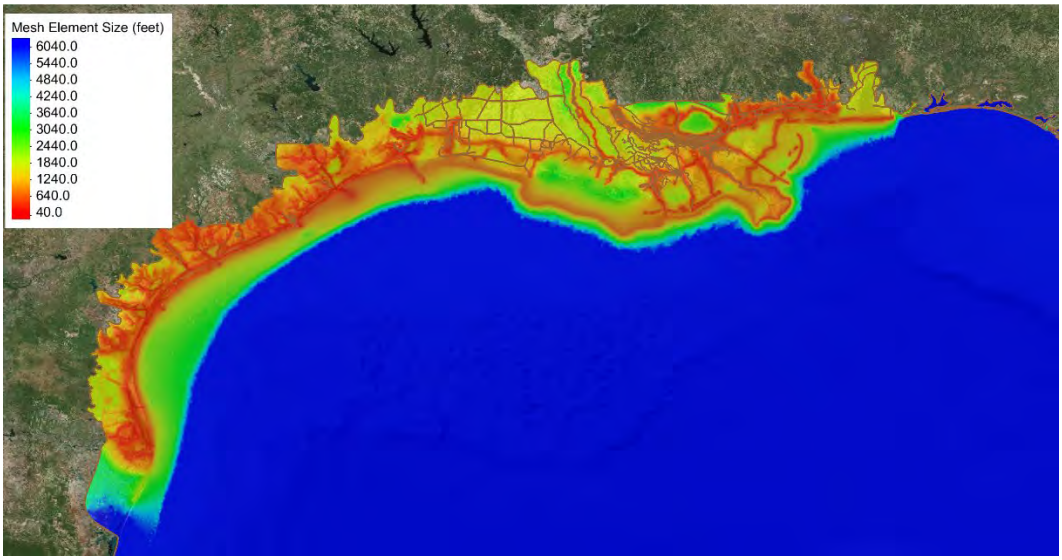

The ADCIRC mesh was adapted from a combination of previously developed and validated ADCIRC meshes. As shown in Figure 27, the Texas FEMA Risk MAP mesh from the 2011 study was used along the entire Texas coastline. At the Texas-Louisiana boarder and continuing eastward along the coast past Mobile, AL, portions of a mesh for southern Louisiana developed for both FEMA and USACE uses (USACE 2011) and most recently used in the post-Hurricane Isaac investigation of the

Hurricane Storm Damage Risk Reduction System (HSDRRS), see (USACE 2013) were used. In the Atlantic and Caribbean, a grid named EC95, which was originally created for computing tidal databases (Hench et al. 1995), served as the base mesh and was used with some localized refinements to improve response and robustness around some of the islands and shallower depths. After the three main meshes had their respective high resolution areas extracted, they were stitched together and the deeper water areas of the Gulf of Mexico were recreated to smooth the transitions between the meshes and to reduce the number of nodes and elements in that area.

Figure 27. Composite map showing the approximate areas where different ADCIRC meshes were combined and created to produce a seamless high resolution mesh for the entire TX-LA-MS coastline.

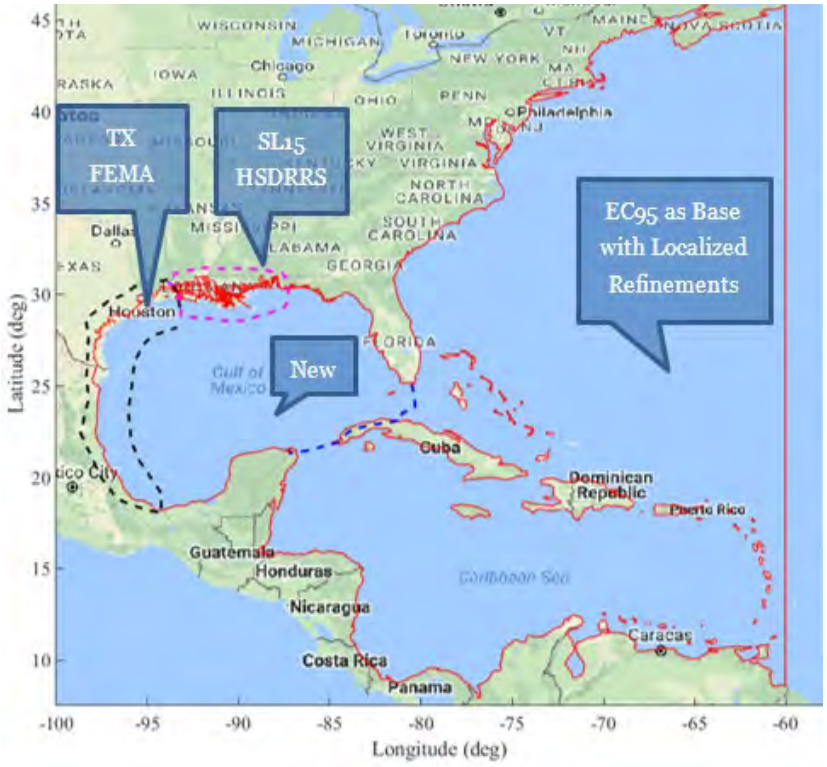

The bathymetry from the TX FEMA mesh and SL15-HSDRRS mesh was given in meters relative to NAVD88. The two sources of bathymetry/topography were maintained for the final meshes in their respective areas. The bathymetry from the TX FEMA mesh was used in the Gulf of Mexico and the areas derived from the EC95 mesh. A view of the bathymetry and topography from the ADCIRC mesh in the TX-LA border area is shown in Figure 28.

Figure 28. A color contour map showing the seamless topography and bathymetry contained in the ADCIRC mesh along the TX-LA border.

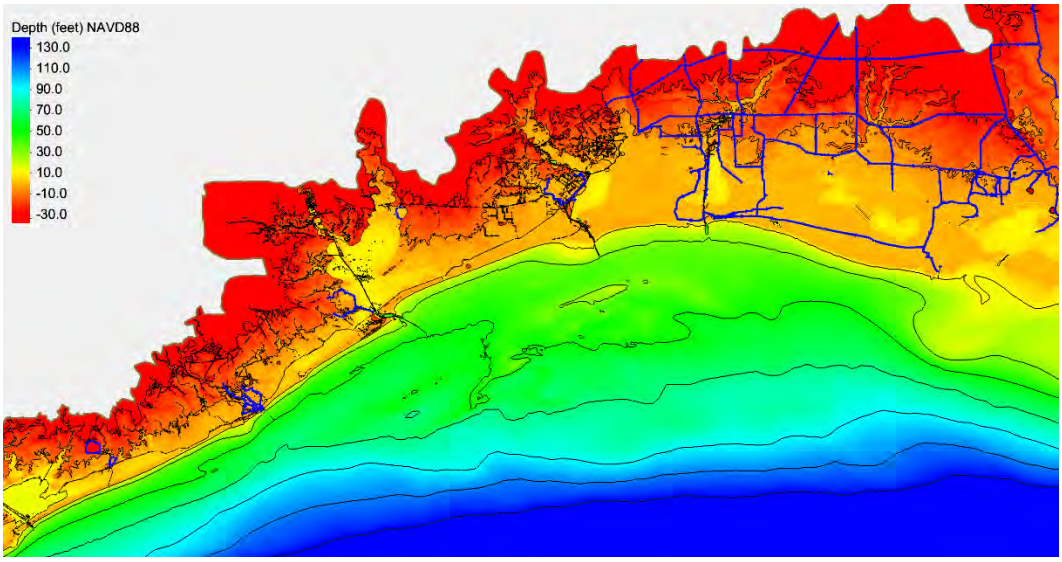

Topography and bathymetry

The topography and bathymetry used in the ADCIRC mesh and the STWAVE grids was the same as used in the TX2008 ADCIRC mesh for the entire Texas coast areas and in the Gulf of Mexico. Inland areas over Louisiana, Mississippi and Alabama used the data derived from the SL15 mesh.

The representation of the existing CSRM systems in the ADCIRC mesh and STWAVE grids used for the prior CTXCS simulations were nearly sufficiently resolved to provide the level of detail required for the with-project conditions and only local modifications in the immediate project areas were required. The ADCIRC mesh and STWAVE grids were modified from the prior simulations to more accurately capture the existing and proposed CSRM measures. Modifications included adding more resolution along the CSRM systems. Wherein the CTXCS prior ADCIRC mesh had element sizes in the range of 90 ft to 900 ft in these areas, the updated with-project ADCIRC mesh has element sizes in the range of 60 ft to 300 ft. Figure 29 and Figure 30 present details of the ADCIRC mesh resolution for both the prior CTXCS mesh and then the refinements made in the project areas. Figure 29 shows the mesh resolution for CTXCS existing where the black lines are existing flood control structures. Figure 30 shows

the mesh resolution and element sizes, for the full beach-dune case, with-project meshes where black lines indicate existing structures and magenta lines indicated new with-project features. It is noted that the ADCIRC model was simulated using a static topo/bathy for the dunes which means morphology changes that may occur during the storm event were not represented in the ADCIRC simulation. For future design efforts during the Preconstruction-Engineering and Design (PED) phase, additional mesh resolution enhancements and updates to the topo/bathy values should be considered.

Figure 29. DCIRC mesh resolution (element size in meters) for the Galveston area from the CTXCS mesh. Conversion is 3.281 ft/m.

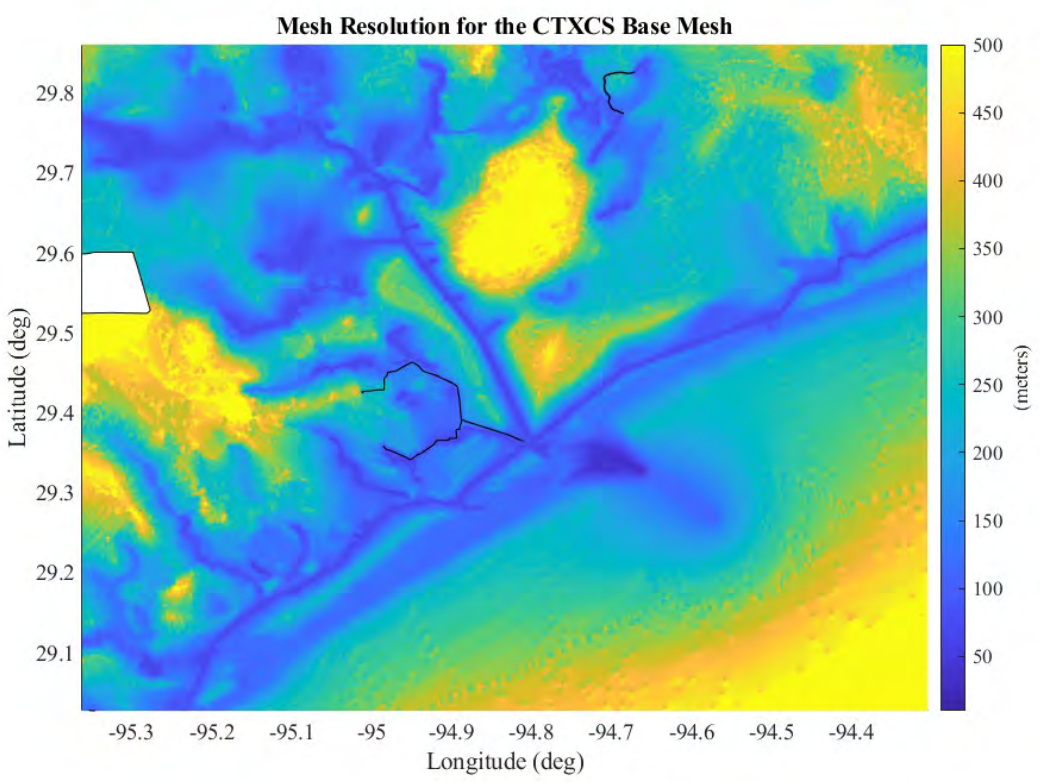

Figure 30. ADCIRC mesh resolution (element size in meters) for the Galveston area under the full beach dune with-project case. Conversion is 3.281 ft/m.

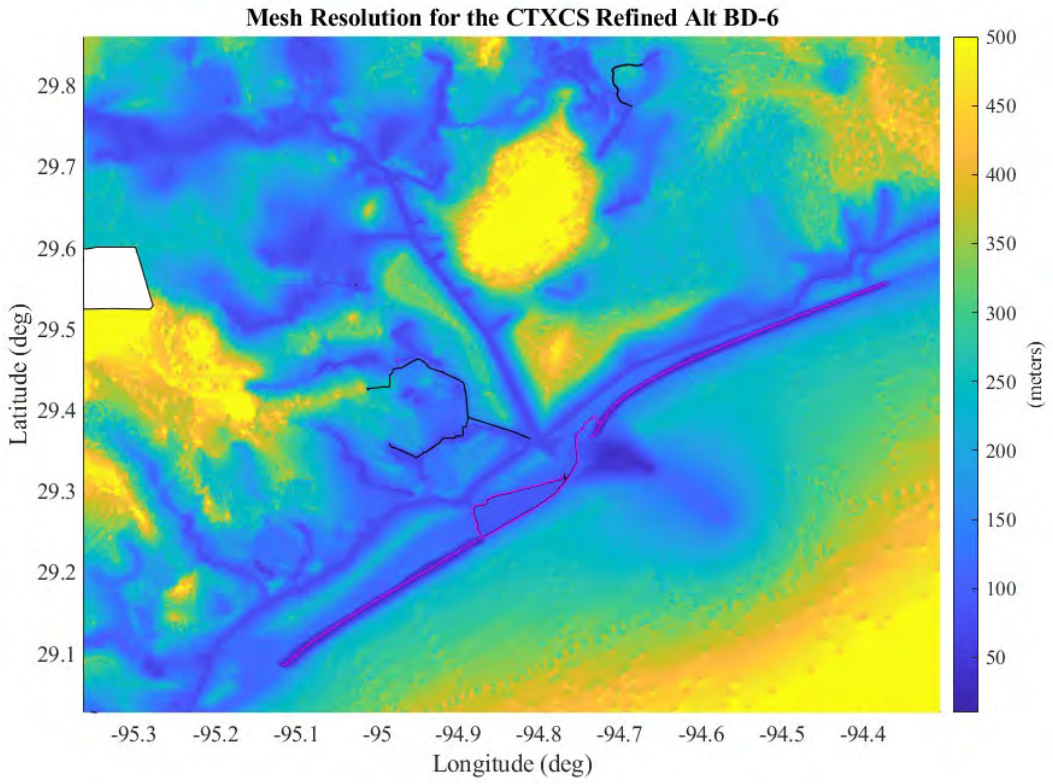

ADCIRC model settings

ADCIRC also makes use of a nodal attribute file (fort.13) that specifies spatially variable model parameters like Manning's n for bottom roughness. Many of the nodal attribute parameters are derived from land cover and land use (LCLU) data that provide classification systems for what is on the Earth's surface at a given location. For wind and coastal hydrodynamic modeling by ADCIRC, LCLU data was used to determine spatially distributed values of bottom friction coefficients (or Manning's n), canopy coefficients, and surface roughness length for the effect of directional wind reduction, in response to spatial changes of land cover and land use over study areas. These parameters were all updated for the CTXCS using the most recent LCLU data.

Two sets of LCLU data were used to specify the above-mentioned model parameters over the entire coasts of Gulf of Mexico. The first LCLU dataset is the United States Geological Survey (USGS) 2011 National Land Cover Database (NLCD 2016, Homer et al. 2015), which covers the Gulf Coast of

the United States. The National Land Cover Database 2011 is the most recent national land cover product created by the Multi-Resolution Land Characteristics (MRLC) Consortium. The NLCD 2011 uses a 29-class land cover classification scheme at a spatial resolution of 98 ft.

The second LCLU dataset used for the study is the Global Land Cover Characterization (GLCC 2017), which is a series of global land cover classification datasets. The spatial resolution of GLCC is 1 km (0.6 mi), much coarser than that in the NLCD 2011 dataset. Therefore, the GLCC dataset was only used for defining land cover properties in the areas beyond the NLCD data coverage. GLCC uses a 20-class land cover classification scheme (Dickenson et al. 1993).

Two river inflows from the Mississippi River and the Atchafalaya River are included in the storm-surge simulations. The inflow boundary (or the river cross-section) of the Mississippi River is located near the USGS gage #07374000 Mississippi River at Baton Rouge, LA. The boundary for the Atchafalaya River is placed near the USGS gage #07381490 Atchafalaya River at Simmesport, LA. Constant river inflows were used for all simulations. A value of approximately 160,000 cfs (cubic feet per second) was used for the Mississippi River and a value of 68,000 cfs was used for the Atchafalaya River. These flow rates are consistent with those used in similar studies, (Dietrich et.al 2010, and Bunya et.al 2010). No riverine inflows within the Texas coast (e.g. Sabine, Neches, and Brazos rivers) were included in the model. Those major river basins were included as topo/bathy features and the mesh nodes and elements were aligned with the river. The ADCIRC mesh extended so far inland, that there were no good “head” water conditions to force the river flux. The flow rates would not have significantly altered the coastal water levels by including the rivers. Furthermore, surge is allowed to propagate up the rivers basins, but did not reach the physical boundaries of the ADCIRC mesh. This is the same approach used in the previous FEMA Flood RiskMap study (FEMA 2011). A separate Texas study investigated the impact of combined hydrology-related (rainfall) and coastal storm surge and concluded that the combined processes would not influence the results reported herein primarily because the two processes are out of phase.

ADCIRC has a model setting for multiplying the magnitude of winds. This setting is sometimes used as an adjustment parameter for historical storms, particularly when the input wind fields do not match observation

data. Its use has also been justified by the relatively infrequent demand to adjust wind fields from a 30 minute averaging window to a 10 minute averaging window. Wind multiplier values of 1.09 to 0.95 are common. A value of 1.0 was used in the CTXCS study. The wind drag formulation for the CTXCS study made use of the Garratt formula. The ADCIRC model's upper limit for wind drag coefficient was set to a value of 0.003, where it is noted that 0.0035 is the default value in the ADCIRC model and values as low as 0.002 have been used. The 0.002 value was also used in the 2010 FEMA Flood RiskMap study for the area (FEMA 2011) along with a wind multiplier of 1.09. The above model settings were used for all storms and both with and without project scenarios. Selection of these values was based on balancing model stability and model accuracy. While certain combinations of values may produce better agreement when modeling historical storms and when comparing model output to measurements, they can also cause the model to be much more unstable. This is a concern when simulating such a wide range of storm conditions as specified within the 660 synthetic storm suite with drastically different initial water levels, e.g. relative sea level rise values. As a result, while these settings produce water levels that were typically lower than observed when comparing to historical events, this was accounted for with a bias correction in the final statistical values which is explained in more detail in Appendix B.

Save points

While the CSTORM model output is saved at mesh nodal locations, a reduced set is saved at save points in order to provide a manageable data set for engineering analysis. For CTXCS, 18332 points were identified that span the coast of Texas. Figure 31 shows save point locations for the project area. Save points were located both on dry land and in nearby water bodies at a fairly high density. Responses at these save points are used to generate extremal statistics, for flood risk calculations and to force engineering response models.

Figure 31. CSTORM save Points in the region with depth indicated by color of dot.

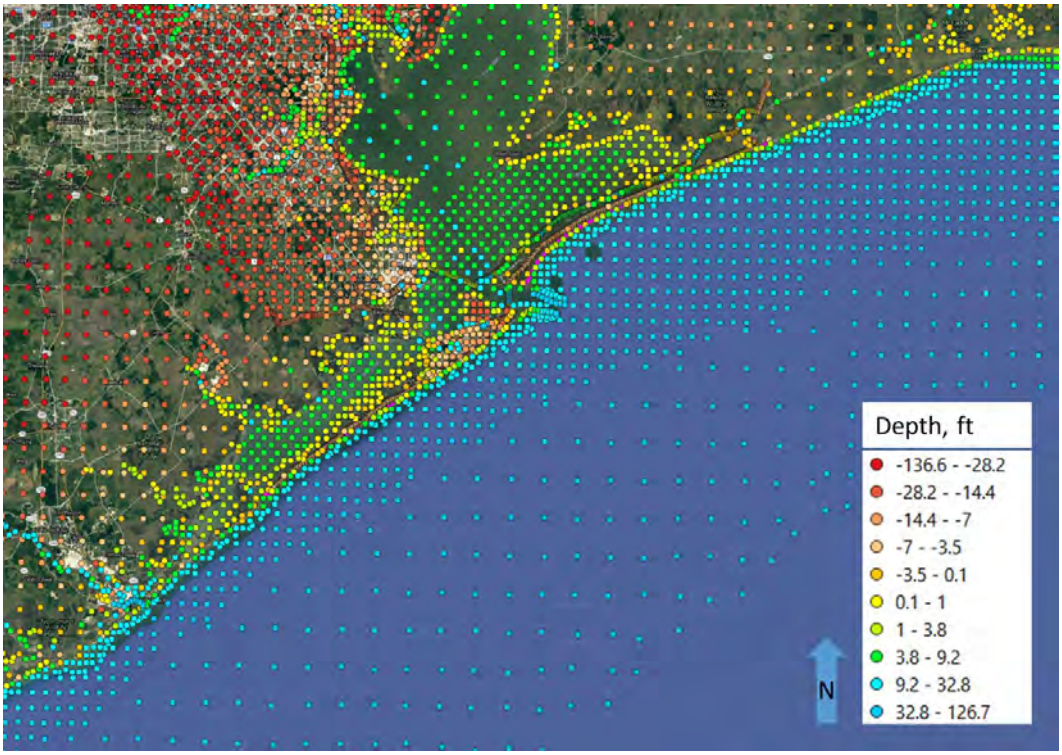

Tides

For modeling storm surges and surge tides for validation storms, the open ocean boundary (60-deg west longitude in Westerink et al. (2011) was forced with 8 tidal constituents. Time-varying tidal elevations specified at nodes along the open ocean boundaries were synthesized using the M2, S2, N2, K1, O1, Q1, P1, and K2 tidal constituents. Constituent information was extracted from a database developed from the TOPEX 7 satellite measurements. Because the model domain is of sufficient size that celestial attraction induces tide within the mesh proper, tide-generating potential functions were included in the simulations, and correspond to the constituents listed above. Tidal forcing was only included for the CSTORM modeling of historical storms and was not used for CSTORM modeling of the synthetic TCs.

Tides were included as an epistemic uncertainty for the statistics of SWL computed from the regionl hydrodynamic modeling. This is described further in Chapter 5. The standard deviation of tidal response is 0.38 ft.

While tides were not included explicitly in the CSTORM synthetic storm modeling, they were included as a random-phase time series in the stochastic morphology simulation modeling as described in Chapter 7.

The local tidal datums for NOAA tide gage Galveston Pier 21 8771450 are as follows:

MHHW: 1.41 ft, MHW: 1.32 ft, MSL: 0.84 ft, NAVD88: 0.46 ft,

MLW: 0.35 ft, MLLW: 0.00 ft.

Relative sea level change

Relative sea level change (RSLC) scenarios were defined according to guidance set forth in USACE ER 1100-2-8162 (USACE 2019) and ETL 1100-2-1 (USACE 2014). The base year for the calculations was 1992 as this was the mid-point of the last National Tidal Datum Epoch which spans 1983 to 2001. The RSLC scenarios use a global mean sea level rise of 1.7 mm/yr and add criteria for different sea level rise acceleration rates. Local ground elevation change due to subsidence and other local factors are included. Figure 32 shows the 3 RSLC curves associated with the project that extend from 1992 (center of tidal epoch) and span the project service life from 2035 to 2085 from the USACe Sea-Level Change Curve Calculator (https://www.usace.army.mil/corpsclimate/Public_Tools_Dev_by_USACE/sea_level_change/). The three curves are:

Low curve representing the linear historical SLC (USACE Low)

NRC Curve I (USACE Intermediate)

Modified NRC Curve III (USACE High)

Figure 32. Relative SLC curves for Gage 8771450 at Galveston Pier 21

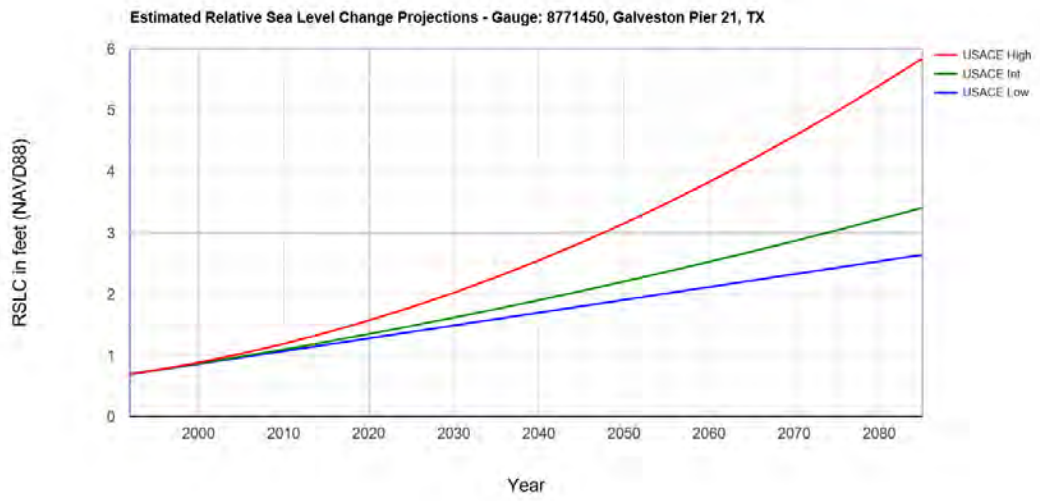

The low curve corresponds to historical change at NOAA Galveston Pier 21 Gage as shown in Figure 33.

Figure 33. Long term monthly mean sea level change time series plot with long-term linear trend for NOAA Gage 8771450 at Galveston Pier 21. Conversion is 3.28ft/m.

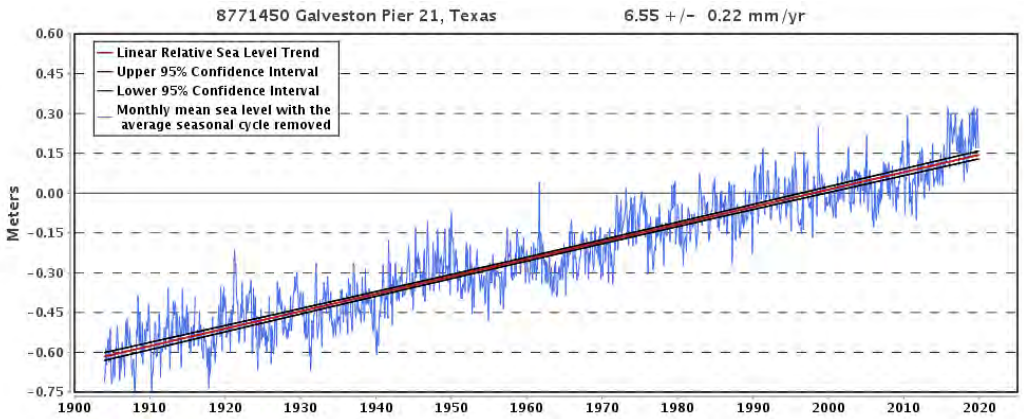

The CSTORM simulations for the full CTXCS study used initial water levels corresponding to 3 different sea levels. Two of these water levels were used to evaluate project alternatives. The three levels corresponded to present time, which at the initiation of the CTXCS was 2017, and a time in the future of roughly 2085. The two distant-in-time RSLCs were 4.92 ft for the high and 2.46 ft for the intermediate, chosen somewhat arbitrarily because the details of the economic life had not been resolved when the simulations were done initially in 2017. For the base case, the RSLC plus other sea level adjustments were used to compute the final geoid offset for

the CSTORM simulations, with data taken from long term NOAA gages. An addition of 0.14 ft was needed to account for the RSLC occurring between 2008 and 2017. This was because the ADCIRC mesh was based on LiDAR from 2008. Besides RSLC, a steric adjustment of 0.39 ft was added to account for regional seasonal variations to sea level primarily due to seasonal water temperature change. Also, an adjustment of 0.38 ft to convert LMSL to NAVD88 was added. The total RSLC and final geoid offsets for the CSTORM simulations were as follows:

SLC0, Present day (2017):

RSLC 2008 – 2017 = 0.14 ft

Geoid offset=0.39 ft steric+(0.38 ft LMSL-NAVD88)+0.14 ft=0.91 ft (rounded to 1 ft)

SLC1, 50 yr Service Life (2035 – 2085), High Curve:

Geoid offset = 1 + 4.92 ft = 5.92 ft (Includes offset 2008 - 2017)

SLC1 most closely corresponds to high curve from USACE 2013 and matches the intermediate-high curve at 50% confidence from NOAA 2017.

SCL2, 50 yr Service Life (2035 – 2085), Intermediate Curve:

Geoid offset=1 + 2.46 ft = 3.46 (Includes offset 2008 - 2017)

SLC2 most closely corresponds to the intermediate curve from USACE 2013 and intermediate-low curve at 50% confidence from NOAA 2017 (e.g. see internet location https://www.usace.army.mil/corpsclimate/Public_Tools_Dev_by_USACE/sea_level_change/).

The preceding values of RSLC were used as Geoid offsets for the CSTORM hydrodynamic simulations of all synthetic TCs. So extremal statistics computed for CSTORM hydrodynamics were based on these point values of RSLC and represent a specific RSLC curve at a specific time. It is important to simulate inland flooding water levels using CSTORM, modeling the important physics rather than linearly superimposing the various water level components. As shown in Melby et al. 2020, the nonlinear residual (NLR), the error between linear superposition and modeling all physics, is large for Texas. They showed that the error can be

the same order of magnitude of the added component for inland flooded areas. So if the added component was, for example, 5 ft, then the error from linear superposition could be roughly 5 ft in inland areas. So for the hydrodynamic modeling, it was critical to use CSTORM to model all important physics.

For the life cycle simulations of beach morphology change, a service life initiation date of 2035 was used. The life cycles were 50 years in duration so they extended to year 2085. For the life cycle simulations, CSTORM SLC0 scenario simulations were used. The RSLC curves shown in Figure 32 were computed within the simulations at the end of each year and the increase in RSLC was linearly added to the SWLs for all storms of the following year. In this case, the CSHORE model was used to transform waves to nearshore so nonlinear interaction and wave setup were included in the CSHORE simulations. As a result, in this case, linear superposition of RSLC with SWL did not result in a NLR error.

Final CSTORM scenarios

The final list of primary scenarios for CSTORM with geoid offset was as follows:

1. Original CTXCS without-project, SLC0.

2. Original CTXCS without-project, SLC1.

3. Original CTXCS without-project, SLC2.

4. With-Project, surge barrier only, SLC0

5. With-project, surge barrier, ring levee, fixed beach-dune and smaller navigation gates at Clear Creek and Dickinson Bayou, SLC0.

6. With-project, surge barrier, ring levee, fixed beach-dune and smaller navigation gates at Clear Creek and Dickinson Bayou, SLC1.

A with-project case, consisting of a surge barrier, ring levee and the fixed beach-dune for SLC0 was run for a reduced set of 20-storms (developed with the genetic algorithm described earlier) and is presented in Appendix D.

5 Local Wave and Water Level Response from Regional CSTORM Modeling

Storm peak responses

Regional surge and wave modeling output at save points included the storm peak responses and time series. Save points 6038 and 5960, shown in Figure 34, are used for illustration of storm responses for the area offshore of the project. The peak responses for the top 10 storms are shown in Table 4 and Table 5 for these two points. The depth at these save points is 46 ft. Figure 35 plots the Gate alternative against the Beach alternative responses. Here the alternatives were as follows

Gate Alternative: closed surge barrier, ring barrier and smaller navigation gates

Beach Alternative: beach, closed surge barrier, ring barrier and smaller navigation gates.

The synthetic TC characteristics are listed in Appendix C. More extensive analysis of CSTORM regional hydrodynamic response is provided in Appendix D. Peak water levels are similar between the two points with the Beach alternative slightly higher. Also, the peak wave heights are similar in the offshore, although with more scatter than SWL. Additional by-storm alternative comparisons are included in Appendix D.

Figure 34. Aerial view of save point locations in project area color shaded by depth. The circled point is save points 6038 and 5960.

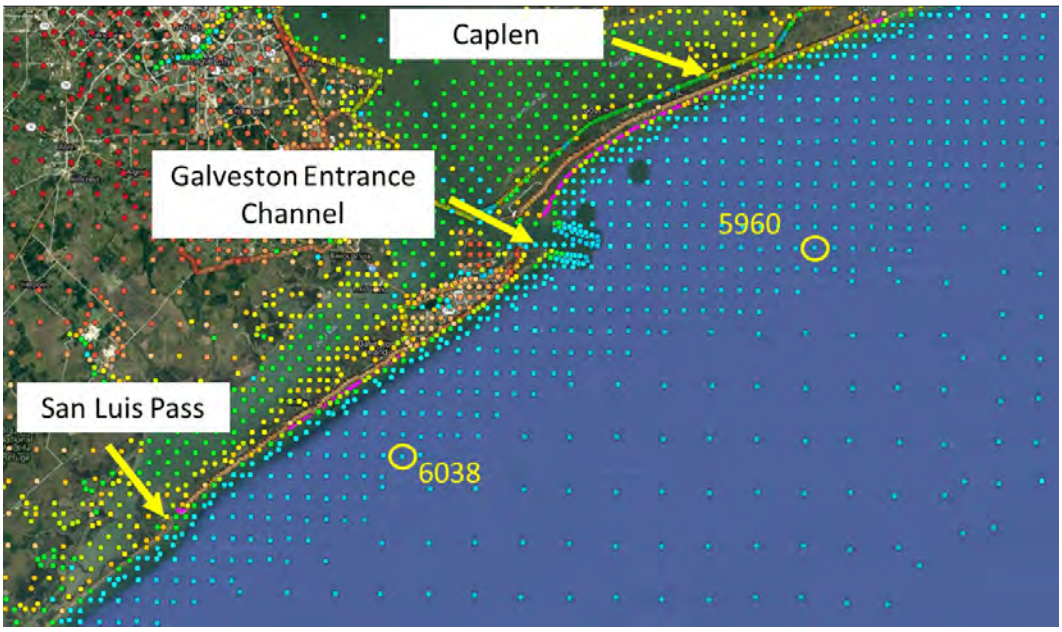

Table 4. CSTORM output peaks for top 10 synthetic storms ranked by SWL for Gate alternative (left side) and Beach alternative (right side) at save point 6038.

SLC 0 – Gate Alternative					SLC 0 – Beach Alternative				
Storm ID	SWL (ft, NAVD88)	H_{m0} (ft)	T_p (s)	MWD (deg, Eucl)	Storm ID	SWL (ft, NAVD88)	H_{m0} (ft)	T_p (s)	MWD (deg, Eucl)
347	17.9	28.6	13.5	211	347	18.8	28.8	13.5	211
342	17.3	33.1	16.3	170	578	17.7	29.0	13.5	125
578	17.1	28.9	13.5	125	342	17.5	33.2	16.3	170
521	16.8	29.4	12.3	160	521	17.1	29.4	12.3	160
633	16.7	29.6	13.5	184	633	16.9	29.7	13.5	184
529	16.3	30.5	14.9	204	529	16.6	30.5	14.9	204
447	16.3	32.0	14.9	187	447	16.4	32.0	14.9	187
449	15.8	31.1	14.9	165	449	16.1	31.1	14.9	165
589	15.6	31.8	14.9	143	589	15.8	31.9	14.9	143
139	15.3	27.6	13.5	194	139	15.5	27.7	12.3	184
					SLC 1- Beach Alternative				
					Storm ID	SWL (ft, NAVD88)	H_{m0} (ft)	T_p (s)	MWD (deg, Eucl)
					347	22.7	30.6	13.5	211
					342	21.7	35.2	16.3	176
					578	21.2	29.6	13.5	141
					521	21.0	30.7	13.5	174
					633	20.9	31.7	13.5	184
					447	20.9	33.9	14.9	197
					529	20.8	31.3	16.3	214
					449	20.1	32.9	14.9	178
					589	19.8	33.6	14.9	143
					139	19.7	28.3	14.9	209

Table 5. CSTORM output peaks for top 10 synthetic storms ranked by SWL for Gate alternative (left side) and Beach alternative (right side) at save point 5960.

SLC 0 – Gate Alternative					SLC 0 – Beach Alternative				
Storm ID	SWL (ft, NAVD88)	H_{m0} (ft)	T_p (s)	MWD (deg, Eucl)	Storm ID	SWL (ft, NAVD88)	H_{m0} (ft)	T_p (s)	MWD (deg, Eucl)
529	19.2	28.7	14.9	156	529	19.8	28.7	14.9	156
633	16.9	25.3	11.2	172	633	17.1	25.0	11.2	173
595	16.2	28.3	13.5	180	595	16.6	28.2	13.5	180
634	16.0	25.2	11.2	180	634	16.3	25.3	11.2	180
342	15.9	26.3	13.5	146	342	16.1	26.6	13.5	146
447	15.7	26.7	13.5	162	347	16.1	24.5	12.3	164
589	15.6	27.6	14.9	126	453	15.8	24.6	11.2	146
347	15.6	24.4	12.3	164	447	15.8	26.8	13.5	162
453	15.2	24.4	11.2	146	589	15.6	27.6	14.9	126
449	15.1	25.2	13.5	150	449	15.3	25.0	13.5	146
					SLC 1- Beach Alternative				
					Storm ID	SWL (ft, NAVD88)	H_{m0} (ft)	T_p (s)	MWD (deg, Eucl)
					529	23.4	30.6	14.9	156
					633	20.9	26.0	12.3	172
					595	20.5	29.3	13.5	190
					342	20.3	28.2	13.5	146
					447	20.1	28.5	13.5	162
					634	20.1	26.1	11.2	183
					347	20.1	25.6	12.3	171
					589	19.6	29.4	14.9	143
					453	19.5	25.2	11.2	146
					449	19.2	26.6	13.5	150

Figure 35. SWL and H_{m0} for top 10 storms ranked by SWL, Gate alternative vs Beach alternative with SLC0. Top plot is save point 6038 while bottom is 5960.

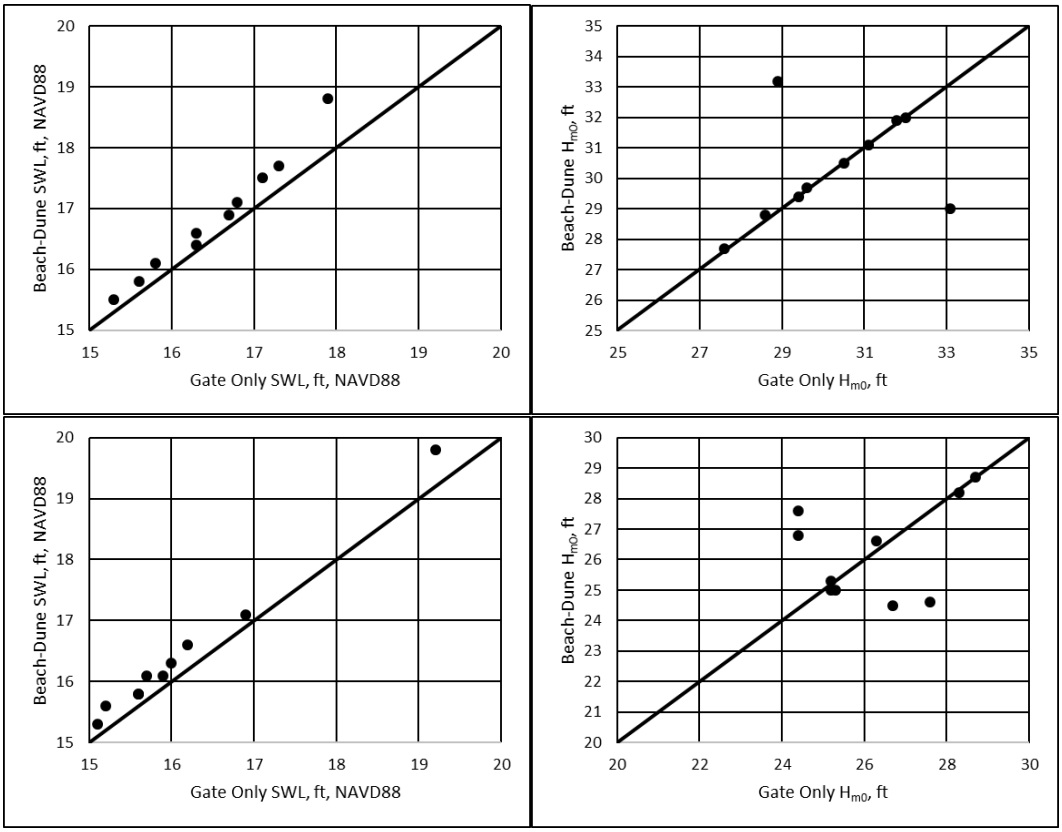

Storm hydrodynamic response hazard

The storm hydrodynamic hazard is stochastic with natural variability. In addition, our estimates using models have inherent error. Uncertainty in flood risk studies is usually grouped according to natural variations in physical processes (aleatory) and errors in our understanding and prediction of these processes (epistemic). This grouping is a simplification and not intended to be a rigorous categorization of all uncertainties. However, it serves the primary purpose for dealing with uncertainty herein. The primary natural variability of hurricane extreme responses is dealt with through the JPM-OS approach and is quantified through the use of the multivariate probability relation Equation A.1. The discrete version of Equation A.1 sums the probability masses of the synthetic TCs combined with epistemic uncertainty of the response estimates to compute the *hazard curve*, an extremal distribution of the response.

Probability masses

The JPM-OS methodology was used to define the CTXCS storm suite and the associated storm probability masses (Nadal-Caraballo et al. 2018a, Nadal-Caraballo et al. 2018c, Nadal-Caraballo et al. 2019). These probability masses provide the relative probabilities of the synthetic events and are required to construct the hazard curves. They are directly related to the storm rates shown in the discrete version of Equation A.1 in Appendix A. The non-exceedance probability of response, such as storm water level, is the product of storm probability mass and conditional joint probability of storm parameters (Equation A.1). Probability masses were computed from the JPM analysis of CTXCS modeling output for 660 TCs and 18332 save points (Nadal-Caraballo et al. 2018a). The CTXCS probability masses were scaled to the smaller number of 170 storms using the methods discussed in Appendix E. As was shown in Figure 19, the hazard curves computed using the reduced storm suite and the revised probability masses are indistinguishable from those computed using the 660 original storms.

Epistemic uncertainty

The epistemic uncertainty that is incorporated in this analysis is discussed in Nadal-Caraballo et al. (2018a) and Melby et al. (2020) and background is summarized in Appendix A. Gonzalez et al. (2019) summarized general uncertainty quantification in probabilistic storm surge models. The uncertainty approach herein is fundamentally based on the work of Resio et al (2013) and Jacobsen et al. (2015). The uncertainties that are considered in the hazard computation for SWL and H_{m0} have been used in recent JPM-OS studies:

1) Errors in hydrodynamic modeling and grids associated with epistemic uncertainty
2) Errors in meteorological modeling associated with simplified PBL winds.
3) Random variations in the Holland B parameter (shape of wind profile).
4) Storm track variations not captured in synthetic storm set.
5) Random astronomical tide phase.

The uncertainty associated with each error is assumed to be unbiased (bias was removed as discussed in Appendix B) and a Gaussian distributed process. This allows the errors to be represented as standard deviations

and their effects to be combined additively. Usually the Holland B uncertainty is proportional while other uncertainties are constant however the ADCIRC model error has also been shown to be proportional to SWL. The total uncertainty is represented by the standard deviation of errors (σ_ε), where the total associated uncertainty is computed as the square root of the sum of the squares of the standard deviations of each independent component uncertainty (σ_i), $\sigma_\varepsilon = \sqrt{\sum_i^n \sigma_i^2}$. The coefficient of variation, given by $\nu=\sigma_\varepsilon/\mu$, where σ_ε and μ, for example, are the standard deviation and mean SWL from the validation study, is usually roughly 20% and this is further divided into a 15% component that is applied within the integration of Equation A.1 and a second component of 13.2% applied to compute confidence limits. This separate grouping of uncertainties is required to assure a smooth uniform hazard curve and was used to compute all hazard curves.

The astronomical tide in Texas is shown in Melby et al. (2020) to be small enough to allow it to be considered an uncertainty associated with the total water level response. This is common practice in Gulf of Mexico flood risk studies. This uncertainty captures the aleatory variability arising from the possibility of the tropical cyclone arriving during any tide phase. The uncertainty is computed as the standard deviation of the predicted tide at a given location and is roughly equal to MHHW - MSL. For the statistical analysis of water levels, the tidal uncertainty of 0.6 ft was applied to SWL, computed as the standard deviation of the hourly record of NOAA water level gage known as Texas Point 8771450 for the predicted tide time series between 2012 and 2019.

Incorporating epistemic uncertainty, the mean and confidence limit hazard curves are computed as $(\lambda_{r(\hat{x})\pm\sigma_r>r})_{mean} \approx \sum_i^n \lambda_i P[\{r(\hat{x})0.15 \leq \sigma_c\} > r|\hat{x},\sigma]$ and $(\lambda_{r(\hat{x})\pm\sigma_r>r})_{CL} \approx \lambda_{r(\hat{x})>r} + z(\lambda_{r(\hat{x})>r} \leq \sigma_c)0.132$, respectively, where: z = Z-score or number standard deviations from the mean hazard curve. For example, the 84% CL has a Z-score = 1.0, the 90% CL has a Z-score = 1.282 and the 98% CL has a Z-score = 2.0. The total error in SWL is capped at 2.5 ft and for H_{m0} at 3.0 ft to avoid large unreasonable error estimates. This is based on the fact that the error is typically constant for large responses. So, combining the SWL cap with tide, $\sigma_c = \sqrt{2.5^2 + 0.67^2}$ and σ_c = 3.0 ft for H_{m0}.

SWL hazards

Figure 36 shows an example of SWL hazard curves for Gate alternative for SLC0 scenario, with the mean and confidence limits. Save points offshore of Galveston Island and Bolivar Peninsula are shown. These are the same save points highlighted in the previous section. Figure 37 shows similar plots for Beach alternative with SLC0 scenario. Figure 38 shows similar plots for Gate and Beach alternatives, respectively, under the SLC1 scenario. Note that the high-frequency tail looks odd for SLC1 with 'thick' confidence bands. This is because the total water level is higher for all water levels so the error is relatively larger for the high-frequency end. Hazard curves for nearshore, overland and the intercoastal waterway (ICWW) points on transects, described in the prior section, are shown in Appendix F.

Extremal statistics results for all scenarios, all parameters, and all save points were provided to the project sponsor in a spreadsheet and plots.

Figure 36. AEP vs SWL for save point 6038 (offshore Galveston Island, on left) and 5960 (offshore Bolivar Peninsula, on right) SLC0, Gate alternative.

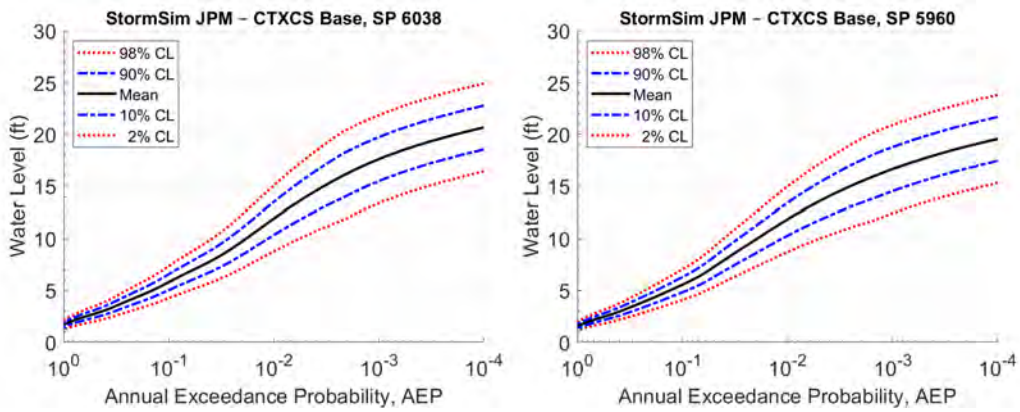

Figure 37. AEP vs SWL for save point 6038 (offshore Galveston Island, on left) and 5960 (offshore Bolivar Peninsula, on right) SLC0, Beach alternative.

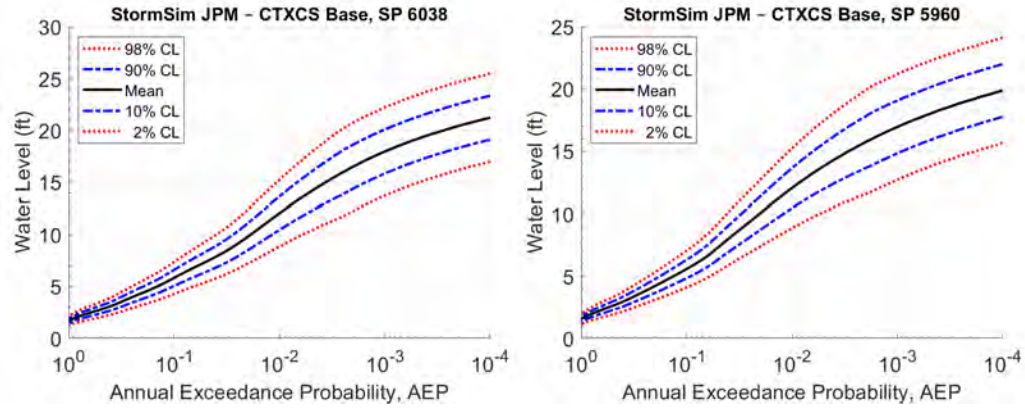

Figure 38. AEP vs SWL for save point 6038 (offshore Galveston Island, on left) and 5960 (offshore Bolivar Peninsula, on right) SLC1, Beach alternative.

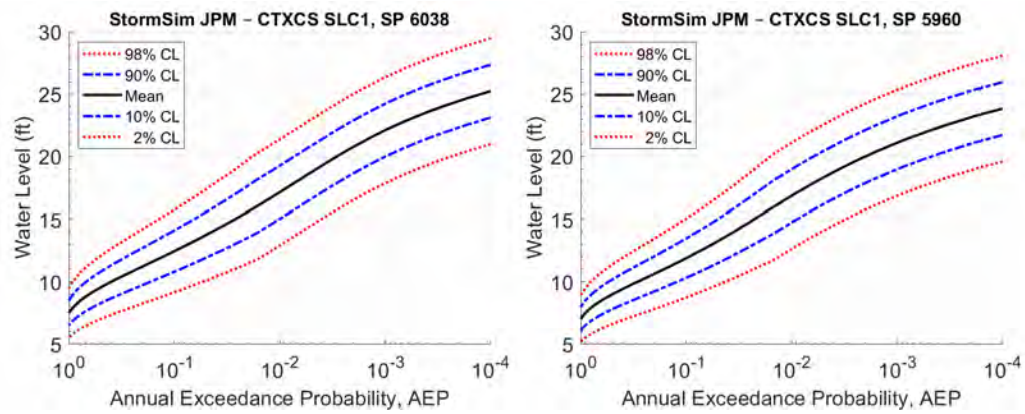

Alternative hazard comparative analyses over the region were conducted. In Appendix F, extremal analysis of CSTORM water levels for save points across the landforms is summarized. The results were reduced to water level transects. Figure 39 shows the transect locations. The save point locations for these transects are shown in Appendix F. Figure 40 through Figure 43 show SWL for 1% AEP at locations across transect for Beach SLC0 alternative and Gate SLC0 alternative. In general, the Beach alternative shows decreased SWLs inshore as expected. However, there are some considerations. First, some of the nearshore points show an increase in SWL in the nearshore, probably mostly due to wave setup. For these locations, there is an increase in SWL from offshore to nearshore and then reduction in water level across the inshore region that includes the dune. The very large rise in nearshore SWL for T1B and T5B as well as the decrease for T3B is probably a result of the way that the CSTORM coupled

ADCIRC and STWAVE averages across nodes in a cell that straddles dry land and not a continuous process as would happen in nature. These results from CSTORM are provided to illustrate hydrodynamics across the large-scale landforms in the absence of morphology change. For the investigation of morphology change described in Chapter 7, the cross-shore hydrodynamic and morphology model CSHORE was used to transform waves from roughly 40 ft depth into shore so these CSTORM outputs on the landforms are not directly relevant to the morphology study.

Figure 39. Hazard transect analysis locations

Figure 40. Hazard transects T1G and T2G with 1% AEP SWL in ft, NAVD

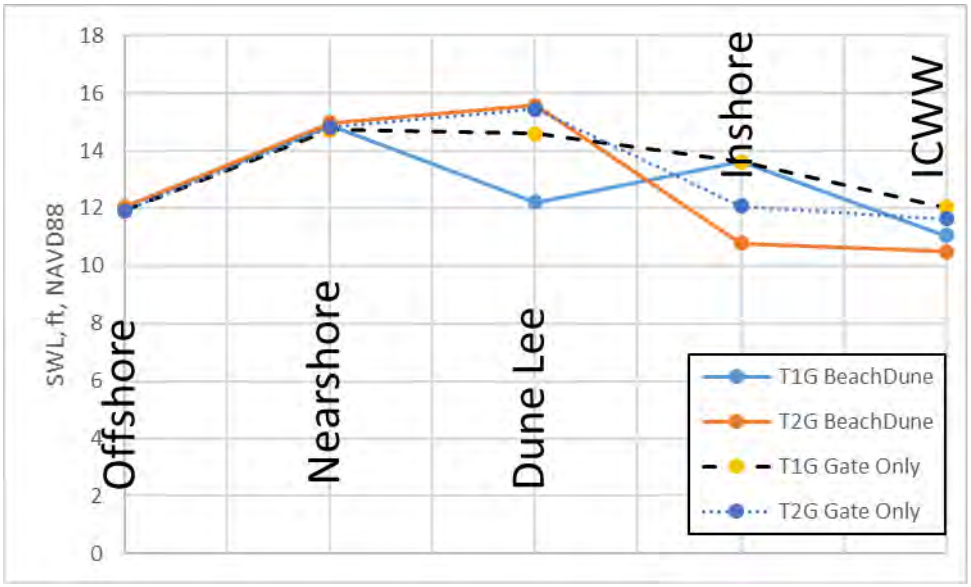

Figure 41. Hazard transects T1B and T2B with 1% AEP SWL in ft, NAVD

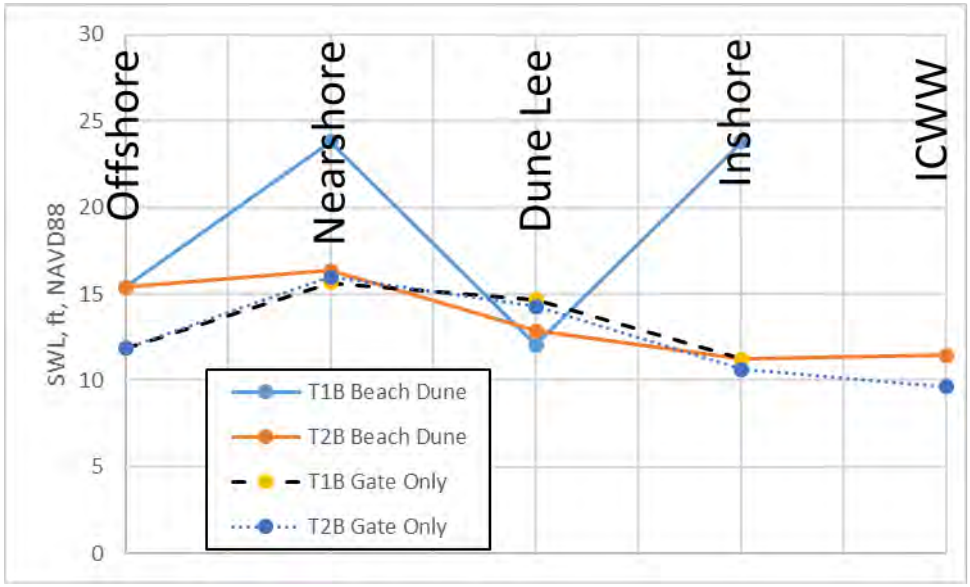

Figure 42. Hazard transects T3B and T4B with 1% AEP SWL in ft, NAVD

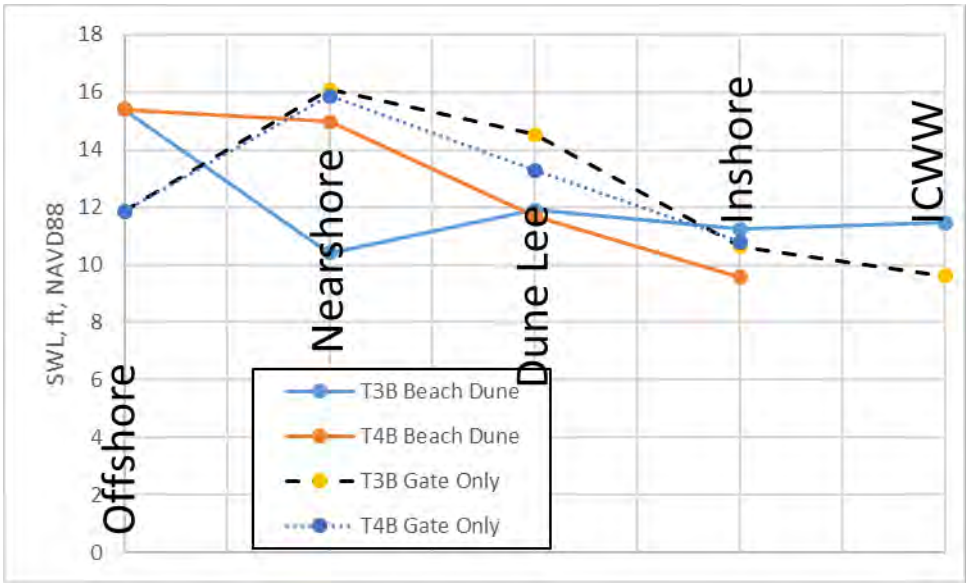

Figure 43. Hazard transects T5B and T6B with 1% AEP SWL in ft, NAVD

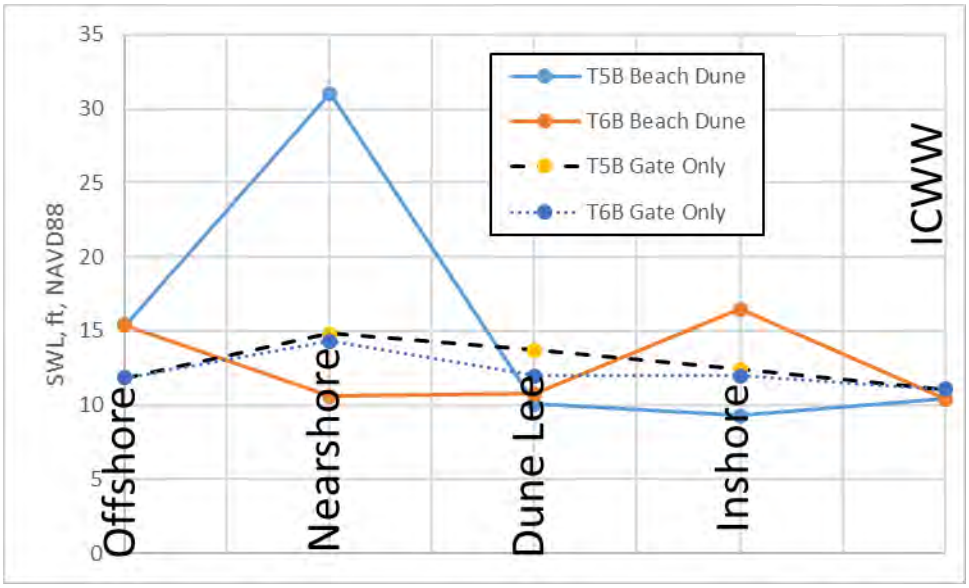

6 Beach Alternatives

Beach profiles

There are 4 reaches analyzed in this study, 2 each on Bolivar and Galveston. They are defined in Table 6 and shown in Figure 44. The general configuration of a beach profile with key features labeled is shown in Figure 45. The alternatives evaluated consist of single dune and dual dune. Bolivar profiles are shown in Figure 46 and Figure 47 for XS1 single and dual dune profiles, respectively, and Figure 48 and Figure 49 for XS2. In these figures, DoC stands for Depth of Closure. The Bolivar profile dimensions are listed in Table 7. Similarly, Galveston profiles are shown in Figure 50 and Figure 51 for XS1 single and dual dunes and Figure 52 and Figure 53 for XS2. The Galveston dune dimensions are listed in Table 8. Quantities are listed in Table 9 and Table 10. Generally, the primary dunes are roughly 10 ft high, extending from elevation 4 ft to 14 ft, NAVD88, while the foredunes for the dual dune configurations are roughly 8 ft high. All dunes have 12 ft wide crests and 1:4 slopes. The berms are about 100 ft wide. The surfzones are generally characterized as wide and shallow-sloping.

Table 6. Beach Alternative Reach Definitions

Description	Length (ft)	Length (mi)	Start Latitude	Start Longitude	End Latitude	End Longitude
Galveston XS1 West	33845	6.41	-95.114	29.087	-95.032	29.145
Galveston XS2 East	63043	11.94	-95.032	29.145	-94.869	29.242
Bolivar XS1 West	69168	13.1	-94.716	29.393	-94.535	29.494
Bolivar XS2 East	63307	11.99	-94.535	29.494	-94.352	29.563

Figure 44. Morphology analysis reaches

Figure 45. Beach components and performance tracking locations

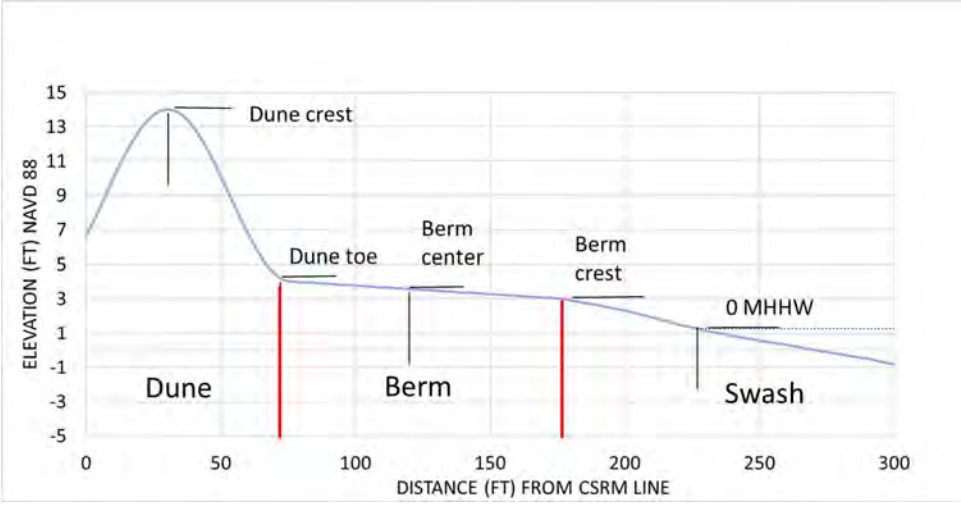

Figure 46. Bolivar Profile XS1 beach and offshore profile. Both single and dual dune profiles are shown.

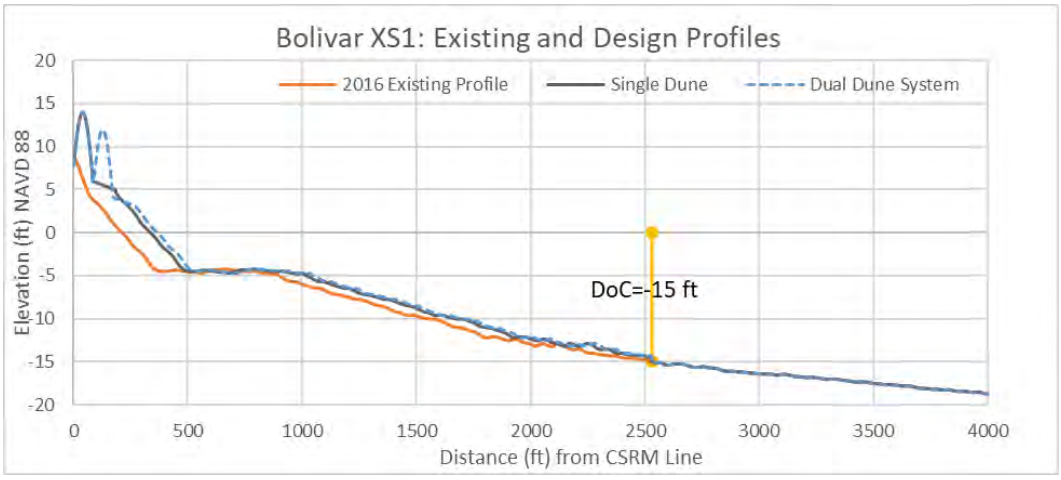

Figure 47. Bolivar Profile XS1 zoomed in to dune and berm. Both single and dual dune profiles are shown.

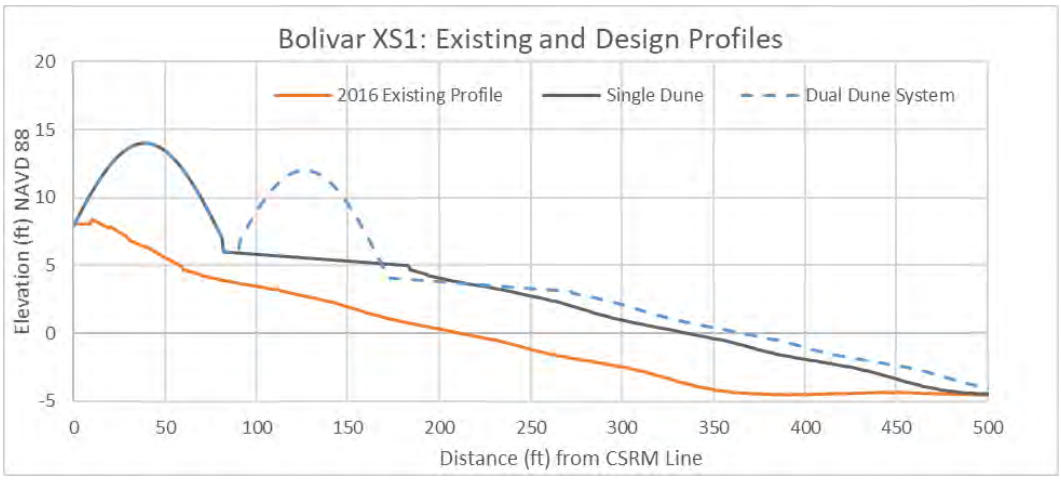

Figure 48. Bolivar Profile XS2 beach and offshore offshore profile. Both single and dual dune profiles are shown.

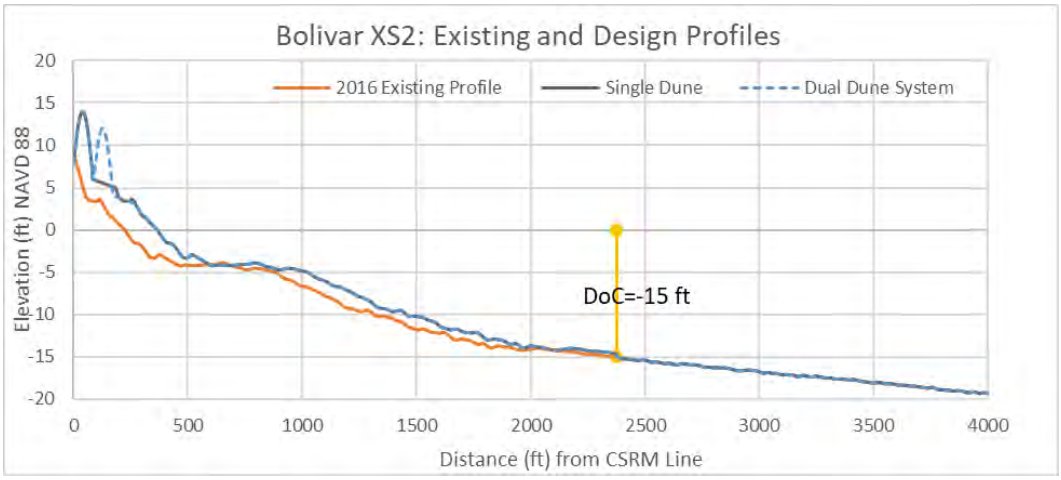

Figure 49. Bolivar Profile XS2 zoomed in to dune and berm. Both single and dual dune profiles are shown.

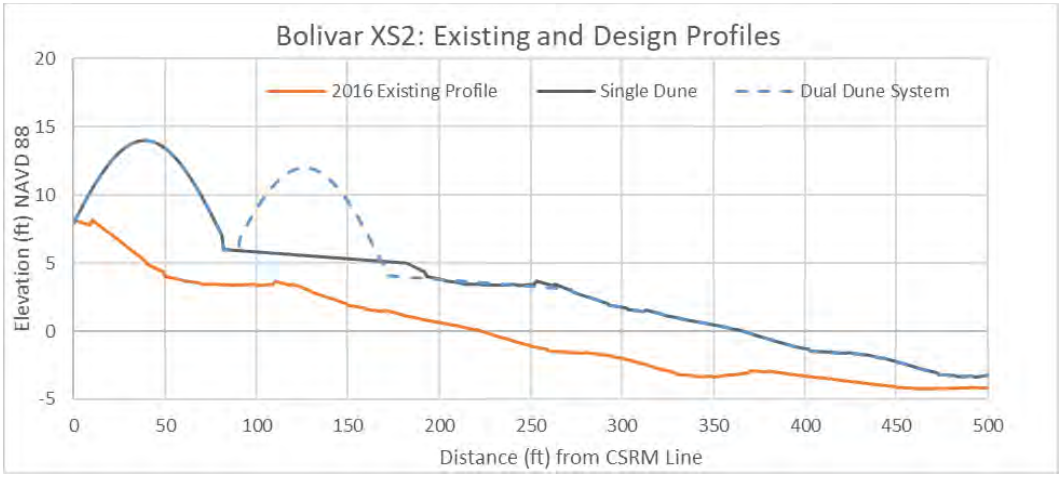

Table 7. Beach feature dimensions in ft for Bolivar Peninsula

Bolivar XS1	Primary Dune Crest	Primary Dune Seaside Toe	Fore-dune Leeside Toe	Fore-dune Crest	Fore-dune Seaside Toe	Berm	MHHW	0 NAVD88	DOC
Single Dune:									
Top Elevation (NAVD88):	14	6	N/A	N/A	N/A	4	1.27	0	-15
Distance from Leeside Toe	36	82	N/A	N/A	N/A	182	313	336	2290
Dual Dune									
Top Elevation (NAVD88):	14	6	6	12	4	4	1.27	0	-15
Distance from Leeside Toe	36	82	90	126	172	272	343	363	2290

Bolivar XS2	Primary Dune Crest	Primary Dune Seaside Toe	Fore-dune Leeside Toe	Fore-dune Crest	Fore-dune Seaside Toe	Berm	MHHW	0 NAVD88	DOC
Single Dune:									
Top Elevation (NAVD88)	14	6	N/A	N/A	N/A	4	1.27	0	-15
Distance from Leeside Toe	36	82	N/A	N/A	N/A	182	344	366	2376
Dual Dune									
Top Elevation (NAVD88)	14	6	6	12	4	4	1.27	0	-15
Distance from Leeside Toe	36	82	90	126	172	272	344	366	2376

Figure 50. Galveston Profile XS1 beach and offshore offshore profile. Both single and dual dune profiles are shown.

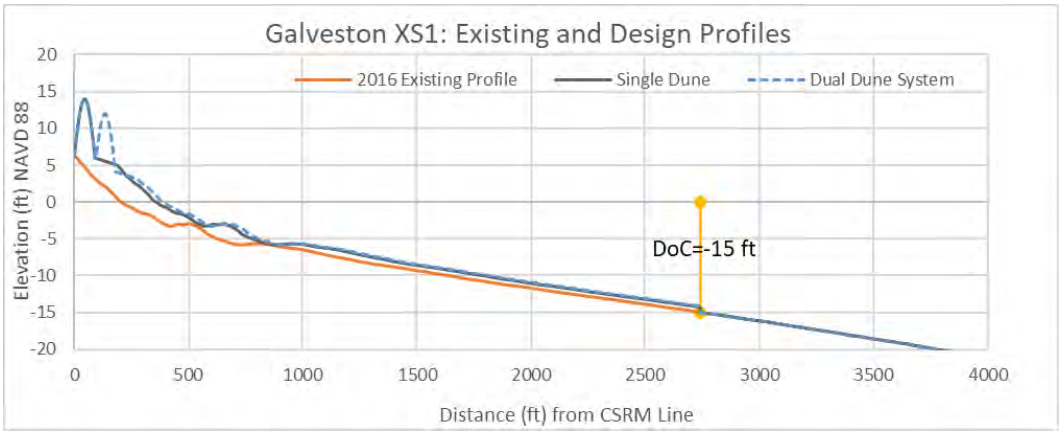

Figure 51. Galveston Profile XS1 zoomed in to dune and berm Both single and dual dune profiles are shown.

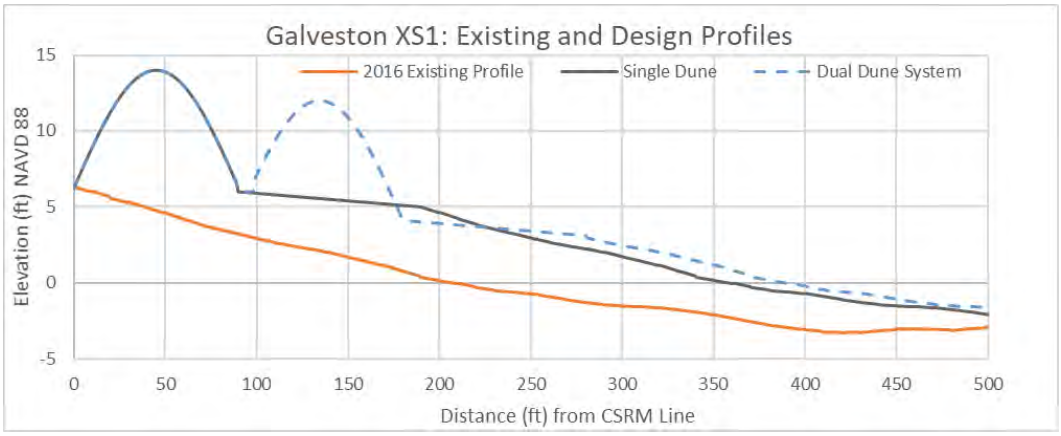

Figure 52. Galveston Profile XS2 beach and offshore offshore profile. Both single and dual dune profiles are shown.

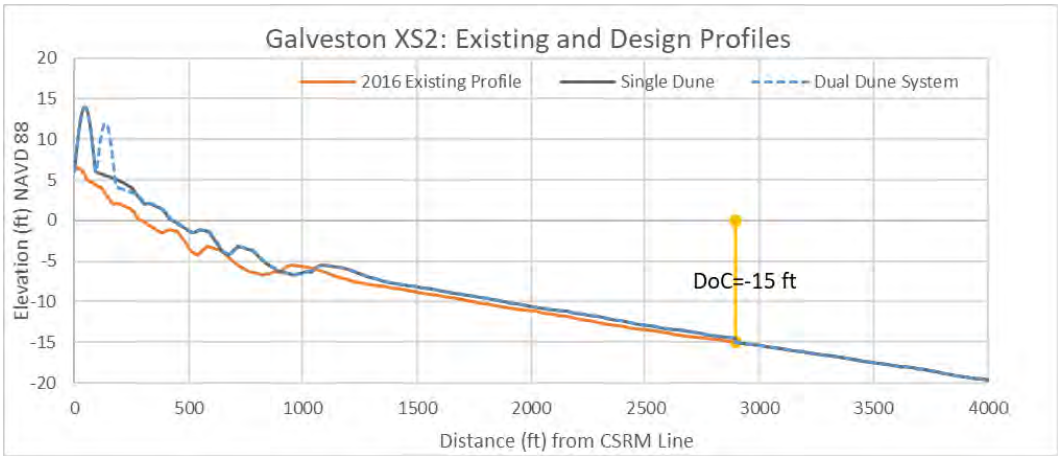

Figure 53. Galveston Profile XS2 zoomed in to dune and berm. Both single and dual dune profiles are shown.

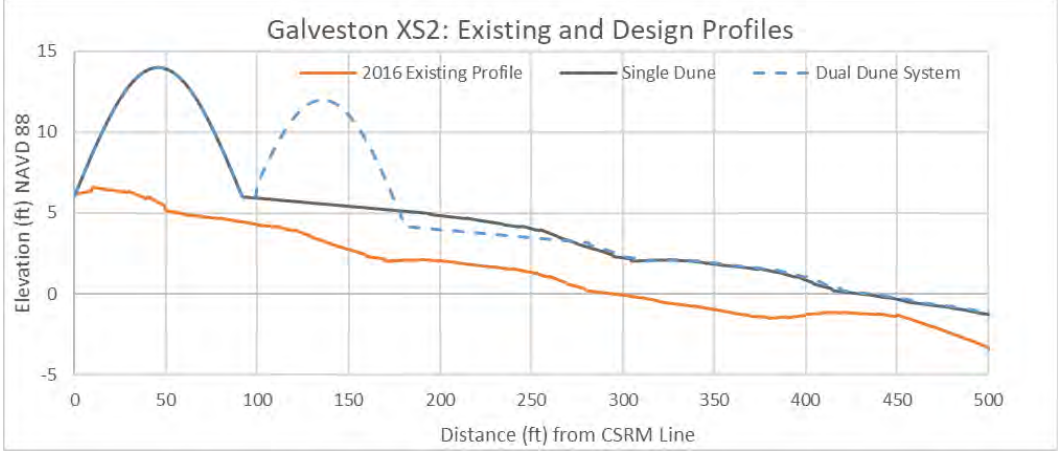

Table 8. Beach feature dimensions in ft for Galveston Island

Galveston XS1	Primary Dune Crest	Primary Dune Seaside Toe	Fore-dune Leeside Toe	Fore-dune Crest	Fore-dune Seaside Toe	Berm	MHHW	0 NAVD88	DOC
Single Dune:									
Top Elevation (NAVD88):	14	6	N/A	N/A	N/A	4	1.27	0	-15
Distance from Leeside Toe	45	90	N/A	N/A	N/A	190	311	358	2742
Dual Dune									
Top Elevation (NAVD88):	14	6	6	12	4	4	1.27	0	-15
Distance from Leeside Toe	45	90	96	134	180	280	342	389	2742

Galveston XS2	Primary Dune Crest	Primary Dune Seaside Toe	Fore-dune Leeside Toe	Fore-dune Crest	Fore-dune Seaside Toe	Berm	MHHW	0 NAVD88	DOC
Single Dune:									
Top Elevation (NAVD88)	14	6	N/A	N/A	N/A	4	1.27	0	-15
Distance from Leeside Toe	46	85	N/A	N/A	N/A	192	381	430	2895
Dual Dune									
Top Elevation (NAVD88)	14	6	6	12	4	4	1.27	0	-15
Distance from Leeside Toe	46	85	96	135	182	282	386	435	2895

Cumulative volume

Table 9 gives cumulative volumes for reaches of beach and surfzone areas per alongshore ft. Table 10 gives total volume if these transects are translated over the alongshore distance of each reach. Note that cy is cubic yards and Mcy is millions of cubic yards. A more detailed analysis is required to accurately determine fill volumes but that is outside the scope of this study. Generally, the analysis herein is looking at average response of the beach and so extending relatively few transects over the entire alongshore reach.

Table 9. Cumulative volumes per ft alongshore for Bolivar Peninsula and Galveston Island dune profiles

Bolivar XS1 (West)	Primary Dune	Transi-tion	Fore-dune	Berm	To MHHW	To 0 NAVD88	To DOC
Initial Volume	(cy/ft)	(cy/ft)	(cy/ft)	(cy/ft)	(cy/ft)	(cy/ft)	(cy/ft)
Single Dune:	16.52	0.00	0.00	11.25	46	48.94	108.18
Dual Dune	16.52	0.66	21.35	14.53	65	68.77	139.50
Bolivar XS2 (East)							
Initial Volume	(cy/ft)	(cy/ft)	(cy/ft)	(cy/ft)	(cy/ft)	(cy/ft)	(cy/ft)
Single Dune:	19	0.00	0.00	10.76	53.30	56.09	124.01
Dual Dune	19	0.77	20.87	13.61	64.87	67.66	135.58
Galveston XS1 (West)							
Initial Volume	(cy/ft)	(cy/ft)	(cy/ft)	(cy/ft)	(cy/ft)	(cy/ft)	(cy/ft)
Single Dune:	21.55	0.00	0.00	13.34	51.89	56.18	131.40
Dual Dune	21.55	0.86	23.11	14.84	69.11	74.40	162.97
Galveston XS2 (East)							
Initial Volume	(cy/ft)	(cy/ft)	(cy/ft)	(cy/ft)	(cy/ft)	(cy/ft)	(cy/ft)
Single Dune:	18.9	0.0	0.0	8.84	46.7	50.13	119.0
Dual Dune	18.9	0.48	19.54	8.03	57.6	60.98	132.3

Table 10. Total idealized volumes for translated transects for Bolivar Peninsula and Galveston Island reaches

Transect	Alongshore Distance (ft)	Total Volume per alongshore ft (cy/ft)	Total Volume per Reach (Mcy)	Total Volume per Landform (Mcy)
Bolivar XS1 (West) Single	69,168	108.18	7.483	15.334
Bolivar XS2 (East) Single	63,307	124.01	7.851	
Bolivar XS1 (West) Dual	69,168	139.50	9.649	18.232
Bolivar XS2 (East) Dual	63,307	135.58	8.583	
Galveston XS1 (West) Single	33,844	131.40	4.447	11.949
Galveston XS2 (East) Single	63,043	119.0	7.502	
Galveston XS1 (West) Dual	33,844	162.97	5.516	13.857
Galveston XS2 (East) Dual	63,043	132.3	8.341	

7 Stochastic Simulation of Response

Morphological modeling was conducted with the numerical software CSHORE (Kobayashi 2009, Johnson et al. 2012) to model the following processes:

1) Morphology change,

2) Nearshore wave transformation and nearshore water levels,

3) Wave runup and wave and steady flow overtopping.

CSHORE includes the following capabilities:

1) Combined wave and circulation current model based on time-averaged continuity, cross-shore and longshore momentum, wave action, and wave roller energy equations,

2) Sediment transport model for suspended sand and bedload,

3) Permeable layer model to account for porous flow and energy dissipation,

4) Irregular wave runup, overtopping and wave transmission,

5) Probabilistic model for an intermittently wet and dry zone,

6) Impermeable and permeable bottoms for the purpose of predicting wave overwash of a dune and mobility of stone,

7) Erosive or fixed clay layer under mobile sediment

8) A vegetation model.

CSHORE is intended to predict short-term changes to the beach-dune system as a result of storm waves and water levels. It is a cross-shore erosion model so it does not account for inter-storm accretion nor does it model long-term alongshore transport. CSHORE computes local alongshore sediment movement and this quantity can be useful but it is storm-focused and highly localized so it is not very well correlated with

long-term alongshore sediment transport along a stretch of shoreline. CSHORE is referred to as one-dimensional because it is a cross-shore model and computes depth-averaged processes. It solves the time-averaged hydrodynamic and sediment mobility mass and momentum conservation equations along a transect from just offshore of the surf zone to the extent of inundation. The solution scheme within CSHORE is efficient and is fast enough to run many 50-year life cycles of storms for several transects in a day. The evolution of the beach and interaction with incident waves and water levels is complex and a priori unknown. So it is important to use a model that is both efficient and accurate so that all possible hazard conditions can be modeled and the worst case scenarios resolved. The present technological state of coastal morphological modeling is highly uncertain so a relatively sophisticated model like CSHORE is still required in order to get reasonable results.

For analysis of the beach morphology and wave overtopping, the following strategy was employed:

1) Input Hazard: Continuous 3-hourly synthetic tropical storm conditions and hourly non-tropical storm conditions for the initial offshore wave and water level hazard at roughly 40 ft depth. Note that the runtime peaks from the CSTORM model were substituted into the 3-hourly time series in order to assure capture of storm peak.

2) Sea level rise (SLR) scenarios: SLR scenarios were defined at 1 year increments. These sea levels were linearly added to the SWL time series of each storm at the 40 ft depth. Linear superposition at this depth avoided introducing nonlinear residual error.

3) Tide: Predicted tidal time series of two years in duration from Galveston Pier 21 gage were used to define the tide. A random phase was selected and then a tidal time series sampled that was then linearly added to the SWL time series of each storm when each storm was sampled. In this way every instance of every storm will have a different tide phase.

4) Uncertainty: Epistemic uncertainty was sampled for each storm and added to the storm responses. Uncertainties were summarized in Chapter 5.

5) Nearshore wave and water level hazard: For each life cycle, CSHORE transformed the continuous time series of waves.

6) Morphology change: Simultaneously with the wave transformation, CSHORE modeled the morphology change over each transect.

7) Wave and overflow overtopping: CSHORE computed overtopping and overflow at each time step.

8) Rehabilitation limit state: The dune crest height was tracked and the entire beach profile was restored to the as-built profile if the eroded dune height was less than half of its original height prior to the next storm. The dune profile and number of rebuilds was tracked and recorded through the life cycles.

Sediment transport parameters

The sediment transport parameters used in CSHORE to model cross shore transport were as follows:

d_{50}=0.15 mm, median grain size diameter

w_f = 0.0165 m/s, fall velocity

s = 2.65, specific gravity

e_B = 0.005, suspension efficiency due to breaking

e_f =0.01, suspension efficiency due to bottom friction

a = 0.2, suspended load parameter

a_o = 0.1, suspended load parameter associated with overtopping

tan ϕ = 0.63, limiting (maximum) slope

b = 0.001, bedload parameter

CSHORE run parameters

DX = 3 m, computational cell size

γ = 0.7, empirical breaker ratio parameter

RWH = 0.02 m, runup wire height

The individual profiles included a sand layer on top of a clay layer. The sand layer for all simulations was 13 ft thick. The clay layer was never exposed in the simulations so it had little effect.

CSHORE simulations of individual storms

Separate from the life cycle simulations, CSHORE was run individually and independently for all storms in order to determine the impact of individual storms on an undamaged beach. Figure 54 shows example damaged profiles for 6 different TCs. The examples are classified into damage levels (DL) relative to the dune height reduction as follows:

DL=0: No noticeable damage to dune
DL=1: 0%< Dune height reduction ≤ 10%
DL=2: 10% < Dune height reduction ≤30%
DL=3: 30% < Dune Height Reduction ≤ 60%
DL=4: 60% < Dune Height Reduction ≤ 80%
DL=5: Dune Height Reduction > 80%

The individual storm simulations showed that the dunes exhibited very little erosion from the non-tropical events and TC storms that had little local response. However, TC storms with significant local hydrodynamic response (high SWL and H_{m0}) produced considerable erosion. The most intense local TC storms had water levels that inundated the dunes and these generally completely eroded the dunes. This case would be equivalent to a breach of the flood constraining capability of the dune. Interestingly, no storms produced much erosion of the berm and beach portion of the profile. The erosive storms usually moved material from the dune to the berm and to the swash area. So the dune acted as a nourishment source for the berm and swash zone. Relatively infrequent severe TC storms tended to erode the dune past the limit state which was defined heuristically as less than 50% of dune height remaining. An additional interesting phenomenon of the CSHORE simulation was that very intense TCs moved sand to the offshore boundary of the model and produced accumulation of sand at the boundary.

Figure 54. Example beach, berm and dune profiles for select TC storms to illustrate damage levels to berm and dune. These are actual starting and ending output profiles from CSHORE.

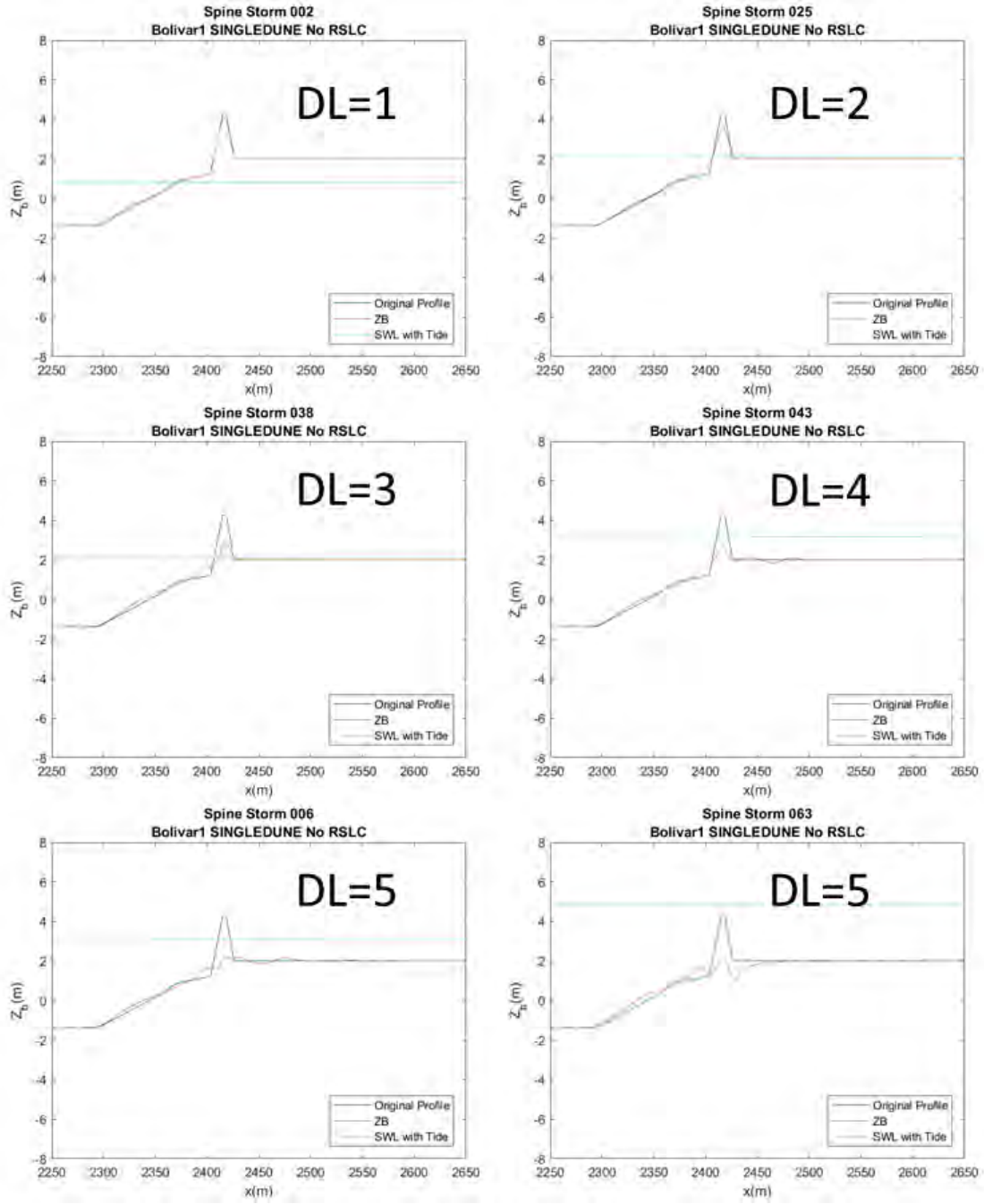

Details of stochastic response simulation approach

For stochastic assessment of the beach morphology, the CSHORE model was embedded in a time-dependent Monte Carlo sampling scheme within the larger StormSim stochastic modeling system. The modeling system is written in Matlab.

Wave and water level life cycles

The forcing included tropical storms and non-tropical storms. The number of storms in a given year followed a Poisson distributed process which depends only on the storm rate. The Poisson distribution for non-tropical storms was based on a storm rate of 0.9211 storms per year and this was based on results from the peaks-over-threshold analysis described in Chapter 3. So over a 50 year life cycle, 46 non-tropical storms were sampled, on average. Each non-tropical storm was an actual historical storm run on random tide. However, epistemic uncertainty associated with water level and wave parameters was added based on a Gaussian copula multi-variate probability density function in order to preserve parameter correlations.

TC Storms were also sampled based on a Poisson distribution where the overall storm rate was 0.6047 storms per year. This storm rate was determined using the Gaussian kernel approach described in Appendix A and Nadal-Caraballo et al. (2018a). So over a 50 year life cycle, about 30 tropical storms are sampled, on average. The storms were further subsampled from 3 separate groups according to their intensity and each group had a specific storm recurrence rate (SRR) (Nadal-Caraballo et al. 2018a).

Low Intensity ($\Delta P \leq 28$ mb): SRR = 0.3471/yr

Mid Intensity (28 mb $< \Delta P <$ 48 mb): SRR = 0.1502/yr

High Intensity ($\Delta P \geq 48$ mb): SRR = 0.1074/yr

Here, $\Delta P = 1013$ mb $- P_{min}$ where P_{min} is the minimum central pressure of the TC. Individual TCs were sampled according to their probability masses. Note that the majority of TCs from the JPM-OS were extreme events so there were relatively few storms in the low and mid intensity groups. The result was that the same storm could be sampled more than once in a life cycle for the lower intensity, relatively frequent, groups of tropical storms.

An StormSim tool randomly samples the individual offshore storm wave and water level time series and tide, and produces the final random 50 year sequences of the waves and water levels for all life cycles with RSLC included. A single run control file includes the names of the external data

files, the sediment parameters and all other inputs. A second StormSim routine is run to read the offshore wave and water level life cycle files, the transect profile elevation data, and the run control file and generate all of the by-storm CSHORE input files. A separate StormSim routine then runs the stochastic simulation by stepping through the life cycle, running each storm in sequence with CSHORE. The life-cycle simulation software steps through each storm, time step by time step, running CSHORE, copying the last damaged profile to the new CSHORE input file, running the next storm, tracking the dune elevation for potential rebuild, rebuilding if the limit state is exceeded and so on. Each life cycle had roughly 72 to 77 storms and sufficient life cycles to achieve a stable solution for each simulation. The runtime was about 2 hours per profile scenario on an average PC and many scenarios can be run simultaneously so all simulations were completed in a single day.

A series of StormSim post-processing codes were run to do the following:

- Compile the results per life cycle including details of the storms sampled, the TC storm parameters, individual damage categories, peak storm SWL and wave characteristics, profile rebuilds, etc.
- Assemble profile parameters as a time series.
- Create animations of profile evolution for every life cycle.
- Assemble overtopping by storm and compute probability distributions.

Convergence

A statistical convergence test was conducted to determine the number of life cycles required to establish a statistically stable solution. The goal was to determine the number of life cycles where additional life cycles produced little change in the average output and variability, defined by standard deviation of output parameters. Figure 55 shows an example of the number of life cycles vs number of rebuilds, Figure 56 shows life cycles vs seaward dune toe elevation difference from as-built, Figure 57 shows life cycles vs berm centerline elevation difference from as-built, Figure 58 shows life cycles vs berm seaward crest elevation difference from as-built, and Figure 59 shows life cycles vs profile elevation at MHHW intersection difference from as-built. These performance tracking locations were defined in Figure 45. These plots show that the output is fairly stable after

20 life cycles. For the life cycle simulations, full stochastic simulations consisted of 30 life cycles.

Figure 55. Example of statistical convergence of number of rebuilds with number of life cycles

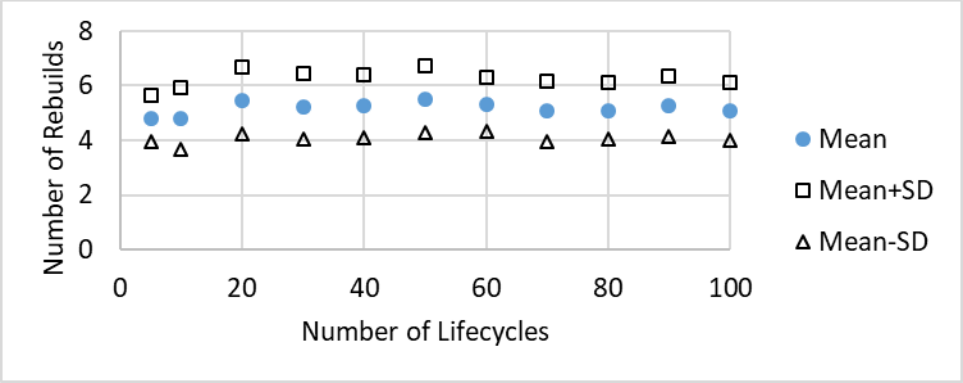

Figure 56. Example of statistical convergence of seaward dune toe elevation difference from as-built with number of life cycles

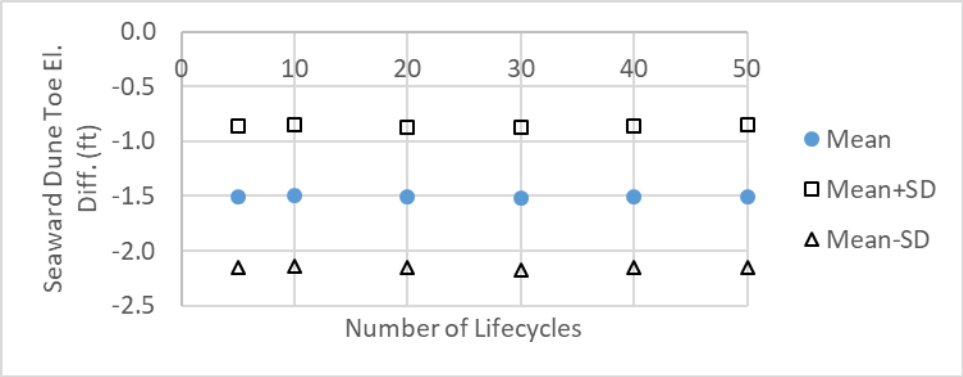

Figure 57. Example of statistical convergence of berm centerline elevation difference from as-built with number of life cycles

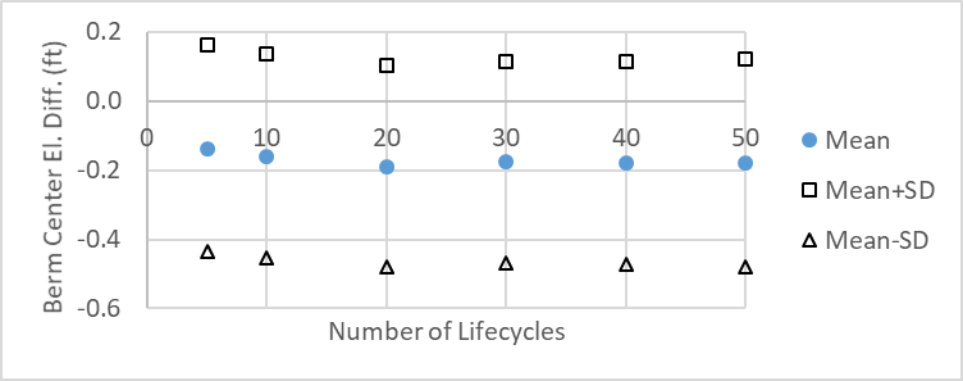

Figure 58. Example of statistical convergence of berm seaward crest elevation difference from as-built with number of life cycles

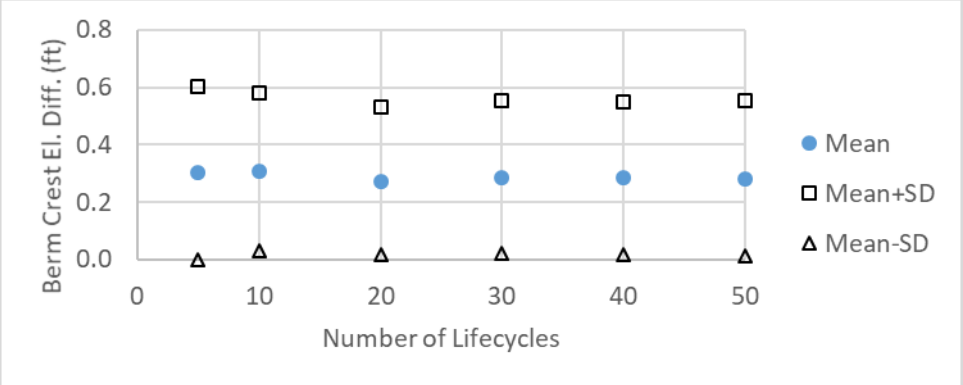

Figure 59. Example of statistical convergence of profile elevation at MHHW intersection difference from as-built with number of life cycles

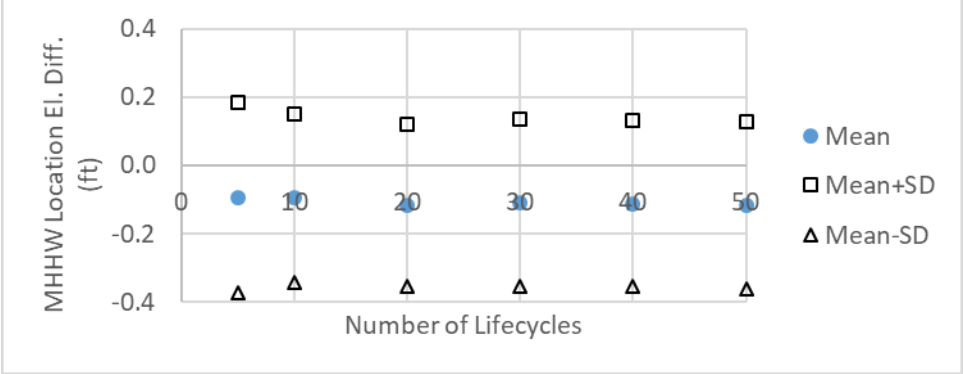

Life cycle simulation limitations

Morphological models like CSHORE do not model the natural recovery of the dune and berm. The natural recovery occurs as a result of quiescent day-to-day waves that move the sand back onto the beach and dune between erosive storm events. It is common in these types of life cycle morphological studies to add elevation to the berm and dune to account for this recovery. The typical recovery addition is 50% of the loss per storm or per year. That was not done herein for several reasons. First, the area is sand limited. There is little new sand entering the system. Further, the very intense hurricanes move sand beyond the active profile so that sand is not likely to be available for recovery. This was observed during the single storm simulations where sand piled up on the seaward CSHORE boundary. Also, the rebuilds that are required are relatively frequent. It is assumed that rebuilds will account for changes in RSLC by building back to an elevation relative to a datum that is adjusted in the long term with RSLC. It would be relatively simple to rerun the simulations with recovery for comparison. However, it was not done herein for the above reasons.

As relative sea level rises, the beach will continually adjust to a new equilibrium profile. This is usually accounted for in studies like this through application of the Bruun rule, where the equilibrium beach profile is steadily adjusted with time. The adjustment includes recession that would occur due to a higher water level stand. The Bruun rule has been criticized as being overly simple (e.g. Anderson et al. 2015, Cooper and Pilkey 2004). It does not account for alongshore sediment transport, assumes a closed system, and assumes unlimited sediment availability, among other things. Depth of closure (DoC) is defined as the shallowest depth at which sediment is not influenced by waves and currents. The idea suggests a fixed point in space. However, the DoC can vary with time depending on storm severity. This part of the U.S. coast is routinely exposed to TCs and these storms move sediment out of what would be considered a normally closed beach-dune sediment mobility system. Intense TC storms can influence sediment transport at much deeper depths than what is considered a typical DoC. TC storms will erode sand out of the system, moving sediment out to deep depths. CSHORE reestablishes equilibrium rapidly after construction and transports sediment in a realistic way and so should account for this process at the storm level. Again, as discussed above, it is assumed that rebuilds will account for changes in RSLC by building back to an elevation relative to a

datum that is adjusted in the long term with RSLC. This concept will need to be accounted for in the management approach.

Long term shoreline recession was not included in the modeling. For Bolivar, it is not required because the shoreline recession in the populated area is near neutral, as discussed in Chapter 2. The small net erosion is mitigated in the stochastic simulations by building back to the original profile. For Galveston, the end effects of the seawall will cause significant erosion. This area will require separate maintenance because it is an odd case. For the remainder of Galveston Island where the net recession is significant, the mitigation will be similar to that described above for RSLC-related recession. That is, the beach rebuilds are assumed to provide recovery of the shoreline with long term adjustment of the project elevations for RSLC.

The above physics limitations and simplifications of the present study may prove to be important for this project and should be investigated further. Several approaches are mentioned that could be employed relatively easily with the CSHORE StormSim life-cycle simulation model.

Life cycle simulation time series results

An example of a time series of profile evolution for a single life cycle is shown in Figure 60 and Figure 61. Additional scenarios are shown in Appendix G. In Figure 60, time series of the profile tracking location elevation differences are plotted versus time over a life cycle. These plots show time series of the difference between the tracking location elevation for the as-built beach and the elevation after each storm. Note that the time (years in the life cycle) axis label at the bottom of the plot applies to all of the subplots. So, for example, for the top plot in Figure 60, the first point on the left hand side is zero indicating that the dune crest is at the as-built elevation and has no erosion at the start of the life cycle. The values of dune crest difference increase with time for the first few years of the life cycle indicating that the crest is eroding until year 6 where the limit state is exceeded, the beach profile is rebuilt and the elevation difference returns to zero. Note that the final dune elevation is not shown in this plot. The 9 rebuilds for this life cycle can be clearly seen. This graphic is typical of the life cycles. The Sea Dune Toe numbers are negative because the toe is always accreting, never eroding. This is not realistic because dunes develop a scarp when they erode but this flaw in the physics is a known

weakness of cross-shore sediment transport models. This does not limit the usefulness of the models to show general beach erosion with time.

Figure 61 shows the same life cycle as shown in Figure 60 but here the profiles after each storm are shown as many brown lines while the initial profile is shown as a heavy green line. The profile tracking locations are denoted as colored vertical lines on this plot. Note that the vertical axis is heavily distorted in this plot. The maximum vertical erosion of the berm crest is about 1 ft. This was typical of all profiles. Similar plots of all of the life cycles and all scenarios look almost indistinguishable from this one. The conclusion from these plots is that the berm and swash area did not show significant erosion throughout the life cycles. However, the dune did degrade with time. Degradation of the dune caused sediment to be transported from the dune to the berm and then to the swash area so the dune acted as a renourishment source for the rest of the beach. This process was very evident in animations of the profile evolution that were produced for every life cycle. A vegetated dune may not renourish quite so efficiently and so, for the performance of the system, there may be relatively less erosion of the vegetated dune and more erosion of the berm than was shown in the simulations. This could be evaluated in the future by including a vegetated dune in the CSHORE simulations. However, for all simulations discussed herein, the dune was not vegetated.

CSHORE models cross-shore sediment transport but not three-dimensional sediment transport alongshore. Breaching of dune would be indicated by the dune crest elevation being reduced to near the elevation of the berm and this was common for severe TCs. However, CSHORE does not model large scale morphological evolution that would characterize barrier island breaching from steady flow either from incoming surge or outgoing drainage after the peak of the storm. That type of process would require modeling that was not done for this study.

Table 11 summarizes the profile tracking location data. In this case, the difference between the initial elevation and the damaged elevation was computed and statistics computed over all life cycles. The mean and standard deviation are provided. The negative differences at the dune toe indicate that the toe always accretes. Depending on the transect, the single or dual dune may accrete more. The berm centerline accretes on Galveston Island but erodes on Bolivar Peninsula. The berm crest virtually always erodes, regardless of the location or the scenario. At the mean, the berm

crest for the Galveston XS1 single dune alternative appears to accrete slightly but at the mean+1SD, it is eroding. Generally the erosion of the berm crest is less than 1 ft at the mean but over 1 ft for the mean+1SD, however, it is on the order of a foot. For Galveston, the berm crest for the dual dune erodes less than the single dune but for Bolivar it is opposite. The MHHW may erode or accrete but it generally shows little average change.

These results show that the sediment is eroded from the dune to the berm and then to the swash area. This morphological transformation is repeatable from life cycle to life cycle and the only significant difference between life cycles and scenarios is the rate at which the dune degrades. Tropical storms are relatively frequent and they cause severe dune erosion. So the dune demands regular maintenance. Because the dune nourishes the berm and swash area, there is no motivation to perform minor maintenance to restore the beach separately from the dune. These two comments will be explored further in the following sections on required dune rebuilds and overtopping.

Figure 60. Time series of profile elevations at select locations for a single life cycle from Alternative Bolivar XS1, single dune, low RSLC

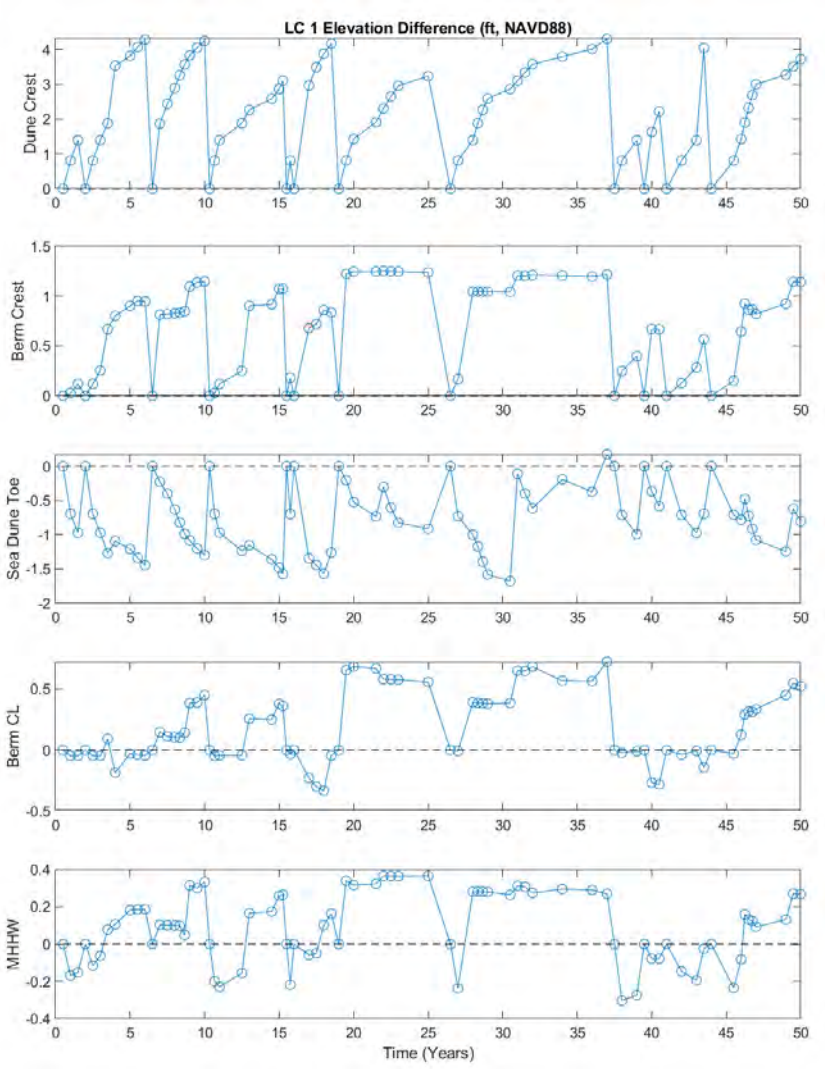

Figure 61. Time series of profile elevations at select locations for a single life cycle from Alternative Bolivar XS1, single dune, low RSLC

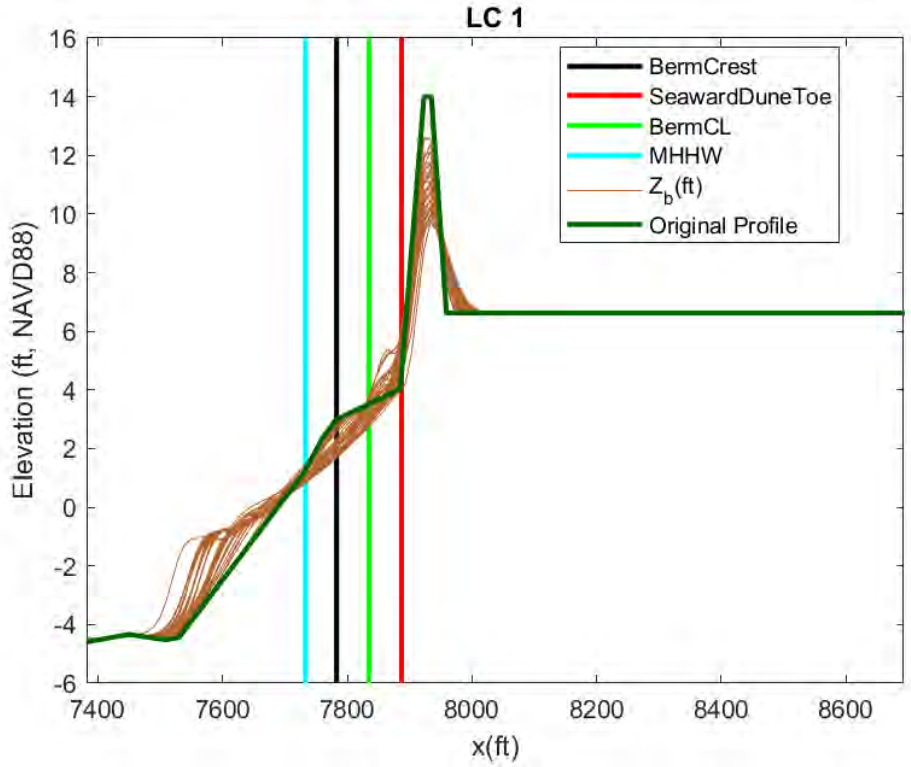

Table 11. Elevation difference summary

Alternative and Scenario	Berm Seaward Crest Elevation Difference (ft)		Seaward Dune Toe Elevation Difference (ft)		Berm Center Line Elevation Difference (ft)		MHHW Elevation Difference (ft)	
	Mean	SD	Mean	SD	Mean	SD	Mean	SD
Bolivar XS1								
SINGLE, Low	0.72	0.43	-0.93	0.56	0.22	0.25	0.10	0.20
SINGLE, High	0.50	0.40	-0.85	0.55	0.04	0.28	-0.08	0.24
DUAL, Low	0.81	0.41	-0.80	0.51	0.31	0.32	0.14	0.20
DUAL, High	0.58	0.39	-0.83	0.50	0.11	0.34	-0.08	0.28
Bolivar XS2								
SINGLE, Low	0.77	0.43	-0.87	0.54	0.25	0.25	0.10	0.16
SINGLE, High	0.54	0.40	-0.82	0.53	0.07	0.29	-0.07	0.22
DUAL, Low	0.84	0.40	-1.45	0.73	0.31	0.31	0.33	0.19
DUAL, High	0.61	0.38	-1.28	0.69	0.12	0.32	0.11	0.26
Galveston XS1								
SINGLE, Low	0.33	0.20	-1.10	0.55	-0.08	0.20	-0.16	0.12
SINGLE, High	0.21	0.20	-1.00	0.56	-0.19	0.27	-0.25	0.18
DUAL, Low	0.40	0.20	-0.95	0.48	-0.06	0.25	-0.18	0.12
DUAL, High	0.23	0.26	-0.95	0.51	-0.21	0.33	-0.33	0.23
Galveston XS2								
SINGLE, Low	-0.64	0.41	-1.37	0.61	-1.37	0.61	-0.29	0.16
SINGLE, High	-0.69	0.49	-1.20	0.63	-1.20	0.63	-0.37	0.24
DUAL, Low	0.46	0.22	-1.74	0.66	-0.03	0.24	0.05	0.13
DUAL, High	0.29	0.27	-1.52	0.65	-0.18	0.29	-0.11	0.24

Another interesting process was infilling of the gap between the dual dunes. Typically, the dual dune would transform into a single dune relatively quickly, depending on the severity of the storms. This is illustrated in Figure 62. In this case, the dune is transformed to a single dune by year 15 of the 50 year life cycle. Again, this process may not be as aggressive if the dune is vegetated. However, dune vegetation may be sparse so at least locally, this process is likely to occur similar to that shown in the model.

Figure 62. Select plots of a dual dune profile at 4 times in a life cycle: undamaged (upper left), year 8 (upper right), year 10 (lower left), and year 15 (lower right). Damaged profile is typical of dual dune and illustrates transition from dual to single dune.

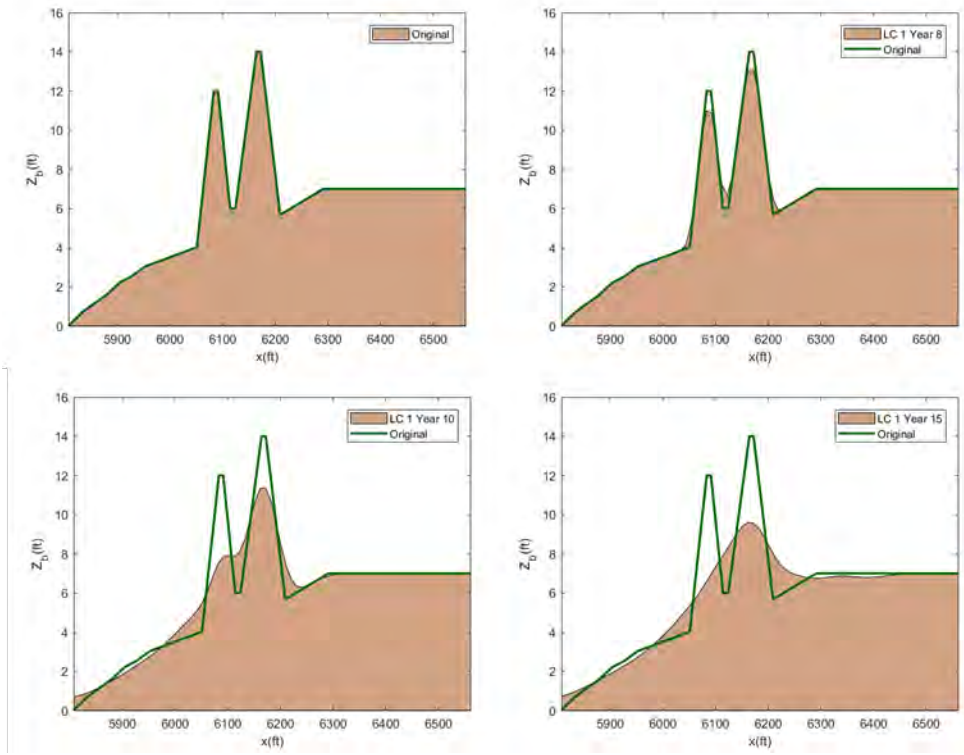

Volume of mobilized sand

The total volume of mobilized sand (erosion+accretion) and the erosion-only volume associated with each rebuild were determined using quadrature numerical integration. The mean and standard deviation across all life cycles were computed and are summarized in Table 12 and Table 13. Table 12 summarizes the erosion only while Table 13summarizes the sum of erosion and accretion.

Table 12. Total eroded volume summary

Alternative and Scenario	Mean Erosion			Standard Deviation (SD) (cy/ft)		Mean+SD
	XS1 (cy/ft)	XS2 (cy/ft)	Total (Mcy)	XS1	XS2	Total (Mcy)
Bolivar						
SINGLE, Low	9.4	9.2	1.2	4.0	3.7	1.8
SINGLE, High	7.8	8.0	1.0	3.2	3.1	1.5
DUAL, Low	17.7	16.3	2.3	5.4	5.1	3.0
DUAL, High	15.3	14.2	2.0	5.0	4.8	2.6
Galveston						
SINGLE, Low	9.4	9.2	0.9	4.0	3.7	1.3
SINGLE, High	7.8	8.0	0.8	3.2	3.1	1.1
DUAL, Low	17.7	16.3	1.6	5.4	5.1	2.1
DUAL, High	15.3	14.2	1.4	5.0	4.8	1.9

Table 13. Total eroded + accreted volume summary

Alternative and Scenario	Mean Erosion			Standard Deviation (SD) (cy/ft)		Mean+SD
	XS1 (cy/ft)	XS2 (cy/ft)	Total (Mcy)	XS1	XS2	Total (Mcy)
Bolivar						
SINGLE, Low	18.8	18.4	2.5	8.0	7.5	3.5
SINGLE, High	15.7	16.0	2.1	6.5	6.3	2.9
DUAL, Low	34.2	32.0	4.4	10.0	9.8	5.7
DUAL, High	30.0	28.0	3.8	9.6	9.4	5.1
Galveston						
SINGLE, Low	18.8	18.4	1.8	8.0	7.5	2.5
SINGLE, High	18.4	17.6	1.7	7.4	7.3	2.4
DUAL, Low	34.2	32.0	3.2	10.0	9.8	4.1
DUAL, High	32.0	30.4	3.0	10.6	9.9	4.0

Rebuild frequency

The primary goal of the stochastic simulation was to determine the most effective renourishment rate. The limit state for rehabilitation is dune height reduction of 50% or more. This parameter was tracked throughout each and every storm. If the limit state was exceeded (the dune height fell below 50% of the original height), the beach profile was rebuilt to the original as-built profile prior to the next storm. A basic renourishment criterion of loss of half of the as-built dune height provided a heuristic optimized CSRM with relatively few periods where there was little to no flood limiting landform while the renourishment rate was roughly consistent with national average rates. As stated in the previous section, other limit state criteria were not necessary because there was relatively little net erosion of the beach seaward of the dune.

The mean and mean+1 standard deviation of number of rebuilds over all life cycles were computed. Table 14 summarizes the rebuild statistics for all alternatives, profiles, and RSLC scenarios. The dual dune required significantly fewer rebuilds than the single dune. The dual dune is being rebuilt on a 6-10 year cycle, depending on the scenario, while the single dune is rebuilt on a 3.5 to 6 year cycle. The high RSLC condition required significantly more rebuilds than the low. The values are plotted in Figure 63.

Figure 63. Number of rebuilds per 50 year life cycle, average and average+1 standard deviation. TB1 is, for example, XS1 Bolivar and T2G is for XS2 Galveston.

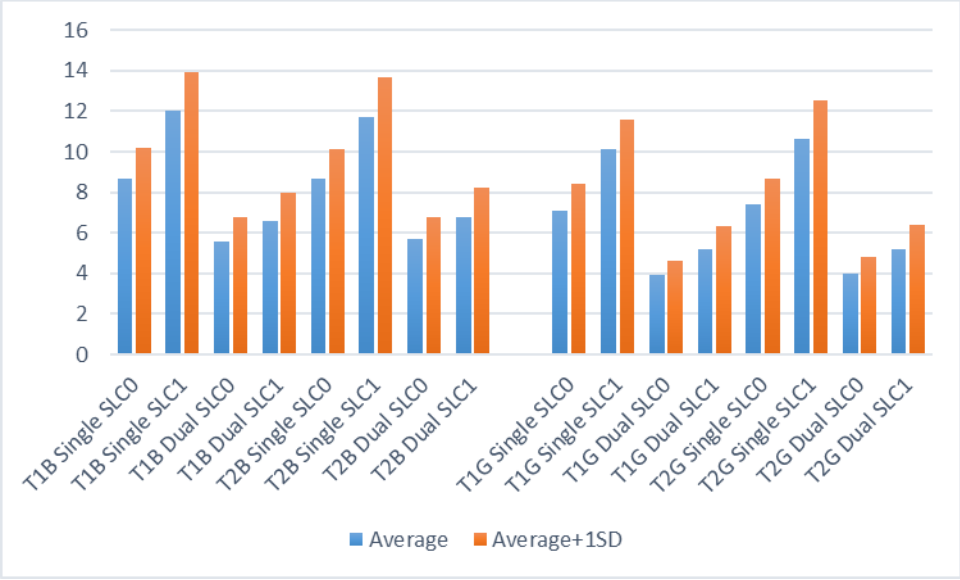

Table 14. Profile rebuild rate for various profiles, alternatives and scenarios

Alternative and Scenario	Number of Rebuilds per 50 years		
	Mean	Standard Deviation	Mean + Standard Deviation
Bolivar1 SINGLEDUNE USACELow RSLC	8.7	1.5	10.2
Bolivar1 SINGLEDUNE USACEHigh RSLC	12.0	2.0	13.9
Bolivar1 DUALDUNE USACELow RSLC	5.6	1.2	6.8
Bolivar1 DUALDUNE USACEHigh RSLC	6.6	1.5	8.0
Bolivar2 SINGLEDUNE USACELow RSLC	8.7	1.4	10.1
Bolivar2 SINGLEDUNE USACEHigh RSLC	11.7	2.1	13.7
Bolivar2 DUALDUNE USACELow RSLC	5.7	1.2	6.8
Bolivar2 DUALDUNE USACEHigh RSLC	6.8	1.3	8.2
Galveston1 SINGLEDUNE USACELow RSLC	7.1	1.3	8.4
Galveston1 SINGLEDUNE USACEHigh RSLC	10.1	1.5	11.6
Galveston1 DUALDUNE USACELow RSLC	3.9	0.8	4.6
Galveston1 DUALDUNE USACEHigh RSLC	5.2	1.1	6.3
Galveston2 SINGLEDUNE USACELow RSLC	7.4	1.3	8.7
Galveston2 SINGLEDUNE USACEHigh RSLC	10.6	1.9	12.5
Galveston2 DUALDUNE USACELow RSLC	4.0	0.8	4.8
Galveston2 DUALDUNE USACEHigh RSLC	5.2	1.2	6.4

Overtopping hazard

Overtopping as a result of both wave and steady overflow occurred during the life cycle simulations. CSHORE computed overtopping at each time step. These values were used to determine a total overtopping per storm using quadrature integration. The values were rank ordered and an empirical distribution computed for each life cycle. A Generalized Pareto distribution was fit to the overtopping data. The mean and confidence intervals of the probability distributions across all life cycles were computed. Example distributions are plotted in Figure 64 through Figure 67. While overtopping for a wide range of AEPs was computed, only the 1% AEP is listed in Table 15 where the values are volume of water (ft^3) per linear ft of shoreline for 1% AEP at 50% and 90% confidence limits.

Figure 64. AEP vs overtopping for Bolivar low RSLC scenario

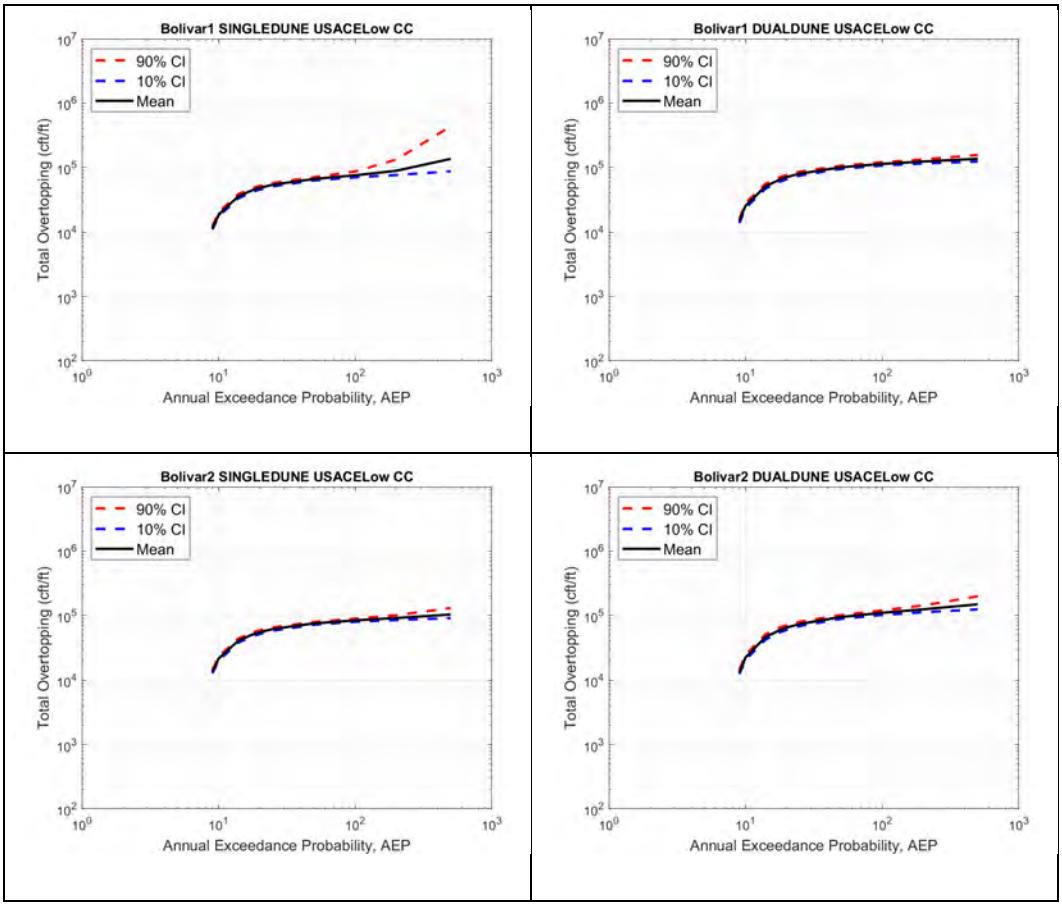

Figure 65. AEP vs overtopping for Bolivar high RSLC scenario

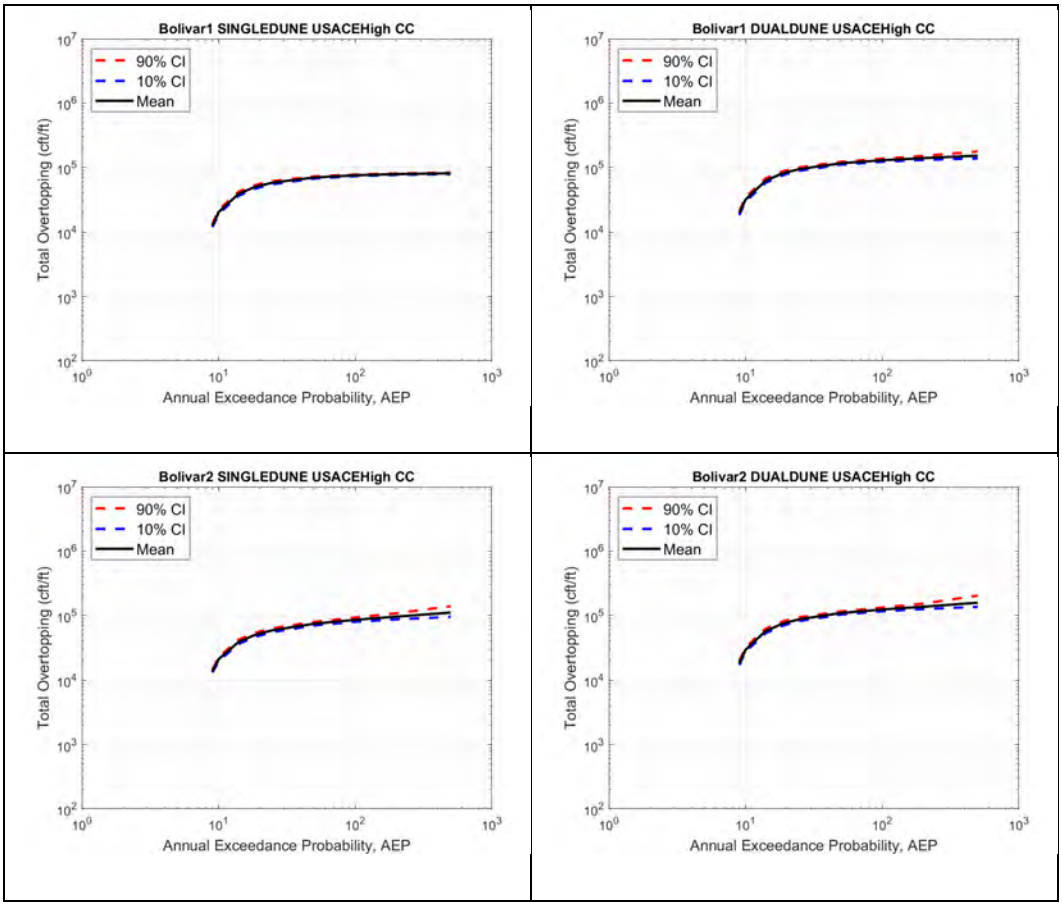

Figure 66. AEP vs overtopping for Galveston low RSLC scenario

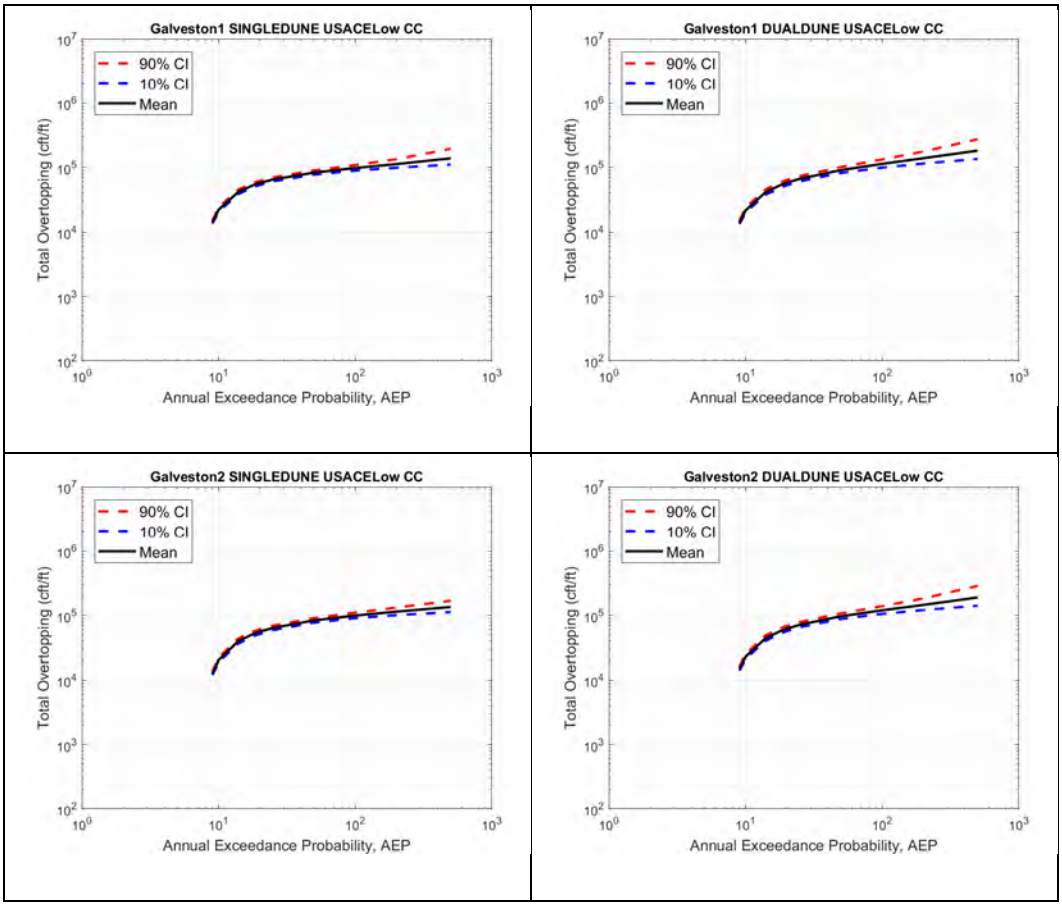

Figure 67. AEP vs overtopping for Galveston high RSLC scenario

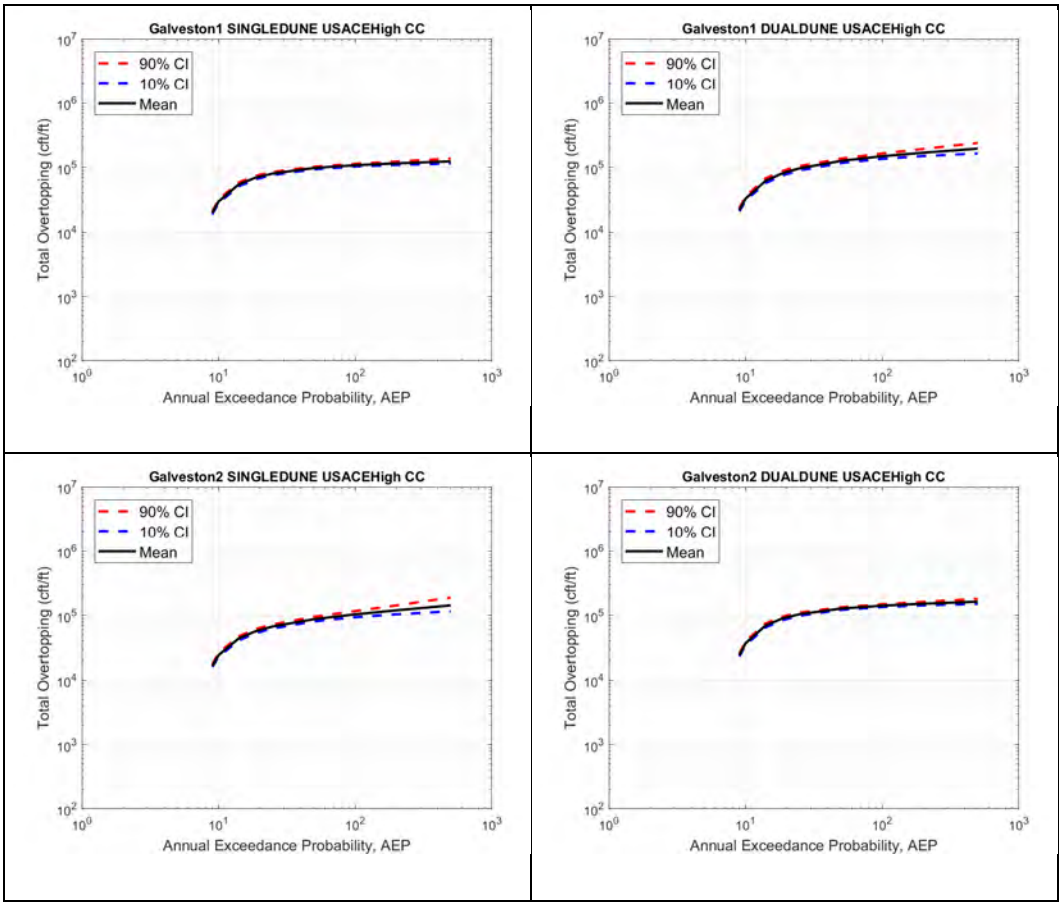

Table 15. Overtopping Q in ft^3/ft for 1% AEP 50% and 90% CLs for all scenarios.

Scenario	Annual Exceedance Probability	
	0.01 at 50%	0.01 at 90%CL
Bolivar1 SINGLEDUNE USACELow RSLC	7.55E+04	8.68E+04
Bolivar1 SINGLEDUNE USACEHigh RSLC	7.56E+04	7.77E+04
Bolivar1 DUALDUNE USACELow RSLC	11.4E+04	12.1E+04
Bolivar1 DUALDUNE USACEHigh RSLC	12.9E+04	13.7E+04
Bolivar2 SINGLEDUNE USACELow RSLC	8.40E+04	8.92E+04
Bolivar2 SINGLEDUNE USACEHigh RSLC	8.56E+04	9.28E+04
Bolivar2 DUALDUNE USACELow RSLC	11.0E+04	12.0E+04
Bolivar2 DUALDUNE USACEHigh RSLC	12.4E+04	13.3E+04
Galveston1 SINGLEDUNE USACELow RSLC	9.80E+04	10.9E+04
Galveston1 SINGLEDUNE USACEHigh RSLC	10.9E+04	11.4E+04
Galveston1 DUALDUNE USACELow RSLC	11.4E+04	13.3E+04
Galveston1 DUALDUNE USACEHigh RSLC	14.9E+04	16.5E+04
Galveston2 SINGLEDUNE USACELow RSLC	9.97E+04	11.1E+04
Galveston2 SINGLEDUNE USACEHigh RSLC	10.4E+04	11.7E+04
Galveston2 DUALDUNE USACELow RSLC	12.0E+04	14.0E+04
Galveston2 DUALDUNE USACEHigh RSLC	14.2E+04	14.9E+04

Overtopping discussion

The 1% AEP overtopping values listed in Table 15 are reasonable. A simple check using the broad crested weir equation with 1% AEP SWL and a completely eroded dune (elevation 5 ft) yields a value of roughly 1e6 ft^3/ft for a typical TC, for comparison.

The 1% AEP overtopping values and the probability distributions shown in this section suggest several interesting performance issues with respect to the dune profiles. The overtopping is large, compared to levees, and would represent significant flood depths in the lee of the dune. It is common to assume that the flood depth in the lee equals the depth on the seaward side of the dune for cases where the dune crest is submerged. During events represented by the 1% exceedance overtopping, that would likely be the case because the dune is likely to be nearly completely eroded. CSHORE showed that this is typically the case. Galveston overtopping rates are higher than those on Bolivar Peninsula.

Overtopping generally increases with RSLC. In addition, the dual dune has greater overtopping at the 1% exceedance level than the single dune. For

the dual dune, there is a longer period between rebuilds, because rebuilds are relatively infrequent, so there is relatively more time when the dune is vulnerable to major overtopping. This has significant implications on sediment management decisions. Based on the number of rebuilds, it appears as though the dual dune is a better alternative because it requires fewer rebuilds. However, the flood risk may be greater because the dune is at a lower elevation for longer periods throughout the life cycle. So the optimal economic approach may be a dual dune with relatively fewer major rehabilitations but additional minor maintenance in order to maintain the dune elevation and lessen the number of major overtopping events. The dual dune rebuild rate of 6 – 10 years could be extended to perhaps 15 – 20 years with minor maintenance to reshape the dune more frequently, thus reducing the risk of catastrophic overtopping events. This can be investigated with the life cycle simulation tool but there are several constraints required and it requires an iterative economic investigation which is beyond the scope of the study reported herein.

8 Summary and Conclusions

The U.S. Army Corps of Engineers Galveston District (SWG) is executing the Coastal Texas Protection and Restoration Feasibility Study (CTXCS) coastal storm risk management (CSRM) project. The project is currently in the feasibility phase. The primary goal is to develop CSRM measures that maximize net national economic development (NED) benefits. The study reported herein evaluated impacts from the following alternatives:

- Roughly 19 miles of beach, berm and dune along Galveston Island and 26 miles of beach, berm and dune along Bolivar Peninsula
- Ring levee around Galveston
- Surge barrier at Bolivar Roads
- Smaller navigation gates at Clear Creek and Dickinson Bayou

As part of the ongoing feasibility phase of the project, this report documents the coastal storm water level (surge, tide, relative sea level rise) and wave hazard and beach morphology modeling. Wave and water level impacts are assessed. Beach response is quantified for life cycles of coastal storms. All wave and water level modeling described herein also included the alternative of a closed surge barrier/navigation gate at Bolivar Roads (Galveston Entrance Channel).

A joint probabilistic model of historical tropical cyclone (TC) parameters was developed that spans the full range of tropical storm hazards from frequent, low-intensity storms to very rare, very intense storms. The probabilistic model describes the continuous spatial and temporal tropical storm coastal flood hazard. This probabilistic model was sampled efficiently to develop a suite of 660 TCs that characterize the coastal storm flood hazard for Texas. This suite was further subsampled efficiently to develop a suite of 170 synthetic tropical storms that effectively capture the flood hazard for the Galveston and Galveston Bay region. Wind and pressure fields were developed for the 660 TCs using the Planetary Boundary Layer (PBL) model.

The CSTORM coupled surge and wave modeling system was used to accurately quantify the surge and wave hazards. New model meshes were developed from very high-resolution land and sub-aqueous surveys for with- and without-project scenarios. With-project meshes include the proposed Bolivar Roads surge barrier, Galveston ring barrier, smaller

navigation gates at Clear Creek and Dickinson Bayou and the beach, berm and dune measures. The new meshes provide the highest resolution regional surge and wave modelling done to-date for the region. The CSTORM model was validated against historical storms and then used to model the 170 synthetic TCs. The storms were run on 2 relative sea level change (RSLC) scenarios for with- and without-project meshes. These RSLC scenarios are: 1. SLC0 corresponding to historical sea level change rate, and 2. SLC1 corresponding to a high rate. A third intermediate RSLC, SLC2, was applied within the morphological modeling.

Flood hazard exposure and impacts of the project features were quantified and are illustrated on a by-storm basis for both moderate and extreme tropical cyclones. By-storm results generally showed significant reduction of water levels in Galveston Bay as a result of the CSRM project features, as expected. Hazard curves for the CSTORM output over the entire state of Texas were computed for the various alternatives and scenarios. Alternatives included no project, with the ring levee and Surge Barrier closed and for the case with the ring levee, Surge Barrier closed and the beach-dune system. Annual exceedance probabilities (AEP) were computed for the range of 1 to 0.0001 for peak storm water level (SWL) and wave height (H_{m0}). Both mean values and confidence limits (CL) were computed at roughly save point locations spanning the Texas coast, both inland and offshore. SWLs at the 1% AEP were reported at specific transects spanning Galveston Island and Bolivar Peninsula. These data generally showed that the 1% AEP SWL increased to around 15 ft in the nearshore as a result of wave setup but decreased across the landforms as a result of the dunes and other high ground.

Historical morphological performance of Galveston Island and Bolivar Peninsula was relevant to the present study. In particular, net alongshore sediment transport rates and shoreline recession/accretion were applicable to the morphological modeling. Prior recent USACE studies covered this topic in detail so the results of those studies were summarized herein.

A suite of historical non-tropical storms was developed using a peaks-over-threshold sampling technique with measured water levels and historical hindcast waves offshore. These storms produced relatively minor responses compared to the tropical storms and did not impact the

extremal statistics of SWL but were required for the morphological modeling because frequent minor events can erode the beach.

The CSHORE beach morphology model was used to model cross-shore sediment transport during significant storm events. Results from prior geomorphological, geologic and beach morphology studies were used as a basis for defining the modeling configurations and constraints. These include the sand and clay layer thicknesses, longshore sediment transport, longterm erosion, and beach sediment gradation. Four reaches were defined spanning the length of the beach-dune alternative, two each for Galveston Island and Bolivar Peninsula. Two dune configurations were modeled, each consisting of single and dual dune configurations. So four total profiles were modeled. All 170 TC storms and all non-tropical storms were modeled individually.

For stochastic assessment of the beach morphology, the CSHORE model was embedded in a time-dependent Monte Carlo sampling scheme within the larger StormSim stochastic modeling system. The climatology consisted of tropical storms and non-tropical storms. The number of storms per year was Poisson distributed which were defined according to the non-tropical and TC historical storm rates. Individual TC storms were sampled according to their probability masses. Each storm was modeled as a time series of wave and water level conditions. A convergence test was conducted and it was determined that 30 life cycles at 50 years each produced a stable statistical response. The waves and water levels for each storm were combined with a random tidal time series and each RSLC scenario. The simulations progressed from time step to time step with CSHORE computing the morphology change for each storm. During the simulation, the damaged profile from a given storm was used as the starting profile for the next event. Beach profile and hydrodynamic parameters including water levels and overtopping were recorded throughout the life cycle. The profiles were tracked at key locations. The beach was rebuilt to the original profile if the dune height reduction exceeded 50%.

Non-tropical storms were shown to produce only slight profile responses but were frequent so the total impact on profile evolution was significant. Tropical storms had dramatic effect on the dune with near complete destruction if the dune crest was submerged. The berm did not show significant erosion throughout the life cycles. However, the dune did

degrade with time. Degradation of the dune caused sediment to be transported from the dune to the berm and then to the swash area of the beach so the dune acted as a somewhat inefficient renourishment source for the berm and beach.

A primary goal of the stochastic simulation was to define the number of rebuilds during a life cycle. A basic renourishment criterion of loss of half of the as-built dune height provided a heuristic optimized CSRM that limited the condition where there was little to no flood limiting landform while requiring a renourishment rate roughly consistent with national average rates. The mean and mean+1 standard deviation of the number of rebuilds from 30 life cycles is reported. It was found that a single dune on Bolivar Peninsula with an initial elevation of 14 ft, NAVD88, yielded renourishment rates of 10.2 and 13.9 rebuilds per 50 years for RSLC scenarios low and high, respectively, at the mean+1SD quantile. That is, in a given 50-year period, at the low RSLC scenario, the beach was rebuilt to the as-constructed condition an average of 10.2 times. These rates are the average across the two reaches. Similarly, a dual dune configuration for Bolivar yielded renourishment rates of 6.8 and 8.1 rebuilds per 50 years. For Galveston Island single dune, the simulation yielded renourishment rates of 8.6 and 12.1 rebuilds per 50 years for RSLC scenarios low, medium and high, respectively. That is, in a given 50-year period, at the low RSLC scenario, the beach was rebuilt to the as-constructed condition an average of 10.2 times. For Galveston Island dual dune, the simulation yielded renourishment rates of 4.6 and 6.4 rebuilds per 50 years for RSLC scenarios low and high, respectively.

Total wave and overflow overtopping for each storm was computed. Probability distributions for each life cycle were computed and then an average and 90% confidence limit were computed across all life cycles. These statistics correspond to overtopping criteria used for levees. In general, the total overtopping at 1% AEP is governed by TC that inundate the dune. The total overtopping at the 1% AEP is roughly 10^6 ft^3/ft. Interestingly, a counter-intuitive outcome was that the dual dune configurations on both Bolivar Peninsula and Galveston Island had higher overtopping than the single dune because the dual dune is not rebuilt as often so the average dune elevation is lower. A potential mitigation of this issue is to stretch out the major rehabilitation rebuilds and add periodic minor maintenance to maintain the height of the dune. These sediment management decisions require economic optimization that could be done

with iterative application of the StormSim morphology model described herein.

References

Anderson, T. R., C.H. Fletcher, M.M. Barbee, L.N. Frazer, B.M. Romine, (2015). "Doubling of coastal erosion under rising sea level by mid-century in Hawaii". Natural Hazards. 78 (1): 75–103. doi:10.1007/s11069-015-1698-6. ISSN 0921-030X

Becker, J. J., D. T. Sandwell, W. H. Smith, J. Braud, B. Binder, J. Depner, D. Fabre, J. Factor, S. Ingalls, S.-H. Kim, R. Ladner, K. Marks, S. Nelson, A. Pharaoh, R. Trimmer, J. Von Rosenberg, G. Wallace, P. and Weatherall, (2009). Global Bathymetry and Elevation Data at 30 Arc Seconds Resolution: SRTM30_PLUS, Marine Geodesy,32(4): 355-371.

Bender, C., J. M. Smith, A. Kennedy, and R. Jensen. (2013). STWAVE simulation of Hurricane Ike: Model results and comparison to data. Coastal Engineering 73: 58–70.

Bunya, S., J. Westerink, J. C. Dietrich, H. J. Westerink, L. G. Westerink, J. Atkinson, B. Ebersole, J. M. Smith, D. Resio, R. Jensen, M. A. Cialone, R. Luettich, C. Dawson, H. J. Roberts, and J. Ratcliff. (2010). A high-resolution coupled riverine flow, tide, wind, wind wave and storm surge model for Southern Louisiana and Mississippi: Part I-Model development and validation. Monthly Weather Review 138:345–377.

Cialone, M A., T. C. Massey, M.E. Anderson, A. S. Grzegorzewski, R. E. Jensen, A. Cialone, D. J. Mark, K. C. Pevey, B. L. Gunkel, T. O. McAlpin, (2015). North Atlantic Coast Comprehensive Study (NACCS) Coastal Storm Model Simulations: Waves and Water Levels. ERDC/CHL TR-15-14. Vicksburg, MS: U.S. Army Engineering Research and Development Center.

Cooper, J. A. G., O.H. Pilkey, (2004). "Sea-level rise and shoreline retreat: time to abandon the Bruun Rule". Global and Planetary Change. 43 (3–4): 157–171. doi:10.1016/j.gloplacha.2004.07.001. ISSN 0921-8181.

Dickinson, R. E., A. Henderson-Sellers, P. J. Kennedy, (1993). Biosphere-Atmosphere Transfer Scheme (BATS) Version le as Coupled to the NCAR Community Climate Model, NCAR Technical Note: NCAR/TN-387+STR, Climate and Global Dynamics Division, National Center for Atmospheric Research, Boulder, Colorado, August, 2993.

Dietrich, J. C., S. Bunya, J. J. Westerink, B. A. Ebersole, J. M. Smith, J. H. Atkinson, R. Jensen, D. T. Resio, R. A. Luettich, C. Dawson, V. J. Cardone, A. T. Cox, M. D. Powell, H. J. Westerink, and H. J. Roberts. (2010). A high-resolution coupled riverine flow, tide, wind, wind wave and storm surge model for Southern Louisiana and Mississippi: Part II-Synoptic description and analysis of Hurricanes Katrina and Rita. Monthly Weather Review 138:378–404.

Dietrich, J. C., J.J. Westerink, A. B. Kennedy, J. M. Smith, R. E. Jensen, M. Zijlema, L. H. Holthuijsen, C. Dawson, R. A. Luettich Jr, M. D. Powell, V. J. Cardone, A. T. Cox, G. W. Stone, H. Pourtaheri, M. E. Hope, S. Tanaka, L. G. Westerink, H. J. Westerink, and Z. Cobell, (2011). "Hurricane Gustav (2008) waves and storm surge: Hindcast, synoptic analysis, and validation in Southern Louisiana." Mon. Weather Rev., 139(8), 2488–2522.

Federal Emergency Management Agency (FEMA) (2011). Flood Insurance Study: Coastal Counties, Texas: Joint Report prepared for Federal Emergency Management Agency by the Department of the Army, U.S. Army Corps of Engineers, Washington DC.

Frey, A., A. Morang, and D.B. King, (2013). Galveston Island, Texas, Sand Management Strategies, ERDC/CHL TR-16-13. Vicksburg, MS: U.S. Army Engineering Research and Development Center.

GLCC (2017). USGS-GLCC Ver.2: Global Land Cover Data Base Version 2.0, https://lta.cr.usgs.gov/glcc/globdoc2_0#intro, Accessed on Jan. 26, 2017.

Gonzalez, V.M., N.C. Nadal-Caraballo, J.A. Melby, M.A. Cialone. 2019. Quantification of uncertainty in probabilistic storm surge models: literature review. ERDC/CHL SR-19-1. Vicksburg, MS: U.S. Army Engineer Research and Development Center.

Hench, J. L., R. A. Luettich, Jr., J. J. Westerink and N. W. Scheffner, (1995), ADCIRC: an advanced three-dimensional circulation model for shelves, coasts and estuaries, report 6: development of a tidal constituent data base for the Eastern North Pacific, Dredging Research Program Technical Report, U.S. Army Corps of Engineers Waterways Experiment Station, Vicksburg, MS.

Homer, C. G., J. A. Dewitz, L. Yang, S. Jin, P. Danielson, G. Xian, J. Coulston, N. D. Herold, J. D. Wickham, K. and Megown, (2015). Completion of the 2011 National Land Cover Database for the conterminous United States-Representing a decade

of land cover change information. Photogrammetric Engineering and Remote Sensing, v. 81, no. 5, p. 345-354

Hope, M. E., J. J. Westerink, A. B. Kennedy, P. C. Kerr, J. C. Dietrich, C. Dawson, C. Bender, J. M. Smith, R. E. Jensen, M. Zijlema, L. H. Holthuijsen, R. A. Luettich, M. D. Powell, V.J. Cardone, A. T. Cox, H. Pourtaheri, H. J. Roberts, J. H. Atkinson, S. Tanaka, H. J. Westerink, and L. G. Westerink. (2013). Hindcast and validation of Hurricane Ike (2008) waves, forerunner, and storm surge. Journal of Geophysical Research 118(9):4424–4460.

Jacobsen, R. W., N. L. Dill, A. Herrin, and M. Beck (2015). Hurricane Surge Hazard Uncertainty in Coastal Flood Protection Design, The J. of Dam Safety. 13(3):21-38.

King, D.B., (2007). Wave and beach processes modeling: Sabine Pass to Galveston Bay, Texas, shoreline erosion feasibility study. Technical Report ERDC/CHL TR-07-6. Vicksburg, MS: U.S. Army Engineer Research and Development Center.

Kobayashi, N. (2009). Documentation of Cross-Shore Numerical Model CSHORE, Research Report CACR-09-06. Center for Applied Coastal Research, University of Delaware, Newark, Delaware.

Johnson, B., Kobayashi, N. and Gravens, M. (2012). Cross-Shore Numerical Model CSHORE for Waves, Currents, Sediment Transport and Beach Profile Evolution, ERDC/CHL TR-12-22 Technical Report, Vicksburg, MS: U.S. Army Engineer Research and Development Center.

Komen, G. J. L. Cavaleri, M. Donelan, K. Hasselmann, S. Hasselmann, and P. A. E. M. Janssen, (1994). Dynamics and modeling of ocean waves. Cambridge University Press, United Kingdom. 532 pp.

Massey, T.C., R. Jensen, M. Cialone, Y. Ding, M. Owensby, N.C. Nadal-Caraballo (2018). A Brief Overview of the Coastal Texas Protection and Restoration Feasibility Study: Coastal Storm Model Simulations of Waves and Water Levels, Vicksburg, MS: U.S. Army Engineer Research and Development Center.

Melby, J. A., N. C. Nadal-Caraballo, J. Ratcliff, T. C. Massey, and R. Jensen, (2015a). Sabine Pass to Galveston Bay Wave and Water Level Modeling, ERDC/CHL Technical Report, Vicksburg, MS: U.S. Army Engineer Research and Development Center.

Melby, J. A., F. Diop, N. C. Nadal-Caraballo, D. Green, and V. M. Gonzalez, (2015b). Coastal Hazards System, Coastal Structures and Solutions to Coastal Disasters Joint Conference (COPRI), 9-11 September 2015, Boston, USA.

Melby, J. A., N. C. Nadal-Caraballo, V. M. Gonzalez, (2017). "Uncertainty in Coastal Structure Reliability", Coasts, Marine Structures and Breakwaters 2017 Conference, ICE, Liverpool, UK.

Melby, J. A., T.C. Massey, A.L. Stehno, N. C. Nadal-Caraballo, S. Misra, V. M. Gonzalez, (2020). Sabine Pass to Galveston Bay, TX, Pre-Construction, Engineering and Design (PED): Coastal Storm Surge and Wave Hazard Assessment, ERDC/CHL Technical Report, Vicksburg, MS: U.S. Army Engineer Research and Development Center.

Morton, R. A. (1974). "Shoreline changes on Galveston Island," Geological Circular 74-2, University of Texas at Austin, Bureau of Economic Geology, Austin, TX.

Morton, R. A. (1975). "Shoreline changes between Sabine Pass and Bolivar Roads, An analysis of historical changes on the Texas gulf shoreline," Geological Circular 75-6, University of Texas at Austin, Bureau of Economic Geology, Austin, TX.

Morton, R. A. (1997). "Gulf shoreline movement between Sabine Pass and the Brazos River, Texas: 1974-1996," Geological Circular 97-3, University of Texas at Austin, Bureau of Economic Geology, Austin, TX.

Nadal-Caraballo, N. C., Melby, J. A., Gonzalez, V. M. and A. T. Cox. (2015). Coastal Storm Hazards from Virginia to Maine. Technical Report ERDC/CHL TR-15-5, US Army Engineer R&D Center, Vicksburg, MS.

Nadal-Caraballo, N. C., A. B. Lewis, V. M. Gonzalez, T. C. Massey, and A. T. Cox. (2018a). Coastal Texas Protection and Restoration Feasibility Study, Probabilistic Modeling of Coastal Storm Hazards, Draft Technical Report, U.S. Army Engineer R&D Center, Vicksburg, MS.

Nadal-Caraballo, N.C., V.M. Gonzalez, and L. Chouinard. 2019. Storm Recurrence Rate Models for Tropical Cyclones. ERDC/CHL TR-19-4. Vicksburg, MS: U.S. Army Engineer Research and Development Center.

NLCD (2016). National Land Cover Database 2016 (NLCD 2016), https://www.mrlc.gov/viewerjs/, accessed on Dec. 1, 2016.

Paine, J. G. and Morton, R. A. (1989). "Shoreline and vegetation-line movement, Texas gulf coast, 1974 to 1982," Geological Circular 89-1, University of Texas at Austin, Bureau of Economic Geology, Austin, TX.

Paine, J. G., S. Mathew, and T. Caudle. (2011). Texas gulf shoreline change rates through 2007. Final Report Prepared for the General Land Office, Bureau of Economic Geology, John A. and Katherine G. Jackson School of Geosciences, University of Texas, Austin.

Resio, D. T., S. J. Boc, L. Borgman, V. Cardone, A. T. Cox, W. R. Dally, R. G. Dean, D. Divoky, E. Hirsh, J. L. Irish, D. Levinson, A. Niedoroda, M. D. Powell, J. J. Ratcliff, V. Stutts, J. Suhada, G. R. Toro, and P. J. Vickery. 2007. White Paper on estimating hurricane inundation probabilities. Consulting Report prepared by USACE for FEMA. Vicksburg, MS: U.S. Army Engineer Research and Development Center.

Resio, D. T., J. L. Irish, J. J. Westerink, N. J. Powell, (2013). The Effect of Uncertainty on Estimates of Hurricane Surge Hazards, Natural Hazards, 66:1443-1459.

SWAN Team (2017). Scientific and Technical Documentation for SWAN Cycle III version 41.20. Technical report from Delft University of Technology.

Tolman, H. L. (2014). User manual and system documentation of WAVEWATCH III Version 4.18. Technical Note. U.S. Department of Commerce., MMAB Contribution no 316.

United States Army Corps of Engineers (USACE). (2006). Louisiana Coastal Protection and Restoration (LACPR) Preliminary Technical Report. New Orleans, LA: U.S. Army Corps of Engineers District.

_____. (2009). Interagency Performance Evaluation Task Force (IPET). Performance evaluation of the New Orleans and southeast Louisiana hurricane protection system. Final Report of the Interagency Performance Evaluation Task Force. Washington, DC: Department of the Army, U.S. Army Corps of Engineers.

_____. (2011). Sabine-Neches Waterway Channel Improvement Project, Southeast Texas and Southwest Louisiana, CEMP-SWD (1105-2-10-a), Galveston, TX: U.S. Army Corps of Engineers District.

_____. (2013). Post Authorization Change Report Appendices, Morganza to the Gulf of Mexico, Louisiana. New Orleans, LA: U.S. Army Corps of Engineers District.

_____. (2014). Procedures to Evaluate Sea Level Change: Impacts, Responses, and Adaptation. Engineer Technical Letter ETL-1100-2-1. Washington, DC: Department of the Army, U.S. Army Corps of Engineers.

_____. (2017a). Final Integrated Feasibility Report – Environmental Impact Statement. Galveston, TX: U.S. Army Corps of Engineers District.

_____. (2019). Incorporating Sea Level Change in Civil Works Programs, ER-1100-2-8162. June 15, Washington, DC: Department of the Army, U.S. Army Corps of Engineers.

Westerink, J., J. C. Dietrich, H. J. Westerink, S. Tanaka, R. Martyr, M. Hope, L. Westerink, J. Atkinson, H. Roberts, R. Clark, S. Zou, Z. Cobell, C. Bender, R. Srinivas, J. Smith, R. Jensen, D. Resio, J. Ratcliff, H. Pourtaheri, N. Powell, D. Elzey, D. Ulm, C. Dawson, J. Proft, C. Szpilka, R. Kolar, K. Dresback, V. Cardone, A. Cox, M. Powell, (2011). Flood Insurance Study: Coastal Counties, Texas, Intermediate Submission 2: Scoping and Data Review, FEMA Region 6, USACE New Orleans District, 15 November 2011.

White, W. A., T. R. Calnan, R. A. Morton, R. S. Kimble, T. G. Littleton, J. H. McGowen, H. S. Nance, and K. E. Schmedes. (1985). Submerged lands of Texas, Galveston-Houston area: Sediments, geochemistry, benthic and macroinvertebrates, and associated wetlands. Austin, TX: Bureau of Economic Geology.

Appendix A White Paper on Prior Studies

Pre-Construction Engineering and Design Modeling of Coastal Hazards (Storm Surge and Waves) for *Sabine to Galveston* Hurricane Flood Protection System

November 26, 2018

Jeffrey Melby, Chris Massey, Norberto Nadal-Caraballo, Victor Gonzalez

US Army Engineer R&D Center, Vicksburg, MS

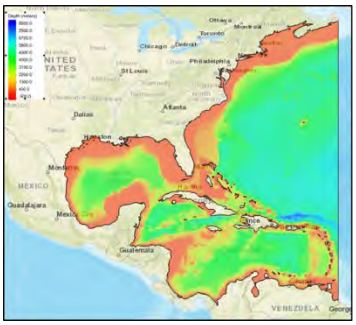

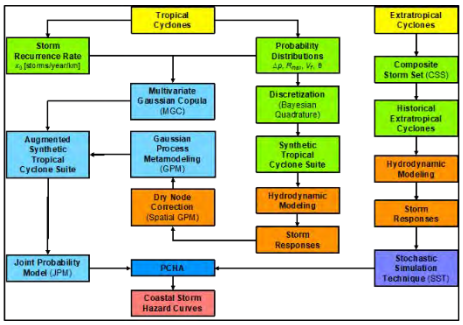

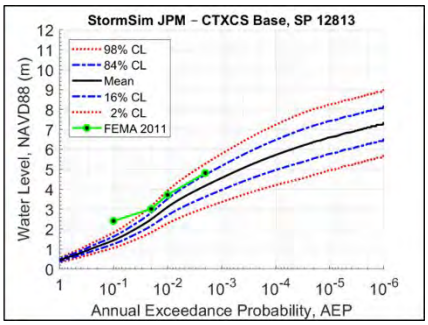

Executive Summary

This white paper presents a summary of recent coastal storm modeling supporting Sabine-to-Galveston coastal flooding analysis. The primary studies are the Federal Emergency Management Agency (FEMA) Region VI Risk Mapping, Analysis and Planning (Risk MAP) study using 2008 conditions (FEMA 2011); the U.S. Army Corps of Engineers (USACE) feasibility study for flood risk management on the Sabine to Galveston portion of the Texas coast (S2G2015) (Melby et al. 2015); and the USACE Coastal Texas Protection and Restoration Feasibility Study (CTXCS) (Massey et al. 2018, Nadal-Caraballo et al. 2018).

Each of these studies took advantage of modern joint probability analysis of tropical storm parameters to develop a suite of tropical storms that adequately reflects the coastal storm hazard. Each study also used modern numerical hydrodynamic modeling of these storms to characterize the regional waves and water levels. However, each study did not fully characterize the hazard. The limitations or weaknesses related to the above modeling can be summarized as follows:

FEMA 2011

- Used separate technologies for Louisiana and Texas modeling creating a discontinuity in statistical response, such as 1% annual chance exceedance surge and wave height, near the LA-TX border
- Older uncoupled surge and wave modeling technologies
- Limited parameter sampling for JPM-OS resulting in poor parameter space resolution
- Limited response surface resulted in poor parameter space resolution in some cases
- Simple windowing approach with 333 km kernel size to determine alongshore spatial variation of storm probability. Estimated frequency of land-falling hurricanes at 1-deg of longitude increments starting at latitude 29.5 deg N which yielded inconsistent frequency distribution.
- Probability masses computed in a crude way, including errors in discretization, and not actual joint probability distribution using a correlation tree.
- Model uncertainty computed for known uncertainty (epsilon) terms but only half of the computed values were used. Uncertainty included in probability integration so result was a hazard curve near the 84% upper confidence limit (one standard deviation above the mean).

- High-fidelity modeling was not conducted in close proximity to hurricane flood protection systems (CSRM).
- Risk assessment of CSRM based primarily on 100 year average recurrence interval water level. Wave impacts, detailed wave analysis in the vicinity of CSRM, and multi-variate probability analysis of hazard was not done.
- Inland wave modeling produced intermittent output and lacked consistent quality to the point that it was not useful to define hazards over the entire flood protection system for engineering design.

S2G2015

This study mostly used FEMA 2011 modeling so the study suffered from some of the same problems as FEMA 2011. However storms where the primary influence was in the Sabine region near the TX-LA border were remodeled using updated surge and wave modeling software and consistent technologies from Louisiana to Texas. Risk assessment of CSRM was still based primarily on 100 year average recurrence interval water level. Wave impacts, detailed wave analysis in the vicinity of CSRM, and multi-variate probability analysis of hazard was limited.

CTXCS

The CTXCS modeling provided significant improvements in both the storm characterization through the JPM-OS and the regional storm surge and wave modeling. The related primary problems mentioned above were resolved in the CTXCS study. In particular, wave modeling is both continuous and of consistent quality throughout the region. The CTXCS modeling will provide a strong foundation for doing with-project regional modeling, detailed wave modeling in the vicinity of the CSRM, multi-variate probability analysis of the hazard, and accurate estimation of CSRM response and related flood risk.

Approach for Present S2G PED Study

The focus in this study is the Freeport, Port Arthur, and Orange County CSRMs. The approach for assessing the flood hazard will utilize the CTX base regional modeling for without-project waves and water levels. It is expected that a response-based approach will be used with the forcing for the hazard being defined by average annual exceedance values from a multivariate probability model. The multivariate response probability model will be conditioned on the JPM-OS storm probability model. Both aleatory and epistemic uncertainties will be included. Event-based modeling will be done with specific modeling

components to validate response-based results. Some details of the approach are being worked out in the first phase of the study but, in general, the expected study approach is as follows:

1. Sample CTX without-project CSTORM modeling corresponding to CSRM reaches (both storm-wise and from the multivariate statistical model.)
2. Refine CTX mesh/grids near CSRMs and include with-project alternatives.
3. Select subset of storms from original CTX modeling that influence statistical responses near CSRMs.
4. Compute with-project regional responses using CSTORM for subset of storms,
5. Construct multi-modal spectra from CTX modeling.
6. Construct Boussinesq near-structure two-dimensional models for CSRMs.
7. Compute response-based hazards (runup, overtopping, forces on walls, shear stresses on levees, etc.) using Boussinesq models and spectra from step 5. This will be done for specific statistical forcing conditions (e.g. 1% annual chance exceedance) and for specific extreme events. A surrogate of the Boussinesq model may be developed if time and funding allow. Empirical response models will be integrated where appropriate.
8. Compute simpler one-dimensional response near structure for both response-based and event-based approaches and compare to step 7 results. Goal is to develop simpler approach that provides adequate accuracy.
9. Sea level rise (SLR) will be incorporated by using the CTX simulations at 3 SLR levels. In this way, nonlinearities from the combination of SLR and surge will be included explicitely.
10. Compare computed hazards to limit states and compute reliability for different CL.
11. Iterate with variations of alternatives if required.

Introduction

The USACE is beginning Preconstruction, Engineering and Design (PED) of Hurricane Flood Protection Systems (CSRM) in the Sabine to Galveston, Texas (S2G) region. A number of flood risk studies have been completed for this region since Hurricane Ike in 2008. This whitepaper discusses modeling needs for the present PED of CSRM. Evaluation of the need focusses on prior flood risk studies conducted for the region since Hurricane Ike and their applicability to the present CSRM study. Three prior studies covered in the paper are the Federal Emergency Management Agency (FEMA) Region VI Risk Mapping, Analysis and Planning (Risk MAP) study using 2008 conditions (FEMA 2011); the U.S. Army Corps of Engineers (USACE) feasibility study for flood risk management on the Sabine to Galveston portion of the Texas coast (S2G2015) (Melby et al. 2015); and the USACE Coastal Texas Protection and Restoration Feasibility Study (CTXCS) (Massey et al. 2018, Nadal-Caraballo et al. 2018). Other studies have been conducted for the region but they either use the above study results for their base flood level or they use something similar. For example, various Galveston barrier studies conducted by Texas A&M-Galveston, Rice University (SSPEED Center), and Jackson State University-ERDC used specific storms for scenario analysis and to represent univariate return intervals.

Additional studies have been conducted by the various flood districts and FEMA (e.g. FEMA 2012a, Lynett 2018, Orange County 2012). Most of the above flood risk assessment studies were based on FEMA 2011 base flood elevations and some included updates to this analysis. Various regional flood risk studies also used specific univariate return interval event-based or scenario approaches primarily based on FEMA 2011 modeling (e.g. USACE SQRA, 2014). So the issues discussed herein are generally applicable to all flood risk studies conducted recently for the region.

While prior S2G region CSRM studies sought to understand flood risk, accurate quantification of risk and resilience was not possible for many reasons. First, most studies have used the FEMA 2011 modeling that has significant weaknesses when applied for engineering design purposes. The primary weaknesses are discussed in this whitepaper. Model uncertainty has not been fully quantified in prior studies. This includes climatology, flood hydrodynamic, and statistical numerical models as well as bathymetric and topographic data and hydrodynamic measurements. Our understanding of, and ability to model, coastal storm flood physics and storm probability combined with improvement of numerical technologies has advanced

significantly in the last 15 years, leading to a reduction of uncertainty. However, perhaps more importantly, only in the last few years has there been increased confidence that the complete range of uncertainty can be included in risk estimates.

Prior studies were founded in event-based analysis. Usually, event-based approaches are in the context of FEMA NFIP studies where a 1% annual chance exceedance (ACE) water level is defined. So the hazards are based on a 1% water level. These hazards include flood depths, wave and steady flow overtopping, hydraulic loads, scour, debris loading, and other responses. For coastal studies where wind and waves are important contributors to these hazards, infrastructure performance prediction for a range of hazards is required for understanding risk and resilience and an NFIP approach is far too simple to properly characterize risk. Hydraulic loads, overtopping, and erosion computation on CSRM structures require careful consideration of the nonlinear hydrodynamic physics and joint probability of wind, waves, and water levels. Event-based approaches often include computation of wave height from a wave height-water level joint probability model and sometimes include computation of wave period, wave direction, and storm duration but this joint probability model is complex. A single statistic, such as the 1% ACE response, is multi-valued for hazards derived from waves and water levels and selection of the worst case requires computation over the entire hyper-surface. While this is not infeasible, it is always challenging and it is common to assume parameter independence or other simplifying assumptions that introduce unknown uncertainty. The focus for many coastal engineering studies is on numerical hydrodynamic models, but errors in computing statistics often overwhelm the numerical model accuracy, as will be discussed in this white paper. The Coastal Hazards System (Melby et al. 2015) (CHS) includes coastal storm climatological and hydrodynamic modeling simulations that span practical probability space. It also includes response statistics that are multi-variate, conditioned on the tropical storm parameters. These data can be leveraged for more accurate event-based design.

Recent advances in hurricane probabilistic modeling and computational capabilities have changed the flood risk paradigm. It is now practical to use response-based approaches to evaluate flood risk and resilience and include known significant uncertainties. Recent response-based approaches facilitate accurate risk and resilience assessment over the continuum of practical probability space. A wide variety of studies have been successfully implemented using response-based modeling including Gravens et al. (2007),

Males and Melby (2012), Melby (2009), Melby et al. (2015a), USACE (2009a), and USACE (2012). The CHS was specifically designed to facilitate the above types of response-based simulations. The above references include discussion of USACE software systems that can read CHS storm simulations and their relative probabilities and perform accurate flood risk computations. These software systems include Beach-fx, Generation II Coastal Risk Model (G2CRM), and StormSim. In addition, HEC-FIA is a response-based risk analysis software package that does similar analysis for inland flooding. This type of approach is a transformational development in flood risk evaluation and its application for S2G using the most recent modeling strategies will guarantee a significant improvement in flood risk understanding and improved actions in mitigating flood risk for the S2G region.

FEMA Region VI's Risk MAP Study

Comprehensive coastal storm modeling was completed for coastal Texas under FEMA Region VI Risk Mapping, Analysis and Planning (Risk MAP) study using storms and bathymetry and topography data available through 2008 (FEMA 2011). This study utilized what has become a standard approach for flood risk studies involving coastlines exposed to tropical cyclones. The study began with Joint Probability Method of Optimum Sampling (JPM-OS) methodology to characterize the probabilistic nature of coastal tropical storms and associated responses including storm wind and pressure fields, surge, and waves. The HURDAT2 database of historical tropical storm climatology was used to define a joint probability model of hurricane parameters. The particular approach utilized a response surface technique and included a fair amount of subjective analysis (FEMA 2011) and this model was sampled to yield a set of 446 synthetic tropical storms, 223 for Texas North and 223 for Texas South.

Characteristics of the JPM-OS approach for FEMA 2011:

- Storm tracks created at regular spacing.
- HURDAT2 database sample 1941 – 2005 landfalling storms. Parameters sampled were landfall location (latitude and longitude), central pressure (C_p), radius to maximum wind speed (R_{max}), translational speed (V_t), and heading direction (θ). As is typical, central pressure deficit $\Delta_p = 1013 - C_p$ was used instead of C_p to describe storm intensity. Joint probability distribution created using these parameters.
- "Optimal sampling" based on engineering judgment. JPM discretization and weights assigned based on expert judgement. Four storm

intensities: 900, 930, 960 (high intensity) and 975 hPa (low intensity) resulting in poor parameter space resolution. The storm suite included 152 low frequency and 71 high frequency storms for TX North and TX South regions.

- Limited response surface (RS) that interpolated surge as a function of central pressure and radius of maximum winds, omitting impacts from other relevant parameters such as translational speed, heading direction, Holland B parameter.
- Initial storm suite on the order of 100-500 tropical cyclones. Increased central pressure and R_{max} parameter resolution through response surface.
- Simple windowing approach with 333 km kernel size to determine alongshore spatial variation of storm probability. Estimated frequency of landfalling hurricanes at 1-deg of longitude increments starting at latitude 29.5 deg N which yielded inconsistent frequency distribution.
- Probability masses computed in a crude way, including errors in discretization, and not actual joint probability distribution using a correlation tree.
- Model uncertainty computed for known uncertainty (epsilon) terms but only half of the computed values were used. Uncertainty included in probability integration so result was a hazard curve near the 84% upper confidence limit (one standard deviation above the mean). This is described below.

Wind and pressure fields for the 446 synthetic storms were created in collaboration between Ocean Weather Inc. (OWI) and ERDC using the Planetary Boundary Layer (PBL) TC96 Model. The model was driven with TROP files of hurricane parameters at 1 hour intervals. A single set of wind and pressure files was created for each storm that covered the Gulf of Mexico (GOM) domain. The GOM domain extended between longitudes -98.0 degrees west to -80.0 degrees west and from 18.0 degrees north to 31.0 degrees north latitude at 0.05 degree resolution. A fifteen 15.0 minute time step between fields for the wind and pressure files was used. The wind and pressure fields were used as forcing for both the wave and surge modeling. Five historical tropical events, Hurricane Carla 1961, Hurricane Allen 1980, Hurricane Bret 1999, Hurricane Rita 2005, and Hurricane Ike 2008 were modeled.

The FEMA study utilized Texas-specific modeling for most of the region but also took advantage of prior modeling that was done for the Louisiana FEMA Risk MAP study (USACE 2009a). Water levels and waves were computed using three different models: 1) the deep water Wave Model (WAM) model (Komen et al. 1994), used for producing offshore wave boundary conditions for use

with 2) the nearshore Steady-state Wave (STWAVE) model (Smith et al. 2001, Massey et al. 2011), and 3) the Advanced Circulation (ADCIRC) model (ADCIRC 2017, Luettich et al. 1992, Kolar et al. 1994), which was used to simulate two-dimensional depth-averaged surge and circulation responses to the storm conditions. The computational domain for storm-surge modeling by ADCIRC contained the western North Atlantic, the Gulf of Mexico, and the Caribbean Sea. It covered an approximately 38° by 38° square area in longitudinal (from 98° W to 60° W) and latitudinal (from 8.0° N to 46° N) directions. The mesh consisted of approximately 3.35 million computational nodes and 6.68 million unstructured triangular elements with an open ocean boundary specified along the eastern edge (60° W longitude). The largest elements were in the deep waters of the Atlantic Ocean and the Caribbean Sea (Figure A1, Figure A2), with element sizes of about 58 km as measured by the longest triangular edge length. The smallest elements resolved detailed geographic features such as tributaries and control structures like levees and roadways. The minimum element size was approximately 14 m. Water depths ranged from almost 8,000 meters in the deep Atlantic to over 100 meters of land elevation (above mean sea level).

For wind and coastal hydrodynamic modeling by ADCIRC, land cover and land use (LCLU) data was used to determine spatially distributed values of bottom friction coefficients (or Manning's *n*), canopy coefficients, and surface roughness length for the effect of directional wind reduction, in response to spatial changes of land cover and land use over the study area. These values were set in ADCIRC's nodal attribute (fort.13) file.

Figure A1. Map showing the ADCIRC model domain with topographic and bathymetric values represented as color contour plots

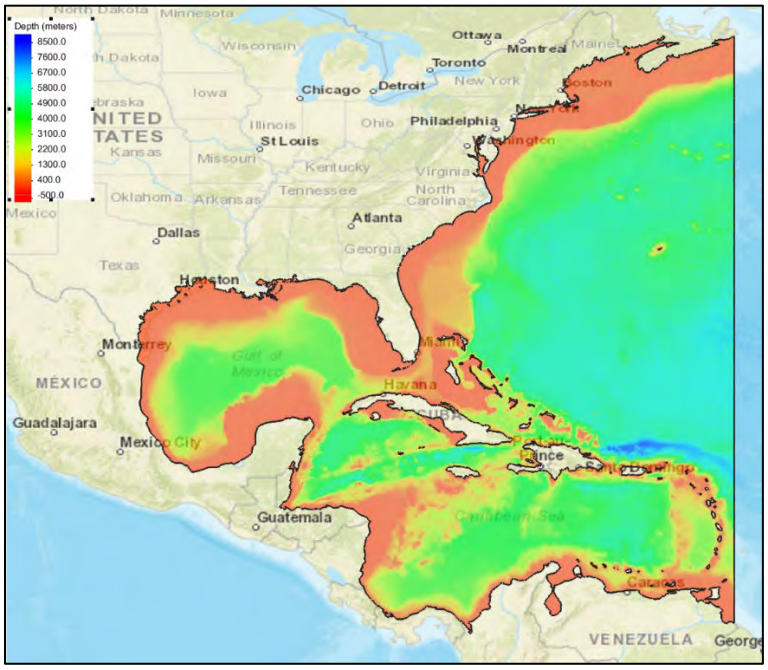

Figure A2. Map showing a close-up view of the topographic/bathymetric values in the TX/LA area of the TX FEMA ADCIRC mesh

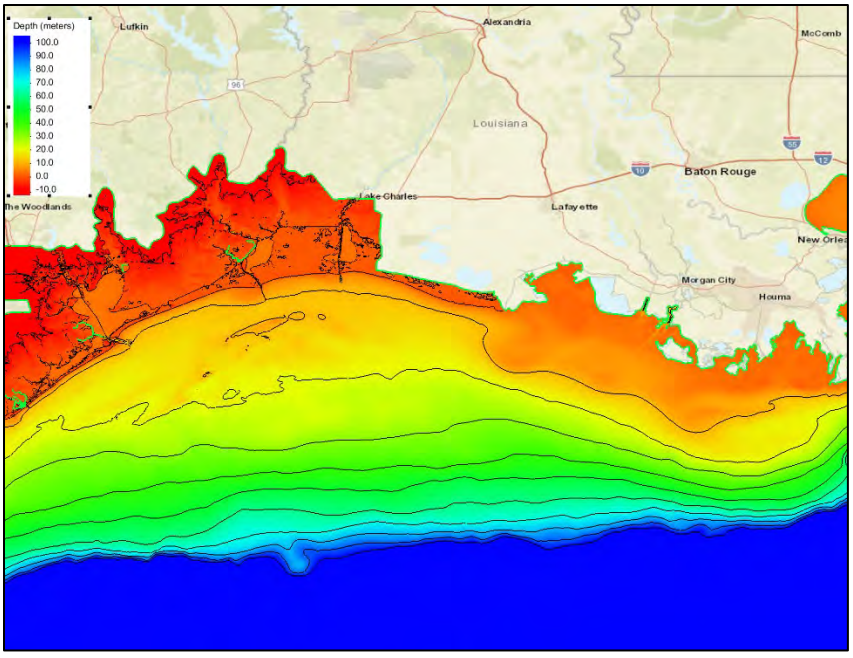

A single WAM grid was used and covered the Gulf of Mexico. Three regional-scale parent grid STWAVE domains covering the coast of Texas were used and

were executed in half-plane mode, which is described later, along with two local-scale "child" grids nested within the parent grids. Each child grid used the same spatial resolution as the parent grid but was executed in full-plane mode. This parent-child nesting was required to both save computational time and to allow for full-plane computations in key areas. At the time of that study, STWAVE was not a parallelized code and thus could not solve large computational domains in full-plane mode due to time constraints and computer memory. The ADCIRC and STWAVE simulations were performed using loose coupling, which means that ADCIRC was run first without wave conditions in order to provide an initial water level to STWAVE. ADCIRC-only water levels and wind fields were then interpolated onto the STWAVE domain to be used as input conditions. The STWAVE parent and child grids were then run and the wave radiation stress gradients computed by STWAVE were interpolated onto the ADCIRC domain. Then ADCIRC was run a second time, including wave stress gradient forcing fields computed by STWAVE. STWAVE model runs were two days in duration and wave conditions were computed every 30 minutes. The STWAVE model was typically started approximately one day prior to landfall of the storm and lasted for one (1) day post landfall. This was standard practice at the time and was done regardless of the size or forward speed of the storm.

Figure A3. Map showing the wave model domains (WAM) and STWAVE used for the TXFEMA study

Figure A4. FEMA study modeling flowchart (FEMA 2011)

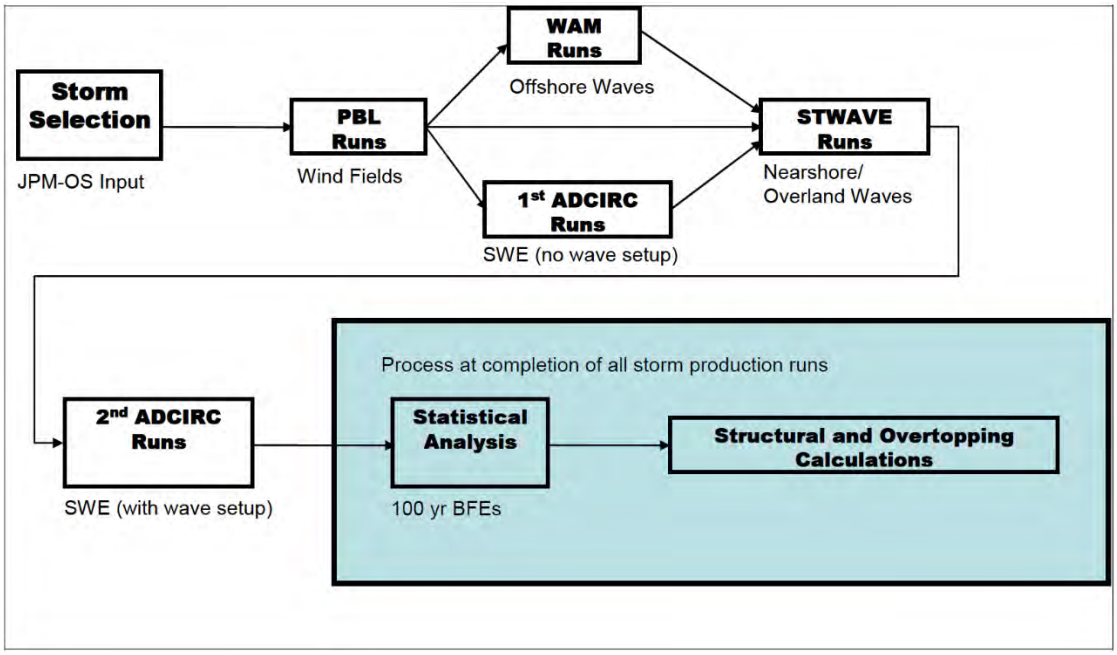

The FEMA Risk MAP Region VI study adopted a set of storms from the Louisiana Risk MAP study known as LA West storms. The modeling and statistics for the LA West region were completed separately from those of Texas and as a result there is a discontinuity in the results that occurs at the TX/LA state lines. Investigations have revealed that the biggest cause of the discontinuity is the different treatment of the wind drag coefficient in ADCIRC between the two studies, resulting in surge differences of 2 to 5 feet. The Garratt wind drag formula was used in the FEMA Texas study with a cap value of 0.002, instead of ADCIRC's default value of 0.0035 which was used in the LA West study. While this lower cap value was used to validate the ADCIRC setup for Hurricane Ike and a few other Texas storms as part of the FEMA study, it is inconsistent with the values used in the Louisiana IPET (IPET 2009) and other FEMA Risk Map studies as well as what was used in the NACCS (Cialone et al 2015).

The annual exceedance probability (AEP) of coastal storm hazards at a given site is a function of three main components: the recurrence rate of storms, the joint probability of characteristic storm parameters, and the individual storm responses. The joint probability of coastal storm hazards can be summarized by means of the JPM integral:

$$\lambda_{r(\hat{x})>r} = \lambda \int P[r(\hat{x}) + \varepsilon > r | \hat{x}, \varepsilon] \, f_{\hat{x}}(\hat{x}) f_{\varepsilon}(\varepsilon) d\hat{x} d\varepsilon$$

$$\approx \sum_i^n \lambda_i \, P[r(\hat{x}) + \varepsilon > r|\hat{x}, \varepsilon] \qquad \text{(A.1)}$$

where $\lambda_{r(\hat{x})>r}$= AEP of storm response r due to forcing vector $\hat{x}$; ε =unbiased error or epsilon term; $P[r(\hat{x}) + \varepsilon > r|\hat{x}, \varepsilon]$ = conditional probability that storm i with parameters $\hat{x}$ generates a response larger than r. The primary storm parameters commonly accounted for in the forcing vector $\hat{x}$ are: distance to reference location (x_0); central pressure deficit (Δp); radius of maximum winds (R_{max}), translation speed (V_f); and heading direction (θ). Secondary parameters may include: Holland B; and astronomical tide. As is typical, a discrete version of equation 1 was employed and a response surface was utilized to achieve a finer computational resolution. In Equation 1, for FEMA studies, it is common practice to include the epistemic uncertainty in the integral so that the AEP is defined at the upper 84% confidence limit. However, in the USACE, this practice has changed to externalize the epistemic uncertainty so that the level of uncertainty can be defined explicitly (Nadal-Caraballo et al. 2015). Epistemic uncertainty arising from modeling inaccuracy was incorporated into the joint probability model. The four uncertainty terms considered were

ε_1: deviation between a storm at a random tide phase and a zero tide level;

ε_2: deviation created by variation of the Holland B parameter;

ε_3: deviation created by variations in tracks approaching the coast; and

ε_4: deviation created primarily by errors in models and grids.

The uncertainties were generally considered independent except ε_4 which was considered to vary linearly with surge.

One of the primary issues that has plagued the reuse of the FEMA 2011 modeling is the inconsistent quality of wave modeling results. Many of the simulated storms had missing wave data. Additionally, it was common for there to be two neighboring points with essentially identical characteristics but very different wave data. These issues occurred in open water and on normally-dry land that was flooded. However, the problems were much more common in interior areas. The reasons for the poor wave data quality is unknown but CTXCS modeling described below did not have these problems.

USACE Sabine to Galveston Feasibility Study (S2G2015)

The following comments apply for both the S2G2015 study and the FEMA Region VI reanalysis for Orange County which were both done by ERDC using the data described below. For the S2G2015 Study, the storm suites, numerical hydrodynamic and statistical models were all updated.

New modeling was conducted for storms that impacted the Sabine region where there was a discontinuity between the Texas and Louisiana modeling as discussed above. The 223 FEMA 2011 TX North storms were used as a basis for the hazard for both Brazoria and Orange Counties. Thirty TX North storms were selected from the original 223 that produced significant flooding in the area of the Orange County CSRM. These storms were remodeled using the Coastal Storm Modeling System (CSTORM-MS) (Massey et al 2011) coupled ADCIRC and STWAVE for both without- and with-project conditions. Additionally, 31 LA West storms were selected that impacted the Sabine region and these were remodeled with CSTORM-MS. Then hazard statistics were computed using the 193 original FEMA-modeled storms, 30 S2G-modeled TX North storms, and 31 S2G-modeled LA West storms for without- and with-project conditions.

The existing ADCIRC and STWAVE setups that were used in the FEMA Risk MAP (FEMA_TX) study were adopted as a starting point, however, modifications to the model input control files were necessary in order to use the newer model source codes, which included the parallel version of STWAVE V6.0 as well as a newer version of ADCIRC's source code, version 50. A further change was that the coupling framework of the Coastal Storm Modeling System was used to perform dynamic two-way model coupling between ADCIRC and STWAVE, instead of the older and more computationally expensive loose file coupling. Since the updated version of STWAVE was now parallelized, nested child domains were not required. Recall they had the same resolution as the parent grids but were much smaller in domain size and used full-plane physics. With the parallelized version of STWAVE, it was possible to use the full-plane version of STWAVE for the full parent grids. For each of the models, the bathymetry and topographic values were left unchanged from the FEMA_TX study.

The ADCIRC mesh was modified to reflect the required increased resolution around the structures. With-project and without-project meshes/grids were constructed with identical resolutions so alternatives could be compared to the no-project base case. The ADCIRC mesh resolution was increased near the

structure and the bathymetry/topography elevations in the original ADCIRC mesh from the FEMA_TX study were linearly interpolated onto the new meshes. In addition, the ADCIRC FEMA_TX nodal attribute values, such as Manning's n values for friction, were also interpolated onto the two new meshes and used without alteration. All the with-project conditions existed within one STWAVE domain, the Texas NE grid. The with-project condition was added to the NE grid by updating the depth file to include the height of the flood wall structures that were a part of the with-project conditions.

Model stability issues were encountered while trying to reproduce the FEMA 2011 ADCIRC model validation results even with no mesh updates. While the ADCIRC model domain was highly resolved, there were issues with some structure features being insufficiently resolved, such as dune systems and jetties, which caused model run time instabilities for ADCIRC. To overcome some of those instabilities, in the FEMA 2011 study, an early form of solution slope limiting was used internally within ADCIRC for some (but not all) of the storms. The exact settings and triggering mechanism for using slope limiting were not able to be recovered for future use so model validations were not reproducible. Another stability issue was that a model setting in ADCIRC that controls the lower limit of bottom friction drag coefficients was set to zero. Setting this limit to zero is physically unrealistic and leads to a major source of model run time instabilities. This setting was employed in order to capture the Hurricane Ike forerunner. By comparison, a more reasonable value of 0.003 was used in the MSCIP study (USACE 2009b), in the Louisiana IPET studies (IPET 2009), and the NACCS study (Cialone et al. 2015). When this latter value is used for Hurricane Ike simulations, the water levels associated with the forerunner do not develop as high as recorded data and are not as high as when the zero value is used. However, when the 0.003 value is used, no slope limiting is required as the ADCIRC model remains stable. As part of another smaller study done for the same area, a value of 0.00026 was used as the lower limit. This value for the bottom friction coefficient (which depends on both water depth and Manning's n values) is consistent with lower limit values found in surge and tide studies of regions that are characterized by fine grain sediment bottoms. While its use improved the model results for storm surge levels for Hurricane Ike, its use requires that slope limiting be applied due to increased instances of model instabilities. As a compromise between model stability and better resolution of the Ike forerunner, a value of 0.003 was used for the S2G2015 study and did not require the use of slope limiting.

The 254 synthetic storms in the S2G2015 study were remapped onto a new joint probability model. The model was built with the approach shown in Figure A5 and discussed below.

Characteristics of the JPM-OS approach for S2G2015:

- Storm tracks created at regular spacing.
- HURDAT2 database sample 1940 – 2013 landfalling and bypassing storms. Parameters sampled were landfall location (latitude and longitude), Δ_p, R_{max}, V_t, and θ. Joint probability distribution created using these parameters.
- "Optimal sampling" based on hybrid approach using Bayesian Quadrature combined with structured discretization. Storm Recurrence Rates (SRR) were computed using Gaussian Kernel Function weighting. Weights for computing probability masses assigned to storms using Bayesian Quadrature resulting in a significant improvement in accuracy of the probability masses. All storm recurrence statistics computed at 200 locations along coast.
- Gaussian Kernel Function (GKF) with an optimized kernel size of 200 km was used to define SRR.
- No response surface was computed.
- Improved estimates of uncertainty (epsilon) terms and these were used to compute various confidence limits around mean rather than being included in hazard curve.
- The probability masses were computed in a more accurate way to better represent response hazard curves. The higher accuracy in the statistical approach resulted in over 1 m error correction over much of the coast.

S2G2015 wave simulations suffered from similar problems that plagued FEMA 2011 in that the inland wave modeling produced intermittent output and lacked consistent quality.

Figure A5. Typical joint probability approach employed by FEMA and USACE (NACCS)

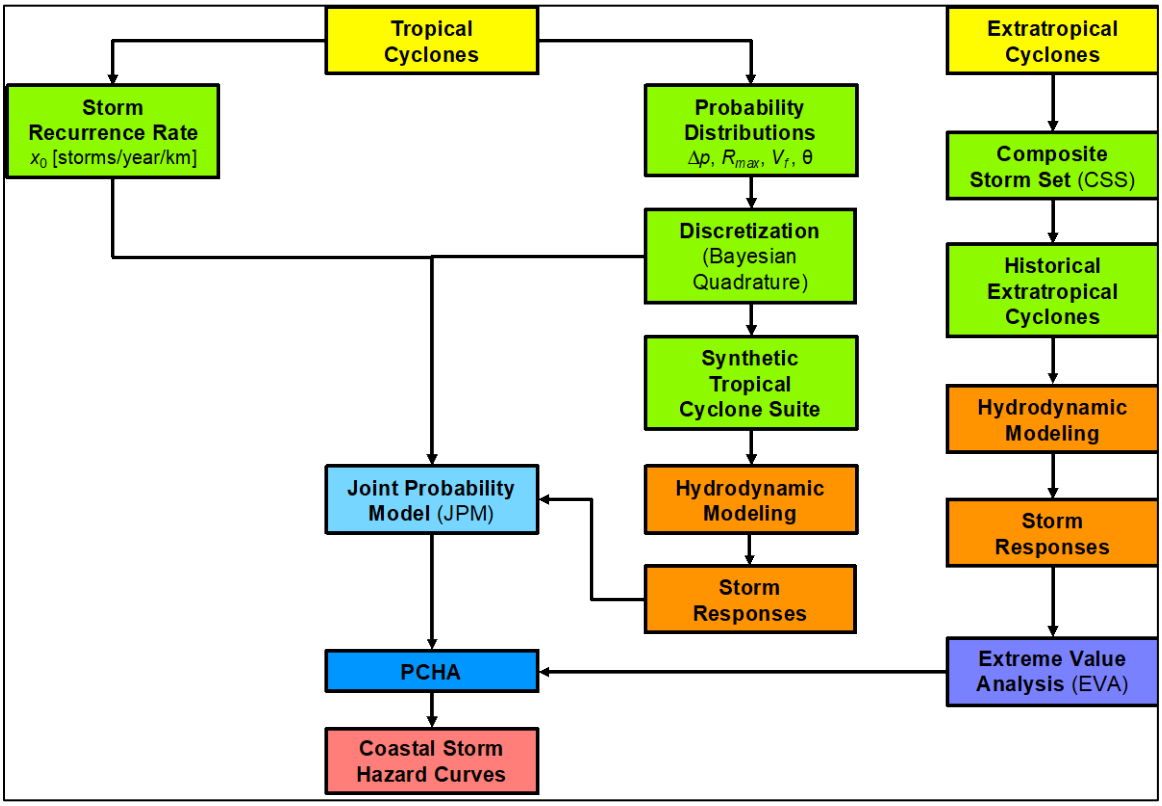

USACE Coastal Texas Protection and Restoration Feasibility Study (CTXCS)

The 2018 CTXCS modeling study was designed to correct the primary deficiencies identified in preceding sections, and apply these corrections over the entire TX coastline. The primary improvements included:

- Improved storm climatology physics and modeling technology
- Improved numerical model physics and modeling technology including fully coupled surge, circulation, and wave models and full plane wave model
- Improved bathymetry, topography, land use, ground cover data
- Increased overall resolution of all numerical models
- Used three wind/pressure domains to increase the extents of data and increased resolution
- Span state margins so there are no spatial discontinuities
- Increased model resolution near HPFS's
- Much broader range of validity tests
- Longer duration of hurricane data
- Improved statistical modeling technology
- Increased resolution of storm probability space
- Improved understanding of both aleatory and epistemic uncertainties
- More consistent modeling across entire probability space
- Model reproducibility
- Incorporation of surrogate meta-modeling technology

The above improvements combine to improve modeling accuracy and reproducibility and allow much more accurate estimation of risk. The surrogate models promote accurate modeling of the continuous storm probability space, which is a new and powerful capability. Further, the CTXCS modeling facilitates improvements in both response-based and event-based risk assessment as a result of the improvements listed above.

The ADCIRC and STWAVE model settings were selected in order to balance model accuracy and stability, while at the same time maintaining consistency with other studies in terms of physical processes. As such, a significant portion of the original ADCIRC mesh from the FEMA_TX Risk MAP study was used without alterations in the nearshore and inland areas. It was necessary to apply localized alterations to the mesh where under-resolved features caused model instabilities. Inland inundation extents were added to the mesh along the entire Louisiana, Mississippi and Alabama coastlines in order to improve

accuracy along the TX-LA border and to accommodate storm tracks that intersected with that portion of the coast. The STWAVE and WAM grid extents are shown in Figure A6. A fourth STWAVE grid was added to cover the Texas/LA coast. The Texas NE STWAVE grid was also recreated in order to change grid cell spacing from 200 meters to 150 meters. This allowed for better representation of with-project features and more accuracy.

Consistent ADCIRC model settings and parameters were selected and validated for using wind drag coefficient caps and the lower limit of bottom drag friction coefficients. Specifically, a lower limit coefficient of 0.002 was used for bottom friction and a Garratt wind drag coefficient cap of 0.003 was also used. It was necessary for solution slope limiting to be applied for some of the most intense storm simulations. In those cases the exact locations, values and procedures for applying it have been documented.

By recording all model changes and using the modern Coastal Storm Modeling System, reproducibility of model results is now certain. Model reproducibility is vitally important for accuracy and quality control, as well as for the current needs of comparing with- and without-project conditions. More details of the changes to the ADCIRC and STWAVE model setup are provided later.

A completely new set of synthetic storm conditions were created for the CTXCS study. In addition, ten historical tropical storms impacting the TX/LA area were selected for model validation and testing. The ten storms are hurricanes Audrey 1957, Carla 1961, Beulah 1967, Allen 1980, Bret 1999, Katrina 2005, Rita 2005, Gustav 2008, Ike 2008 and Isaac 2012. Three sets of wind and pressure fields were created for each of the storms, a Western North Atlantic (WNAT) domain, a Gulf of Mexico domain and a LandFall domain that was allowed to move from one storm track to another. The WNAT domain extended between 99.0 degrees west and 55.0 degrees west longitude and from 5.0 degrees north to 35.0 degrees north at 0.20 degree grid spacing. The GOM mesh extended between 98.0 degrees west to 80.0 degrees west longitude and from 18.0 degrees north to 30.96 degrees north latitude at 0.08 degree grid spacing. The LandFall domains were allowed to move depending on the storm track, however the domain size and resolution was the same for all storms, namely a 0.02 degree grid resolution was specified and the domain size was 3.0 degrees by 3.0 degrees centered on landfall locations. Using three domains with varying degrees of resolution and domain extents allows for proper resolution of deep water waves from outside the Gulf of Mexico, allows

for basin to basin scale interactions for circulation and improved resolution/definition of the storm at landfall locations.

As in the studies described above, the JPM-OS was used to characterize the probabilistic nature of coastal storms and associated responses. The HURDAT2 database of historical storms and their associated climatology was used as a data source for the JPM analysis. A joint probability model of hurricane parameters was sampled to yield a set of 660 synthetic tropical storms. Wind and pressure fields for the storms were created in collaboration between OWI and ERDC. The discrete set of storms provides an efficient but complete representation of the full range of potential storms that could impact the Texas coast. A total of 82 master storm tracks were created. For these tracks, four key storm parameters were perturbed: θ, Δ_p, R_{max}, and V_t. Storm intensities ranged from very low intensity storms with Δ_p = 8 mb to catastrophic category 5 hurricanes (on the Saffir-Simpson Wind Scale) with Δ_p = 148 mb. R_{max} ranged from approximately 5 miles (approx. 8 km) for very small storms to 66 miles (approx. 107 km) for very large storms. V_t ranged from 4 mph (approx. 7 km/h) to 27 mph (approx. 44 km/h). Further details of the JPM-OS approach and synthetic storm suite can be found in Nadal et al. (2018).

The Wave Model (WAM) was used to model the deep water wave contributions for each of the storms. The FEMA_TX study setup for the WAM model parameters was used and is considered standard. A single WAM grid system was used but was enlarged. The CTXCS domain is defined for the coastal areas of the state of Texas, in particular from the Texas-Louisiana state line to the U.S.-Mexico border. Accurately estimating the offshore wave conditions for the entire coastal area of Texas required developing the wave field grid for the entire Gulf of Mexico and extending into the Caribbean Sea and a small part of the western basin of the Atlantic Ocean. The WAM model was validated against the ten historical events.

The primary purpose of the WAM offshore wave generation is to provide boundary condition wave estimates to STWAVE as part of the input to the CSTORM simulations. The forms of the boundary condition wave estimates are defined by two-dimensional wave spectra that vary in space (x & y) and time, covering a discrete range of frequencies f, and directions θ. Setting the boundary locations for STWAVE is dependent on the nearshore, local domains defined in the CSTORM simulations, used specifically as input to STWAVE (Massey et al., 2011). As noted earlier, the full-plane version of STWAVE was

used for all grid domains. The bathymetry, topography, and Manning's *n* bottom friction values were interpolated from the updated ADCIRC mesh to be described later. A grid resolution of 200 m was selected for all the grids except for the TX-N grid, encompassing Galveston Bay, which used a 150 m value.

Figure A6. Maps showing the STWAVE grid boundaries in relation to the WAM boundary used for the CTXCS

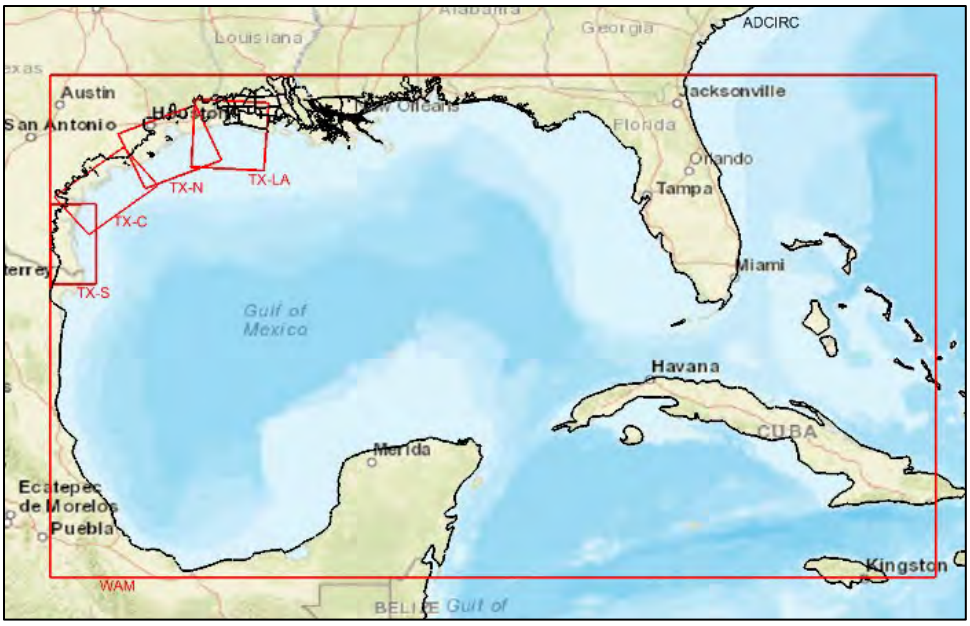

The STWAVE model setups and changes were also validated for the historical storms. STWAVE model simulation duration and time between wave computations was allowed to vary depending on the storm characteristics. Storms were grouped into three categories for nearshore wave conditions, fast moving storms, moderate forward speed and slow forward speed. Corresponding to these conditions, STWAVE times between wave computations was 15 minutes, 30 minutes and 60 minutes. Nearshore wave computations started when the leading outer edge of the storm center was located at approximately 4 times the radius of maximum winds away from any STWAVE domain. STWAVE computations were continued until the trailing outer edge of the storm was located approximately 4 times the radius of the maximum winds away from any STWAVE domain. Furthermore, all storms had at least 24 wave conditions computed and a maximum of 265. Roughly 2/3 of all storms used a 30 minute wave snap and the remaining were evenly split between 15 minute and 60 minute snaps. This methodology for defining the duration and frequency of nearshore wave conditions produces significant

improvement in accuracy of storm responses over the Texas FEMA Risk Map study.

The ADCIRC mesh developed and used for the coastal Texas study was adapted from a combination of previously developed and validated ADCIRC meshes. The Texas FEMA Risk MAP mesh from the 2011 study was used as a base mesh along the entire Texas coastline. At the Texas-Louisiana boarder and continuing eastward along the coast past Mobile, AL, portions of a mesh for southern Louisiana developed for both FEMA and USACE uses (USACE 2011) were used. This mesh is sometimes called the SL15 mesh and was most recently used in the post-Hurricane Isaac investigation of the Hurricane Storm Damage Risk Reduction System (HSDRRS), see USACE (2012b).

Then in the Atlantic and Caribbean, a grid named EC95, which was originally created for computing tidal databases (Hench et al. 1995), served as the base mesh and was used with some localized refinements to improve response and robustness around some of the islands and shallower depths. After the three main meshes (TX FEMA., Southern LA, and EC95) had their respective high resolution areas extracted, they were stitched together and the deeper water areas of the Gulf of Mexico were recreated to smooth the transitions between the meshes and to reduce the number of nodes and elements in that area. The bathymetry from the TX FEMA mesh and SL15-HSDRRS mesh was given in meters relative to NAVD88 and was maintained for the final meshes in their respective areas. The bathymetry from the TX FEMA mesh was used in the Gulf of Mexico and the areas derived from the EC95 mesh.

Figure A7 shows a color-fill topographic/bathymetric map of the topography/bathymetry values used in the CTXCS ADCIRC mesh. Notice also in Figure A7 the levee and roadway structures being represented in the ADCIRC mesh in the LA portion of the domain. These structures were not a part of the TX FEMA mesh. The CTXCS ADCIRC mesh has a total of 4.5 million computational nodes and 9.0 million unstructured elements. Maximum and minimum element sizes are in the same range as the TX FEMA mesh, ranging from approximately 14 meters to 58 km.

Figure A7. A color contour map showing the seamless topography and bathymetry contained in the CTXCS ADCIRC mesh along the TX-LA border

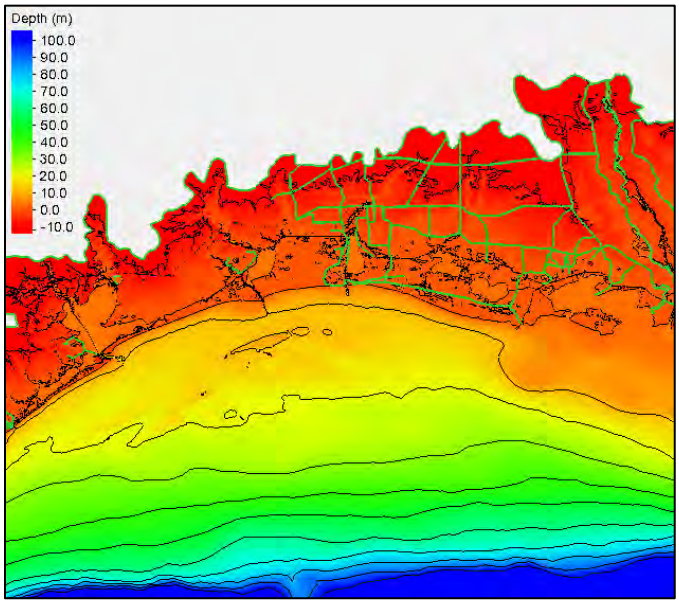

For wind and coastal hydrodynamic modeling by ADCIRC, LCLU data was used to determine spatially distributed values of bottom friction coefficients (or Manning's *n*), canopy coefficients, and surface roughness length for the effect of directional wind reduction, in response to spatial changes of land cover and land use over study areas. These parameters were all updated for the CTXCS using the most recent LCLU data, primarily from the USGS.

Two river inflows from the Mississippi River and the Atchafalaya River are included in the storm-surge simulations. The inflow boundary (or the river cross-section) of the Mississippi River is located near the USGS gage #07374000 Mississippi River at Baton Rouge, LA. The boundary for the Atchafalaya River is placed near the USGS gage #07381490 Atchafalaya River at Simmesport, LA. Constant river inflows were used for all simulations. A value of approximately 160,00 cfs (cubic feet per second) was used for the Mississippi River and a value of 68,000 cfs was used for the Atchafalaya River. Rivers in the TX area of the domain were included in the ADCIRC mesh, but were not forced with any inflow data. The ADCIRC domain extends so far inland that the rivers at the boundary of the model domain are too small to produce significant forcing.

Validation simulations for the CSTORM coupled ADCIRC + STWAVE were performed for historical hurricanes Brett, Carla, Ike, Rita, Katrina, Gustav, and

Isaac. These storms were selected for their historical significance to the Texas coastline and for the availability of measurement data.

Three different sets of water level conditions were modeled for the CTXCS: a base value representing present day conditions, a sea level rise value of 1.5 meters and a sea level rise value of 0.75 meters.

The 660 synthetic storms were sampled from a new joint probability model. The model and storm sampling follow an approach similar to that described above. However significant improvements have been integrated. The approach is illustrated in Figure A8 and described below.

Figure A8. USACE's "new" Probabilistic Coastal Hazard Analysis (StormSim-PCHA) (Nadal-Caraballo et al. 2018)

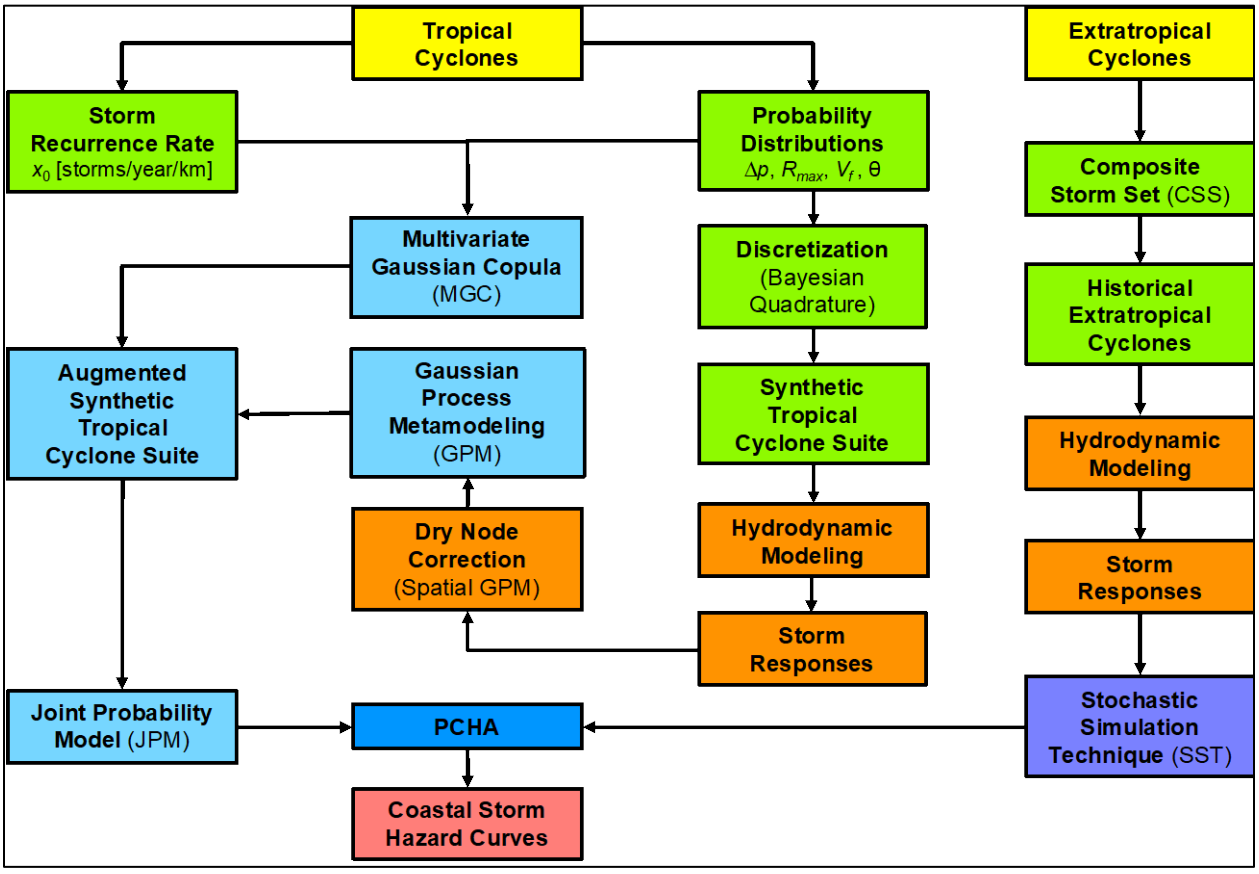

Characteristics of the JPM-OS approach for CTXCS (Nadal-Caraballo et al. 2018):

- Storm tracks created at regular spacing.

- HURDAT2 database sample 1940 – 2017 landfalling and bypassing storms. Parameters sampled were landfall location (latitude and longitude), Δ_p, R_{max}, V_t, and θ. Joint probability distribution created using these parameters.
- A hybrid optimal sampling method was employed for the discretization of the marginal distributions of tropical cyclone parameters. To ensure optimum coverage of both probability and parameter spaces, as well as spatial coverage of the study area, a structured discretization approach was used for the Δ_p and θ marginal distributions. The discretization of the R_{max} and V_t marginal distributions was performed using the Bayesian Quadrature method. Holland B was estimated as a function of Δ_p, R_{max}, and latitude.
- A higher resolution statistical analysis was performed at +200 CRLs throughout the Texas coastline.
- Since intense tropical cyclones (TC) behave differently from weak ones, for CTXCS, storms were separated into three partitions: low-intensity TCs (8 hPa ≤ Δ_p < 28 hPa), medium intensity (28 hPa ≤ Δ_p < 48 hPa) and high-intensity TCs (Δ_p ≥ 48 hPa). Similar partitioning was done by Toro in Mississippi, but had not been done for LA or TX. CTXCS had the following intensities: 148, 138, 128, 118, 108, 98, 88, 78, 68, 58, 48 hPa (high); 38, 28 hPa (medium); 18, 8 hPa (low)
- The GKF was reconceived as a point-based approach accounting for all storms above a given intensity threshold (e.g., all TCs with Δ_p ≥ 8 hPa), each with the appropriate distance-weight. This is different from previous methods used to compute SRR using capture zones (weight of 1 inside; weight of 0 outside), and even from previous applications of the GKF where a capture zone was used first to screen storms and then the SRR computed. The latter can result in underestimation of SRR. Also, the new point-based approach allows for the partitioning of TCs by intensity.
- The distance-weighting GKF methodology was used to compute the TC parameter distance-weighted mean values and marginal probabilistic distributions for each JPM-OS parameter. For each of the TC parameter distributions, a distance-weighted mean was computed based on the distances between the track point of higher intensity and the CRLs. The marginal distributions were fitted to the distance-adjusted TC parameters. The purpose of this Gaussian process is to maximize the use of available historical data while properly characterizing the storm climatology given the latitude-dependency of the TC parameters.
- Improved estimates of uncertainty (epsilon) terms used to compute various confidence limits around mean rather than being included in hazard curve.

The impact of the increased number of storm intensities can be seen in Figure A9. Here the base CTXCS is plotted with mean and two sets of confidence limits while the FEMA 2011 plot is the short green line. The FEMA 2011 under-sampling of storm intensities results in the high frequency tail being high by a meter. In addition, by including the epsilon terms in the JPM integral, the curve is close to the 84% upper confidence limit.

Figure A9. Comparison of hazard curves for FEMA 2011 and CTXCS (Nadal-Caraballo et al. 2018)

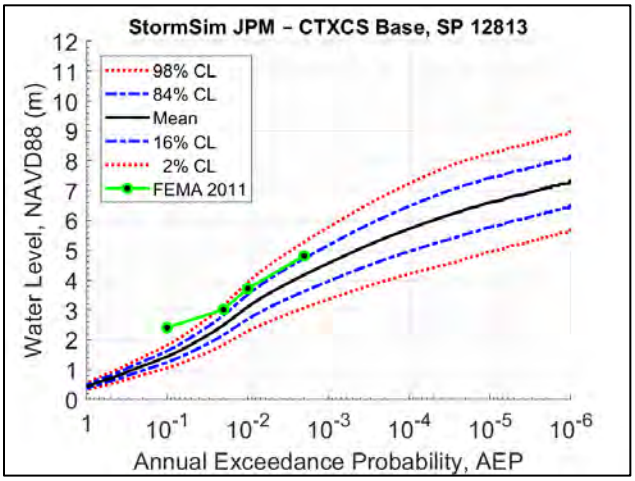

The main improvement of the new PCHA JPM approach used in the CTXCS is incorporation of a surrogate model (Gaussian Process Metamodeling (GPM)) as substitute for a response surface (RS). While the FEMA-TX RS only accounted for Δ_p and R_{max}, GPM accounts for all storm parameters: Δ_p and R_{max}, V_t, θ, and Holland B. The GPM is used to augment the storm sampling by accurately computing parameter values. Where not used, interpolated values have been shown to introduce additional uncertainty in water surface elevations with root-mean-square deviation on the order of 0.70 m (CPRA 2013). The added uncertainty is seldom quantified in these studies.

Figure A10 shows a comparison of several JPM approaches for a specific point located in the North Atlantic Coast Comprehensive Study Region. Note the green curve, which was produced using the above method without the GPM, and the top black curve, which was computed with GPM. In this case, the GPM-augmented storm suite consisted of approximately 200,000 storms. Over the range of extremes of interest the difference is roughly 1 m and the method without GPM is not conservative. Of course, much finer (greater) parameter and probability resolution is expected to produce more accurate results, but this could translate to higher or lower surge hazard magnitude compared to

standard JPM approaches, depending on location within study area – it will not necessarily be always higher than standard JPM.

Figure A10. Comparison of hazard curves for several JPM approaches

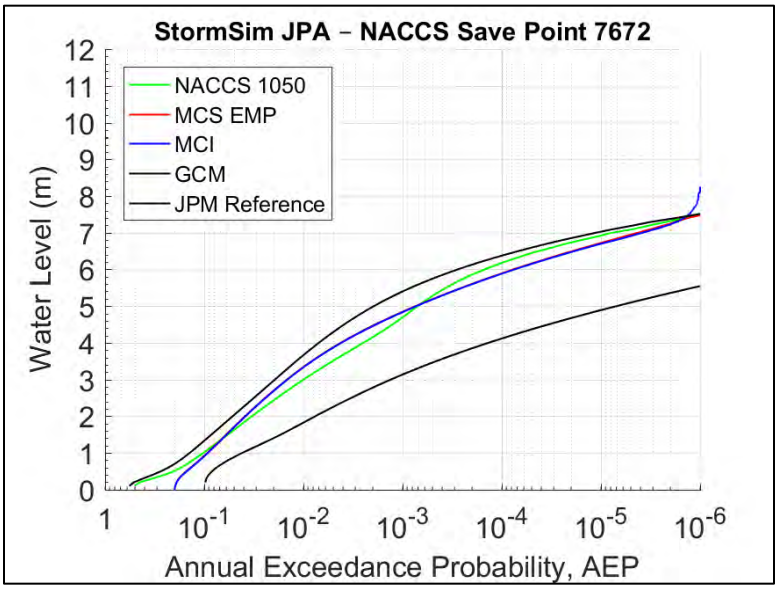

An additional improvement in the methods is the use of Multivariate Gaussian Copula (MGC). Unlike all previous JPM studies which use 1:1 conditional probabilities, MGC allows to, for the first time, have an explicit joint probability model accounting for the (univariate) extreme value distributions of all storm parameters and their corresponding correlations.

Nearshore hydraulic modeling is complicated by the fact that near to, and within, the surf zone, the processes are highly nonlinear and waves and water levels are strongly correlated. The resulting hazards include wave runup, wave and/or steady flow overtopping and wave forces and these are also relatively complicated processes. Historically, these processes were modeled using empirical relations and simple statistical models (e.g. USACE 1984) and errors were unknown. In particular, most empirical models do not account for spatially varying bathymetry that impacts wave transformation, runup and overtopping and are limited to the ranges of parameter combinations from laboratory studies.

Modern analysis includes numerical modeling of nearshore waves and water levels using either phase averaged models (e.g. STWAVE, CMS-WAVE, SWAN, CSHORE) or phase resolving models (e.g. COULWAVE, BOUSS2D, COBRAS, OpenFOAM, FLUENT, Proteus). FEMA uses WHAFIS for nearshore responses

and this is an empirical model that is not typically very accurate. FEMA has begun to apply CSHORE as a replacement for WHAFIS for some projects (FEMA 2012b, Johnson 2012, Johnson et al. 2012, Melby 2012). Most of the phased-averaged models include relatively simple characterizations of wave breaking based on the statistical wave characteristics while phase resolving models attempt to model the surf zone for each wave. In addition, many phase resolving models can model runup and overtopping to some extent. CHSHORE is the only phase averaged model in the list above that can model runup and overtopping and it runs very quickly so it is attractive for risk simulations where thousands of events are required. COULWAVE and BOUSS2D have both been successfully applied to projects within S2G (Lynett 2018, Melby et al. 2015). These Boussinesq models would be expected to be much more accurate than the phase averaged models in the nearshore. They model nonlinear phenomena, such as wave breaking, diffraction and infragravity waves, that are not explicitly modeled by phase averaged models. However, phase resolving may not be more accurate than empirical models for complex phenomena, such as wave overtopping, that are heavily dependent on real fluid effects like friction and dissipation resulting from very rough and porous surfaces unless calibrated. The downside is that they are resource intensive, with both a large computational burden and requiring significant post-processing effort and skill.

Nearshore Boussinesq and RANS models are applied in two horizontal dimensions and in one (transect models). CSHORE is a one-dimensional model. Two-dimensional wave models can take into account wave refraction, diffraction and oblique reflection. Often in the nearshore, waves align with shore-parallel contours and refraction and diffraction are not important. In that case, transect models are often adequate. In addition, the condition of shore-parallel wave crests is often the worst case so it is conservative to assume this. However, in areas where diffraction and refraction are predominant, such as the Freeport inlet and Dow thumb area, a two-dimensional Boussinesq model is required. An initial task with the present study is to compare the various approaches for nearshore wave transformation and adopt the best methods.

Lynett (2018) modeled the nearshore area of Freeport with two-dimensional COULWAVE models using a response-based approach. This captured physics not modeled with previous phase resolving models. However, COULWAVE does not include wind-wave generation so wind waves generated on flood waters landward of the coast were not reproduced.

References for Appendix A

ADCIRC (2017). ADCIRC Utility Programs, http://adcirc.org/home/related-software/adcirc-utility-programs/, accessed on Aug. 1, 2017

Cialone, Mary A., Massey, T.C., Anderson, Mary E., Grzegorzewski, Alison S., Jensen, Robert E., Cialone, Alan, Mark, David J., Pevey, Kimberly C., Gunkel, Brittany L., McAlpin, Tate O. (2015). North Atlantic Coast Comprehensive Study (NACCS) Coastal Storm Model Simulations: Waves and Water Levels. ERDC/CHL TR-15-14. Vicksburg, MS: U.S. Army Engineering Research and Development Center.

Federal Emergency Management Agency (FEMA) 2011. Flood Insurance Study: Coastal Counties, Texas: Scoping and Data Review. Joint Report prepared for Federal Emergency Management Agency by the Department of the Army, U.S. Army Corps of Engineers, Washington DC.

_____2012a. Technical Support Data Notebook DFIRM Update for Brazoria County, Texas Coastal Flood Hazard Analysis Deliverable. FEMA Region VI report.

_____2012b. Great Lakes Coastal Guidelines Update. FEMA Region V report.

Gravens, Mark B., Richard M. Males, Richard M., and Moser, David A. (2007). *Beach-fx: Monte Carlo Life-Cycle Simulation Model for Estimating Shore Protection Project Evolution and Cost Benefit Analyses*, Shore and Beach, Vol. 75, No. 1, Winter, pages 12-19.

Hench, J.L., R.A. Luettich, Jr., J.J. Westerink and N.W. Scheffner, 1995, ADCIRC: an advanced three-dimensional circulation model for shelves, coasts and estuaries, report 6: development of a tidal constituent data base for the Eastern North Pacific, Dredging Research Program Technical Report, U.S. Army Corps of Engineers Waterways Experiment Station, Vicksburg, MS.

IPET. 2009. Performance Evaluation of the New Orleans and Southeast Louisiana Hurricane Protection System. Final Report of the Interagency Performance Evaluation Task Force. Department of the Army, U.S. Army Corps of Engineers, Washington, DC.

Johnson, B. D. 2012. Lake Michigan: Prediction of Sand Beach and Dune Erosion for Flood Hazard Assessment. Great Lakes Coastal Flood Study, 2012 Federal Inter-Agency Initiative, ERDC/CHL TR-12-16, U.S. Army Engineer R&D Center, Vicksburg, MS.

Johnson, B. D., Kobayashi, N., Gravens, M. 2012. Cross-Shore Numerical Model CSHORE for Waves, Currents, Sediment Transport and Beach Profile Evolution. Great Lakes Coastal Flood Study, 2012 Federal Inter-Agency Initiative, ERDC/CHL TR-12-22, U.S. Army Engineer R&D Center, Vicksburg, MS.

Kolar, R. L., W.G. Gray, J.J. Westerink, and R.A. Luettich. (1994). Shallow water modeling in spherical coordinates: Equation formulation, numerical implementation, and application. Journal of Hydraulic Research, 32 (1), 3-24.

Komen, G.J. L. Cavaleri, M. Donelan, K. Hasselmann, S. Hasselmann, and P.A.E.M. Janssen, (1994). Dynamics and modeling of ocean waves. Cambridge University Press, United Kingdom. 532 pp.

Luettich, R. A., Jr., J.J. Westerink, N.W. Scheffner, N. W. (1992). ADCIRC: An advanced three-dimensional circulation model for shelves, coasts, and estuaries. Technical Report DRP-92-6, U.S. Army Engineer Research and Development Center, Vicksburg, MS.

Lynett, P.J., Kalligeris, N. (2018). Velasco Drainage District Levee Overtopping, Valesco Drainage District contract report.

Males, R. M., and Melby, J. A. (2012). "Monte Carlo simulation model for economic evaluation of rubble mound breakwater protection in harbors," Frontiers of Earth Science Journal, Springer, vol. 5 issue 4 December 2011. p. 432 - 441.

Massey, T.C., Jensen, R.E., Bryant, M.A., Ding, Y., Owensby, M.E., and Nadal-Caraballo, N.C. (2018). Coastal Texas Protection and Restoration Feasibility Study: Coastal Storm Model Simulations: Waves and Water Levels. Draft ERDC/CHL Technical Report. Vicksburg, MS: U.S. Army Engineering Research and Development Center.

Massey, T. C., M.E. Anderson, J.M. Smith, J. Gomez, and R. Jones. (2011). *STWAVE: Steady-state spectral wave model user's manual for STWAVE,*

Version 6.0. ERDC/CHL SR-11-1.U.S. Army Engineer Research and Development Center, Vicksburg, MS.

Melby, J.A., N.C. Nadal-Caraballo, and J. Winkelman. (2015a). Point Judith, Rhode Island, Breakwater Risk Assessment. ERDC/CHL TR-15-13. Vicksburg, MS: U.S. Army Engineer Research and Development Center.

Melby, J.A., Nadal-Caraballo, N.C., Ratcliff, J.J., Massey, C.T., Jensen, R.E. (2015b). Sabine Pass to Galveston Bay Wave and Water Level Modeling, Draft Technical Report, U.S. Army Engineer R&D Center, Vicksburg, MS.

Melby, J.A. (2009). Time-dependent life-cycle analysis of coastal structures," Proc. Coastal Structures 2007, World Scientific, 1842-1853.

Melby, J.A. (2012). "Wave runup prediction for flood hazard assessment," Technical Report ERDC/CHL TR-12-24, U.S. Army Engineer Research and Development Center, Vicksburg, MS. 111 pgs.

Melby, J. A., Thompson, E. F., Cialone, M. A., Smith, J. M., Borgman, L. E., Demirbilek, Z., Hanson, J. L., and Lin, L. (2005). "Life-Cycle Analysis of Mid Bay and Poplar Island Projects, Chesapeake Bay, Maryland," Technical Report ERDC/CHl TR-05-12, U.S. Army Engineer Research and Development Center, Vicksburg, MS.

Melby, J.A., Diop, F., Nadal-Caraballo, N.C.., Green, D., Gonzalez, V. (2015). "Coastal Hazards System", Coastal Structures and Solutions to Coastal Disasters Conference, ASCE, Boston, MA.

Nadal-Caraballo, N.C., Lewis, A.B., Gonzalez, V.M., Massey, T.C. and Cox, A.T. (2018). Coastal Texas Protection and Restoration Feasibility Study, Probabilistic Modeling of Coastal Storm Hazards, Draft Technical Report, U.S. Army Engineer R&D Center, Vicksburg, MS.

Orange County 2012. Flood Protection Planning Study Hurricane Flood Protection System, Orange County, Texas. Report prepared for Orange County, Orange County EDC and The Texas Water Development Board.

Smith, J. M., A.R. Sherlock, and D.T. Resio. (2001). *STWAVE: Steady-state spectral wave model user's manual for STWAVE, Version 3.0*. ERDC/CHL

SR-01-1. U.S. Army Engineer Research and Development Center, Vicksburg, MS.

United States Army Corps of Engineers (USACE). (2006). Louisiana Coastal Protection and Restoration (LACPR) Preliminary Technical Report. Provided to United States Congress.

_____. 2009a. *Louisiana Coastal Protection and Restoration (LACPR) Final Technical Report*. New Orleans District, Mississippi Valley Division, USACE.

_____. 2009b. *Mississippi Coastal Improvements Program (MSCIP), Hancock, Harrison, and Jackson Counties, Mississippi*. Mobile, AL: Mobile District, South Atlantic Division, USACE.

_____. 2012. Hurricane and Storm Damage Reduction System Design Guidelines, New Orleans District, Mississippi Valley Division, USACE.

_____. 2014. Freeport Hurricane Flood Protection, Semi-Quantitative Risk Assessment Report. US Army Engineer Galveston District.

Westerink, J.J., R.A. Luettich Jr., J.C. Feyen, J.H. Atkinson, C. Dawson, H.J. Roberts, M.D. Powell, J.P. Dunion, E.J. Kubatko, and H. Portaheri. (2008). A basin- to channel-scale unstructured grid hurricane storm surge model applied to southern Louisiana. Monthly Weather Review, 136, 833–864.

Westerink, J., Dietrich, J., Westerink, H., Tanaka, S., Martyr, R., Hope,M., Westerink, L., Atkinson, J., H. Roberts, R. Clark, S. Zou, Z. Cobell, C. Bender, R. Srinivas, J. Smith, R. Jensen, D. Resio, J. Ratcliff, H. Pourtaheri, N. Powell, D. Elzey, D. Ulm, C. Dawson, J. Proft, C. Szpilka, R. Kolar, K. Dresback, V. Cardone, A. Cox, M. Powell, (2011). Flood Insurance Study: Coastal Counties, Texas, Intermediate Submission 2: Scoping and Data Review, FEMA Region 6, USACE New Orleans District, 15 November 2011,

Appendix B CSTORM Modeling Validation and Assessment

Validation and Bias Correction

Validation simulations for the CSTORM coupled ADCIRC + STWAVE were performed for historical hurricanes Brett, Carla, Ike, Rita, Katrina, Gustav, and Isaac. These storms were selected for their historical significance to the Texas coastline and for the availability of measurement data. Due to the brevity of this summary report, only portions of the results will be shown. In Figure B1, time series plot comparisons of measured versus modeled water surface elevations are shown at NOAA gauge station (8771450) located at Galveston Pier 21. The time series comparisons are for Hurricanes Brett, Ike, Katrina, Rita and Gustav. Modeled water levels for Bret are approximately 0.3 meters (1 feet) higher than measured for the entire simulation. For Hurricane Ike, the model results are about 0.2 meters (approx. 8 inches) high leading up to the peak of the storm and then are about 0.5 meters (1.6 feet) low. Model results are about 0.2 meters (approx. 8 inches) higher than measured for Hurricane Katrina and similarly for Hurricane Rita, although the peak of the storm surge is represented very well. Hurricane Gustav shows the model over estimating the peak water levels and under representing the full water level range (tide range). The peaks are over estimated by about 0.25m (10 inches), mostly as a vertical offset for the peaks when compared to measured values and the tidal range is under estimated by approximately 0.2m (8 inches).

Figure B1. Plots showing time series of water levels (in meters NAVD88) at the NOAA tide gauge station located at Galveston Pier 21 (ID 8771450). Results are shown for (a) Hurricane Brett, (b) Hurricane Ike, (c) Hurricane Katrina, (d) Hurricane Rita and (e) Hurricane Gustav.

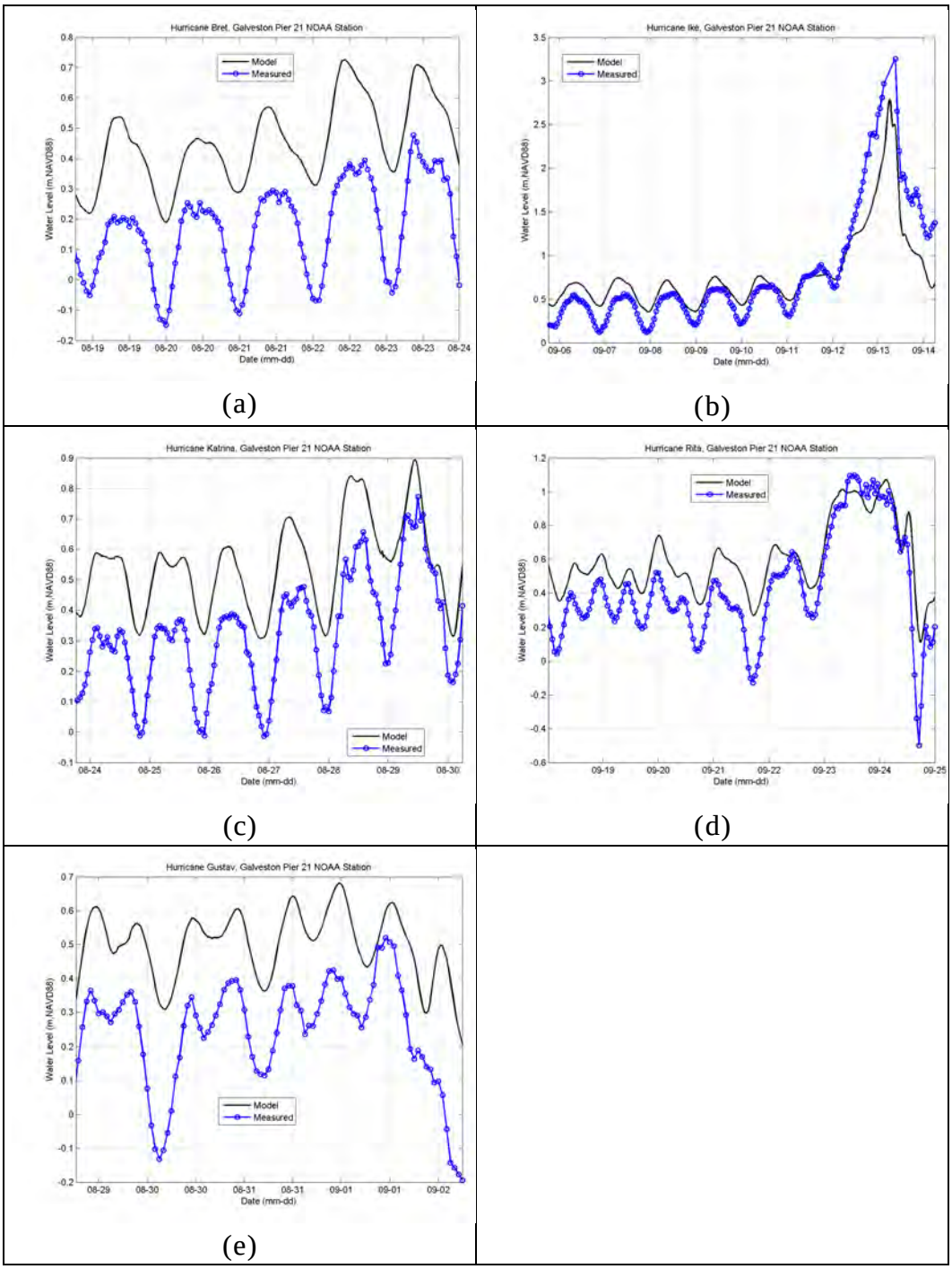

In Figure B2, time series plot comparisons of measured versus modeled water surface elevations are shown at NOAA gauge station (8774770)

located at Rockport. The time series comparisons are for Hurricanes Brett, Ike, Katrina, Rita and Gustav. Modeled water levels for Bret are approximately 0.05 meters (2 inches) lower than measured prior to the arrival of the storm peak, then the model results at the peak of the event are approximately 0.2 meters (8 inches) lower than observed. The phasing of the tides is very good and the gradual building of the water levels is good around Aug. 22, 1999. For Hurricane Ike, the model results are about 0.1 meters (approx. 4 inches) low leading until approximately Sept. 9, 2008 then the forerunner growth for the model is under represented by about 0.2 meters and peak surge is under represented by 0.6 meters (approx. 2 feet). Model results are about 0.05 meters (approx. 2 inches) lower than measured for Hurricane Katrina leading up to the peak which is under-represented by 0.075 meters (3 inches). For Hurricane Rita, the model under predicts by approximately 0.1 meters (4 inches) prior to the arrival of the storm. Then the peak is under estimated by 0.45 meters (1.5 ft). Hurricane Gustav shows the model under estimating the peak water level by 0.2 meters (8 inches).

Figure B2. Plots showing time series of water levels (in meters NAVD88) at the NOAA tide gauge station located at Rockport (ID 8774770). Results are shown for (a) Hurricane Brett, (b) Hurricane Ike

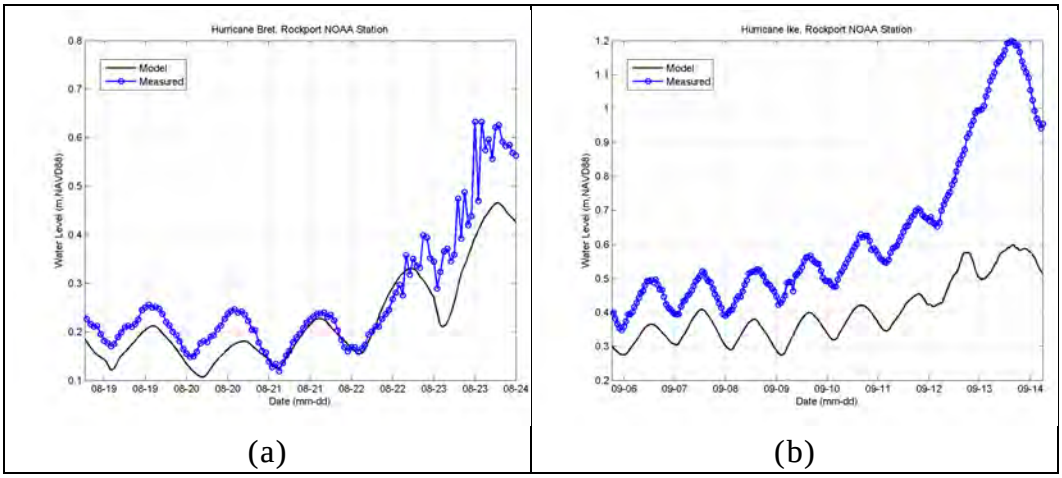

(a) (b)

In Figure B3, time series plot comparisons of measured versus modeled water surface elevations are shown at NOAA gauge station (8779770) located at Port Isabel, TX for Hurricanes Brett, Ike, Katrina, Rita and Gustav. Modeled water levels for Bret are approximately 0.2 meters (approx. 8 inches) higher than measured leading up to the peak at which point the model overestimates the peak by about 0.3 meters (approx. 1

foot). For Hurricane Ike, the model results are about 0.1 meters (approx. 4 inches) high leading up to the peak of the storm and then are about 0.3 meters (approx. 10 inches) low, this could be due to errors in representing the winds near this area for Ike in particular. For Hurricane Katrina, the model results are about 0.2 meters (approx. 8 inches) higher than measured leading up the peak of the storm and then overestimate the peak by about 0.25 meters. Model results are about 0.15 meters (approx. 6 inches) higher than measured for Hurricane Rita and are about 0.1 meters (approx. 4 inches) below the peak observed. For Hurricane Gustav, the model over predicts the water levels by about 0.12 meters (5 inches) at the peaks and does under represents the tidal range by not allowing the water levels to drop as low as measured values. The modeled tidal surge range at Port Isabel, TX is about 0.25 meters (10 inches) compared to 0.45 meters (17 inches) for Katrina and Rita.

Figure B3. Plots showing time series of water levels (in meters NAVD88) at the NOAA tide gage station (ID 8770475) located at Port Isabel, TX. Results are shown for (a) Hurricane Rita, (b) Hurricane Ike, and (c) Hurricane Harvey.

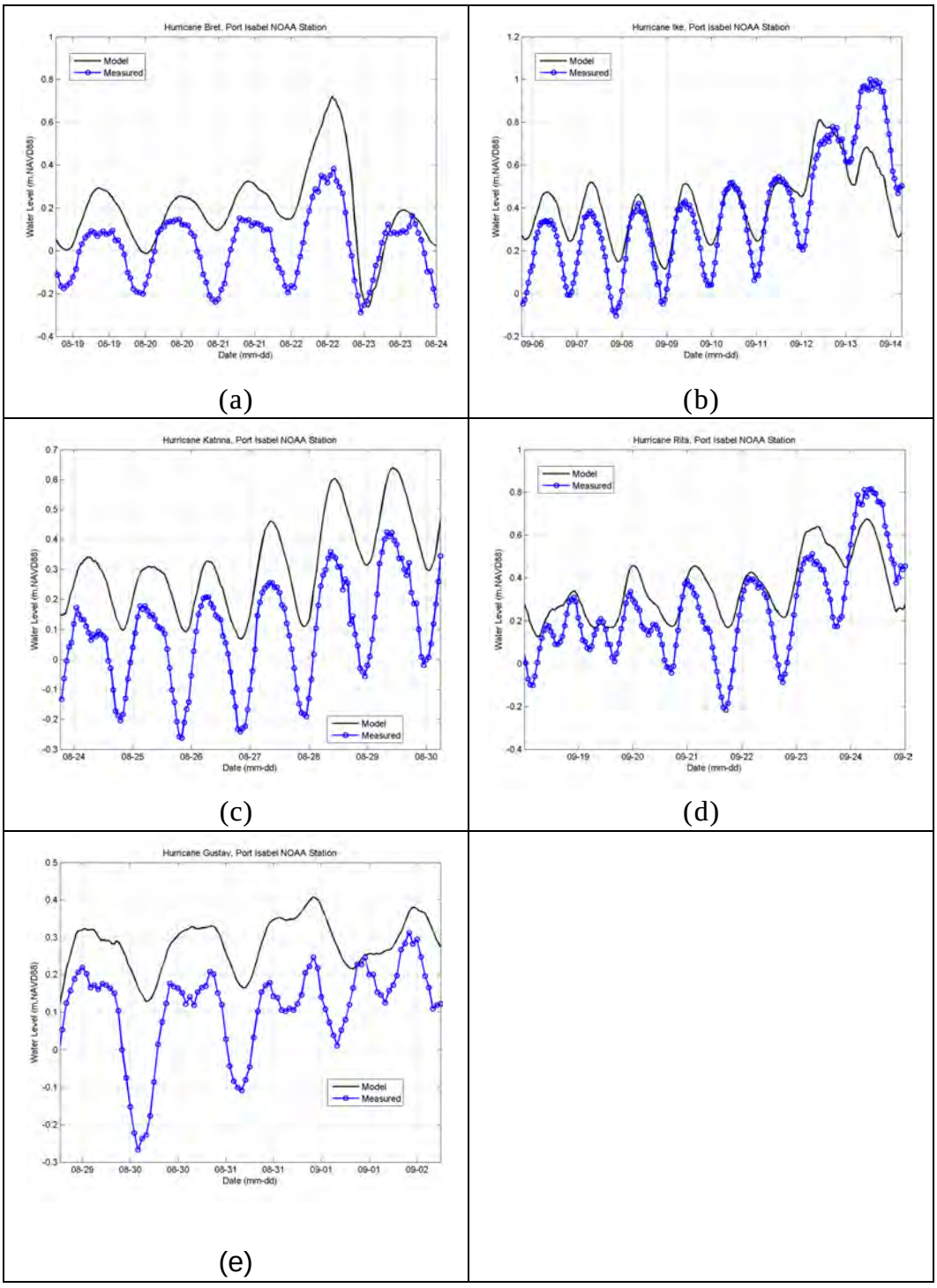

In Figure B4, time series plot comparisons of measured versus modeled water surface elevations are shown at NOAA gauge station (8770570) located at Sabine Pass North in TX for Hurricanes Brett, Ike, Katrina, Rita and Gustav. At this station, the model has a tendency to under estimate the water levels with some similar vertical offsets. The peaks appear to be off by 0.2 to 1.0 meter for the various storms presented in similar fashion to the other stations.

In Figure B5, maximum water surface levels scatter plots and the corresponding point location differences are shown for Hurricane Brett and Carla, both of which did not have many measurement values. For Hurricane Brett, all measured versus modeled differences are less than 0.5 meters (approx. 1.6 feet) with a cross correlation coefficient of 0.41. For Hurricane Carla only 20 percent of the model versus measured result differences are less than 0.5 meters (1.6 feet), with the majority of the model results being lower than measured by about 1 meter (3.3 feet).

Similarly, in Figure B6 maximum water surface levels scatter plots and corresponding point location difference are shown for Hurricanes Ike and Rita. Approximately 45 percent of all model versus measurement differences are within 0.5 meters (1.6 feet) and an overall cross correlation coefficient of 0.71. The model tends to underestimate surge levels by about 0.8 meters (2.6 feet). For Hurricane Rita the cross correlation coefficient is 0.24 and approximately 59 percent of all locations show modeled versus measured differences of less than 0.5 meters (1.6 feet). For Rita, only a few measurement locations were located in Texas.

Figure B7 shows the maximum water surface elevations for Hurricanes Gustav and Isaac and Figure B8 shows the same for Hurricane Katrina.

Figure B4. Plots showing time series of water levels (in meters NAVD88) at the NOAA tide gauge station located at Sabine Pass North in TX (ID 8770570. Results are shown for (a) Hurricane Brett, (b) Hurricane Ike, (c) Hurricane Katrina, (d) Hurricane Rita and (e) Hurricane Gustav.

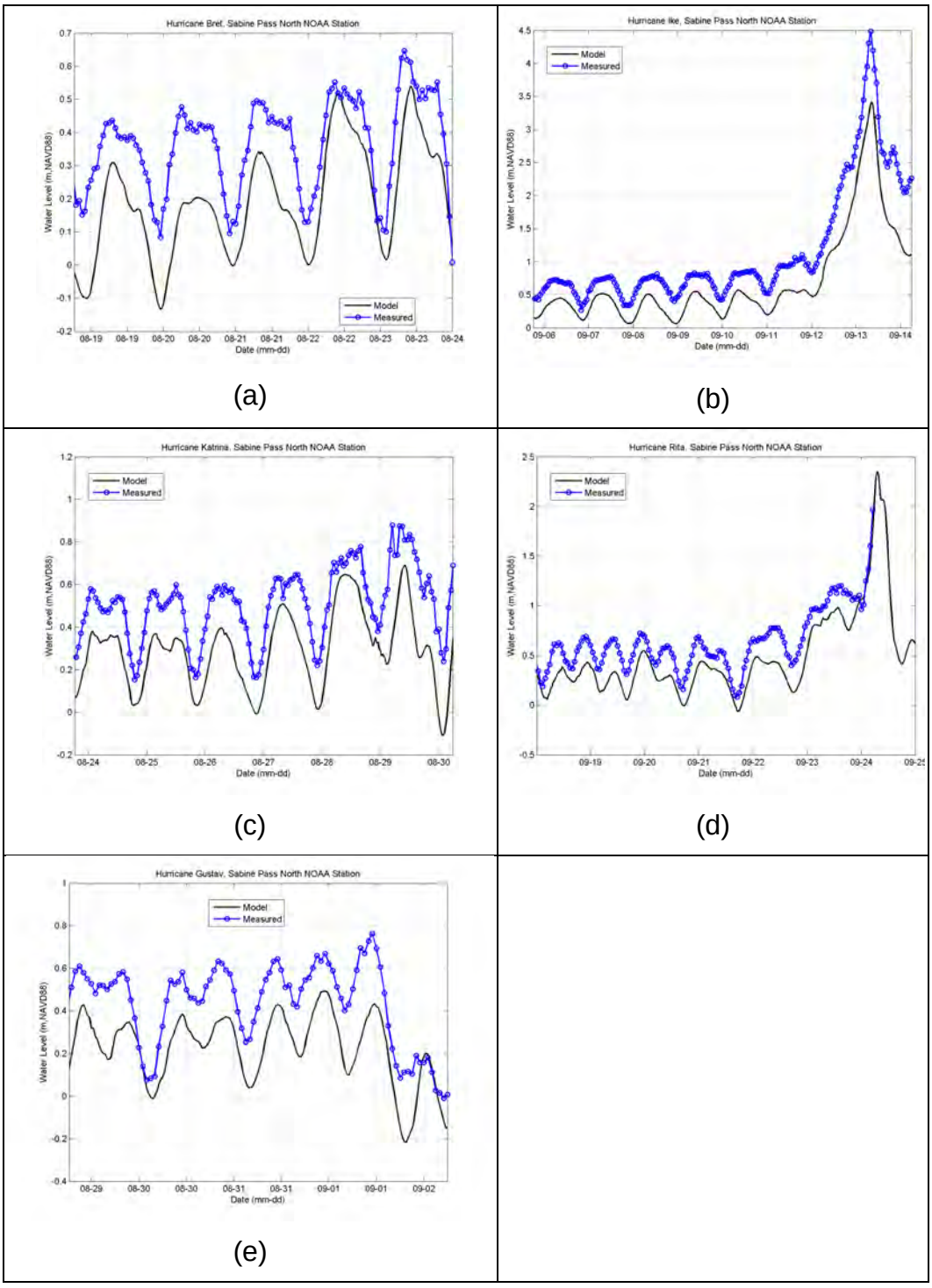

Figure B5. Scatter plots and the corresponding measurement locations plotted on a map for Hurricanes Brett and Carla (results shown in meters).

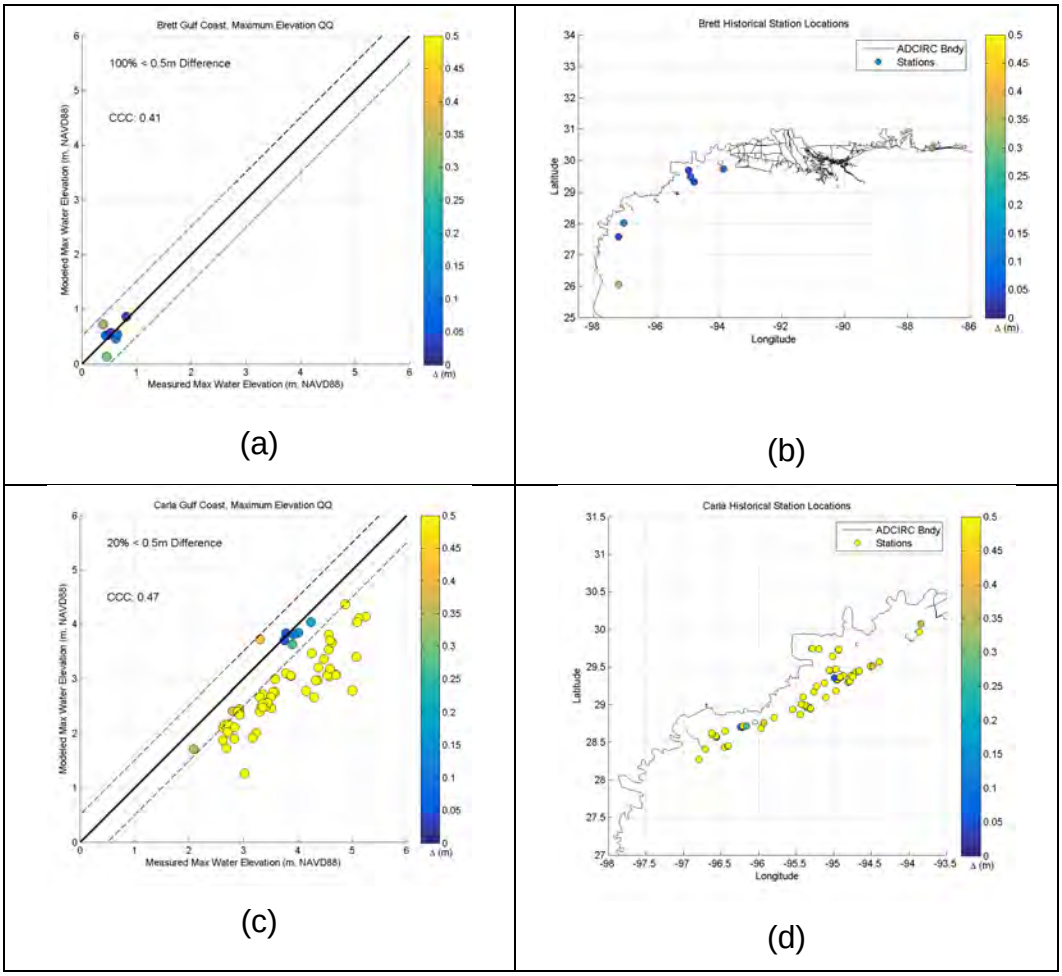

Figure B6. Scatter plots and the corresponding measurement locations plotted on a map for Hurricanes Ike and Rita.

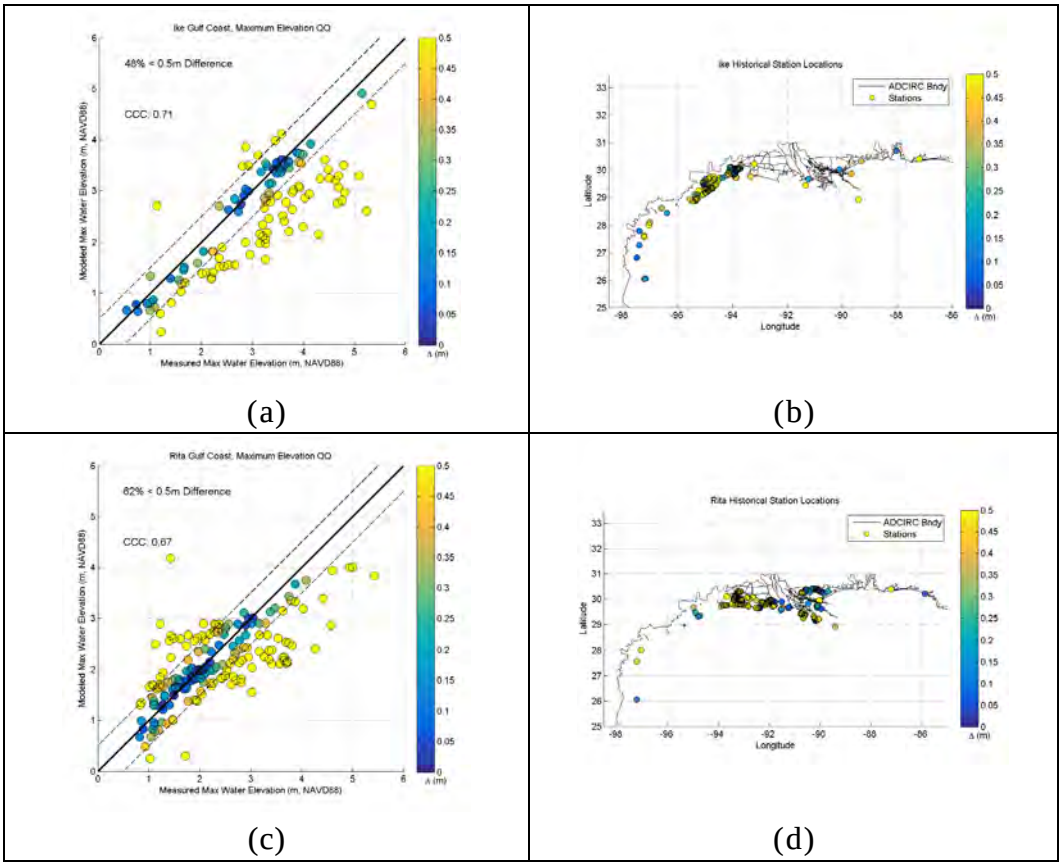

Figure B7. Scatter plots and the corresponding measurement locations plotted on a map for Hurricanes Gustav and Isaac.

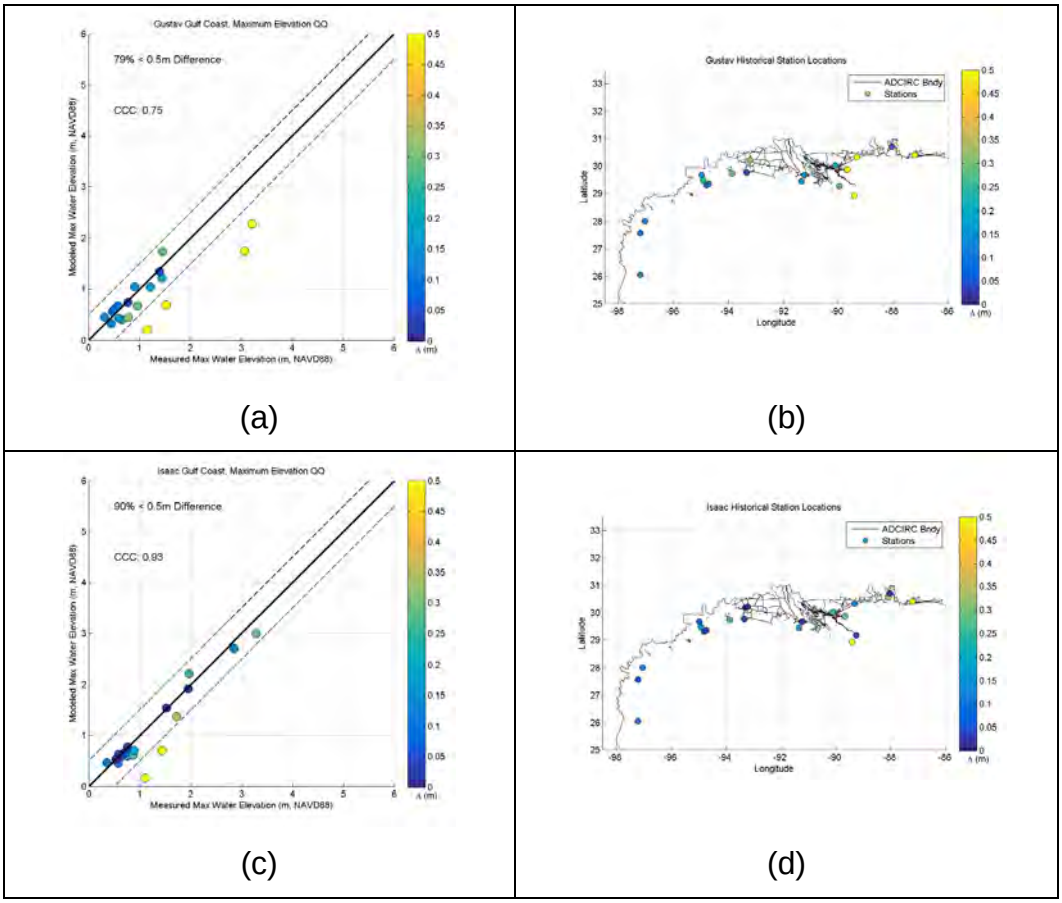

Figure B8. Scatter plots and the corresponding measurement locations plotted on a map for Hurricane Katrina.

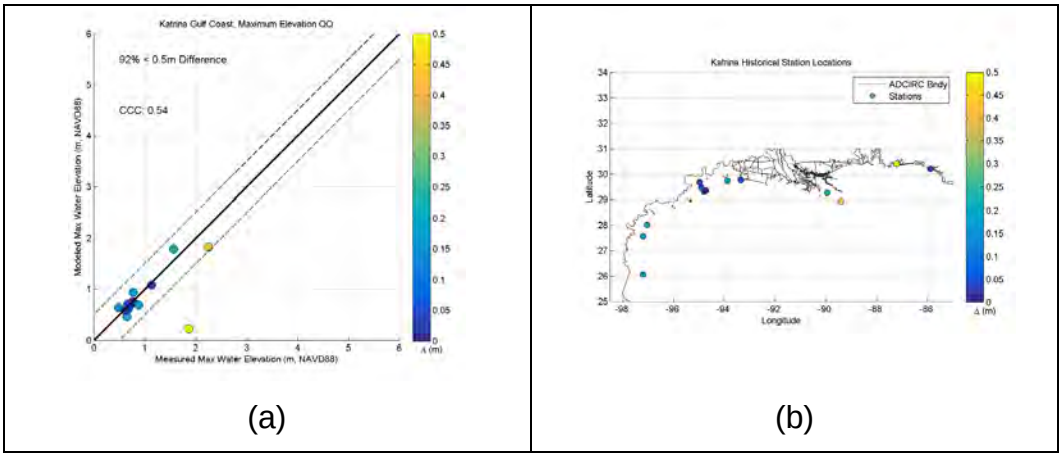

(a) (b)

Bias Correction

Validation statistics for CSTORM output were computed. SWL bias is evident in the validation plots shown above. Bias was computed for all validation storms and all validation points. These points include high water marks and gage measurements. A smooth SWL bias surface was generated using a Gaussian kernel with an optimized radius of 7 km. The surface computed using the measurements was mapped onto the 18332 CTXCS save points. Figure B9 and B10 show the SWL bias surface in the vicinity of Galveston Island and Bolivar Peninsula, respectively. The very tiny numbers in the plot correspond to the bias values at the points and these values are described by the point color. This bias was applied to all SWLs of the synthetic TC storms. Generally, the bias was negative so SWL values in the synthetic storms were increased.

Figure B9. CSTORM SWL bias in vicinity of Galveston Island mapped onto save points

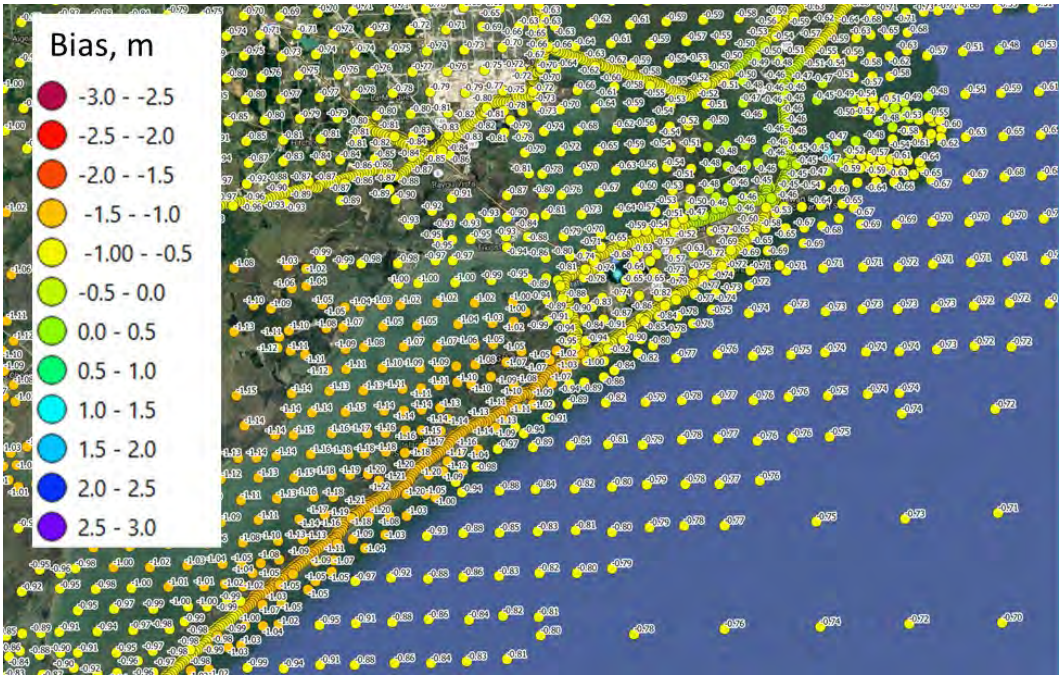

Figure B10. CSTORM SWL bias in vicinity of Bolivar Peninsula mapped onto save points

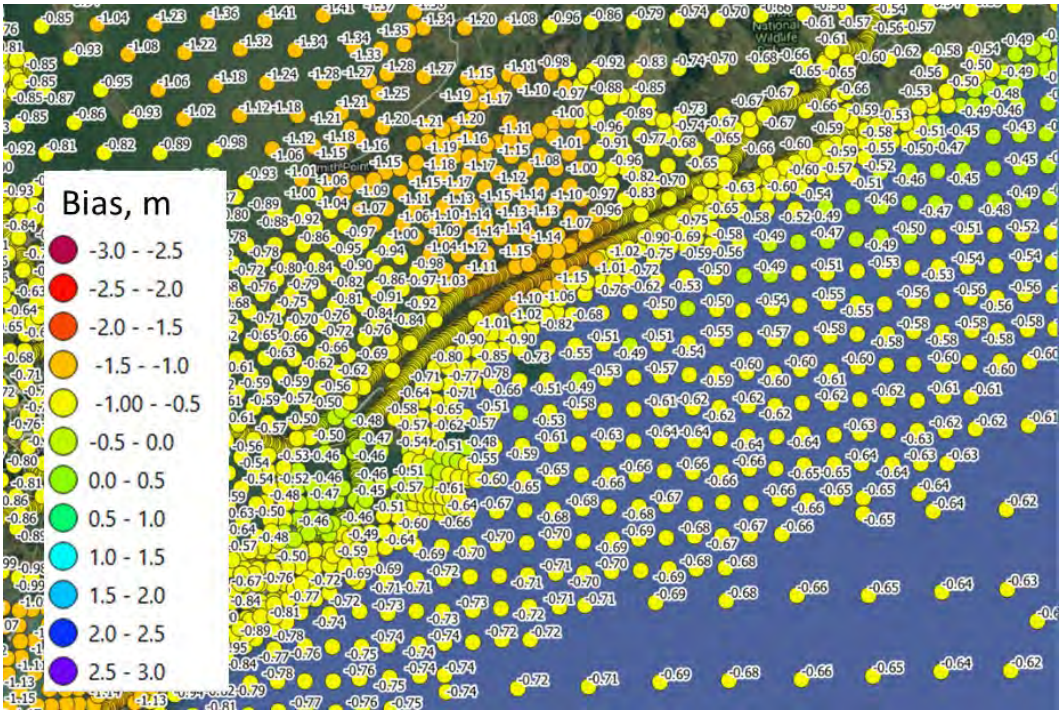

Appendix C. Historical and Synthetic Tropical Cyclones

JPM-OS methodology is described in Appendix A. In this approach, historical tropical storms from 1938 to 2017 from the HURDAT2 database that impacted the Texas coastline were extracted. These storms are tropical cyclones and well parameterized by track (heading θ, landfall location), intensity (minimum central pressure, P), size (radius to maximum winds, R_{max}) and forward speed (V_r). Central pressure is further defined according to the deficit from far-field atmospheric pressure, ΔP = 1013 mb - P_{min}. The historical TCs are listed in Table C1.

Table C1. List of select historical TCs affecting the Coastal Texas study region during the 1938–2017 period.

Year	NHC ID	TC Name	Maximum Wind Speed (km/h)	Minimum Central Pressure (hPa)
1938	3	UNNAMED	157	969
1938	7	UNNAMED	93	996
1940	2	UNNAMED	157	975
1940	6	UNNAMED	83	999
1941	1	UNNAMED	93	996
1941	2	UNNAMED	204	953
1942	2	UNNAMED	130	983
1942	3	UNNAMED	185	962
1943	1	UNNAMED	167	971
1943	6	UNNAMED	157	972
1944	5	UNNAMED	93	996
1945	2	UNNAMED	65	1004
1945	5	UNNAMED	185	962
1946	1	UNNAMED	65	1004
1947	1	UNNAMED	83	999
1947	3	UNNAMED	130	983
1949	11	UNNAMED	176	967
1950	8	HOW	74	1002
1954	3	ALICE	176	967

1954	5	BARBARA	93	997
1955	5	UNNAMED	83	999
1957	2	AUDREY	204	953
1957	3	BERTHA	102	994
1958	1	ALMA	102	994
1958	5	ELLA	176	969
1958	7	GERDA	93	999
1959	5	DEBRA	139	982
1960	1	UNNAMED	93	996
1961	3	CARLA	278	909
1963	4	CINDY	130	983
1964	3	ABBY	102	994
1967	13	BEULAH	259	922
1968	3	CANDY	111	992
1970	4	CELIA	204	953
1970	13	FELICE	111	992
1971	11	FERN	148	976
1971	13	EDITH	259	922
1973	10	DELIA	111	990
1975	7	CAROLINE	185	962
1977	5	ANITA	278	909
1978	4	AMELIA	83	999
1978	9	DEBRA	93	997
1979	6	CLAUDETTE	83	999
1979	12	ELENA	65	1004
1980	4	ALLEN	306	889
1980	11	DANIELLE	93	997
1980	16	JEANNE	157	975
1982	5	CHRIS	102	994
1983	3	ALICIA	185	962
1983	4	BARRY	130	985
1985	4	DANNY	148	979
1985	12	JUAN	139	980
1986	2	BONNIE	139	982

1987	3	UNNAMED	74	1002
1988	2	BERYL	83	999
1989	2	ALLISON	83	1000
1989	4	CHANTAL	130	985
1989	14	JERRY	139	982
1993	2	ARLENE	65	1004
1995	4	DEAN	74	1002
1998	3	CHARLEY	111	992
1998	6	FRANCES	102	994
1999	3	BRET	232	937
2000	5	BERYL	83	1000
2001	1	ALLISON	93	996
2002	6	FAY	93	997
2002	13	LILI	232	938
2003	4	CLAUDETTE	148	979
2003	8	ERIKA	120	989
2003	11	GRACE	65	1004
2004	9	IVAN	269	917
2005	5	EMILY	259	925
2005	18	RITA	287	903
2007	5	ERIN	93	997
2007	9	HUMBERTO	148	979
2008	4	DOLLY	157	975
2008	5	EDOUARD	102	994
2008	9	IKE	232	935
2010	1	ALEX	176	967
2010	10	HERMINE	111	990
2011	4	DON	83	1000
2011	13	LEE	93	996
2015	2	BILL	93	997
2017	3	CINDY	93	996
2017	9	HARVEY	176	967

A joint probability model of the tropical storm parameters was constructed and discretized to develop a suite of synthetic tropical storms that defines the entire hazard from low-intensity frequent storms to high-intensity very infrequent storms. The upper limit of the storm parameters extends beyond all historical events but only to reasonable extremes; that is, the upper limits of parameters are only slightly larger than the historical storm extents. The associated AEPs of wave and water level responses span the range from 0.1 to 10-4. The final storm list of 660 storms with track landfalls extending over the entire Texas coast and from well into Mexico to Florida is provided in Table C2. Table C3 provides a reduced list of 170 storms that are a subset of the 660 storms and were determined to be optimal for SWL and overtopping hazard for the region. These 170 storms were used as the part of the hazard, along with non-tropical events, for the morphology modeling.

Table C2. List of 660 storms for CTXCS that provided the basis for which storms were sampled. Cells are colored alternating blue and gray by Master Track group,for readability.

Storm Number	Texas Region	Master Track	Θ (deg)	ΔP (hPa)	R_{max} (km)	V_f (km/h)
1	2	1	-100	148	19.7	9.5
2	2	1	-100	128	19.4	30.9
3	2	1	-100	108	12.7	20.1
4	2	1	-100	88	74.7	15.3
5	2	1	-100	68	33.1	12.2
6	2	1	-100	48	14.9	33.7
7	2	1	-100	28	82.1	20.0
8	2	1	-100	8	22.6	10.6
9	2	2	-100	148	11.9	10.0
10	2	2	-100	128	33.9	38.3
11	2	2	-100	108	20.9	12.9
12	2	2	-100	88	9.1	19.8
13	2	2	-100	68	64.6	31.5
14	2	2	-100	48	95.6	11.2
15	2	2	-100	28	49.2	23.2
16	2	2	-100	8	18.4	9.3
17	2	3	-100	148	23.0	10.6
18	2	3	-100	128	29.2	23.0
19	2	3	-100	108	8.0	18.9
20	2	3	-100	88	16.8	8.0
21	2	3	-100	68	25.4	29.2
22	2	3	-100	48	70.5	19.2

23	2	3	-100	28	126.7	21.8
24	2	3	-100	8	42.2	11.4
25	2	4	-100	148	18.2	28.3
26	2	4	-100	128	8.5	11.5
27	2	4	-100	108	59.2	14.5
28	2	4	-100	88	46.0	15.8
29	2	4	-100	68	48.9	8.0
30	2	4	-100	48	44.4	20.3
31	2	4	-100	28	19.7	20.6
32	2	4	-100	8	86.6	29.6
33	2	5	-100	148	10.4	11.1
34	2	5	-100	128	24.1	21.0
35	2	5	-100	108	31.6	8.0
36	2	5	-100	88	20.2	27.8
37	2	5	-100	68	73.3	13.2
38	2	5	-100	48	53.0	20.9
39	2	5	-100	28	9.9	9.8
40	2	5	-100	8	119.2	35.9
41	2	6	-100	148	13.2	18.2
42	2	6	-100	128	9.5	23.8
43	2	6	-100	108	22.7	22.7
44	2	6	-100	88	58.3	13.8
45	2	6	-100	68	70.2	9.8
46	2	6	-100	48	23.7	9.3
47	2	6	-100	28	64.1	34.6
48	2	6	-100	8	20.5	24.2
49	2	7	-100	148	8.6	32.6
50	2	7	-100	128	21.3	26.1
51	2	7	-100	108	19.2	10.4
52	2	7	-100	88	47.8	24.4
53	2	7	-100	68	15.1	18.3
54	2	7	-100	48	106.3	15.4
55	2	7	-100	28	58.9	11.1
56	2	7	-100	8	35.5	24.9
57	2	8	-100	148	27.3	44.6
58	2	8	-100	128	14.8	17.9
59	2	8	-100	108	37.7	9.5
60	2	8	-100	88	23.7	14.3
61	2	8	-100	68	10.8	30.3
62	2	8	-100	48	91.2	28.7
63	2	8	-100	28	44.7	23.9

64	2	8	-100	8	79.7	19.1
65	1	9	-100	148	12.5	25.7
66	1	9	-100	128	44.5	24.5
67	1	9	-100	108	15.9	30.3
68	1	9	-100	88	26.1	12.8
69	1	9	-100	68	8.0	24.8
70	1	9	-100	48	87.1	12.6
71	1	9	-100	28	69.7	29.1
72	1	9	-100	8	12.1	17.0
73	1	10	-100	148	14.9	8.0
74	1	10	-100	128	17.0	26.9
75	1	10	-100	108	8.8	15.0
76	1	10	-100	88	70.5	14.8
77	1	10	-100	68	41.5	22.6
78	1	10	-100	48	34.6	19.7
79	1	10	-100	28	85.6	17.8
80	1	10	-100	8	37.7	11.0
81	2	11	-80	138	15.4	23.9
82	2	11	-80	118	19.3	13.0
83	2	11	-80	98	40.4	26.3
84	2	11	-80	78	79.8	10.3
85	2	11	-80	58	12.7	31.2
86	2	11	-80	38	30.6	10.7
87	2	11	-80	18	101.0	25.2
88	2	12	-80	138	33.8	14.2
89	2	12	-80	118	31.2	23.6
90	2	12	-80	98	14.6	13.4
91	2	12	-80	78	19.4	18.5
92	2	12	-80	58	27.3	34.0
93	2	12	-80	38	107.3	24.9
94	2	12	-80	18	58.2	8.9
95	2	13	-80	138	25.2	32.3
96	2	13	-80	118	16.5	22.2
97	2	13	-80	98	11.7	13.9
98	2	13	-80	78	40.9	20.8
99	2	13	-80	58	35.9	10.3
100	2	13	-80	38	97.2	25.7
101	2	13	-80	18	20.2	30.0
102	2	14	-80	138	14.5	38.7
103	2	14	-80	118	17.9	17.3
104	2	14	-80	98	37.5	9.4

105	2	14	-80	78	90.6	15.2
106	2	14	-80	58	17.5	16.1
107	2	14	-80	38	66.4	26.5
108	2	14	-80	18	53.2	19.3
109	2	15	-80	138	24.4	8.0
110	2	15	-80	118	23.0	24.3
111	2	15	-80	98	15.5	14.4
112	2	15	-80	78	30.3	8.0
113	2	15	-80	58	60.3	11.7
114	2	15	-80	38	81.6	22.0
115	2	15	-80	18	12.0	12.4
116	2	16	-80	138	11.6	19.3
117	2	16	-80	118	40.5	8.0
118	2	16	-80	98	8.0	16.5
119	2	16	-80	78	20.7	36.5
120	2	16	-80	58	68.0	23.1
121	2	16	-80	38	56.2	15.8
122	2	16	-80	18	30.6	15.6
123	2	17	-80	138	30.5	19.9
124	2	17	-80	118	20.0	10.5
125	2	17	-80	98	28.9	27.1
126	2	17	-80	78	11.8	25.0
127	2	17	-80	58	45.2	35.8
128	2	17	-80	38	120.5	13.0
129	2	17	-80	18	48.4	12.8
130	2	18	-80	138	19.9	22.5
131	2	18	-80	118	8.0	19.6
132	2	18	-80	98	26.6	9.9
133	2	18	-80	78	24.7	33.2
134	2	18	-80	58	62.8	19.9
135	2	18	-80	38	32.5	18.5
136	2	18	-80	18	92.5	16.6
137	2	19	-80	138	12.4	33.7
138	2	19	-80	118	23.8	15.6
139	2	19	-80	98	69.3	23.2
140	2	19	-80	78	9.3	11.8
141	2	19	-80	58	47.2	8.9
142	2	19	-80	38	38.6	22.7
143	2	19	-80	18	60.8	26.9
144	1	20	-80	138	15.9	10.0
145	1	20	-80	118	14.5	27.6

146	1	20	-80	98	58.2	33.8
147	1	20	-80	78	34.6	21.5
148	1	20	-80	58	39.5	8.0
149	1	20	-80	38	72.1	23.4
150	1	20	-80	18	8.0	10.6
151	1	21	-80	138	21.0	15.2
152	1	21	-80	118	13.1	9.0
153	1	21	-80	98	53.1	8.0
154	1	21	-80	78	58.1	19.0
155	1	21	-80	58	20.7	15.0
156	1	21	-80	38	44.9	19.0
157	1	21	-80	18	78.2	9.3
158	1	22	-80	138	12.0	20.5
159	1	22	-80	118	42.3	8.5
160	1	22	-80	98	8.9	15.9
161	1	22	-80	78	22.1	38.7
162	1	22	-80	58	70.9	23.8
163	1	22	-80	38	58.7	16.3
164	1	22	-80	18	32.7	16.1
165	1	23	-80	138	10.0	15.8
166	1	23	-80	118	9.3	14.0
167	1	23	-80	98	48.9	17.0
168	1	23	-80	78	31.7	30.6
169	1	23	-80	58	55.6	16.6
170	1	23	-80	38	11.7	14.9
171	1	23	-80	18	41.5	8.0
172	2	24	-60	148	23.8	11.6
173	2	24	-60	128	10.0	32.1
174	2	24	-60	108	30.5	42.9
175	2	24	-60	88	41.0	23.0
176	2	24	-60	68	19.5	12.7
177	2	24	-60	48	100.6	11.6
178	2	24	-60	28	46.9	18.3
179	2	24	-60	8	51.7	15.0
180	2	25	-60	148	15.3	17.0
181	2	25	-60	128	22.6	28.8
182	2	25	-60	108	14.3	27.4
183	2	25	-60	88	79.8	18.6
184	2	25	-60	68	18.0	15.1
185	2	25	-60	48	73.5	32.2
186	2	25	-60	28	66.8	10.2

187	2	25	-60	8	49.3	25.8
188	2	26	-60	148	8.3	30.3
189	2	26	-60	128	22.0	10.5
190	2	26	-60	108	20.1	19.5
191	2	26	-60	88	31.1	35.0
192	2	26	-60	68	22.4	15.6
193	2	26	-60	48	112.9	15.9
194	2	26	-60	28	89.4	18.9
195	2	26	-60	8	26.8	15.5
196	2	27	-60	148	20.3	24.9
197	2	27	-60	128	13.7	40.7
198	2	27	-60	108	35.1	28.3
199	2	27	-60	88	21.4	8.9
200	2	27	-60	68	89.1	13.6
201	2	27	-60	48	67.7	13.5
202	2	27	-60	28	11.9	14.8
203	2	27	-60	8	59.3	30.9
204	2	28	-60	148	15.7	9.0
205	2	28	-60	128	12.6	21.7
206	2	28	-60	108	43.8	24.9
207	2	28	-60	88	27.3	36.9
208	2	28	-60	68	59.7	18.9
209	2	28	-60	48	40.4	16.5
210	2	28	-60	28	107.2	11.5
211	2	28	-60	8	8.0	11.9
212	2	29	-60	148	25.9	20.7
213	2	29	-60	128	15.9	18.5
214	2	29	-60	108	45.7	8.5
215	2	29	-60	88	13.5	28.7
216	2	29	-60	68	38.1	19.5
217	2	29	-60	48	16.6	8.4
218	2	29	-60	28	97.6	12.9
219	2	29	-60	8	67.5	22.8
220	2	30	-60	148	10.7	31.4
221	2	30	-60	128	26.5	12.0
222	2	30	-60	108	25.4	15.5
223	2	30	-60	88	38.0	39.1
224	2	30	-60	68	110.1	14.6
225	2	30	-60	48	13.2	22.2
226	2	30	-60	28	29.8	12.0
227	2	30	-60	8	76.5	27.5

228	2	31	-60	148	16.1	8.5
229	2	31	-60	128	24.9	16.2
230	2	31	-60	108	36.3	35.7
231	2	31	-60	88	35.2	10.4
232	2	31	-60	68	16.6	23.3
233	2	31	-60	48	21.9	35.4
234	2	31	-60	28	54.0	15.2
235	2	31	-60	8	156.4	17.5
236	2	32	-60	148	17.3	14.2
237	2	32	-60	128	11.6	19.1
238	2	32	-60	108	55.5	24.1
239	2	32	-60	88	39.5	9.9
240	2	32	-60	68	43.3	32.8
241	2	32	-60	48	29.0	22.9
242	2	32	-60	28	27.7	13.3
243	2	32	-60	8	103.0	9.7
244	1	33	-60	148	20.9	34.0
245	1	33	-60	128	23.4	15.2
246	1	33	-60	108	9.6	16.6
247	1	33	-60	88	53.7	8.5
248	1	33	-60	68	23.9	8.5
249	1	33	-60	48	36.5	27.7
250	1	33	-60	28	102.2	30.3
251	1	33	-60	8	54.2	12.3
252	1	34	-60	148	13.5	12.6
253	1	34	-60	128	20.6	29.8
254	1	34	-60	108	10.3	23.4
255	1	34	-60	88	32.5	26.0
256	1	34	-60	68	67.3	8.9
257	1	34	-60	48	131.7	24.3
258	1	34	-60	28	42.5	13.8
259	1	34	-60	8	44.5	28.5
260	1	35	-60	148	13.9	19.4
261	1	35	-60	128	25.6	17.4
262	1	35	-60	108	28.4	10.9
263	1	35	-60	88	10.2	16.9
264	1	35	-60	68	94.6	21.9
265	1	35	-60	48	46.5	25.1
266	1	35	-60	28	51.6	8.0
267	1	35	-60	8	62.0	13.2
268	1	36	-60	148	17.7	12.1

269	1	36	-60	128	10.5	19.7
270	1	36	-60	108	29.4	13.9
271	1	36	-60	88	42.6	42.0
272	1	36	-60	68	28.4	26.4
273	1	36	-60	48	30.9	23.6
274	1	36	-60	28	148.0	15.7
275	1	36	-60	8	16.3	12.8
276	1	37	-60	148	11.6	13.2
277	1	37	-60	128	39.0	10.0
278	1	37	-60	108	27.4	29.3
279	1	37	-60	88	12.4	30.9
280	1	37	-60	68	50.9	27.3
281	1	37	-60	48	11.4	9.8
282	1	37	-60	28	119.2	19.4
283	1	37	-60	8	24.7	18.0
284	2	38	-40	138	10.4	16.3
285	2	38	-40	118	9.9	16.1
286	2	38	-40	98	50.9	17.6
287	2	38	-40	78	33.1	31.8
288	2	38	-40	58	57.9	17.1
289	2	38	-40	38	13.5	15.3
290	2	38	-40	18	43.8	8.4
291	2	39	-40	138	16.3	10.5
292	2	39	-40	118	15.1	28.5
293	2	39	-40	98	61.3	28.0
294	2	39	-40	78	36.1	22.1
295	2	39	-40	58	41.4	8.5
296	2	39	-40	38	75.1	19.6
297	2	39	-40	18	10.0	11.0
298	2	40	-40	138	18.3	9.0
299	2	40	-40	118	26.4	34.5
300	2	40	-40	98	9.9	21.2
301	2	40	-40	78	63.1	16.3
302	2	40	-40	58	32.4	26.1
303	2	40	-40	38	24.8	8.9
304	2	40	-40	18	81.5	18.2
305	2	41	-40	138	8.0	12.6
306	2	41	-40	118	49.9	11.0
307	2	41	-40	98	30.0	39.5
308	2	41	-40	78	51.7	13.2
309	2	41	-40	58	24.0	12.1

310	2	41	-40	38	19.1	33.3
311	2	41	-40	18	140.8	19.8
312	2	42	-40	138	21.7	24.7
313	2	42	-40	118	10.6	20.2
314	2	42	-40	98	41.9	10.4
315	2	42	-40	78	37.7	22.8
316	2	42	-40	58	98.1	21.1
317	2	42	-40	38	15.4	12.0
318	2	42	-40	18	34.9	36.3
319	2	43	-40	138	10.8	16.9
320	2	43	-40	118	37.3	29.5
321	2	43	-40	98	17.5	24.6
322	2	43	-40	78	46.0	8.5
323	2	43	-40	58	88.3	14.1
324	2	43	-40	38	61.2	30.6
325	2	43	-40	18	16.1	13.3
326	2	44	-40	138	8.8	44.2
327	2	44	-40	118	44.4	12.5
328	2	44	-40	98	21.4	19.3
329	2	44	-40	78	8.0	26.6
330	2	44	-40	58	77.1	30.0
331	2	44	-40	38	26.7	13.4
332	2	44	-40	18	111.0	21.6
333	2	45	-40	138	26.1	29.0
334	2	45	-40	118	11.8	31.8
335	2	45	-40	98	22.4	11.9
336	2	45	-40	78	27.5	13.7
337	2	45	-40	58	80.5	12.6
338	2	45	-40	38	85.1	37.1
339	2	45	-40	18	24.3	22.3
340	1	46	-40	138	12.8	35.1
341	1	46	-40	118	24.7	16.7
342	1	46	-40	98	75.0	23.9
343	1	46	-40	78	10.5	12.3
344	1	46	-40	58	49.2	9.4
345	1	46	-40	38	40.7	24.1
346	1	46	-40	18	63.5	27.8
347	1	47	-40	138	32.0	21.2
348	1	47	-40	118	20.7	10.0
349	1	47	-40	98	31.2	29.0
350	1	47	-40	78	13.0	25.8

351	1	47	-40	58	51.3	37.9
352	1	47	-40	38	129.2	13.9
353	1	47	-40	18	50.8	13.7
354	1	48	-40	138	15.0	41.1
355	1	48	-40	118	18.6	17.8
356	1	48	-40	98	38.9	10.9
357	1	48	-40	78	98.4	15.7
358	1	48	-40	58	19.1	17.6
359	1	48	-40	38	69.2	27.4
360	1	48	-40	18	55.7	20.4
361	1	49	-40	138	20.5	23.2
362	1	49	-40	118	8.6	20.8
363	1	49	-40	98	27.7	11.4
364	1	49	-40	78	26.1	34.7
365	1	49	-40	58	65.3	20.5
366	1	49	-40	38	34.5	20.2
367	1	49	-40	18	96.6	17.1
368	1	50	-40	138	27.0	30.1
369	1	50	-40	118	15.8	18.4
370	1	50	-40	98	20.4	30.0
371	1	50	-40	78	42.5	9.4
372	1	50	-40	58	43.3	9.8
373	1	50	-40	38	140.7	16.9
374	1	50	-40	18	46.1	31.2
375	1	51	-40	138	8.4	13.1
376	1	51	-40	118	53.8	11.5
377	1	51	-40	98	32.4	42.5
378	1	51	-40	78	53.7	14.2
379	1	51	-40	58	25.6	13.1
380	1	51	-40	38	21.0	35.0
381	1	51	-40	18	153.3	21.0
382	1	52	-40	138	13.2	25.5
383	1	52	-40	118	29.1	14.5
384	1	52	-40	98	33.6	35.4
385	1	52	-40	78	72.1	16.8
386	1	52	-40	58	9.6	18.2
387	1	52	-40	38	49.3	9.8
388	1	52	-40	18	66.3	23.7
389	2	53	-20	148	8.9	17.6
390	2	53	-20	128	35.4	9.0
391	2	53	-20	108	40.6	32.7

392	2	53	-20	88	15.7	26.9
393	2	53	-20	68	34.8	20.1
394	2	53	-20	48	55.2	14.0
395	2	53	-20	28	21.7	8.4
396	2	53	-20	8	133.9	19.7
397	2	54	-20	148	16.5	14.8
398	2	54	-20	128	8.0	16.8
399	2	54	-20	108	15.1	37.6
400	2	54	-20	88	51.6	25.2
401	2	54	-20	68	45.1	34.3
402	2	54	-20	48	62.5	10.3
403	2	54	-20	28	93.3	8.9
404	2	54	-20	8	14.2	18.6
405	2	55	-20	148	12.9	37.1
406	2	55	-20	128	20.0	12.5
407	2	55	-20	108	47.7	39.9
408	2	55	-20	88	33.8	23.7
409	2	55	-20	68	12.3	17.2
410	2	55	-20	48	25.4	29.7
411	2	55	-20	28	112.8	16.2
412	2	55	-20	8	39.9	20.2
413	2	56	-20	148	18.7	15.3
414	2	56	-20	128	32.6	43.8
415	2	56	-20	108	13.5	26.5
416	2	56	-20	88	24.9	20.4
417	2	56	-20	68	76.7	20.7
418	2	56	-20	48	79.9	8.0
419	2	56	-20	28	75.6	24.6
420	2	56	-20	8	10.1	16.0
421	2	57	-20	148	14.2	21.3
422	2	57	-20	128	37.0	9.5
423	2	57	-20	108	39.1	34.1
424	2	57	-20	88	14.6	21.0
425	2	57	-20	68	53.0	16.2
426	2	57	-20	48	18.4	8.9
427	2	57	-20	28	36.0	36.7
428	2	57	-20	8	143.6	20.8
429	1	58	-20	148	8.0	20.0
430	1	58	-20	128	30.3	15.7
431	1	58	-20	108	16.7	9.9
432	1	58	-20	88	17.9	21.6

433	1	58	-20	68	30.0	38.3
434	1	58	-20	48	76.6	17.0
435	1	58	-20	28	38.1	10.6
436	1	58	-20	8	125.9	33.9
437	1	59	-20	148	16.9	26.5
438	1	59	-20	128	9.0	20.4
439	1	59	-20	108	26.4	11.9
440	1	59	-20	88	60.9	13.3
441	1	59	-20	68	26.9	11.3
442	1	59	-20	48	83.3	40.3
443	1	59	-20	28	23.7	31.5
444	1	59	-20	8	64.7	16.5
445	1	60	-20	148	9.2	27.4
446	1	60	-20	128	13.1	13.0
447	1	60	-20	108	64.0	16.0
448	1	60	-20	88	36.6	9.4
449	1	60	-20	68	62.1	36.1
450	1	60	-20	48	57.6	17.5
451	1	60	-20	28	33.9	16.7
452	1	60	-20	8	107.8	14.6
453	1	61	-20	148	21.5	15.9
454	1	61	-20	128	14.2	33.3
455	1	61	-20	108	18.4	17.1
456	1	61	-20	88	63.7	10.9
457	1	61	-20	68	9.4	16.7
458	1	61	-20	48	38.4	18.0
459	1	61	-20	28	78.8	27.1
460	1	61	-20	8	28.9	8.0
461	1	62	-20	148	29.1	22.0
462	1	62	-20	128	16.4	22.3
463	1	62	-20	108	11.1	20.7
464	1	62	-20	88	66.9	17.5
465	1	62	-20	68	31.5	28.2
466	1	62	-20	48	60.0	12.1
467	1	62	-20	28	17.8	21.2
468	1	62	-20	8	70.4	38.5
469	1	63	-20	148	9.5	39.1
470	1	63	-20	128	27.3	34.8
471	1	63	-20	108	23.6	12.4
472	1	63	-20	88	86.6	11.3
473	1	63	-20	68	20.9	11.7

474	1	63	-20	48	65.1	25.9
475	1	63	-20	28	15.8	22.5
476	1	63	-20	8	56.7	8.4
477	1	64	-20	148	9.8	22.7
478	1	64	-20	128	41.4	13.6
479	1	64	-20	108	17.5	9.0
480	1	64	-20	88	44.3	29.8
481	1	64	-20	68	101.3	17.8
482	1	64	-20	48	48.6	21.6
483	1	64	-20	28	13.9	25.4
484	1	64	-20	8	73.4	10.1
485	1	65	-20	148	11.0	23.4
486	1	65	-20	128	31.4	11.0
487	1	65	-20	108	33.9	25.7
488	1	65	-20	88	29.9	22.3
489	1	65	-20	68	84.5	10.3
490	1	65	-20	48	42.4	10.7
491	1	65	-20	28	8.0	28.1
492	1	65	-20	8	90.3	26.6
493	2	66	0	138	22.3	17.5
494	2	66	0	118	13.8	9.5
495	2	66	0	98	55.5	8.5
496	2	66	0	78	60.5	19.6
497	2	66	0	58	22.3	15.5
498	2	66	0	38	47.1	20.8
499	2	66	0	18	85.0	9.7
500	2	67	0	138	17.3	11.0
501	2	67	0	118	33.4	40.3
502	2	67	0	98	23.5	19.9
503	2	67	0	78	15.6	27.5
504	2	67	0	58	111.5	24.6
505	2	67	0	38	8.0	17.4
506	2	67	0	18	116.8	11.5
507	2	68	0	138	13.7	26.3
508	2	68	0	118	30.1	15.1
509	2	68	0	98	34.9	37.2
510	2	68	0	78	75.7	17.3
511	2	68	0	58	11.2	18.7
512	2	68	0	38	51.5	10.2
513	2	68	0	18	69.1	24.4
514	1	69	0	138	28.0	36.8

515	1	69	0	118	17.2	22.9
516	1	69	0	98	12.7	14.9
517	1	69	0	78	44.2	23.5
518	1	69	0	58	37.7	10.7
519	1	69	0	38	102.0	28.4
520	1	69	0	18	22.2	32.6
521	1	70	0	138	23.0	27.2
522	1	70	0	118	11.2	19.0
523	1	70	0	98	43.5	9.0
524	1	70	0	78	39.3	24.2
525	1	70	0	58	104.1	21.8
526	1	70	0	38	17.3	12.5
527	1	70	0	18	37.1	39.0
528	1	71	0	138	17.8	11.5
529	1	71	0	118	34.6	43.3
530	1	71	0	98	24.5	20.5
531	1	71	0	78	16.9	28.5
532	1	71	0	58	121.3	25.3
533	1	71	0	38	9.8	17.9
534	1	71	0	18	123.5	11.9
535	1	72	0	138	9.6	18.1
536	1	72	0	118	27.3	21.5
537	1	72	0	98	64.9	18.7
538	1	72	0	78	47.8	29.5
539	1	72	0	58	14.3	19.3
540	1	72	0	38	53.9	8.4
541	1	72	0	18	75.1	34.3
542	1	73	0	138	9.2	13.6
543	1	73	0	118	46.9	25.1
544	1	73	0	98	36.2	31.2
545	1	73	0	78	68.8	9.9
546	1	73	0	58	8.0	27.0
547	1	73	0	38	22.9	8.0
548	1	73	0	18	39.3	14.2
549	1	74	0	138	29.2	31.2
550	1	74	0	118	12.5	33.0
551	1	74	0	98	25.6	12.4
552	1	74	0	78	28.8	14.7
553	1	74	0	58	84.2	13.6
554	1	74	0	38	88.8	39.9
555	1	74	0	18	26.4	23.0

556	1	75	0	138	18.8	9.5
557	1	75	0	118	28.2	36.1
558	1	75	0	98	10.8	21.8
559	1	75	0	78	65.8	17.9
560	1	75	0	58	34.1	27.9
561	1	75	0	38	28.6	9.3
562	1	75	0	18	88.6	18.7
563	1	76	0	138	11.2	18.7
564	1	76	0	118	38.8	30.6
565	1	76	0	98	18.4	25.4
566	1	76	0	78	49.7	8.9
567	1	76	0	58	92.9	14.5
568	1	76	0	38	63.8	31.9
569	1	76	0	18	18.1	14.7
570	2	77	20	148	19.2	35.4
571	2	77	20	128	11.1	14.1
572	2	77	20	108	21.8	17.7
573	2	77	20	88	55.9	18.0
574	2	77	20	68	47.0	10.8
575	2	77	20	48	20.1	18.6
576	2	77	20	28	25.7	39.4
577	2	77	20	8	94.3	23.5
578	1	78	20	148	22.2	41.5
579	1	78	20	128	15.3	8.0
580	1	78	20	108	42.1	13.4
581	1	78	20	88	8.0	19.2
582	1	78	20	68	39.8	21.3
583	1	78	20	48	50.7	30.9
584	1	78	20	28	31.8	9.3
585	1	78	20	8	113.2	13.7
586	1	79	20	148	12.2	24.1
587	1	79	20	128	17.6	14.6
588	1	79	20	108	11.9	31.5
589	1	79	20	88	49.6	33.5
590	1	79	20	68	36.4	9.4
591	1	79	20	48	9.7	26.8
592	1	79	20	28	135.9	14.3
593	1	79	20	8	31.1	22.1
594	1	80	20	148	11.3	16.4
595	1	80	20	128	28.3	36.4
596	1	80	20	108	24.5	11.4

597	1	80	20	88	19.1	32.1
598	1	80	20	68	80.4	24.0
599	1	80	20	48	8.0	13.0
600	1	80	20	28	56.4	17.3
601	1	80	20	8	46.9	21.5
602	1	81	20	148	24.8	18.8
603	1	81	20	128	12.1	27.8
604	1	81	20	108	32.7	21.3
605	1	81	20	88	22.5	11.8
606	1	81	20	68	57.3	41.2
607	1	81	20	48	121.0	14.5
608	1	81	20	28	40.3	26.3
609	1	81	20	8	33.3	14.1
610	1	82	20	148	14.6	29.3
611	1	82	20	128	18.2	8.5
612	1	82	20	108	52.5	22.0
613	1	82	20	88	11.3	16.4
614	1	82	20	68	55.1	14.1
615	1	82	20	48	27.2	14.9
616	1	82	20	28	61.5	33.0
617	1	82	20	8	83.1	8.9
618	1	83	20	148	10.1	13.7
619	1	83	20	128	18.8	25.3
620	1	83	20	108	50.0	18.3
621	1	83	20	88	28.6	12.3
622	1	83	20	68	13.7	25.6
623	1	83	20	48	32.7	37.5
624	1	83	20	28	72.6	12.4
625	1	83	20	8	98.4	32.3
626	1	84	40	138	14.1	8.5
627	1	84	40	118	22.3	26.7
628	1	84	40	98	47.0	12.9
629	1	84	40	78	14.3	12.7
630	1	84	40	58	53.4	22.4
631	1	84	40	38	92.9	21.4
632	1	84	40	18	14.1	15.1
633	1	85	40	138	36.3	14.7
634	1	85	40	118	32.3	25.9
635	1	85	40	98	16.5	15.4
636	1	85	40	78	23.4	20.2
637	1	85	40	58	29.0	40.7

638	1	85	40	38	113.4	29.4
639	1	85	40	18	72.0	10.2
640	1	86	40	138	19.3	12.1
641	1	86	40	118	35.9	38.0
642	1	86	40	98	19.4	22.5
643	1	86	40	78	55.9	11.3
644	1	86	40	58	30.7	11.2
645	1	86	40	38	42.8	11.1
646	1	86	40	18	131.3	28.8
647	1	87	40	138	23.7	21.8
648	1	87	40	118	25.5	12.0
649	1	87	40	98	13.6	18.1
650	1	87	40	78	18.1	41.6
651	1	87	40	58	73.9	28.9
652	1	87	40	38	78.3	14.4
653	1	87	40	18	28.5	17.6
654	1	88	40	138	16.8	28.1
655	1	88	40	118	21.5	13.5
656	1	88	40	98	45.2	32.4
657	1	88	40	78	84.7	10.8
658	1	88	40	58	15.9	32.5
659	1	88	40	38	36.5	11.6
660	1	88	40	18	105.7	26.0

Table C3. List of 170 tropical cyclone with associated storm parameters used for this project. Storm number is the same as storm number in Table C2.

Storm Number	Texas Region	Master Track	θ (deg)	ΔP (hPa)	R_{max} (km)	V_f (km/h)
10	2	2	-100	128	33.9	38.3
32	2	4	-100	8	86.6	29.6
38	2	5	-100	48	53	20.9
43	2	6	-100	108	22.7	22.7
44	2	6	-100	88	58.3	13.8
52	2	7	-100	88	47.8	24.4
54	2	7	-100	48	106.3	15.4
59	2	8	-100	108	37.7	9.5
62	2	8	-100	48	91.2	28.7
66	1	9	-100	128	44.5	24.5
68	1	9	-100	88	26.1	12.8
73	1	10	-100	148	14.9	8
74	1	10	-100	128	17	26.9
76	1	10	-100	88	70.5	14.8
77	1	10	-100	68	41.5	22.6
105	2	14	-80	78	90.6	15.2
111	2	15	-80	98	15.5	14.4
117	2	16	-80	118	40.5	8
139	2	19	-80	98	69.3	23.2
144	1	20	-80	138	15.9	10
146	1	20	-80	98	58.2	33.8
147	1	20	-80	78	34.6	21.5
151	1	21	-80	138	21	15.2
153	1	21	-80	98	53.1	8
154	1	21	-80	78	58.1	19
158	1	22	-80	138	12	20.5
159	1	22	-80	118	42.3	8.5
160	1	22	-80	98	8.9	15.9
161	1	22	-80	78	22.1	38.7
167	1	23	-80	98	48.9	17
195	2	26	-60	8	26.8	15.5
211	2	28	-60	8	8	11.9
224	2	30	-60	68	110.1	14.6
229	2	31	-60	128	24.9	16.2
238	2	32	-60	108	55.5	24.1
244	1	33	-60	148	20.9	34
245	1	33	-60	128	23.4	15.2

247	1	33	-60	88	53.7	8.5
248	1	33	-60	68	23.9	8.5
252	1	34	-60	148	13.5	12.6
253	1	34	-60	128	20.6	29.8
254	1	34	-60	108	10.3	23.4
255	1	34	-60	88	32.5	26
256	1	34	-60	68	67.3	8.9
260	1	35	-60	148	13.9	19.4
261	1	35	-60	128	25.6	17.4
262	1	35	-60	108	28.4	10.9
264	1	35	-60	68	94.6	21.9
268	1	36	-60	148	17.7	12.1
269	1	36	-60	128	10.5	19.7
270	1	36	-60	108	29.4	13.9
272	1	36	-60	68	28.4	26.4
275	1	36	-60	8	16.3	12.8
276	1	37	-60	148	11.6	13.2
277	1	37	-60	128	39	10
327	2	44	-40	118	44.4	12.5
328	2	44	-40	98	21.4	19.3
330	2	44	-40	58	77.1	30
333	2	45	-40	138	26.1	29
337	2	45	-40	58	80.5	12.6
338	2	45	-40	38	85.1	37.1
341	1	46	-40	118	24.7	16.7
342	1	46	-40	98	75	23.9
344	1	46	-40	58	49.2	9.4
347	1	47	-40	138	32	21.2
348	1	47	-40	118	20.7	10
349	1	47	-40	98	31.2	29
351	1	47	-40	58	51.3	37.9
352	1	47	-40	38	129.2	13.9
354	1	48	-40	138	15	41.1
355	1	48	-40	118	18.6	17.8
356	1	48	-40	98	38.9	10.9
357	1	48	-40	78	98.4	15.7
359	1	48	-40	38	69.2	27.4
363	1	49	-40	98	27.7	11.4
364	1	49	-40	78	26.1	34.7
365	1	49	-40	58	65.3	20.5
376	1	51	-40	118	53.8	11.5

384	1	52	-40	98	33.6	35.4
385	1	52	-40	78	72.1	16.8
414	2	56	-20	128	32.6	43.8
422	2	57	-20	128	37	9.5
423	2	57	-20	108	39.1	34.1
434	1	58	-20	48	76.6	17
435	1	58	-20	28	38.1	10.6
437	1	59	-20	148	16.9	26.5
439	1	59	-20	108	26.4	11.9
440	1	59	-20	88	60.9	13.3
441	1	59	-20	68	26.9	11.3
442	1	59	-20	48	83.3	40.3
445	1	60	-20	148	9.2	27.4
446	1	60	-20	128	13.1	13
447	1	60	-20	108	64	16
448	1	60	-20	88	36.6	9.4
449	1	60	-20	68	62.1	36.1
450	1	60	-20	48	57.6	17.5
453	1	61	-20	148	21.5	15.9
454	1	61	-20	128	14.2	33.3
455	1	61	-20	108	18.4	17.1
456	1	61	-20	88	63.7	10.9
458	1	61	-20	48	38.4	18
461	1	62	-20	148	29.1	22
462	1	62	-20	128	16.4	22.3
463	1	62	-20	108	11.1	20.7
464	1	62	-20	88	66.9	17.5
465	1	62	-20	68	31.5	28.2
466	1	62	-20	48	60	12.1
471	1	63	-20	108	23.6	12.4
472	1	63	-20	88	86.6	11.3
481	1	64	-20	68	101.3	17.8
486	1	65	-20	128	31.4	11
504	2	67	0	58	111.5	24.6
508	2	68	0	118	30.1	15.1
510	2	68	0	78	75.7	17.3
514	1	69	0	138	28	36.8
515	1	69	0	118	17.2	22.9
517	1	69	0	78	44.2	23.5
518	1	69	0	58	37.7	10.7
519	1	69	0	38	102	28.4

521	1	70	0	138	23	27.2
522	1	70	0	118	11.2	19
523	1	70	0	98	43.5	9
524	1	70	0	78	39.3	24.2
525	1	70	0	58	104.1	21.8
528	1	71	0	138	17.8	11.5
529	1	71	0	118	34.6	43.3
530	1	71	0	98	24.5	20.5
531	1	71	0	78	16.9	28.5
532	1	71	0	58	121.3	25.3
535	1	72	0	138	9.6	18.1
536	1	72	0	118	27.3	21.5
537	1	72	0	98	64.9	18.7
538	1	72	0	78	47.8	29.5
540	1	72	0	38	53.9	8.4
543	1	73	0	118	46.9	25.1
545	1	73	0	78	68.8	9.9
564	1	76	0	118	38.8	30.6
573	2	77	20	88	55.9	18
574	2	77	20	68	47	10.8
578	1	78	20	148	22.2	41.5
579	1	78	20	128	15.3	8
580	1	78	20	108	42.1	13.4
583	1	78	20	48	50.7	30.9
586	1	79	20	148	12.2	24.1
587	1	79	20	128	17.6	14.6
588	1	79	20	108	11.9	31.5
589	1	79	20	88	49.6	33.5
590	1	79	20	68	36.4	9.4
594	1	80	20	148	11.3	16.4
595	1	80	20	128	28.3	36.4
596	1	80	20	108	24.5	11.4
597	1	80	20	88	19.1	32.1
598	1	80	20	68	80.4	24
606	1	81	20	68	57.3	41.2
613	1	82	20	88	11.3	16.4
620	1	83	20	108	50	18.3
626	1	84	40	138	14.1	8.5
627	1	84	40	118	22.3	26.7
628	1	84	40	98	47	12.9
630	1	84	40	58	53.4	22.4

631	1	84	40	38	92.9	21.4
633	1	85	40	138	36.3	14.7
634	1	85	40	118	32.3	25.9
637	1	85	40	58	29	40.7
638	1	85	40	38	113.4	29.4
641	1	86	40	118	35.9	38
643	1	86	40	78	55.9	11.3
649	1	87	40	98	13.6	18.1
655	1	88	40	118	21.5	13.5
657	1	88	40	78	84.7	10.8

Appendix D. CSTORM Water Surface Elevation Comparisons for various Alternatives

Comparison at 6 Save Point Locations for 9 storms and 4 Conditions

This section presents time series comparisons of water surface elevations for four conditions, without-project, gate only (BD Alt2), the gate, beach-dune and ring levees with navigation gates at Clear Creek and Dickinson Bayous (BD Alt6), and the gate, beach-dune and ring levee (BD Alt3). Six save point locations are used for this comparison near the Houston Shipping Channel, starting at the mouth of Galveston Bay at the inlet and moving northward through the inlet and stopping near Morgan's Point. See Figure D1 for a map indicating the location of the points. A sampling of 9 of the 170 storms is used to illustrate the water level impacts of alternatives in relation to different storm characteristics. The storms selected provide a variety of angles of approach in relation to the project area along with different intensities and sizes. Each image below contains a side-by-side comparison of water levels on the right hand side and wind speed, wind direction and surface level atmospheric pressure on the left hand side. Note that since the winds and pressure do not change significantly from one save point to an adjacent save point, the images on the left hand side alternate between showing normalized wind vectors over time and a combination of wind speed and atmospheric pressure.

Storm 66, D2, has a rather rare track, in that the storm moves from north to south as it is moving from east to west. The storm also tracks well to the south of the project alternatives. Under these storm conditions, the with-project conditions do not generally lower water in the bay over the without-project condition. This is due to the fact that the ADCIRC model has the large surge barrier gate closed for the entire length of the simulation, which is not something that would occur in practice. The ADCIRC model currently only allows the gate to be open for the entire simulation or closed for the entire simulation. Since the gate is closed, Galveston Bay does not "draw down" water nearly as much as when the gate is open during the storms approach to landfall, which is when the winds blow toward the south. This can clearly be seen at each of the save points inside the bay.

Storm 154, Figure D3, is a slow moving and rather large storm with peak wind speeds over 120 mph. The track of the storm has it making landfall to the south of the project area and with an angle that is acute to the shoreline. This type of track, like the one for storm 66, also sets up persistent winds toward the south, ahead of the storm that would tend to drive water out of Galveston Bay. Again, as in the case of storm 66, the with-project conditions have the large surge barrier gate closed for the entire simulation duration which prevents water from exiting the bay ahead of the storm landfall and even causes water to pile up against the "backside" or bay side of the structure. For the two with-project cases that include the beach-dune components (BD Alt3 and BD Alt6), all the water levels in the bay are lower after the peak water levels are reached, which is virtually the same for each with-project condition shown. This is most likely due to the fact that less water entered the bay across the barrier islands to the north along Bolivar Roads and to the south of Galveston Island.

Storm 270, Figure D4, is an intense, but small sized storm that has a very slow forward motion. Peak wind speeds reach over 140 mph. The track has the storm making landfall just north of Galveston Island at an acute angle but almost perpendicular angle to the shoreline. On the southern end of Galveston Bay at save points 12965 and 15063, the effects of the gate being closed ahead of the storm is again seen as water is driven toward the backside of the gate. As the winds shift toward the north, water moves from the south of the bay to the north, with lower water elevations for the with-project cases compared to the without-project at save points 15602 and 15801.

Storm 342, Figure D5, is a large sized storm with a rather slow forward speed. It has maximum wind speed around 109 mph. The track has the storm making landfall south of the project location at an angle nearly perpendicular to the shoreline. This type of track angle and landfall location in proximity to the project area is where the with-project conditions show significant reductions in water levels at each of the save points along Galveston Bay. Without-project water levels at the northern most save point, 15854, are approximately 18 feet at the peak, while the full project BD Alt 6 has a peak water level of about 8 feet, the gate only option, BD Alt 2, has a peak water level of about 12 feet at the same save point.

Storm 384, Figure D6, is a very intense storm with wind speeds over 160 mph. It is a moderate sized storm and has a forward speed of just over 19 kts. The storm tracks well to the north of the project areas and is likely an event for which the surge barrier gate may not be closed. The peak water levels without the project are only around 2 feet inside the bay, but are only around 1 foot for each of the with-project conditions. The storm location and approach angle relative to the project area, would have water being driven into the bay by the northerly winds ahead of the storm. As the storm passes, the wind direction changes to the south and begins to push water out of the bay.

Storm 447, Figure D7, is a large sized storm with a slow forward speed and winds topping 105 mph. It makes landfall just to the south of the project area and with a nearly perpendicular, albeit slightly obtuse, angle to the shoreline. This condition illustrates the lowering of water levels for the with-project conditions. Similar to storm 342, water levels without the project peak at over 20 feet in the northern most save point and about 15 feet at save point 12965 just inside the bay on the southern side. Each with-project condition reduces water levels significantly in the bay, ranging from about a 6 foot reduction in the southern save points to over 12 feet at the northern save points. The with-project BD Alt6 has the lowest water levels in the bay, followed by BD Alt3 and then the gate only option of BD Alt2.

Storm 456, Figure D8, is a weak tropical storm with wind speed just over 85 mph and a very slow forward motion at only 5.9 kts. It is a moderate sized storm making landfall right over Galveston Island at a nearly perpendicular angle to the shoreline. Examining the wind speeds between day 7.6 and 8.0 at save points 12965 and 15602, the double peak with a rapid decrease in wind speed is indicative of the eye-wall of the storm passing over those locations. Each with-project condition provides significant reductions in water levels at each of the save points inside the bay. At save point 15854, the northern most location, the reduction ranges from almost 10 feet for BD Alt6 and BD Alt3 to 5 feet for Alt2. On the southern end, save point 15063 has a peak water level of nearly 14 feet without the project and only 4 feet with BD Alt6 and BD Alt3 and 8 feet for BD Alt2.

Storm 578, Figure D9, is a very strong storm with wind speeds over 210 mph and minimum central pressure of 865 mb. It is small in size and

moving with a relatively fast forward speed. The track of the storm is from the south moving northward, with landfall south of the project area and at a very obtuse angle relative to the shoreline. The storm passes on the landward, western side of the project area. Each of the with-project alternatives performs nearly identically under these conditions. At save points on the southern side of the bay, points 12965 and 15063 in particular, the bay water level drops by approximately 5 feet from normal levels as opposed to rising between 4 and 8 feet for the without-project case. This is directly due to the winds blowing northward forcing water northward as can be seen at save point 15854, for example. However, under the with-project cases, there is less water in the bay due to the surge barrier gate being closed and, therefore, the peaks of the water levels are between 1 and 2 feet lower at save points 15801 and 15854.

Storm 633, Figure D10, is a strong storm with winds reaching 170 mph and is moderate in size. It is a slow moving storm that would be considered a by-passing storm that moves along the coastline of Texas from the south to the north. The path of the storm and the rotation of the winds would tend to drive water northward along the coast and push water into the bay through the mouth at Bolivar Roads. Each with-project condition reduces the peak water levels by about the same amount over the without-project case. Differences in water levels between the with-project alternatives are seen as the storm peak winds move past the save point locations and the wind direction switches to a more southern direction. During those later times in the storm, after day 5.5, the water levels for the gate only option, BD Alt2, allow more water to flow back out and over the existing barrier islands than the BD Alt3 and BD Alt6 which have higher dunes and retain more water.

Figure D1. Map showing the locations of six (6) save points where time series plots of water surface elevation, wind speed, wind direction and atmpshperic pressure are presented. The color contours are topo/bathy in units of meters (NAVD88) taken from the ADCIRC mesh.

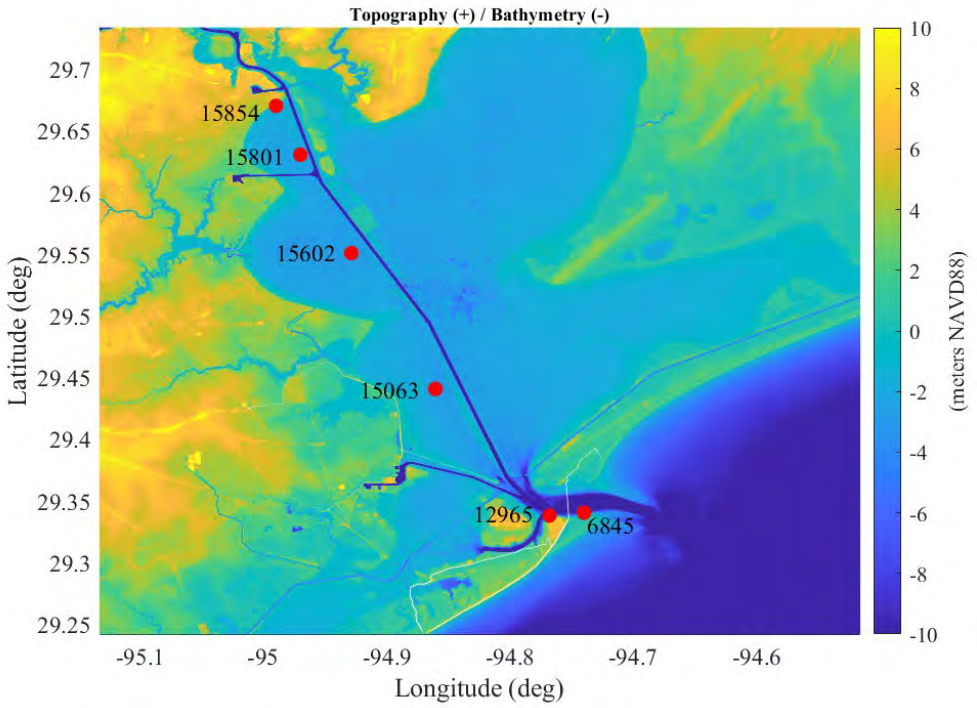

Figure D2. Comparsion of water surface elevation for storm 0066 (right hand side) at six (6) save point locations for four (4) different configurations. The left hand side shows the corresponding wind direction (as normalized vectors), wind speed and athmospheric pressure. Note that images are arranged so that the northernmost save point is at the top of the image and the point outside the mouth of Galveston Bay is at the bottom.

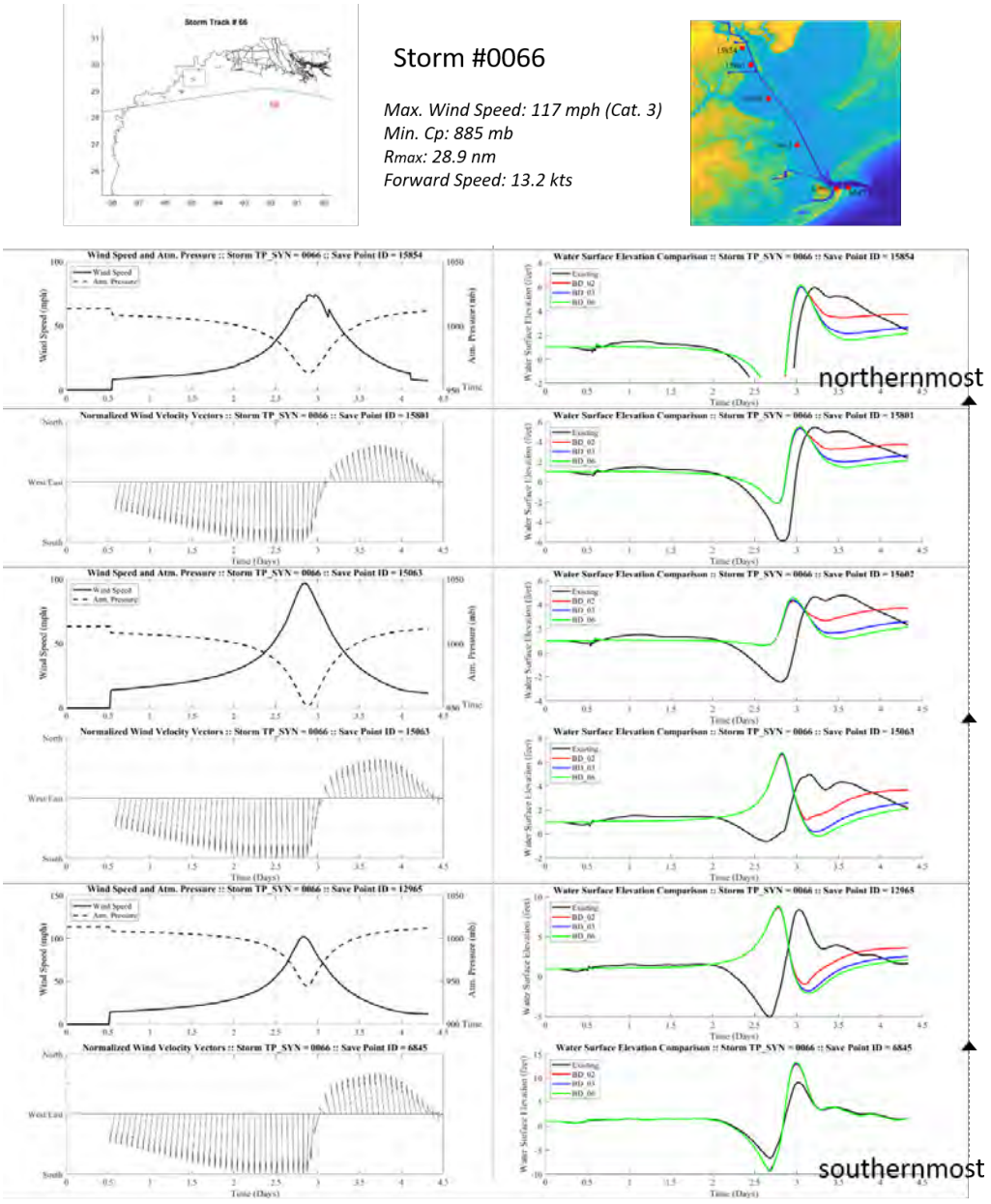

Figure D3. Comparsion of water surface elevation for storm 0154 (right hand side) at six (6) save point locations for four (4) different configurations. The left hand side shows the corresponding wind direction (as normalized vectors), wind speed and athmospheric p

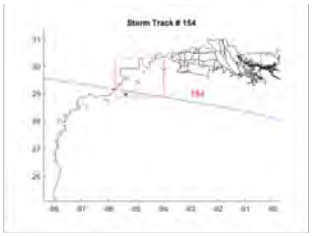

Storm #0154

Max. Wind Speed: 121 mph (Cat. 3)
Min. Cp: 935 mb
Rmax: 39.7 nm
Forward Speed: 10.3 kts

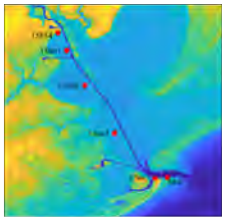

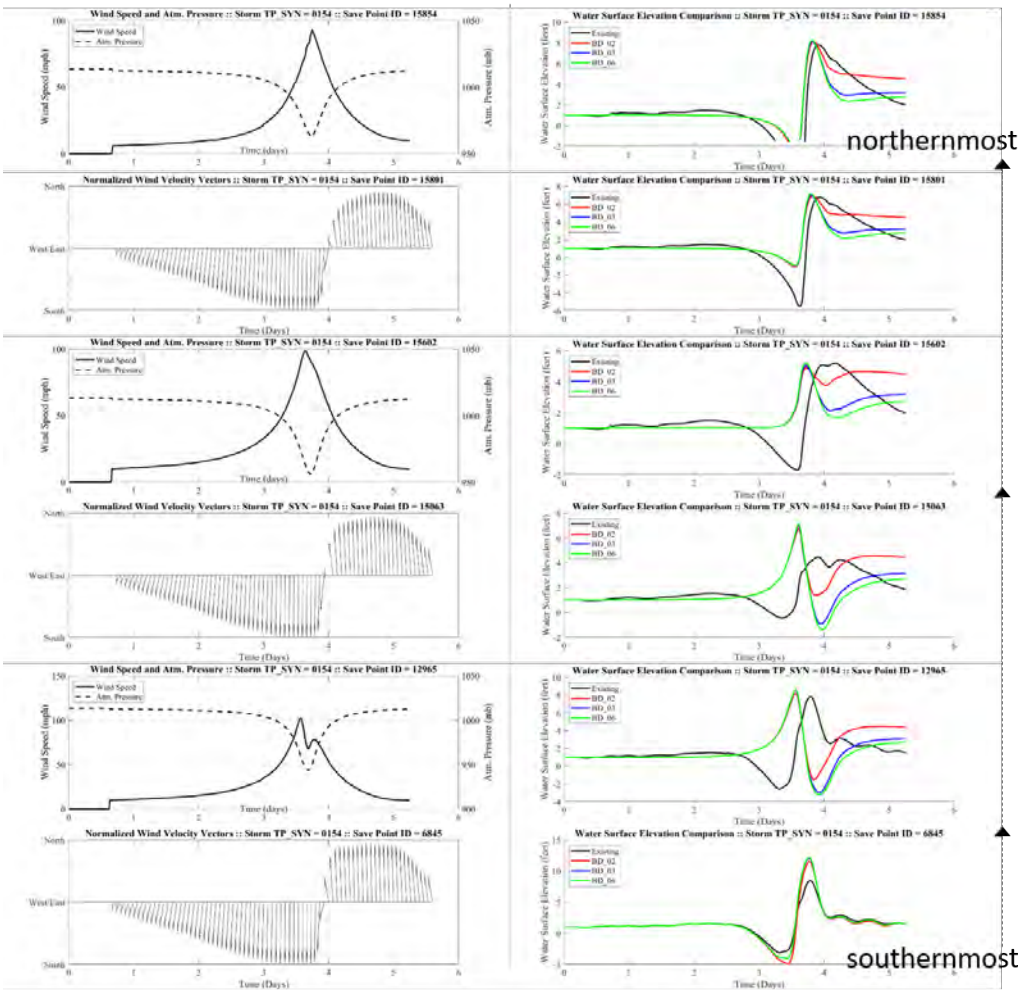

Figure D4. Comparsion of water surface elevation for storm 0270 (right hand side) at six (6) save point locations for four (4) different configurations. The left hand side shows the corresponding wind direction (as normalized vectors), wind speed and athmospheric p

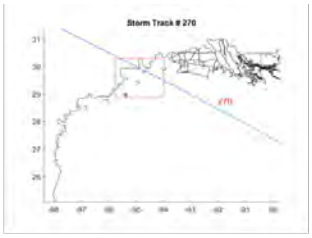

Storm #0270

Max. Wind Speed: 143 mph (Cat. 4)
Min. Cp: 905 mb
Rmax: 17.8 nm
Forward Speed: 7.5 kts

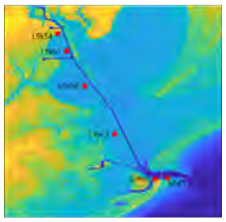

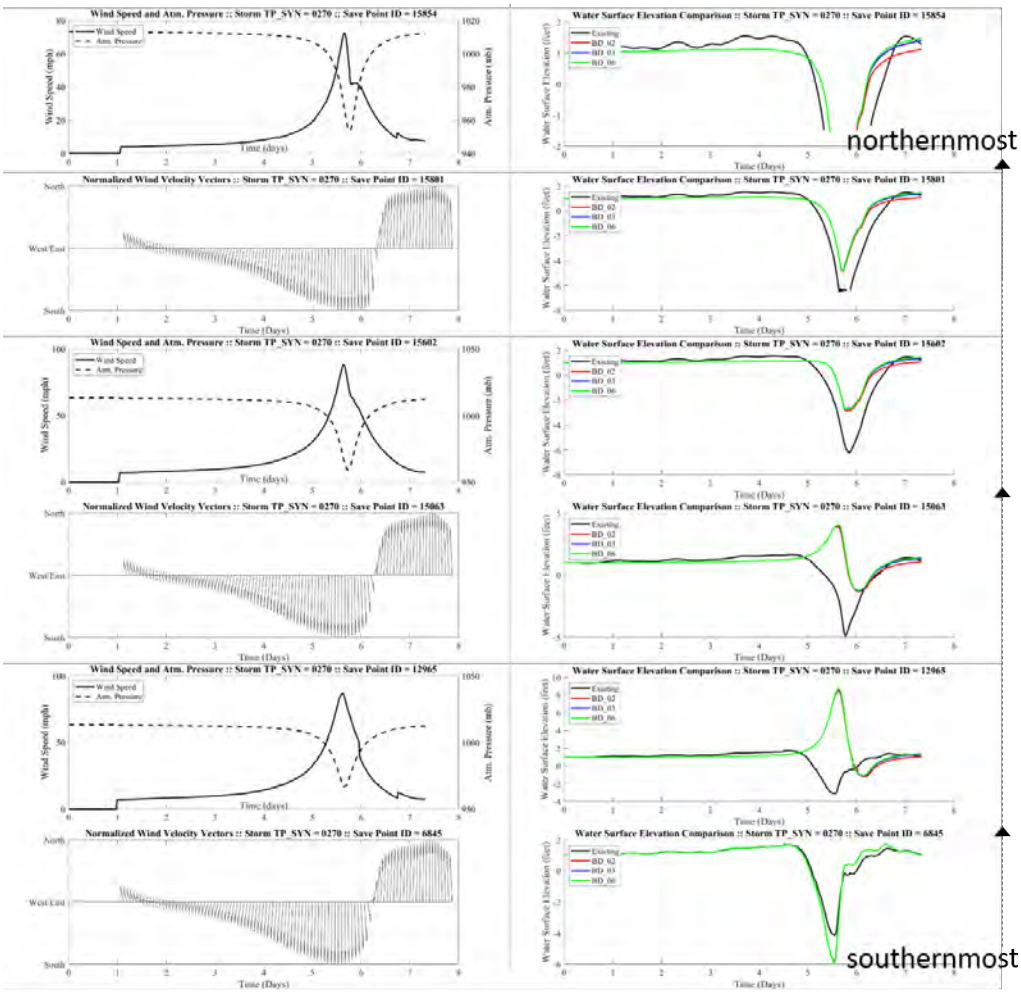

Figure D5. Comparsion of water surface elevation for storm 0342 (right hand side) at six (6) save point locations for four (4) different configurations. The left hand side shows the corresponding wind direction (as normalized vectors), wind speed and athmospheric p

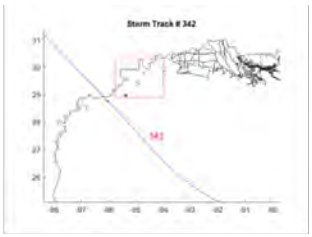

Storm #0342

Max. Wind Speed: 109 mph (Cat. 2)
Min. Cp: 915 mb
Rmax: 54.1 nm
Forward Speed: 12.9 kts

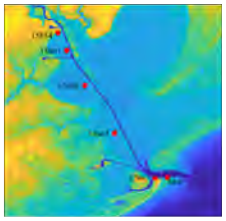

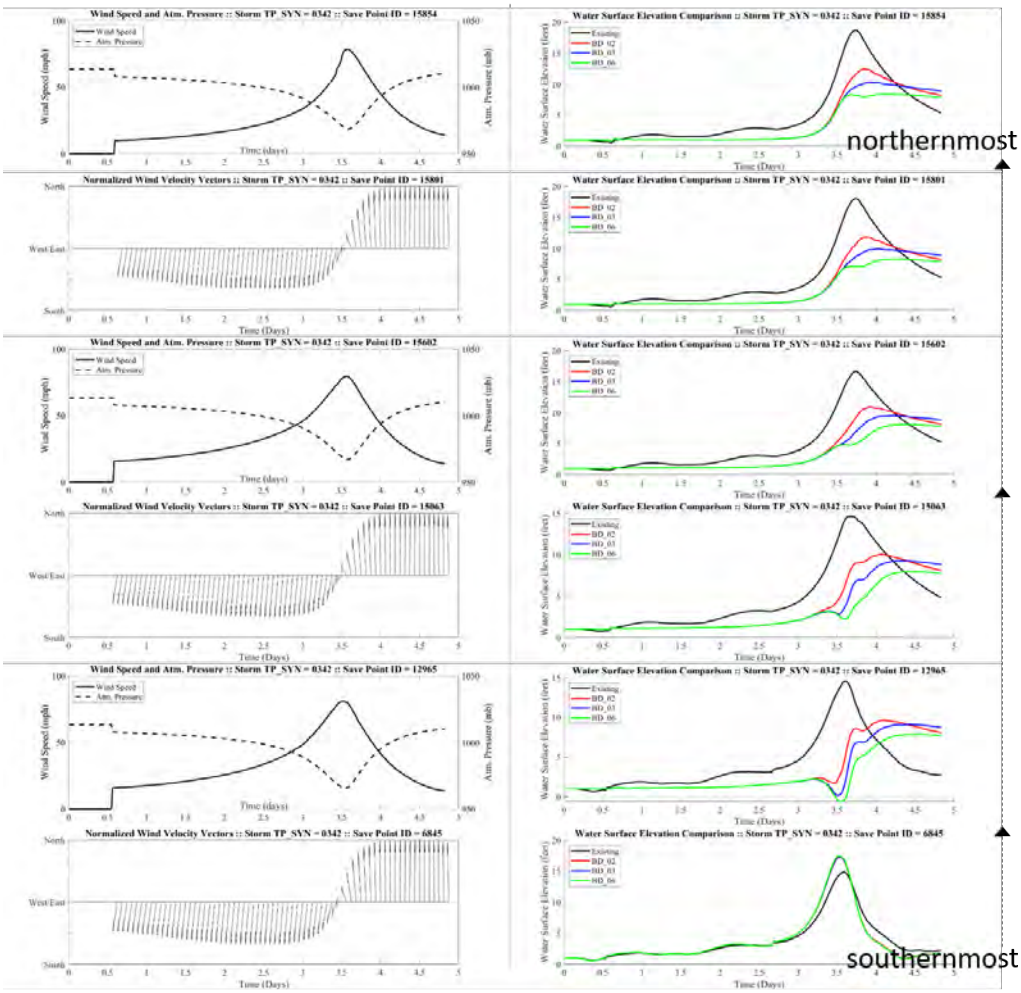

Figure D6. Comparsion of water surface elevation for storm 0384 (right hand side) at six (6) save point locations for four (4) different configurations. The left hand side shows the corresponding wind direction (as normalized vectors), wind speed and athmospheric p

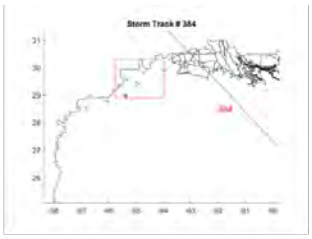

Storm #0384

Max. Wind Speed: 162 mph (Cat. 5)
Min. Cp: 915 mb
Rmax: 20.8 nm
Forward Speed: 19.1 kts

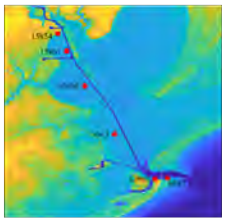

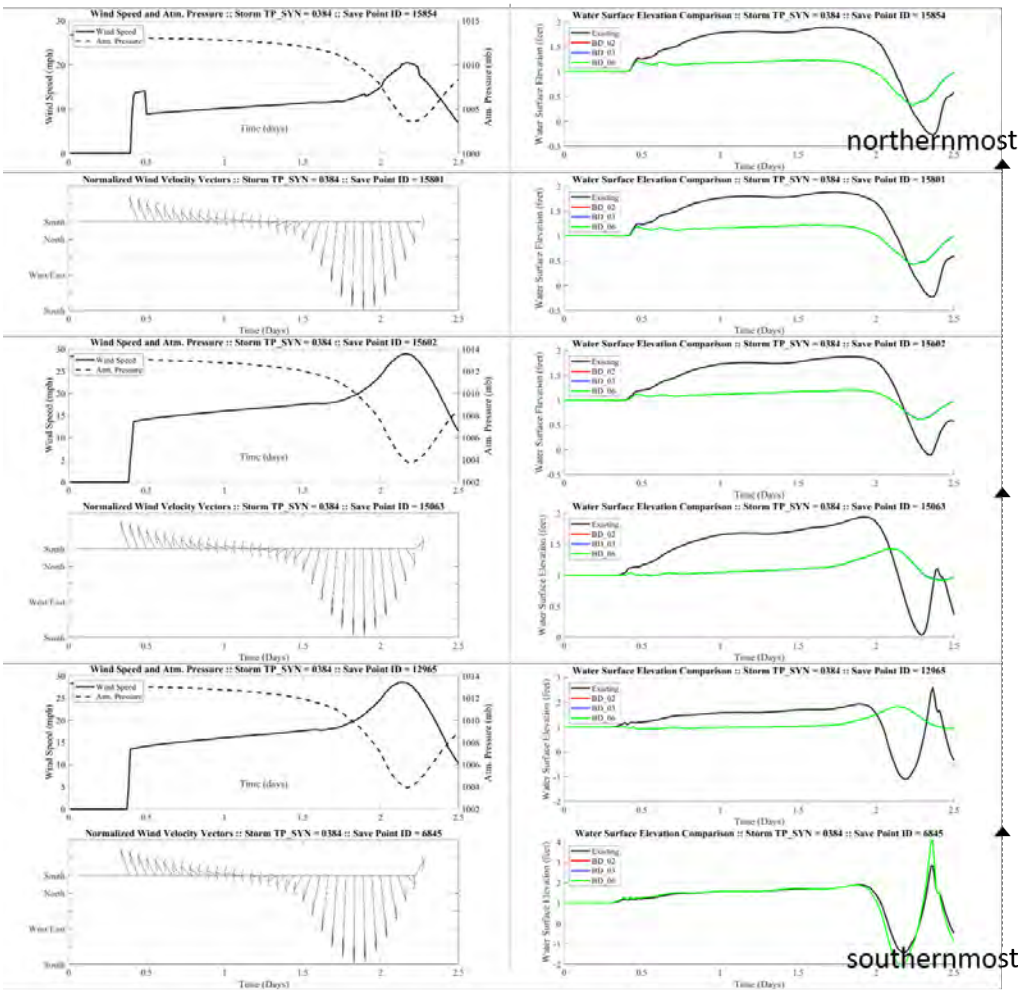

Figure D7. Comparsion of water surface elevation for storm 0447 (right hand side) at six (6) save point locations for four (4) different configurations. The left hand side shows the corresponding wind direction (as normalized vectors), wind speed and athmospheric p

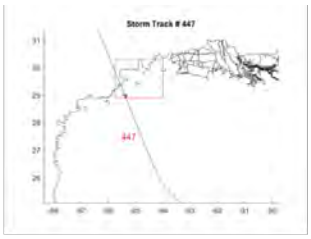

Storm #0447

Max. Wind Speed: 105 mph (Cat. 2)
Min. Cp: 905 mb
Rmax: 44.6 nm
Forward Speed: 8.6 kts

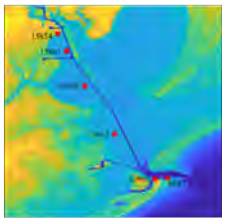

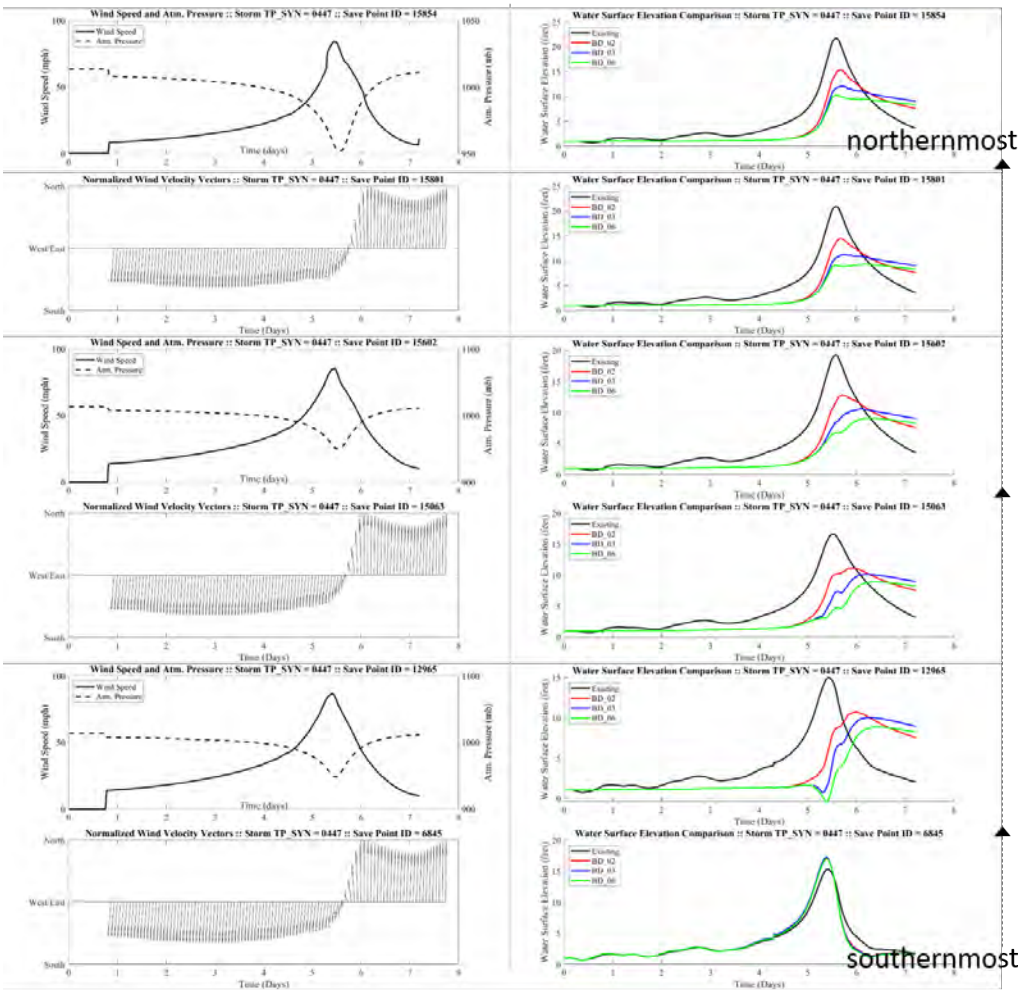

Figure D8. Comparsion of water surface elevation for storm 0456 (right hand side) at six (6) save point locations for four (4) different configurations. The left hand side shows the corresponding wind direction (as normalized vectors), wind speed and athmospheric p

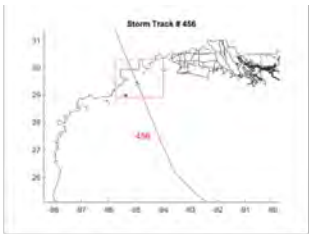

Storm #0456

Max. Wind Speed: 87 mph (Cat. 1)
Min. Cp: 925 mb
Rmax: 44.3 nm
Forward Speed: 5.9 kts

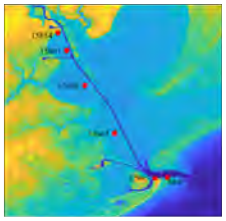

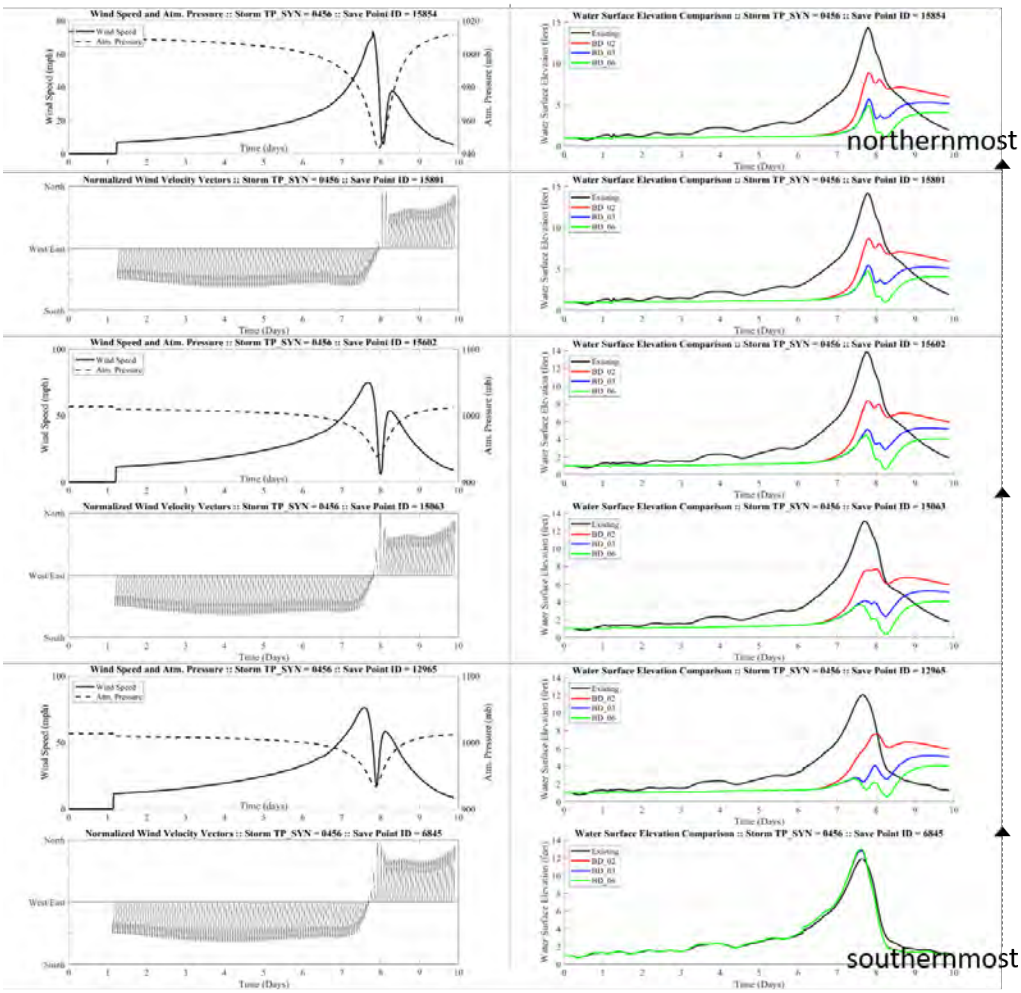

Figure D9. Comparsion of water surface elevation for storm 0578 (right hand side) at six (6) save point locations for four (4) different configurations. The left hand side shows the corresponding wind direction (as normalized vectors), wind speed and athmospheric p

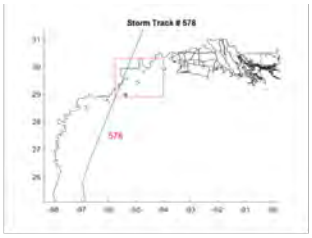

Storm #0578

Max. Wind Speed: 210 mph (Cat. 5)
Min. Cp: 865 mb
Rmax: 12.8 nm
Forward Speed: 22.4 kts

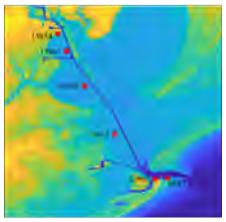

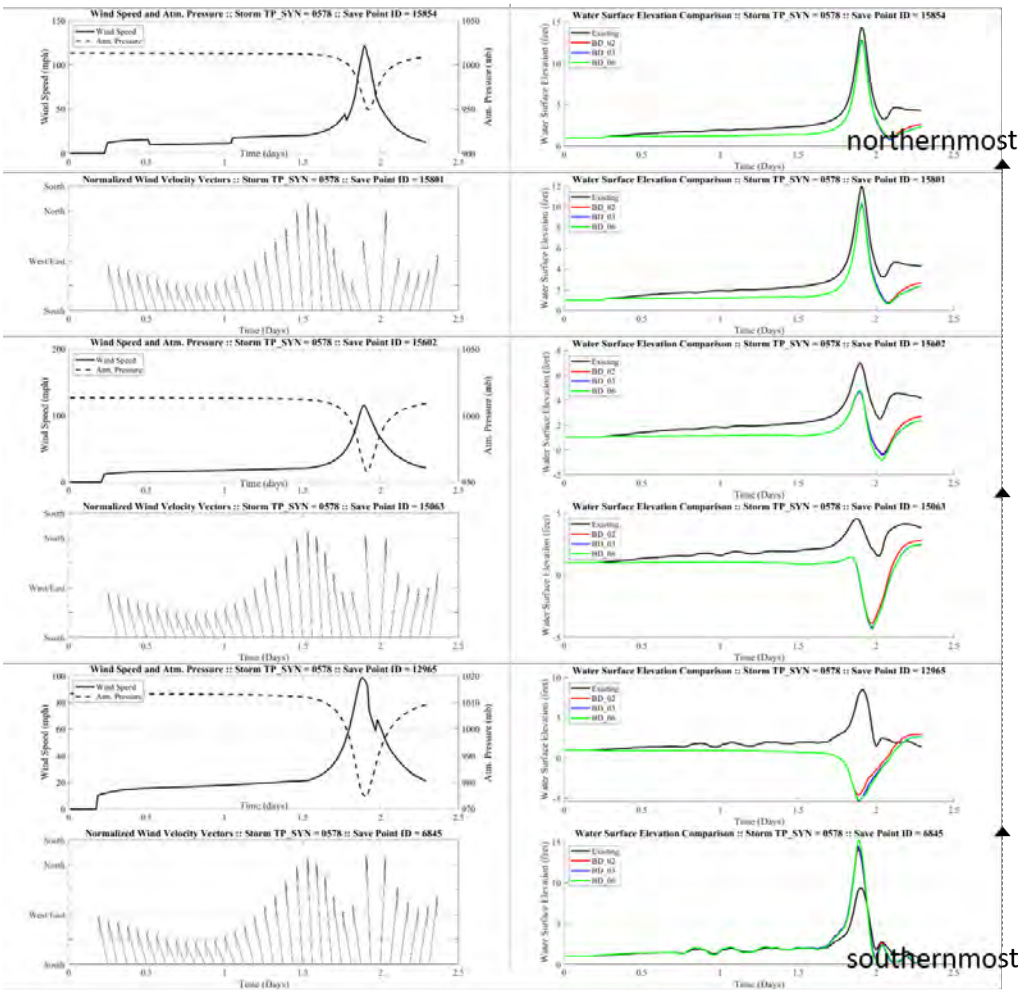

Figure D10. Comparsion of water surface elevation for storm 0633 (right hand side) at six (6) save point locations for four (4) different configurations. The left hand side shows the corresponding wind direction (as normalized vectors), wind speed and athmospheric p

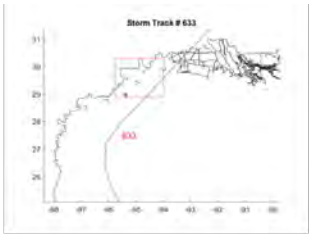

Storm #0633

Max. Wind Speed: 170 mph (Cat. 5)
Min. Cp: 875 mb
Rmax: 22.7 nm
Forward Speed: 7.9 kts

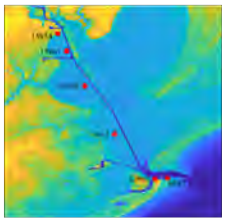

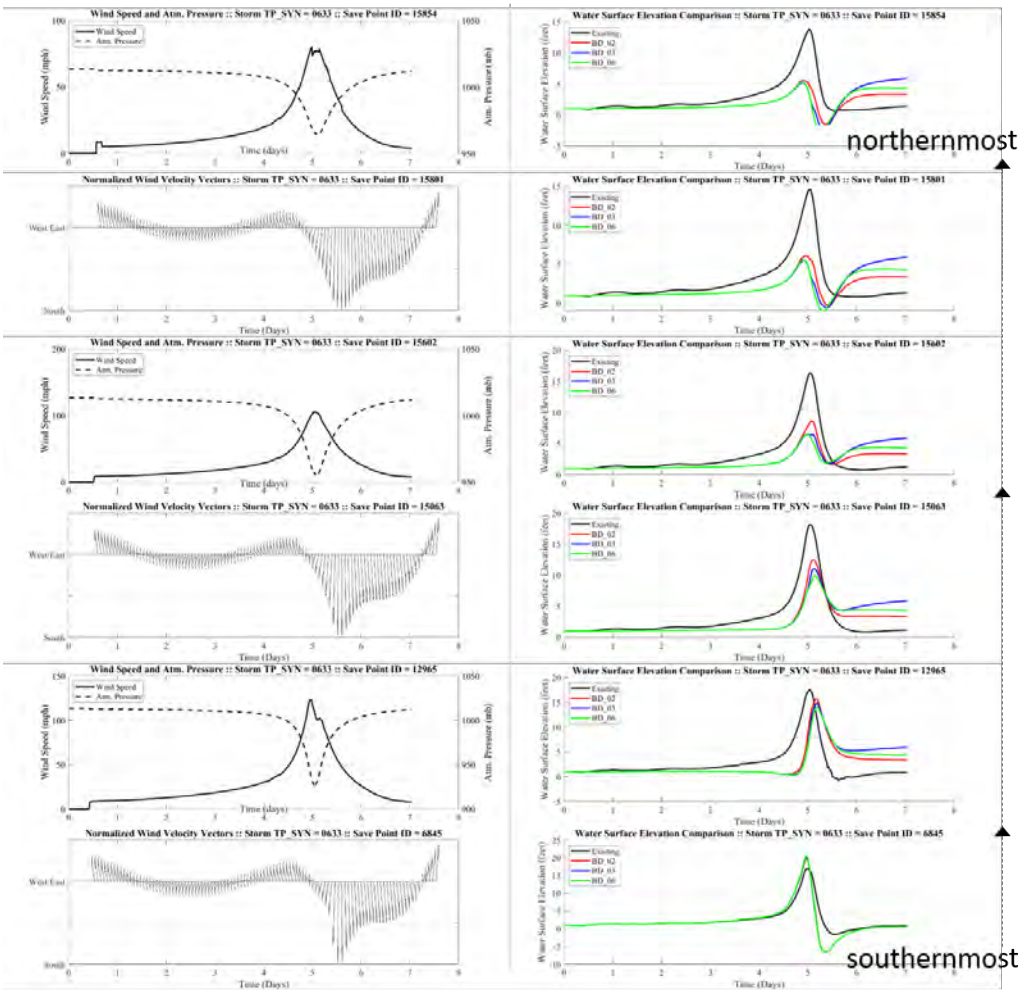

CSTORM Maximum Water Surface Elevation Comparisons for Without-Project vs Beach-Dune Alterative

Maximum water surface elevations for 20 of the 170 storms are presented below for without-project (existing conditions) and full beach dune (BD Alt6). These figures are presented to illustrate the general impacts to maximum water surface elevations when considering this with-project alternative under different storm conditions. Figure D11 shows a map with the general layout of the representation of the alternative in the ADCIRC model. The bright green lines represent the with-project features, including the gate surge barrier, the beach-dune system, the ring levee around the back side of Galveston Island and two smaller navigation gates, one at Dickinson Bayou and the other at Clear Creek.

Figure D11: Map showing the ADCIRC model representation of the full beach dune and gate system, labeled as BD_Alt6.

Figure D12. Comparison of maximum water surface elevations color contour plots from the CSTORM coupled ADCIRC+STWAVE simulations for storm 0066 under without-project and with-project BD_Alt2.

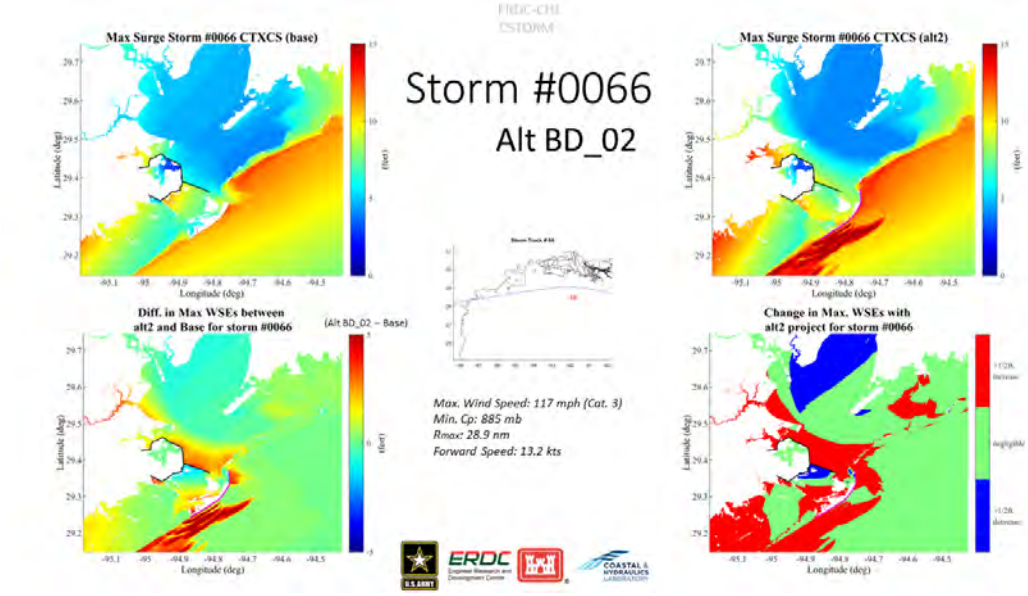

Figure D13. Comparison of maximum water surface elevations color contour plots from the CSTORM coupled ADCIRC+STWAVE simulations for storm 0073 under without-project and with-project BD_Alt2. .

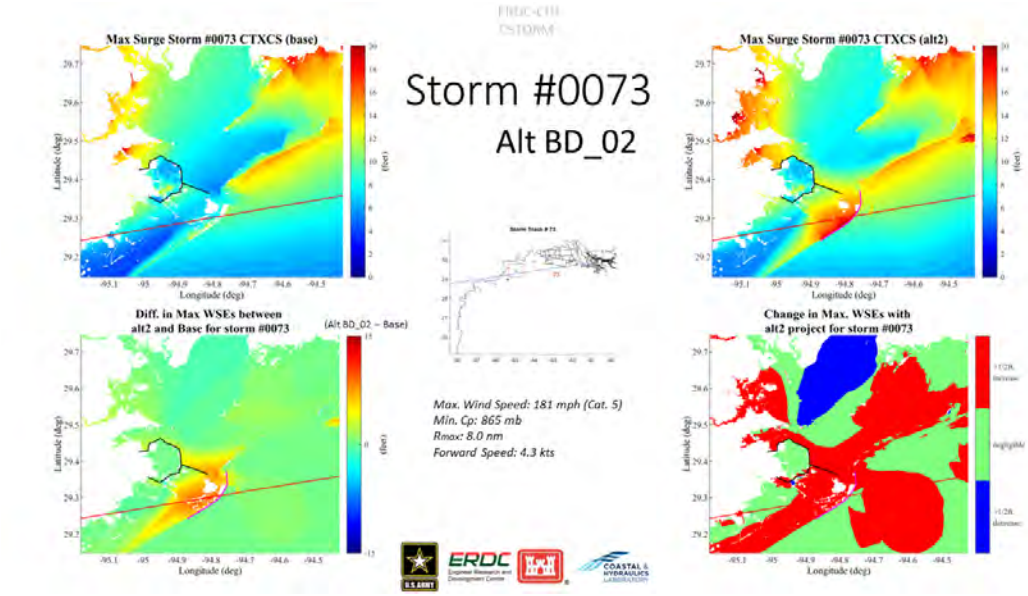

Figure D14. Comparison of maximum water surface elevations color contour plots from the CSTORM coupled ADCIRC+STWAVE simulations for storm 0077 under without-project and with-project BD_Alt2.

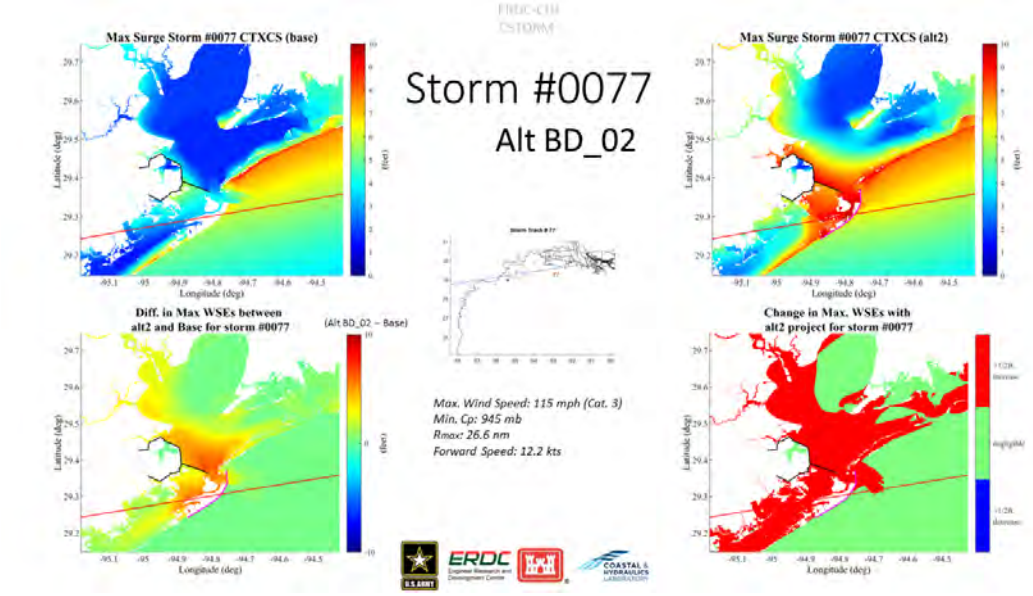

Figure D15. Comparison of maximum water surface elevations color contour plots from the CSTORM coupled ADCIRC+STWAVE simulations for storm 0154 under without-project and with-project BD_Alt2.

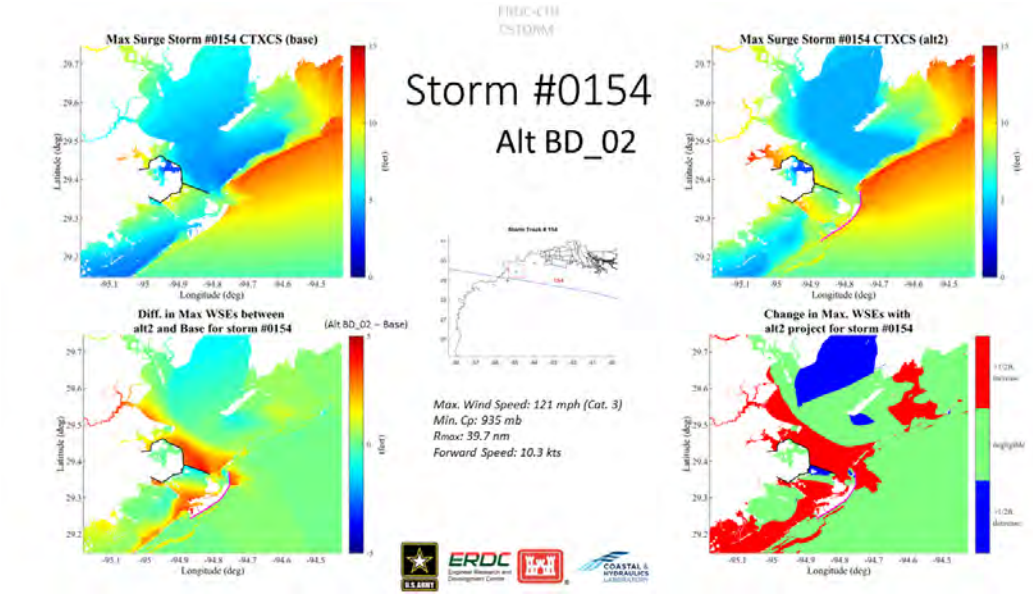

Figure D16. Comparison of maximum water surface elevations color contour plots from the CSTORM coupled ADCIRC+STWAVE simulations for storm 0159 under without-project and with-project BD_Alt2.

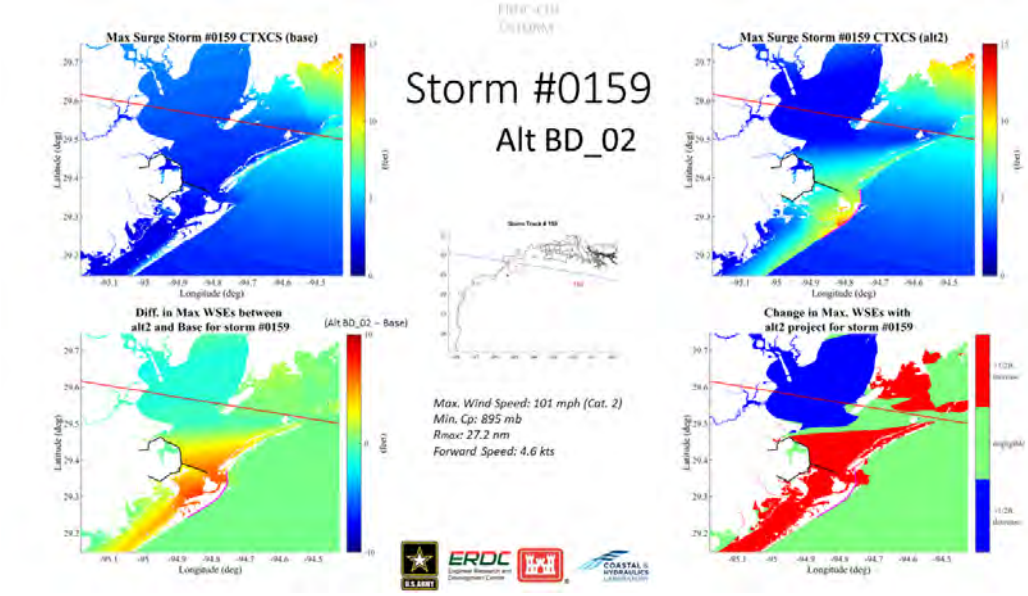

Figure D17 Comparison of maximum water surface elevations color contour plots from the CSTORM coupled ADCIRC+STWAVE simulations for storm 0167 under without-project and with-project BD_Alt2.

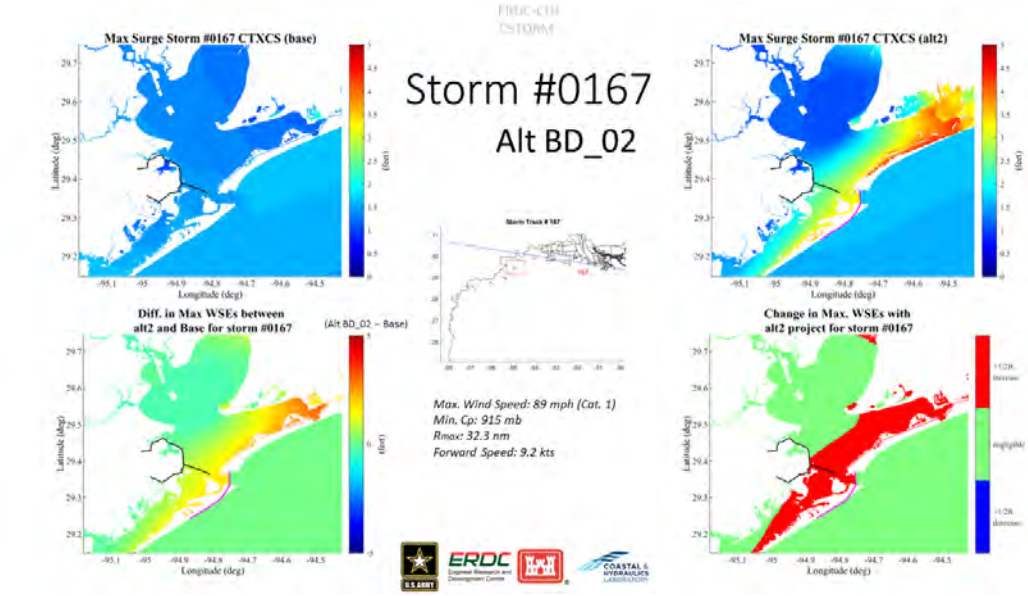

Figure D18. Comparison of maximum water surface elevations color contour plots from the CSTORM coupled ADCIRC+STWAVE simulations for storm 0270 under without-project and with-project BD_Alt2.

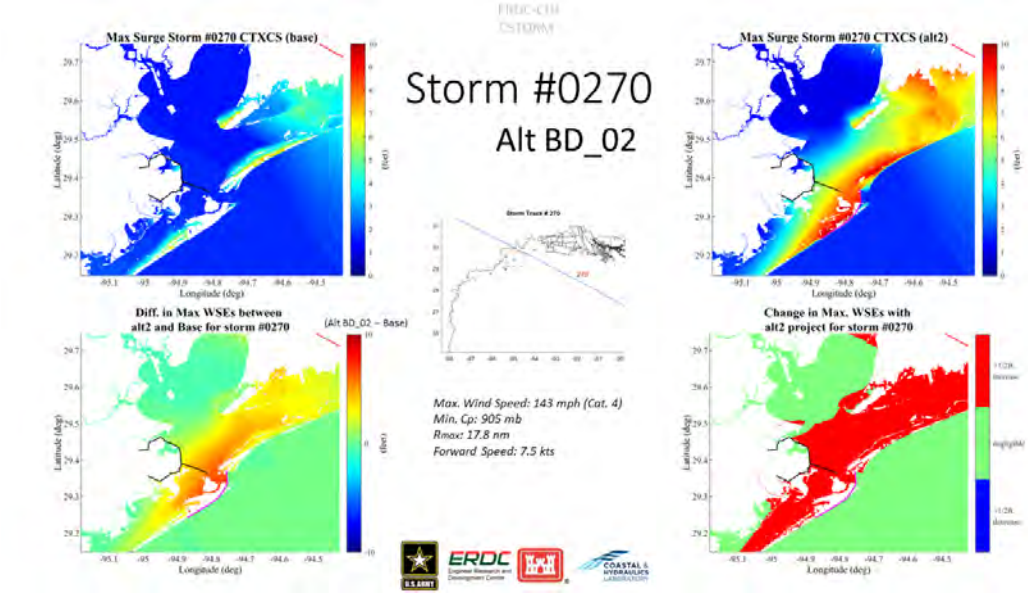

Figure D19. Comparison of maximum water surface elevations color contour plots from the CSTORM coupled ADCIRC+STWAVE simulations for storm 0277 under without-project and with-project BD_Alt2.

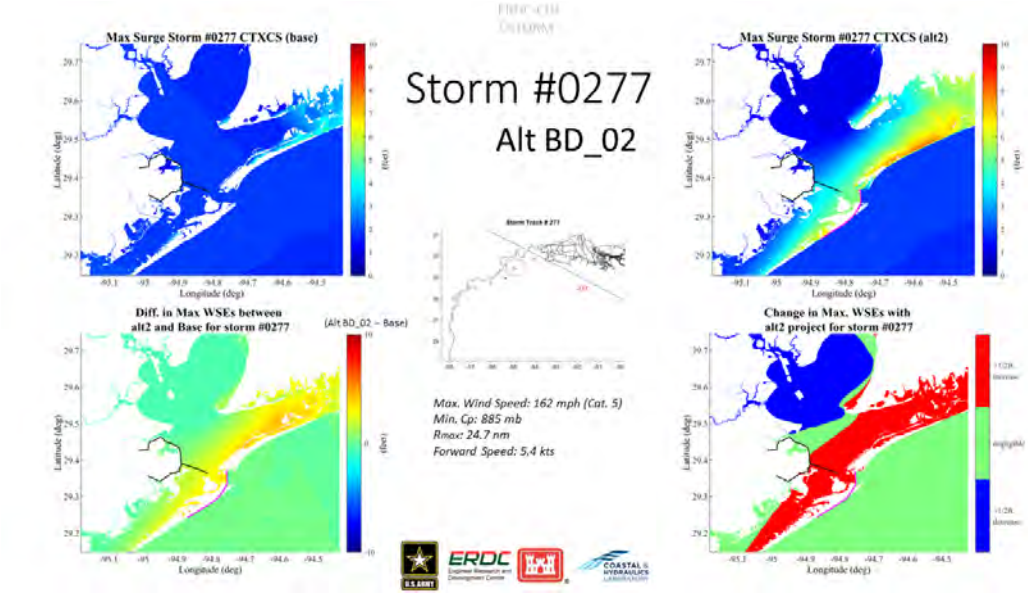

Figure D20. Comparison of maximum water surface elevations color contour plots from the CSTORM coupled ADCIRC+STWAVE simulations for storm 0342 under without-project and with-project BD_Alt2.

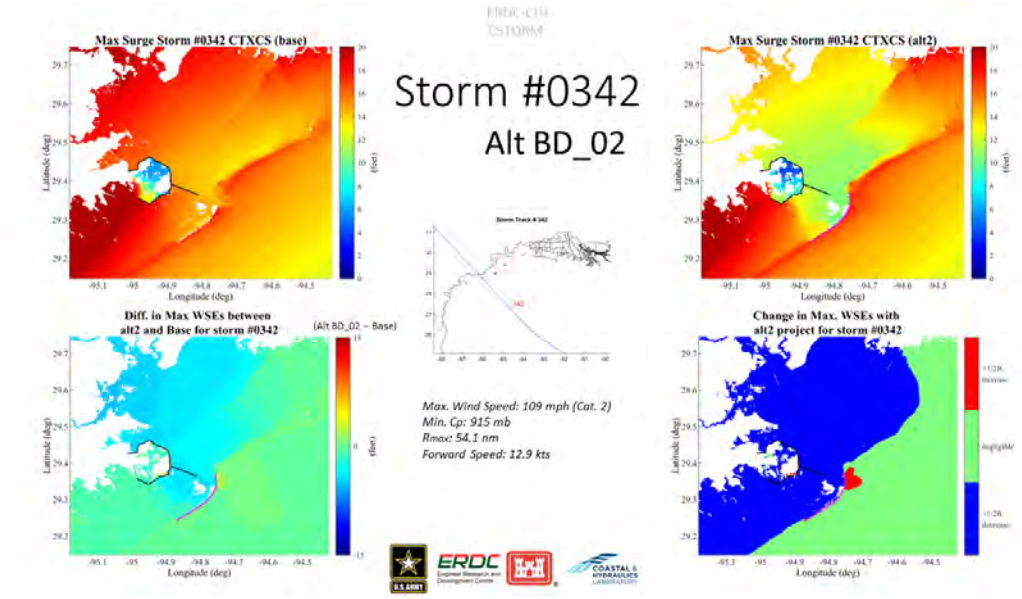

Figure D21. Comparison of maximum water surface elevations color contour plots from the CSTORM coupled ADCIRC+STWAVE simulations for storm 0356 under without-project and with-project BD_Alt2.

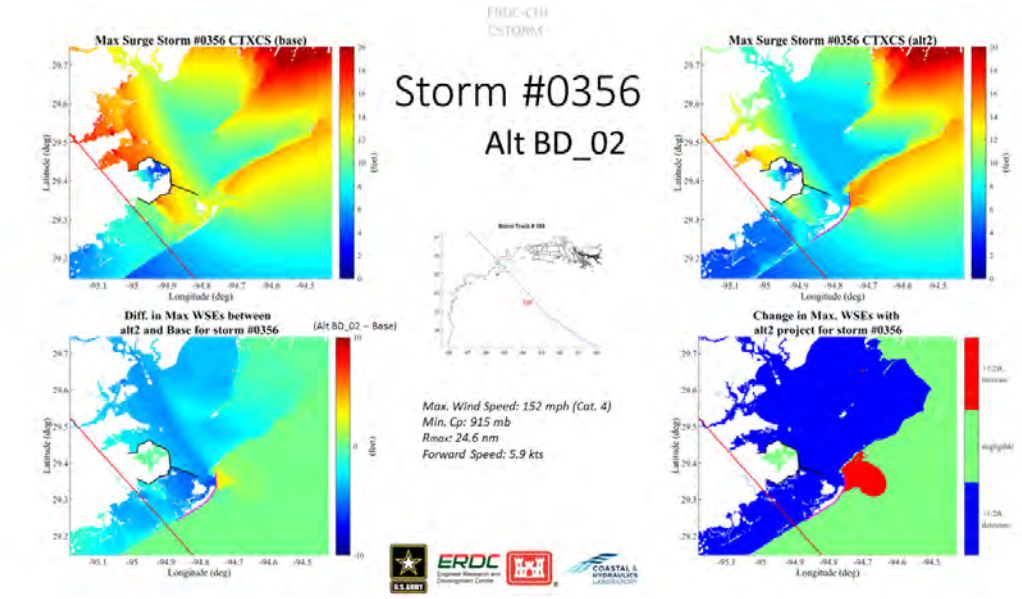

Figure D22. Comparison of maximum water surface elevations color contour plots from the CSTORM coupled ADCIRC+STWAVE simulations for storm 0384 under without-project and with-project BD_Alt2.

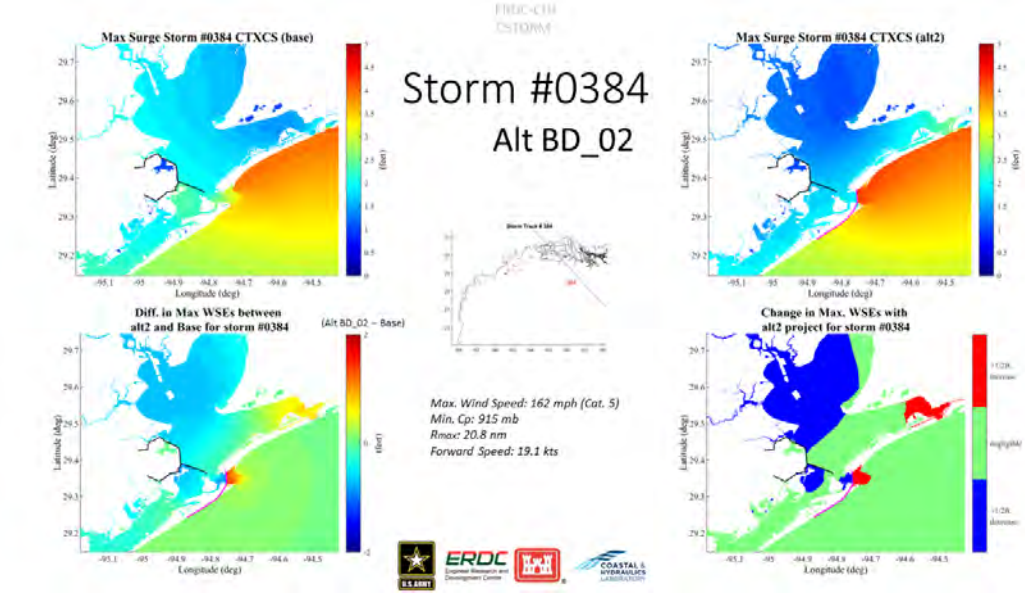

Figure D23. Comparison of maximum water surface elevations color contour plots from the CSTORM coupled ADCIRC+STWAVE simulations for storm 0437 under without-project and with-project BD_Alt2.

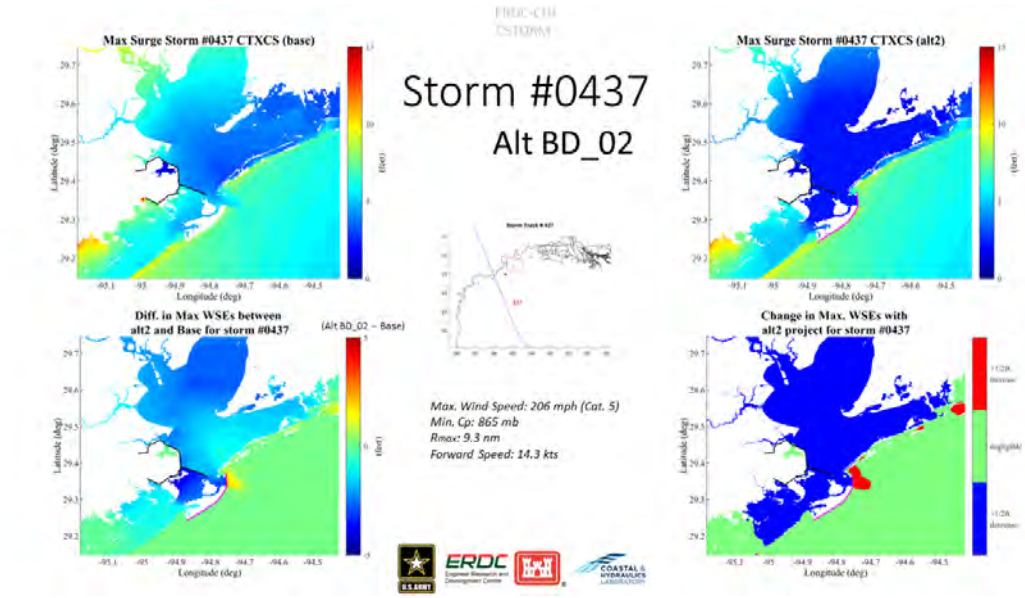

Figure D24. Comparison of maximum water surface elevations color contour plots from the CSTORM coupled ADCIRC+STWAVE simulations for storm 0447 under without-project and with-project BD_Alt2.

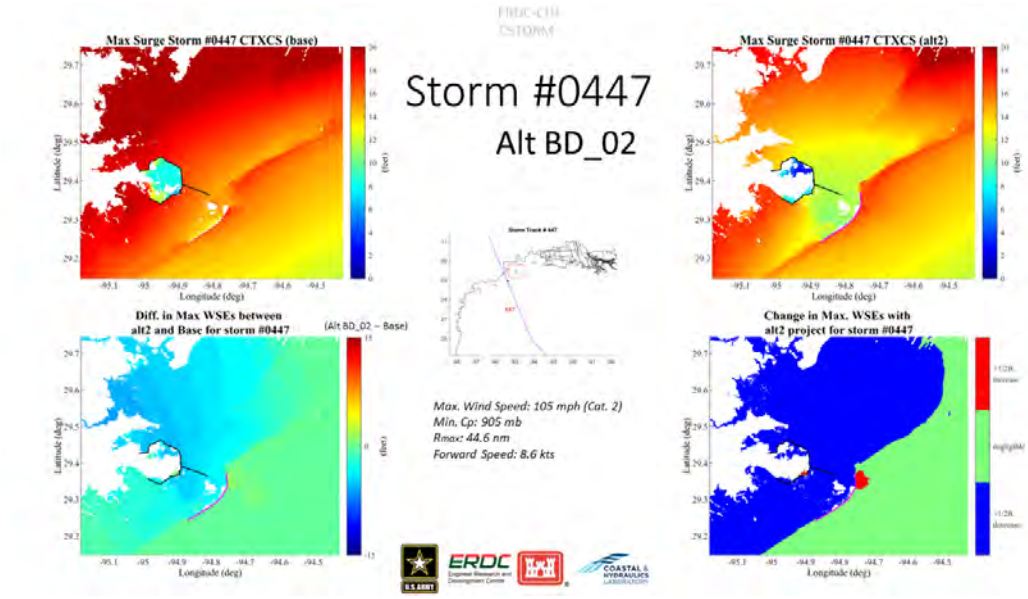

Figure D25. Comparison of maximum water surface elevations color contour plots from the CSTORM coupled ADCIRC+STWAVE simulations for storm 0453 under without-project and with-project BD_Alt2.

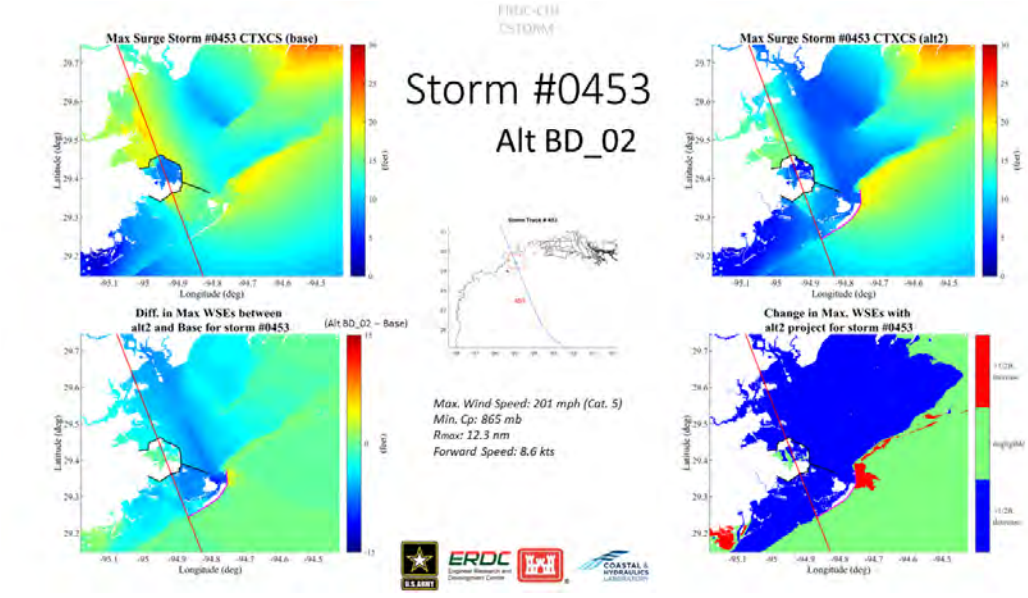

Figure D26. Comparison of maximum water surface elevations color contour plots from the CSTORM coupled ADCIRC+STWAVE simulations for storm 0456 under without-project and with-project BD_Alt2.

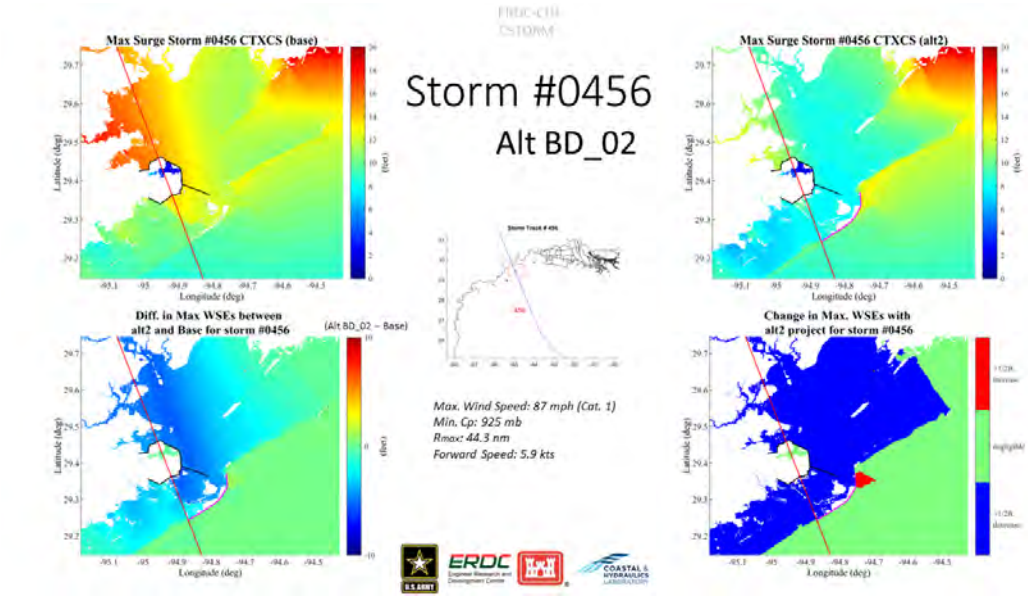

Figure D27. Comparison of maximum water surface elevations color contour plots from the CSTORM coupled ADCIRC+STWAVE simulations for storm 0461 under without-project and with-project BD_Alt2.

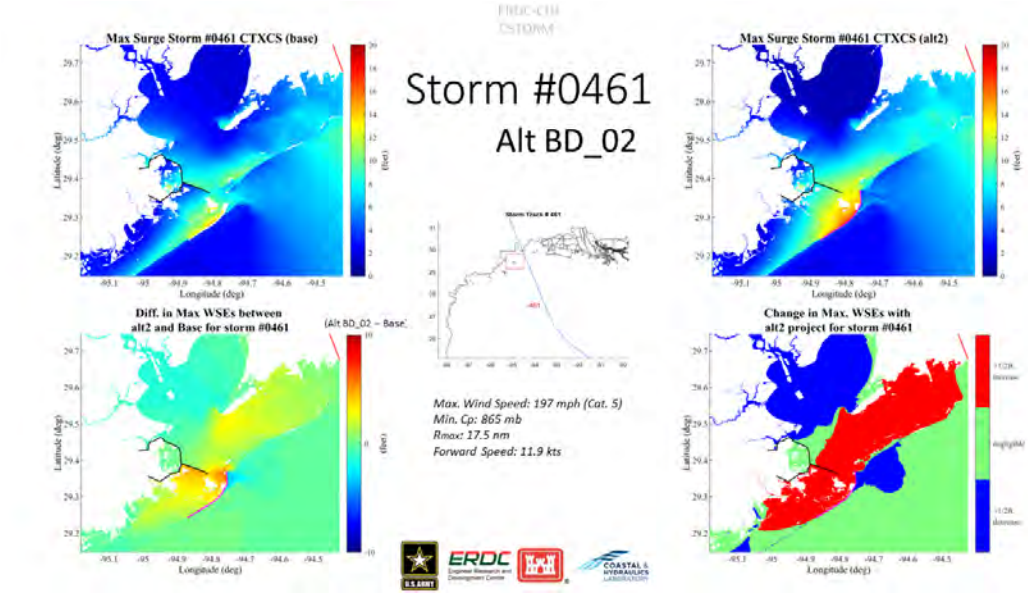

Figure D28. Comparison of maximum water surface elevations color contour plots from the CSTORM coupled ADCIRC+STWAVE simulations for storm 0529 under without-project and with-project BD_Alt2.

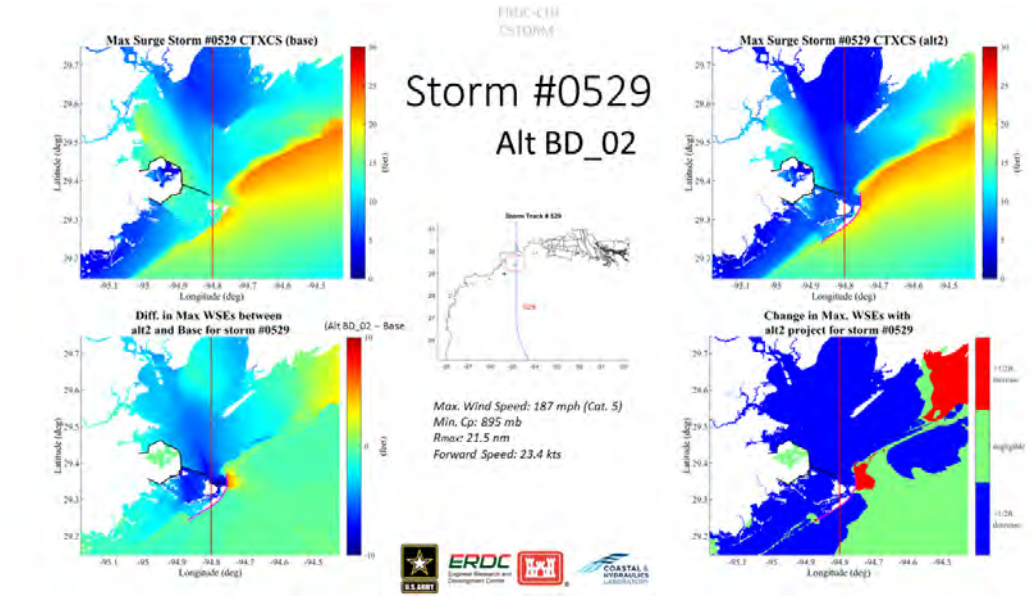

Figure D29. Comparison of maximum water surface elevations color contour plots from the CSTORM coupled ADCIRC+STWAVE simulations for storm 0578 under without-project and with-project BD_Alt2.

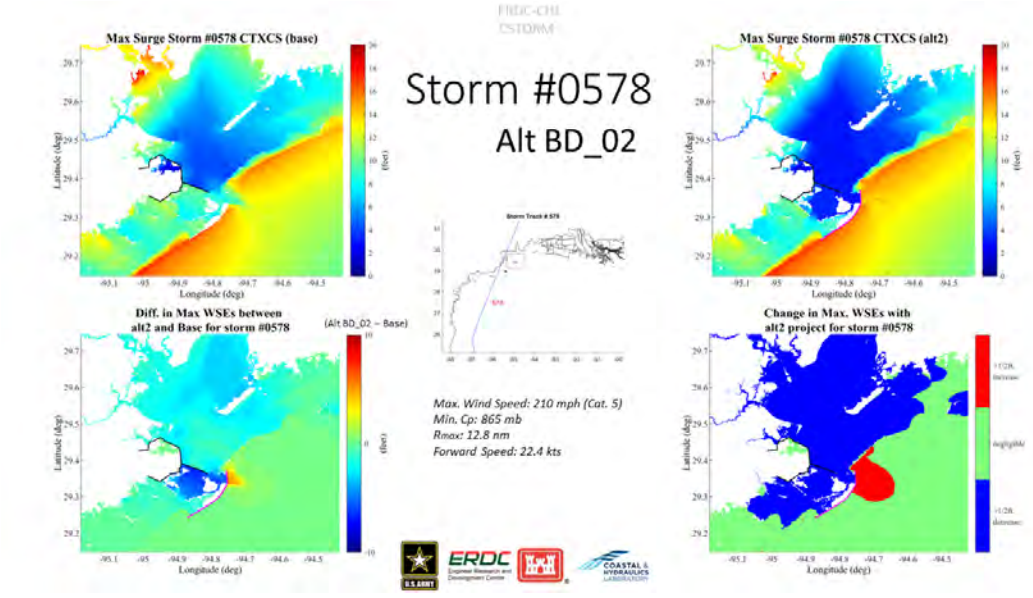

Figure D30. Comparison of maximum water surface elevations color contour plots from the CSTORM coupled ADCIRC+STWAVE simulations for storm 0595 under without-project and with-project BD_Alt2.

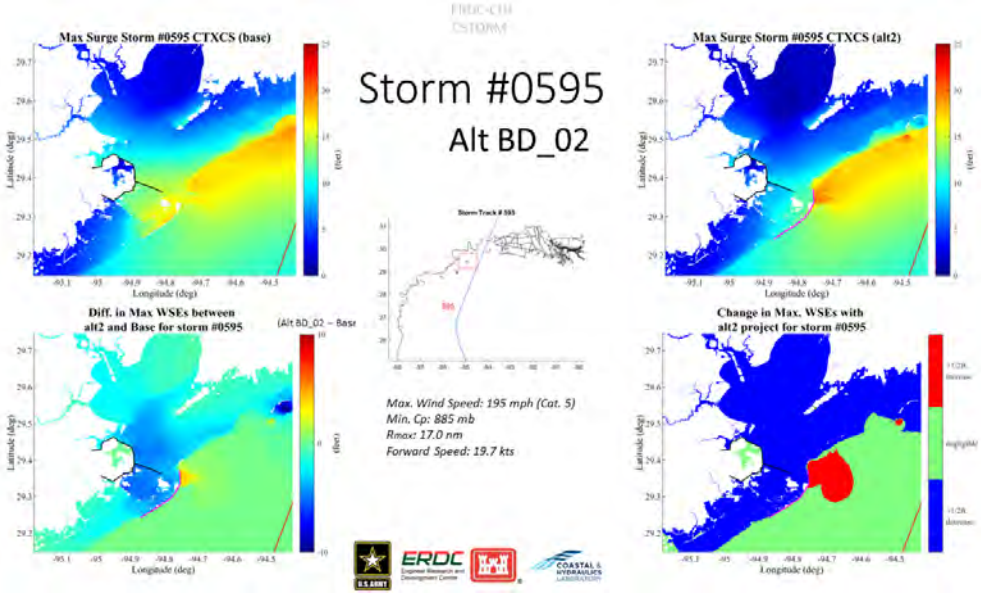

Figure D31. Comparison of maximum water surface elevations color contour plots from the CSTORM coupled ADCIRC+STWAVE simulations for storm 0633 under without-project and with-project BD_Alt2.

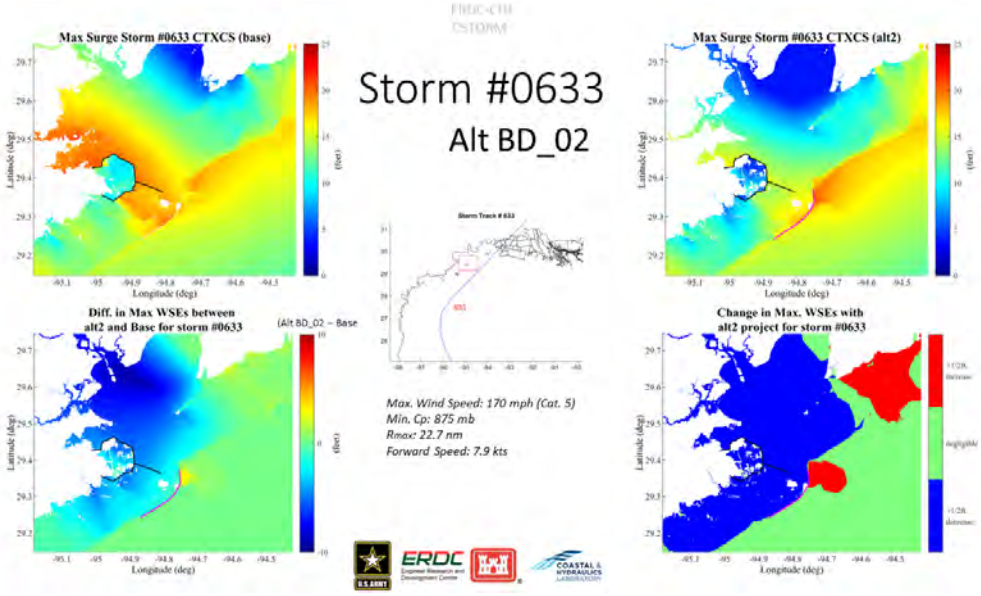

CSTORM Maximum Water Surface Elevation Comparisons for Without-Project vs Beach-Dune Alterative 2

Maximum water surface elevations for 20 of the 170 storms are presented below for without-project (existing conditions) and the gate barrier, beach-dune and ring levee on the backside of Galveston Island (BD Alt3) with-project condition. These figures are presented to illustrate the general impacts to maximum water surface elevations when considering this with-project alternative under different storm conditions. Figure D32 shows a map with the general layout of the representation of the alternative in the ADCIRC model. The bright green lines represent the with-project features the gate surge barrier and some existing structures as well.

Figure D32. Map showing the ADCIRC model representation of the gate only with-project condition, labeled as BD_Alt3.

Figure D33. Comparison of maximum water surface elevations color contour plots from the CSTORM coupled ADCIRC+STWAVE simulations for storm 0066 under without-project and with-project BD_Alt3. .

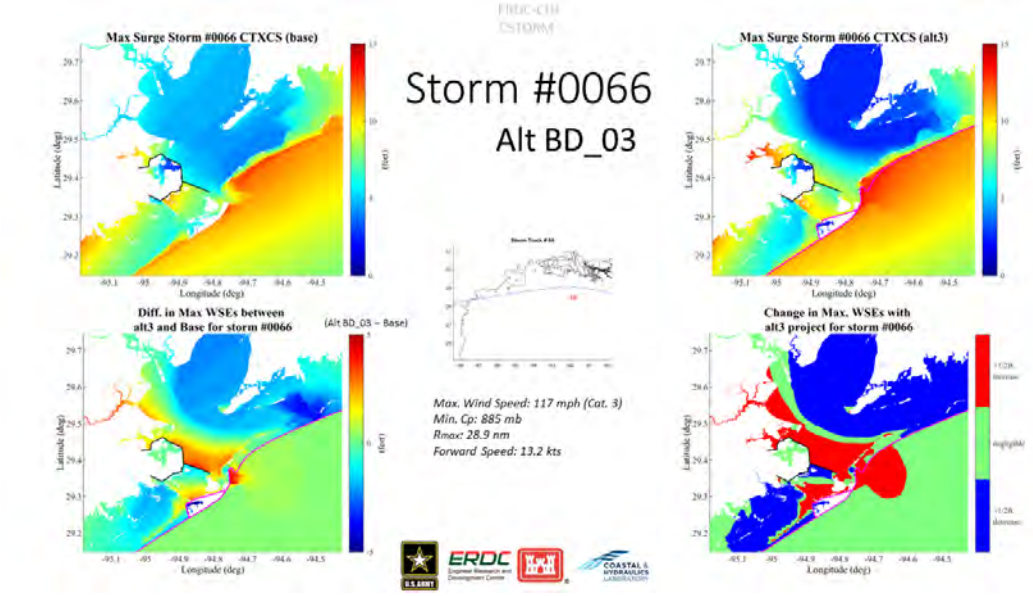

Figure D34. Comparison of maximum water surface elevations color contour plots from the CSTORM coupled ADCIRC+STWAVE simulations for storm 0073 under without-project and with-project BD_Alt3.

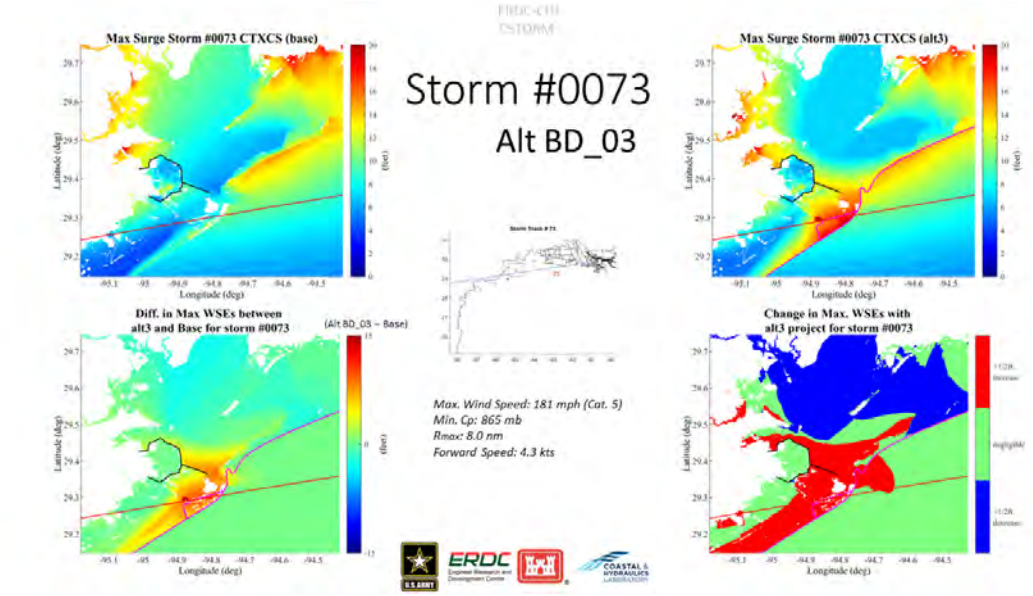

Figure D35. Comparison of maximum water surface elevations color contour plots from the CSTORM coupled ADCIRC+STWAVE simulations for storm 0077 under without-project and with-project BD_Alt3.

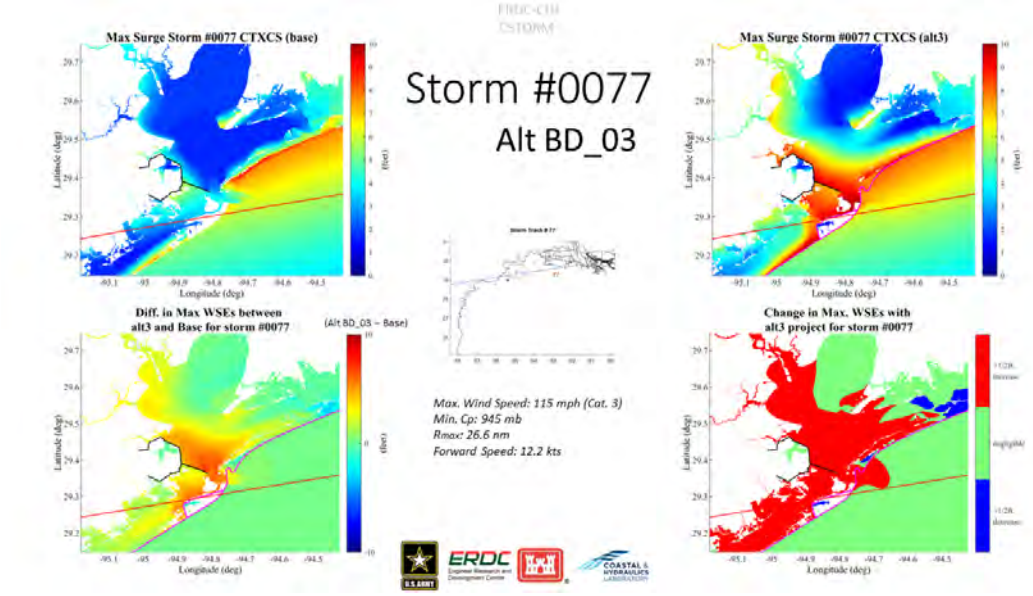

Figure D36. Comparison of maximum water surface elevations color contour plots from the CSTORM coupled ADCIRC+STWAVE simulations for storm 0154 under without-project and with-project BD_Alt3.

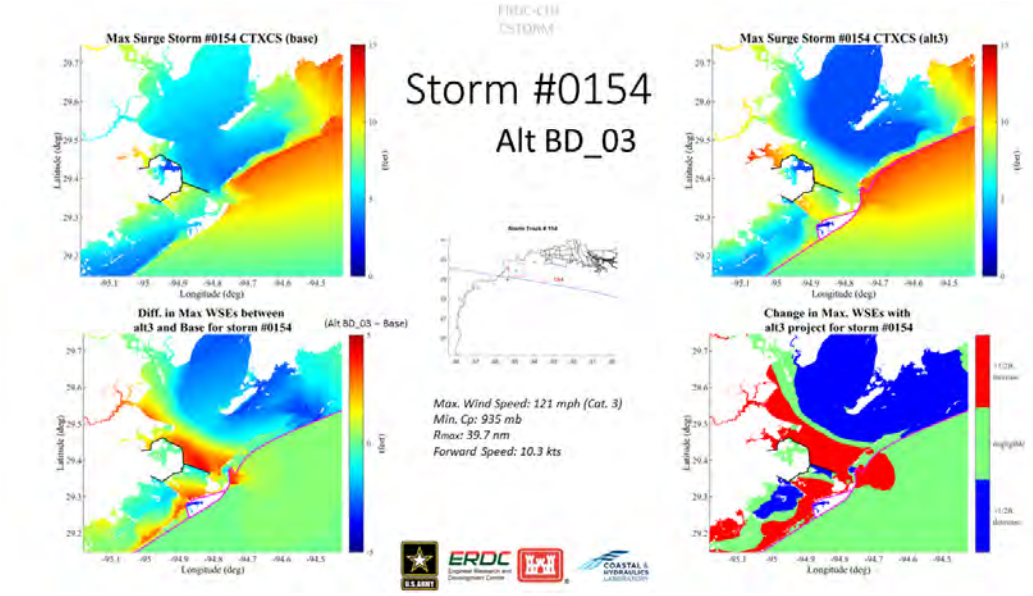

Figure D37. Comparison of maximum water surface elevations color contour plots from the CSTORM coupled ADCIRC+STWAVE simulations for storm 0159 under without-project and with-project BD_Alt3.

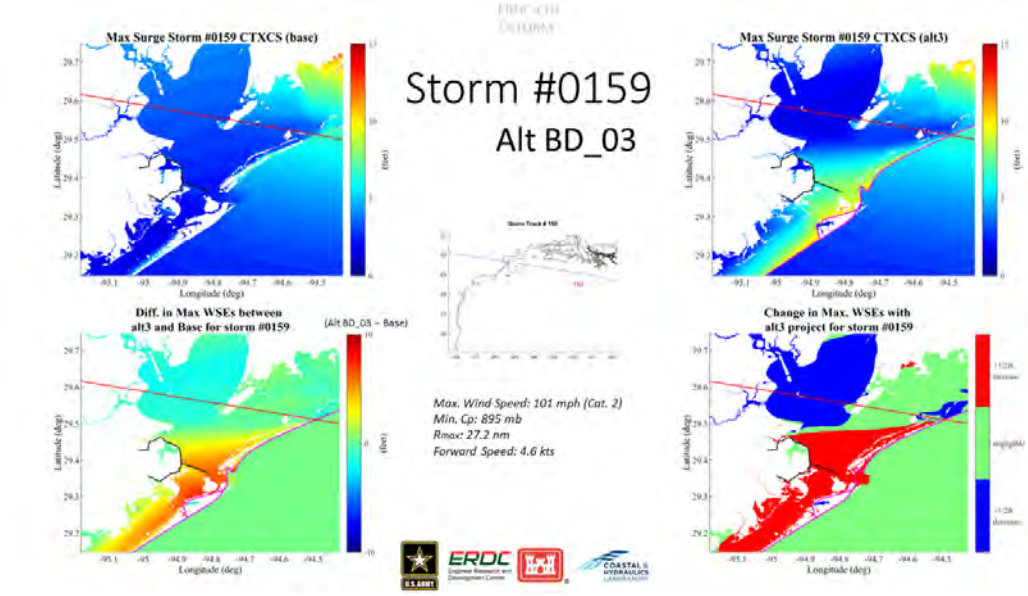

Figure D38. Comparison of maximum water surface elevations color contour plots from the CSTORM coupled ADCIRC+STWAVE simulations for storm 0167 under without-project and with-project BD_Alt3.

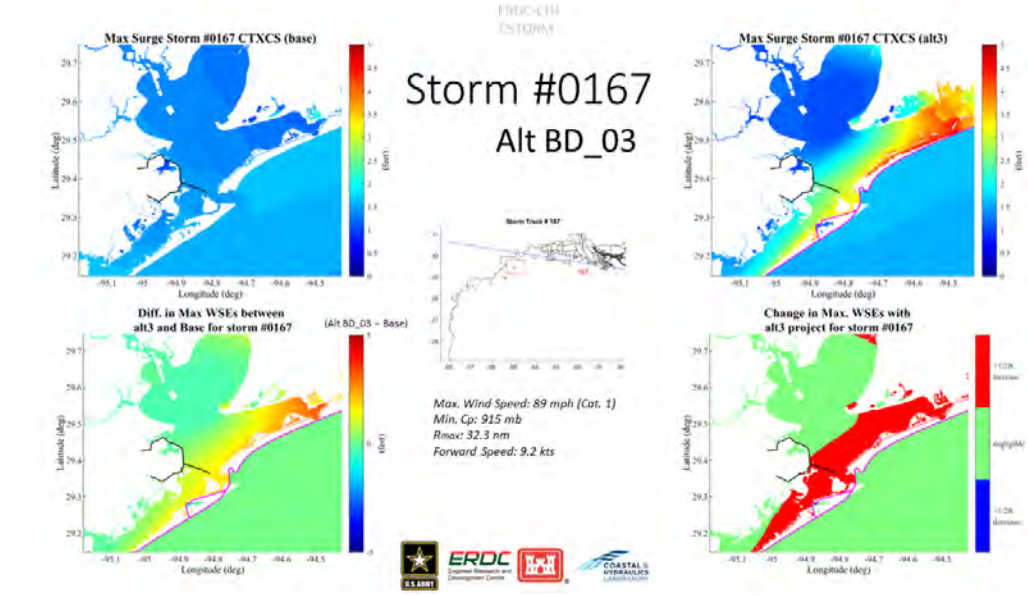

Figure D39. Comparison of maximum water surface elevations color contour plots from the CSTORM coupled ADCIRC+STWAVE simulations for storm 0270 under without-project and with-project BD_Alt3.

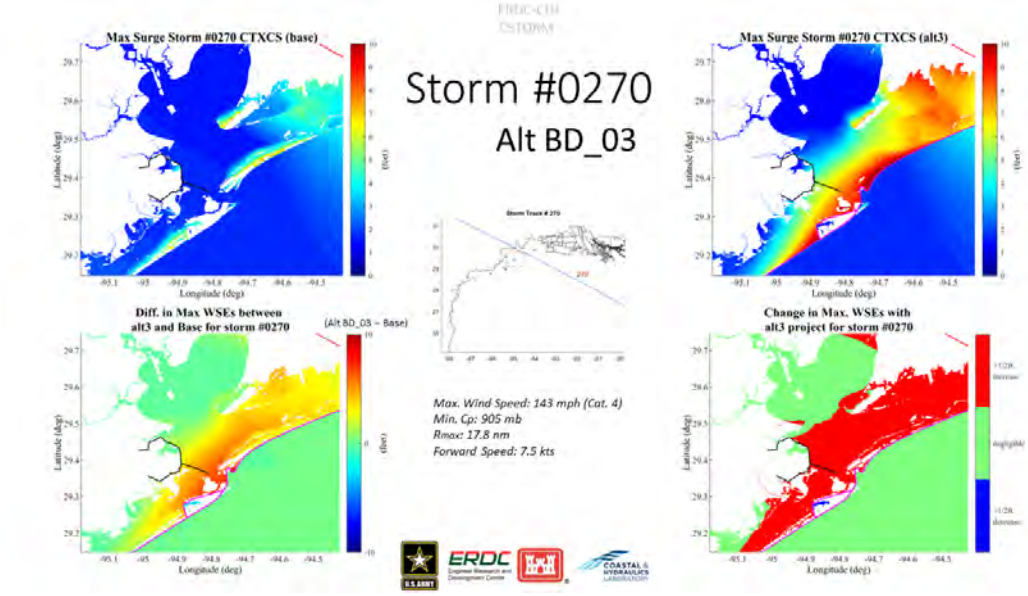

Figure D40. Comparison of maximum water surface elevations color contour plots from the CSTORM coupled ADCIRC+STWAVE simulations for storm 0277 under without-project and with-project BD_Alt3.

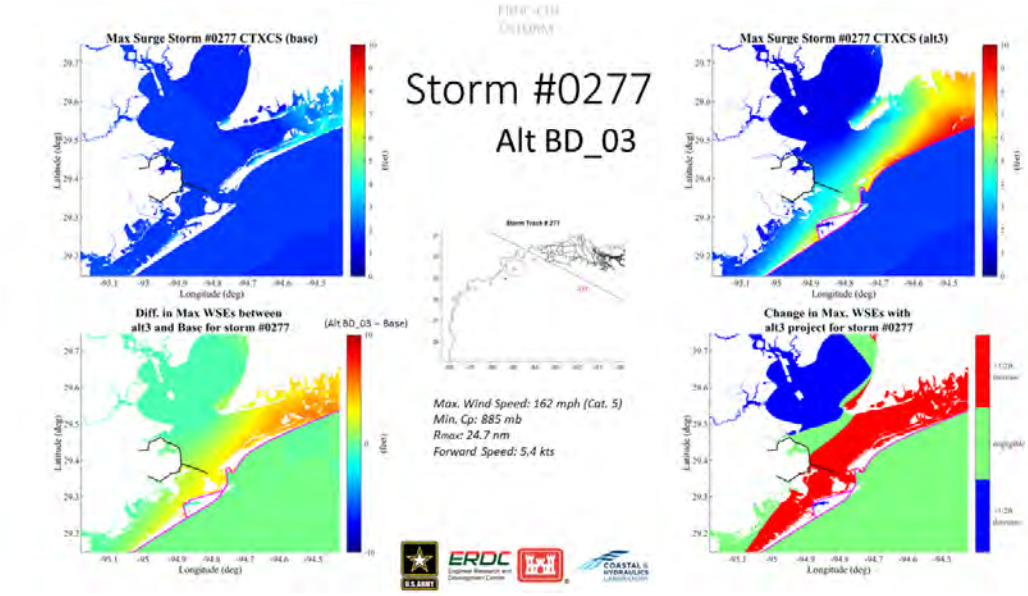

Figure D41. Comparison of maximum water surface elevations color contour plots from the CSTORM coupled ADCIRC+STWAVE simulations for storm 0342 under without-project and with-project BD_Alt3.

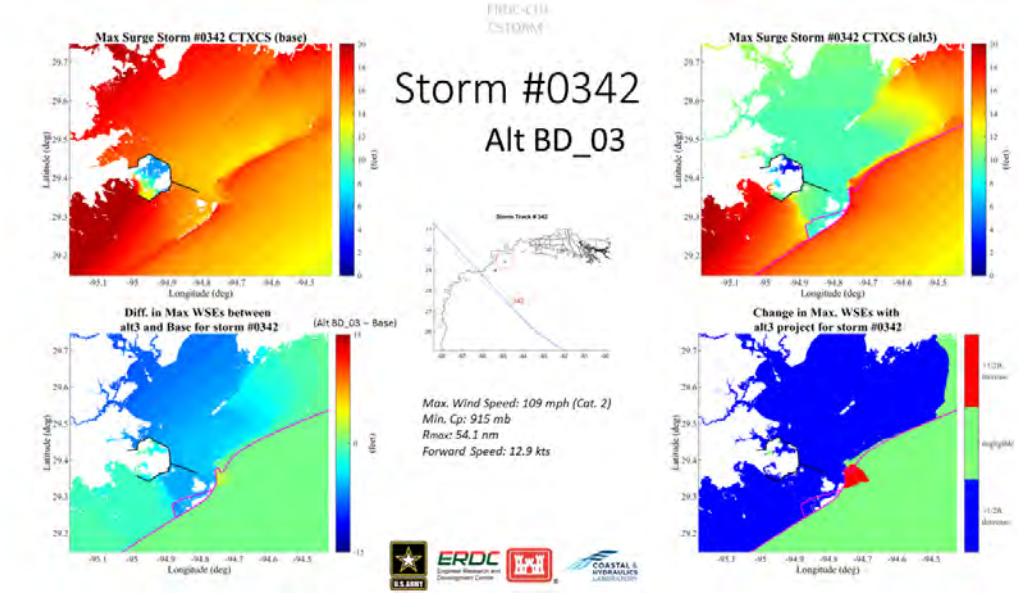

Figure D42. Comparison of maximum water surface elevations color contour plots from the CSTORM coupled ADCIRC+STWAVE simulations for storm 0356 under without-project and with-project BD_Alt3.

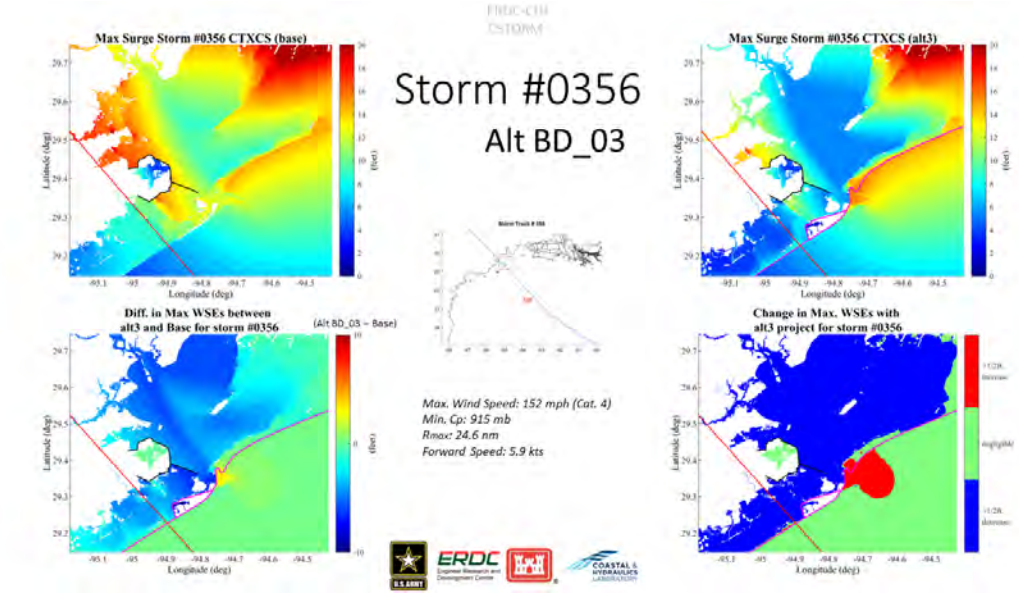

Figure D43. Comparison of maximum water surface elevations color contour plots from the CSTORM coupled ADCIRC+STWAVE simulations for storm 0384 under without-project and with-project BD_Alt3.

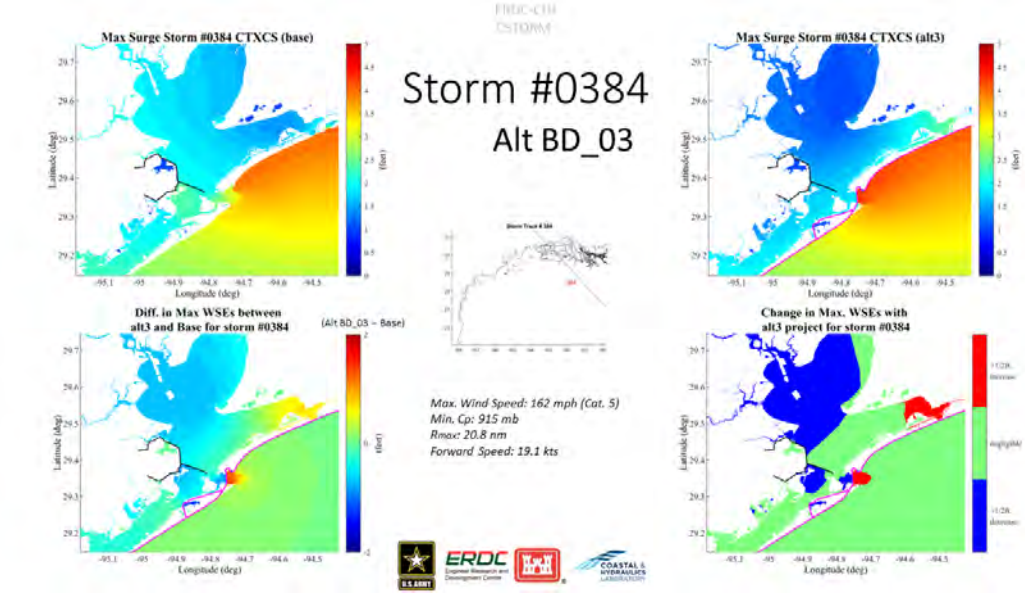

Figure D44. Comparison of maximum water surface elevations color contour plots from the CSTORM coupled ADCIRC+STWAVE simulations for storm 0437 under without-project and with-project BD_Alt3.

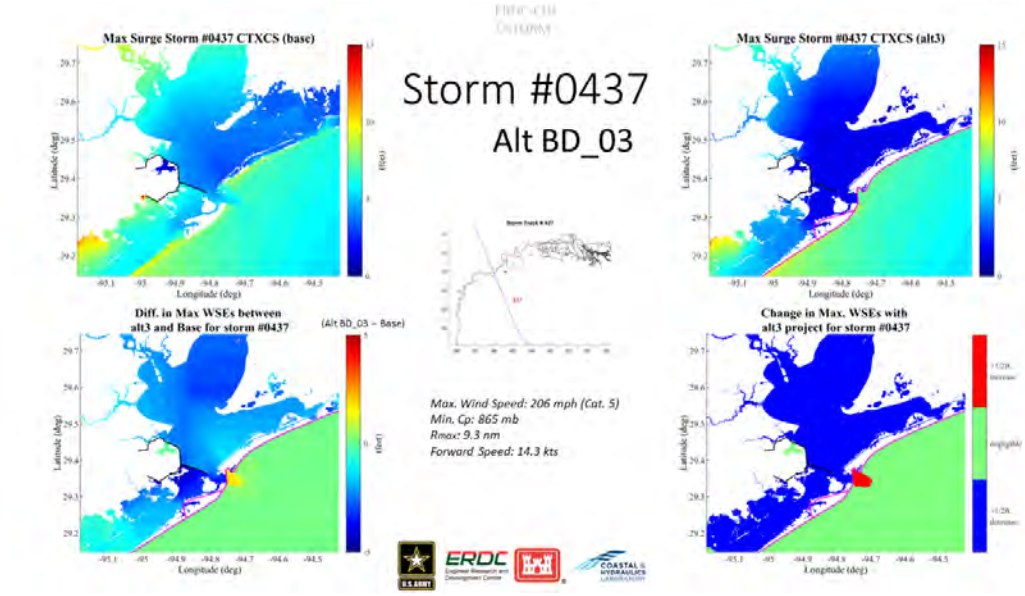

Figure D45. Comparison of maximum water surface elevations color contour plots from the CSTORM coupled ADCIRC+STWAVE simulations for storm 0447 under without-project and with-project BD_Alt3.

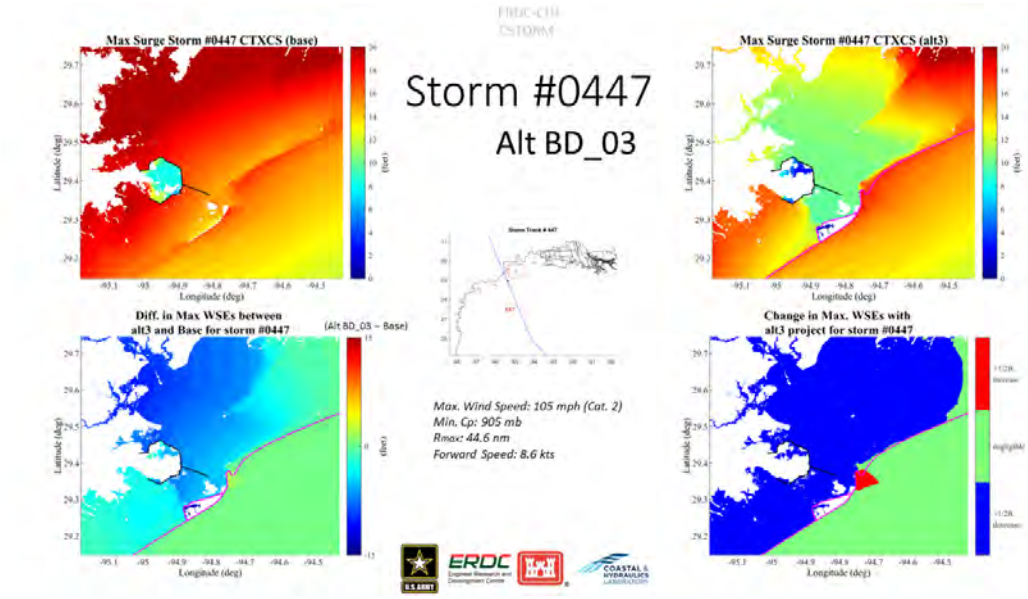

Figure D46. Comparison of maximum water surface elevations color contour plots from the CSTORM coupled ADCIRC+STWAVE simulations for storm 0453 under without-project and with-project BD_Alt3.

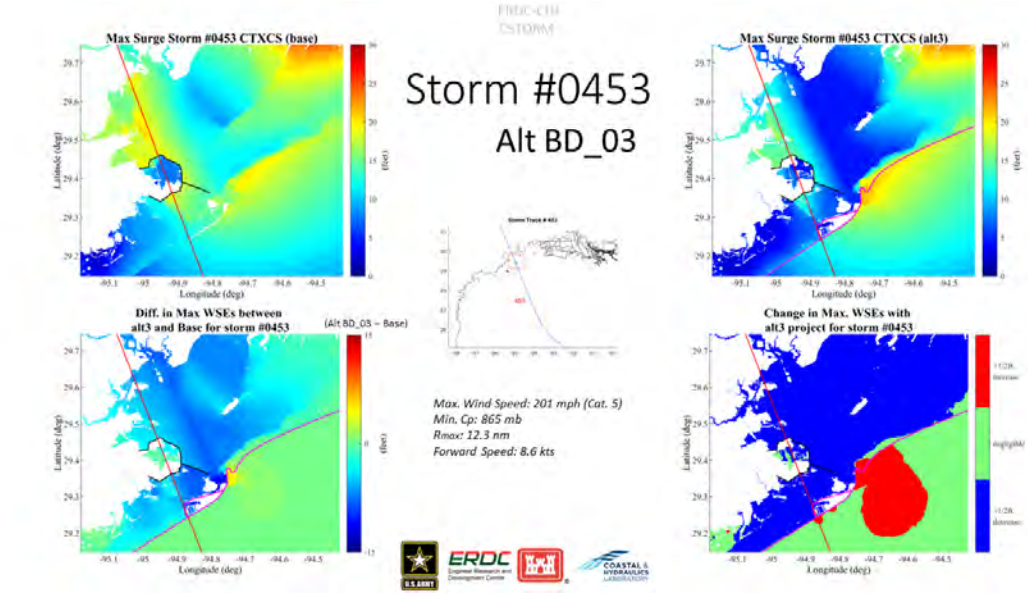

Figure D47. Comparison of maximum water surface elevations color contour plots from the CSTORM coupled ADCIRC+STWAVE simulations for storm 0456 under without-project and with-project BD_Alt3.

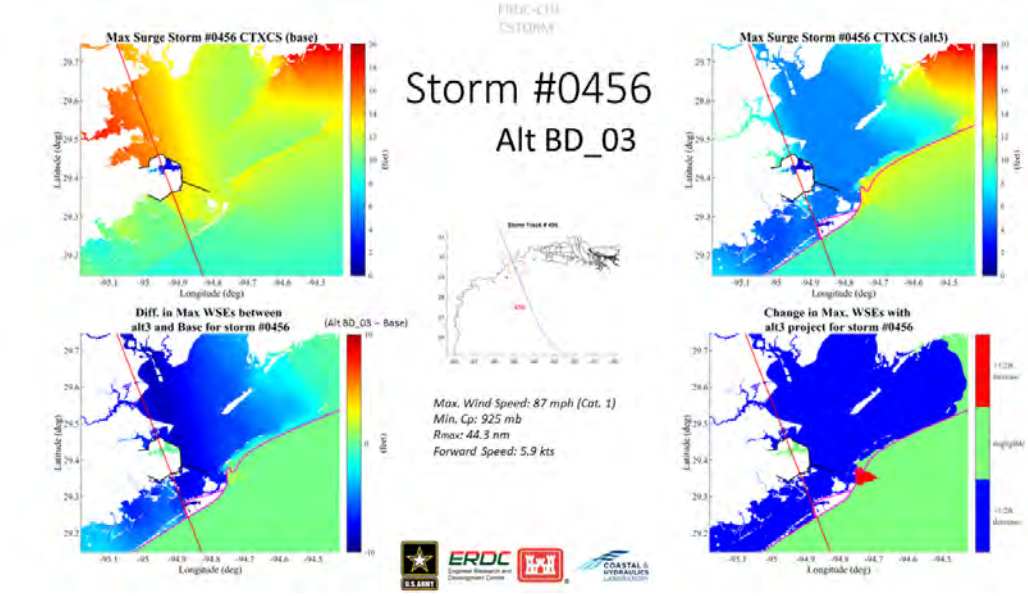

Figure D48. Comparison of maximum water surface elevations color contour plots from the CSTORM coupled ADCIRC+STWAVE simulations for storm 0461 under without-project and with-project BD_Alt3.

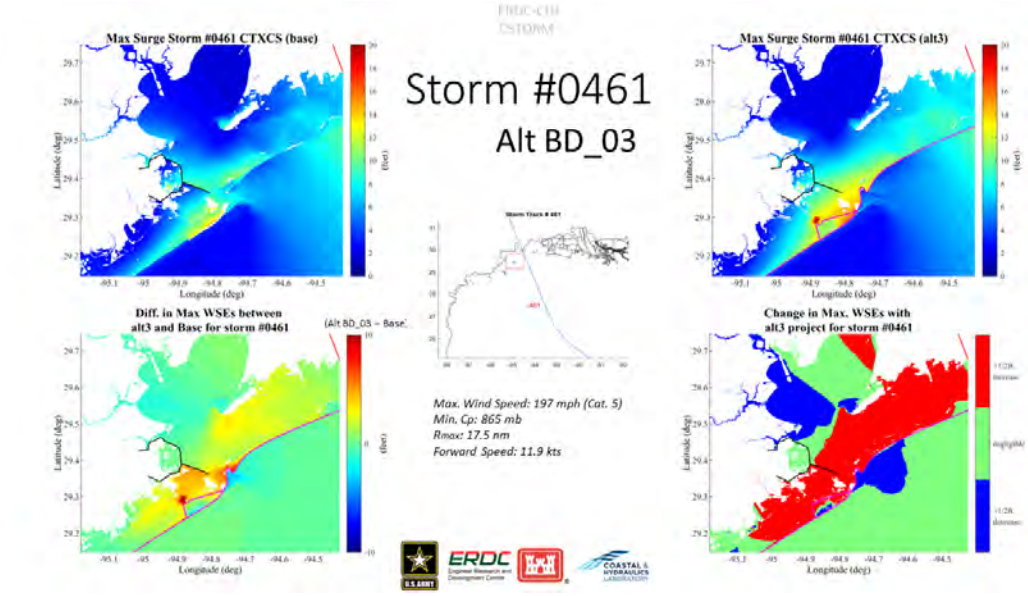

Figure D49. Comparison of maximum water surface elevations color contour plots from the CSTORM coupled ADCIRC+STWAVE simulations for storm 0529 under without-project and with-project BD_Alt3.

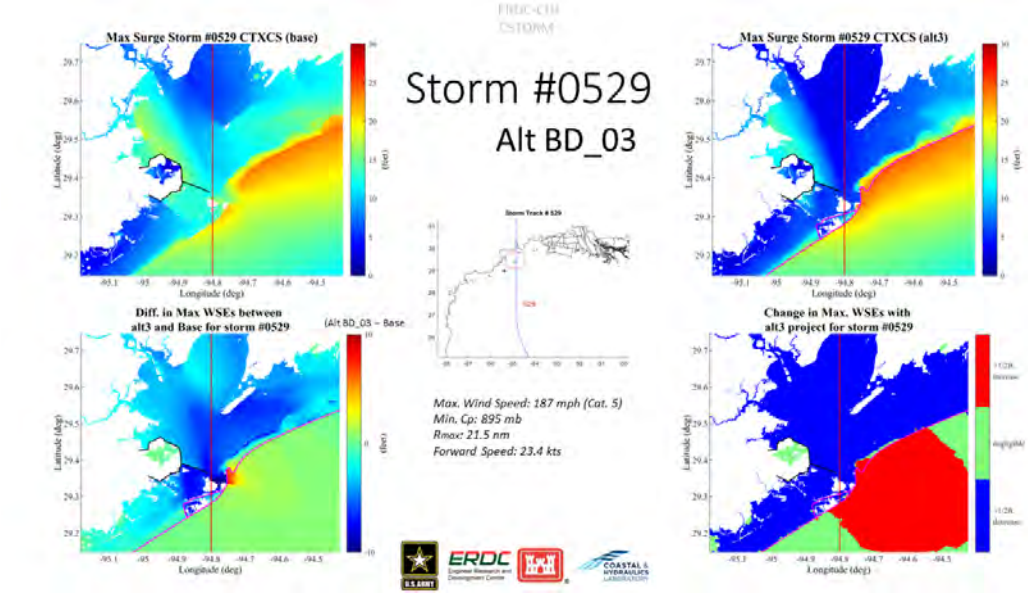

Figure D50. Comparison of maximum water surface elevations color contour plots from the CSTORM coupled ADCIRC+STWAVE simulations for storm 0578 under without-project and with-project BD_Alt3.

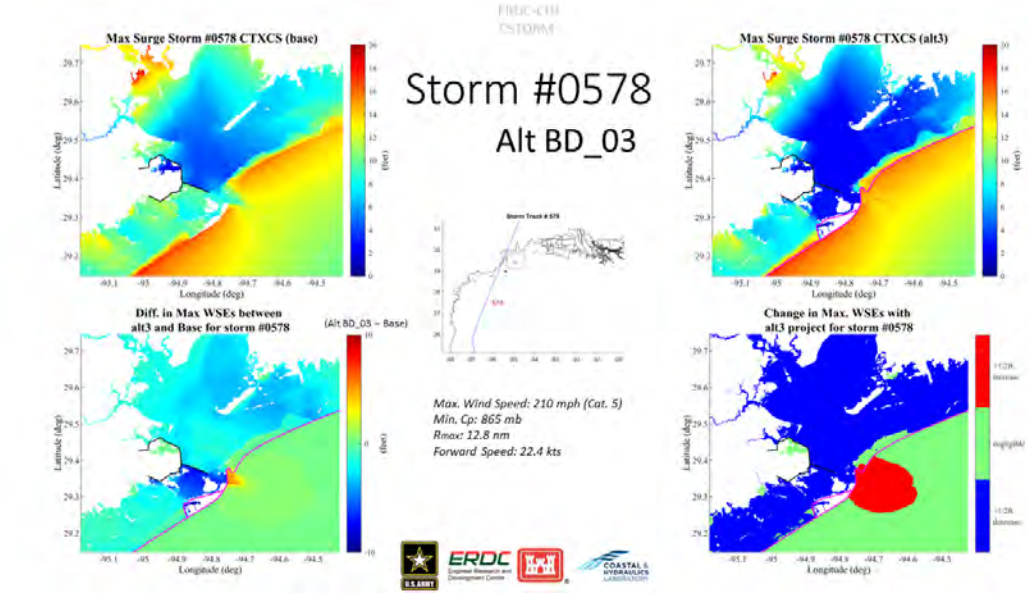

Figure D51. Comparison of maximum water surface elevations color contour plots from the CSTORM coupled ADCIRC+STWAVE simulations for storm 0595 under without-project and with-project BD_Alt3.

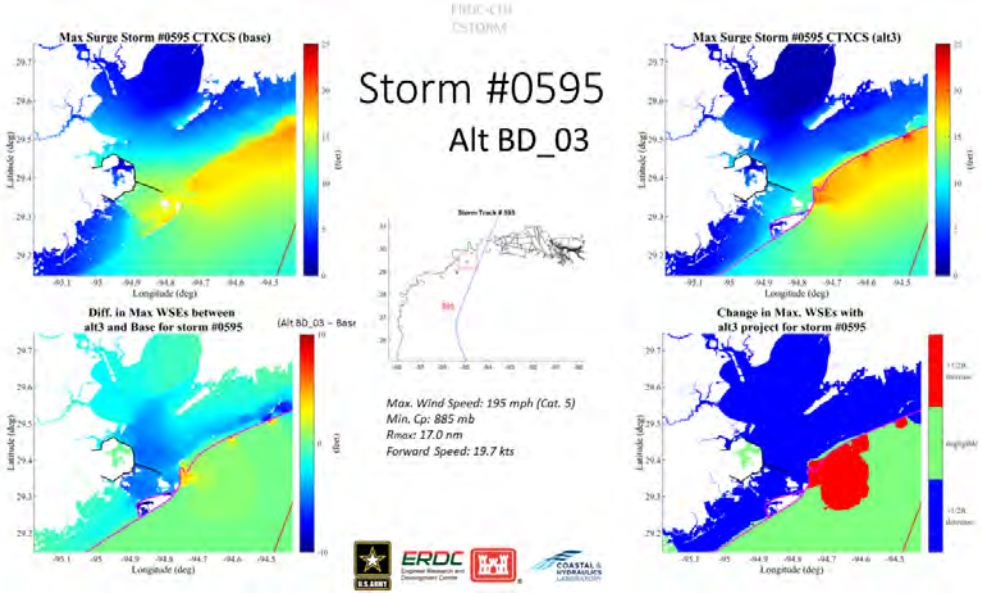

Figure D52. Comparison of maximum water surface elevations color contour plots from the CSTORM coupled ADCIRC+STWAVE simulations for storm 0633 under without-project and with-project BD_Alt3.

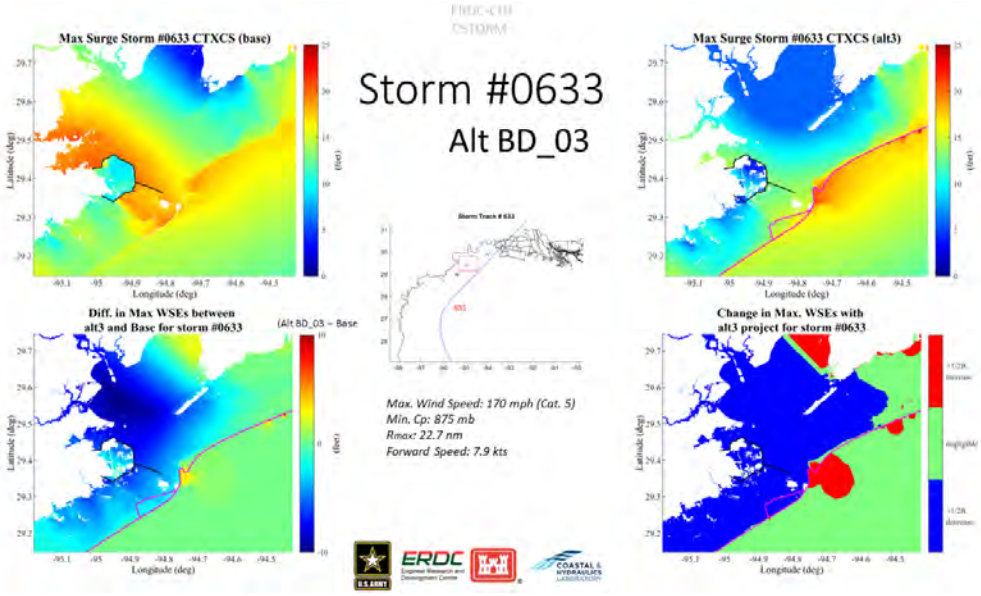

CSTORM Maximum Water Surface Elevation Comparisons for Without-Project vs Beach Dune Alterative 5

Maximum water surface elevations for 20 of the 170 storms are presented below for without-project (existing conditions) and the gate barrier, beach-dune, ring levee on the backside of Galveston Island, and High Island extension (BD Alt5) with-project condition. These figures are presented to illustrate the general impacts to maximum water surface elevations when considering this with-project alternative under different storm conditions. Figure D53 shows a map with the general layout of the representation of the alternative in the ADCIRC model. The bright green lines represent the with-project features the gate surge barrier and some existing structures as well.

Figure D53. Map showing the ADCIRC model representation of the gate barrier, beach dune/berm, ring levee on the backside of Galveston Island and High Island extension, labeled as BD_Alt5.

Figure D54. Comparison of maximum water surface elevations color contour plots from the CSTORM coupled ADCIRC+STWAVE simulations for storm 0066 under without-project and with-project BD_Alt5.

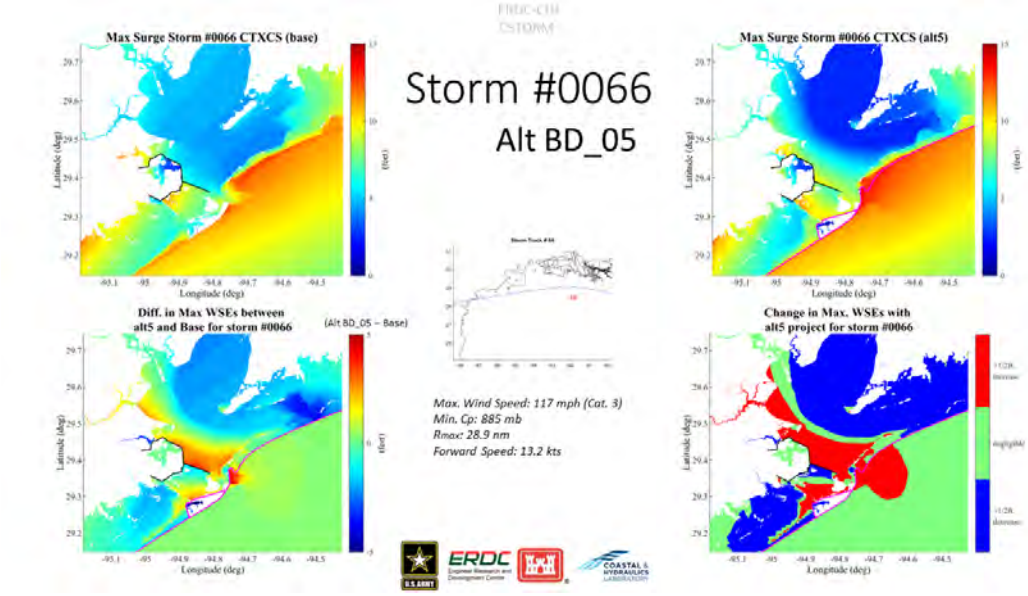

Figure D55. Comparison of maximum water surface elevations color contour plots from the CSTORM coupled ADCIRC+STWAVE simulations for storm 0073 under without-project and with-project BD_Alt5.

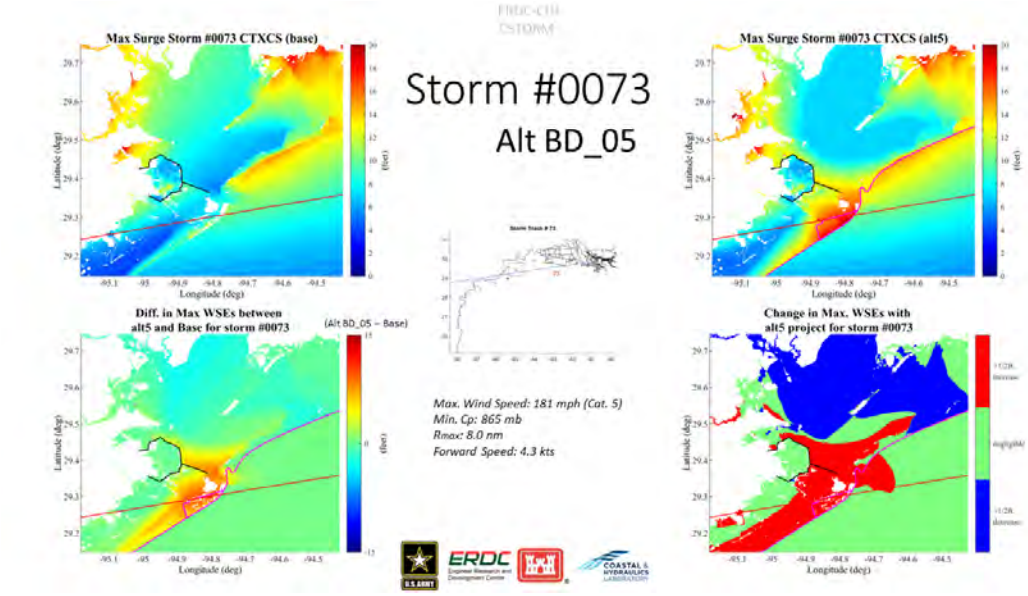

Figure D56. Comparison of maximum water surface elevations color contour plots from the CSTORM coupled ADCIRC+STWAVE simulations for storm 0077 under without-project and with-project BD_Alt5.

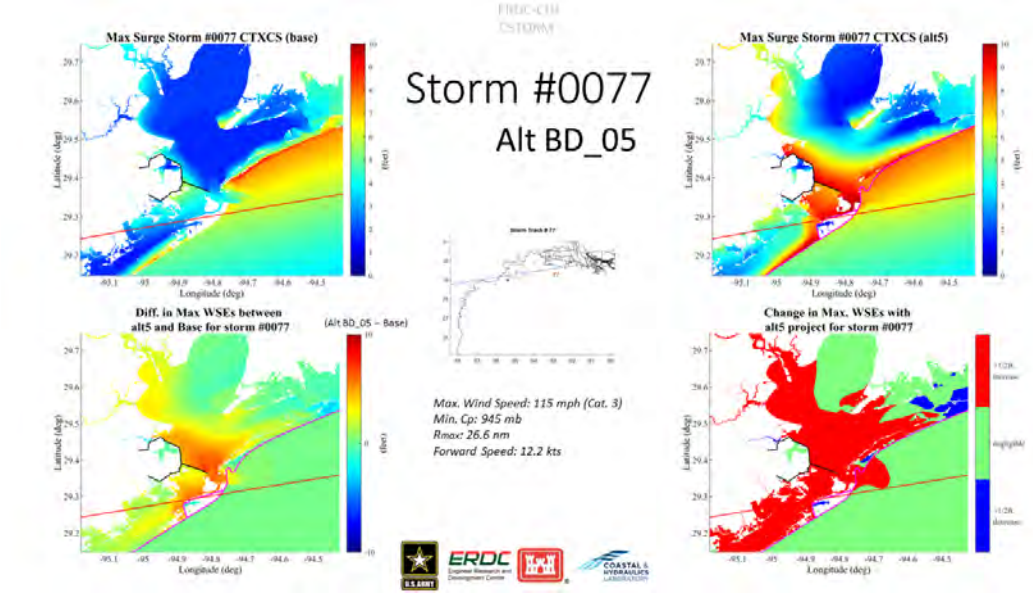

Figure D57. Comparison of maximum water surface elevations color contour plots from the CSTORM coupled ADCIRC+STWAVE simulations for storm 0154 under without-project and with-project BD_Alt5.

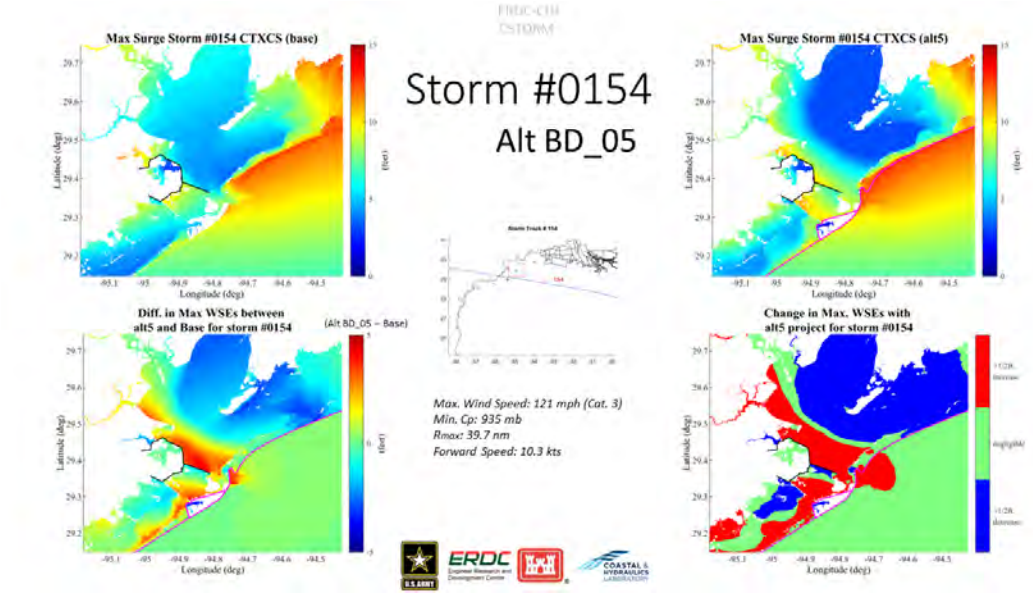

Figure D58. Comparison of maximum water surface elevations color contour plots from the CSTORM coupled ADCIRC+STWAVE simulations for storm 0159 under without-project and with-project BD_Alt5.

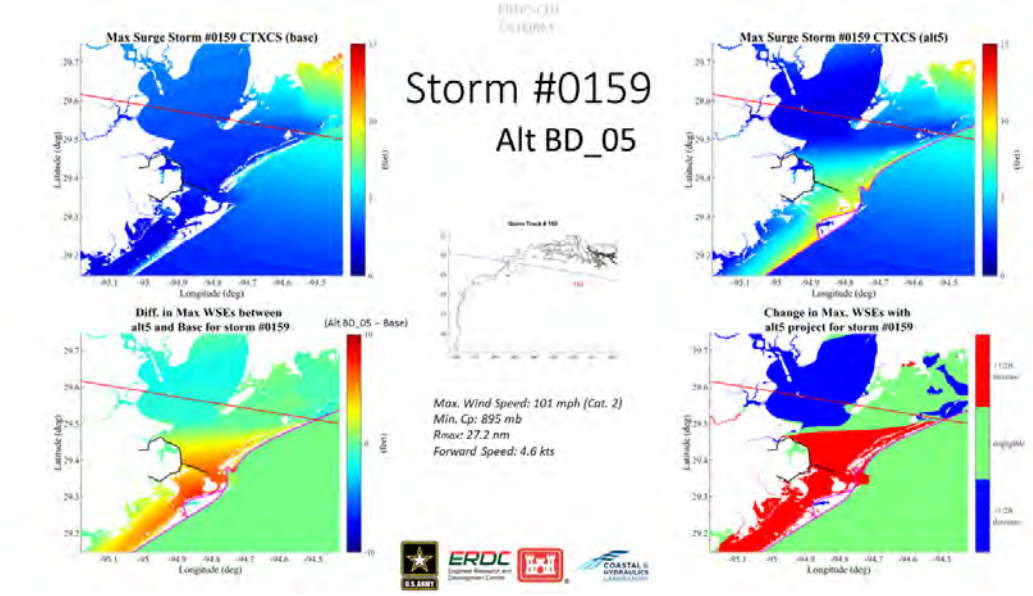

Figure D59. Comparison of maximum water surface elevations color contour plots from the CSTORM coupled ADCIRC+STWAVE simulations for storm 0167 under without-project and with-project BD_Alt5.

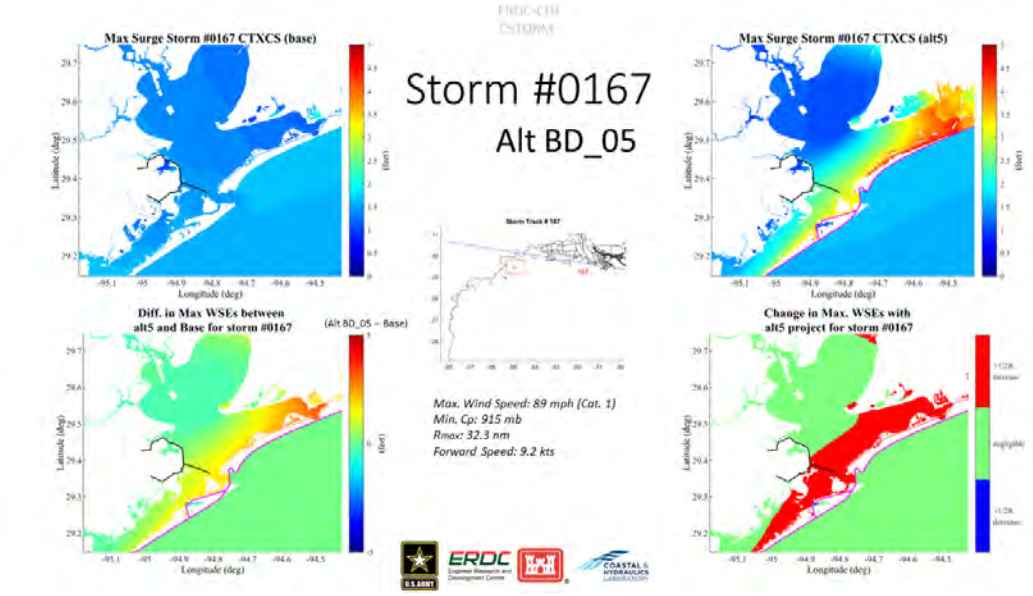

Figure D60. Comparison of maximum water surface elevations color contour plots from the CSTORM coupled ADCIRC+STWAVE simulations for storm 0270 under without-project and with-project BD_Alt5.

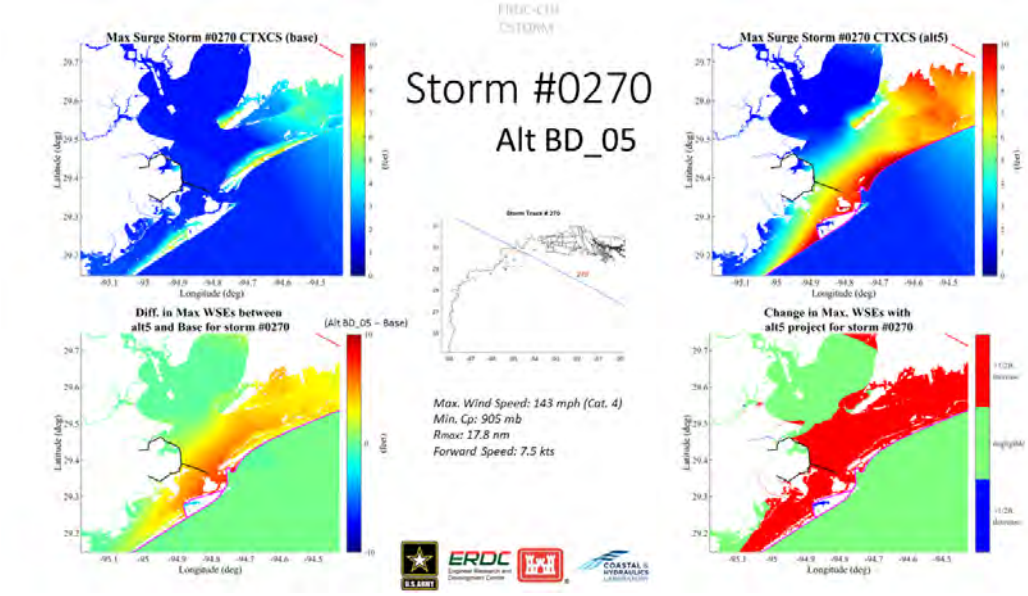

Figure D61. Comparison of maximum water surface elevations color contour plots from the CSTORM coupled ADCIRC+STWAVE simulations for storm 0277 under without-project and with-project BD_Alt5.

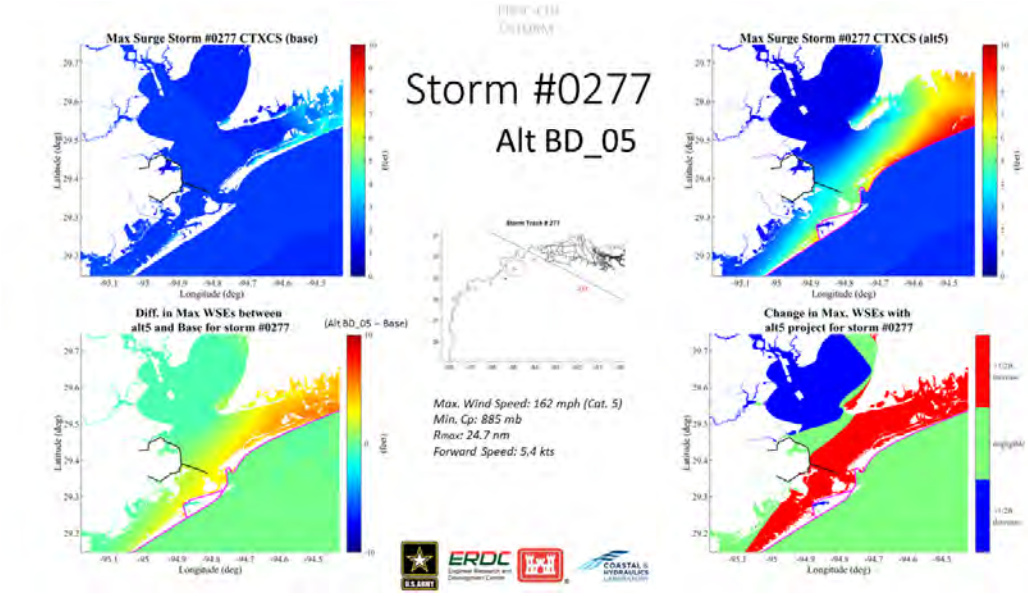

Figure D62. Comparison of maximum water surface elevations color contour plots from the CSTORM coupled ADCIRC+STWAVE simulations for storm 0342 under without-project and with-project BD_Alt5.

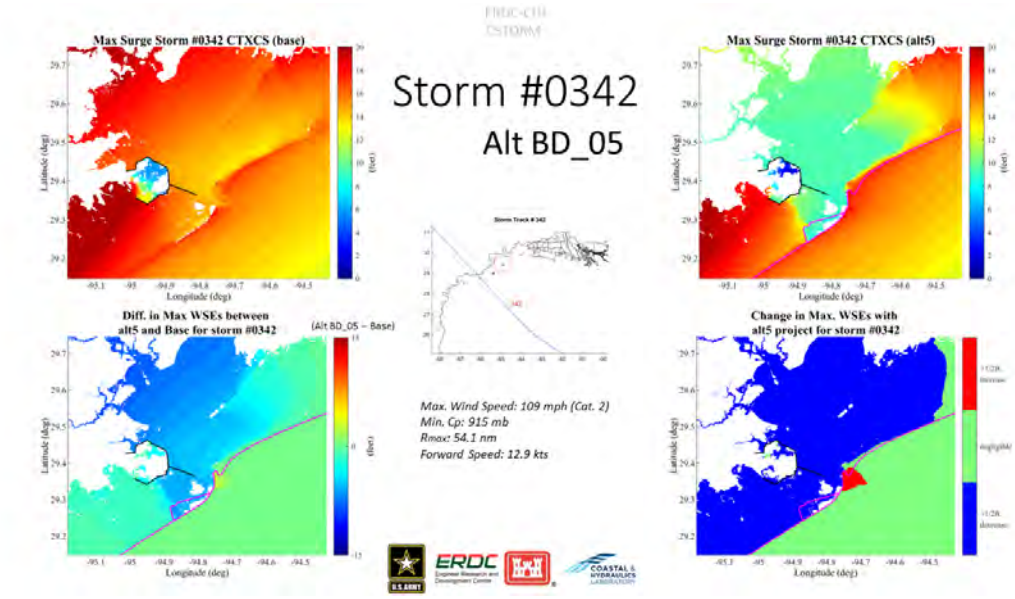

Figure D63. Comparison of maximum water surface elevations color contour plots from the CSTORM coupled ADCIRC+STWAVE simulations for storm 0356 under without-project and with-project BD_Alt5.

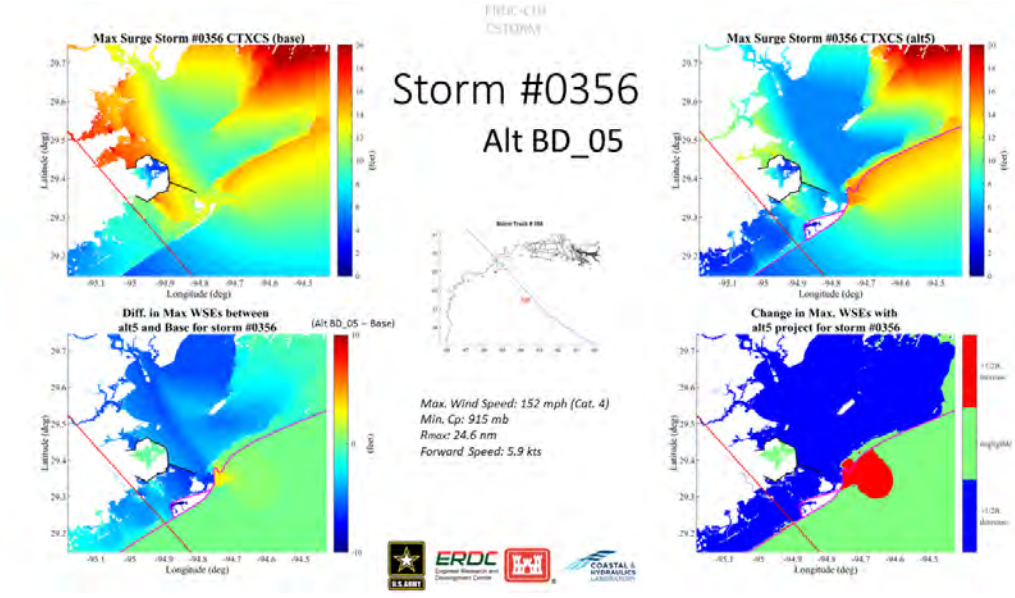

Figure D64. Comparison of maximum water surface elevations color contour plots from the CSTORM coupled ADCIRC+STWAVE simulations for storm 0384 under without-project and with-project BD_Alt5.

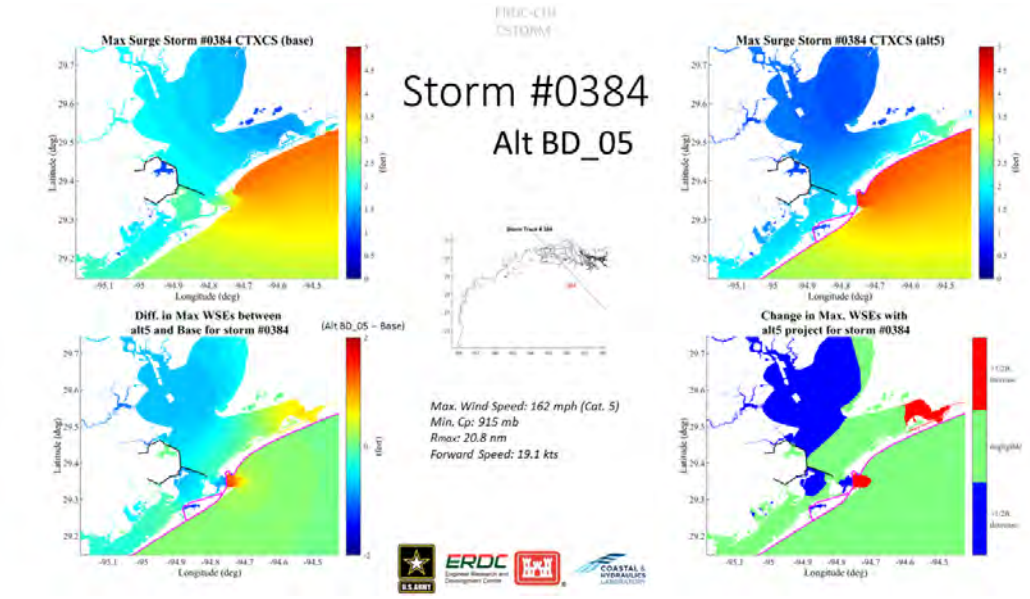

Figure D65. Comparison of maximum water surface elevations color contour plots from the CSTORM coupled ADCIRC+STWAVE simulations for storm 0437 under without-project and with-project BD_Alt5.

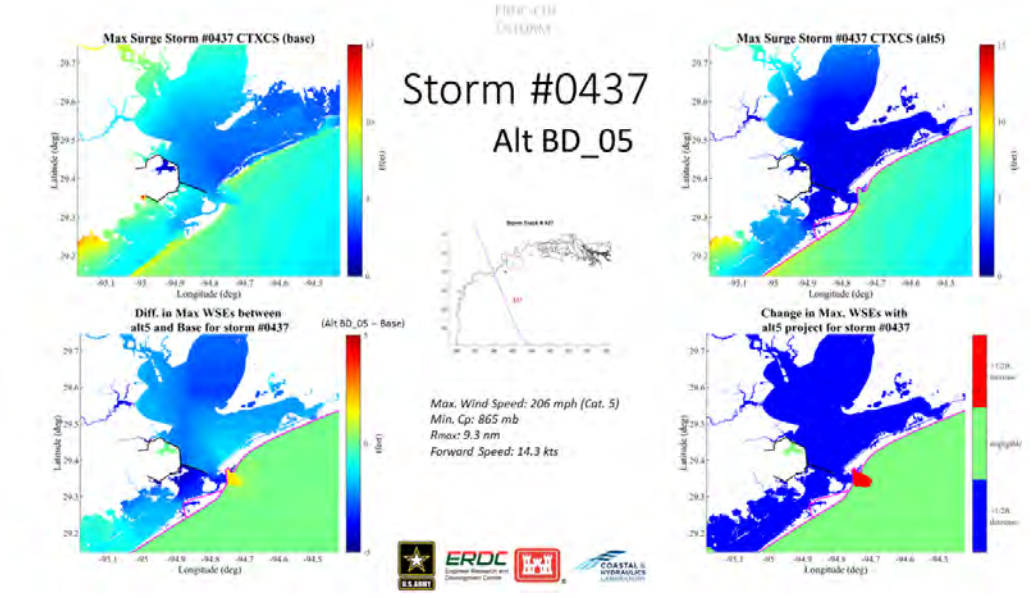

Figure D66. Comparison of maximum water surface elevations color contour plots from the CSTORM coupled ADCIRC+STWAVE simulations for storm 0447 under without-project and with-project BD_Alt5.

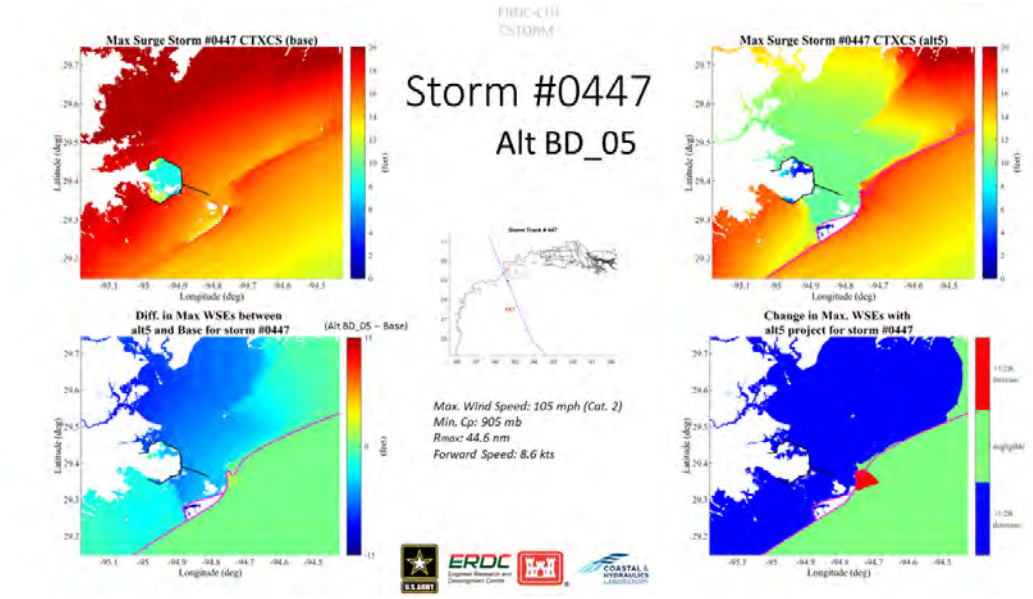

Figure D67. Comparison of maximum water surface elevations color contour plots from the CSTORM coupled ADCIRC+STWAVE simulations for storm 0453 under without-project and with-project BD_Alt5.

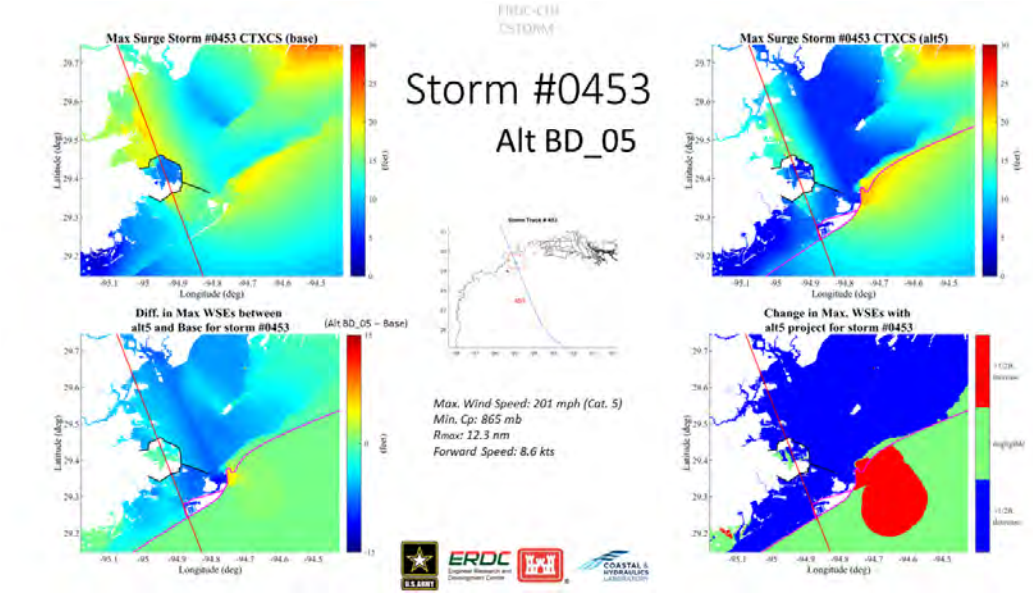

Figure D68. Comparison of maximum water surface elevations color contour plots from the CSTORM coupled ADCIRC+STWAVE simulations for storm 0456 under without-project and with-project BD_Alt5.

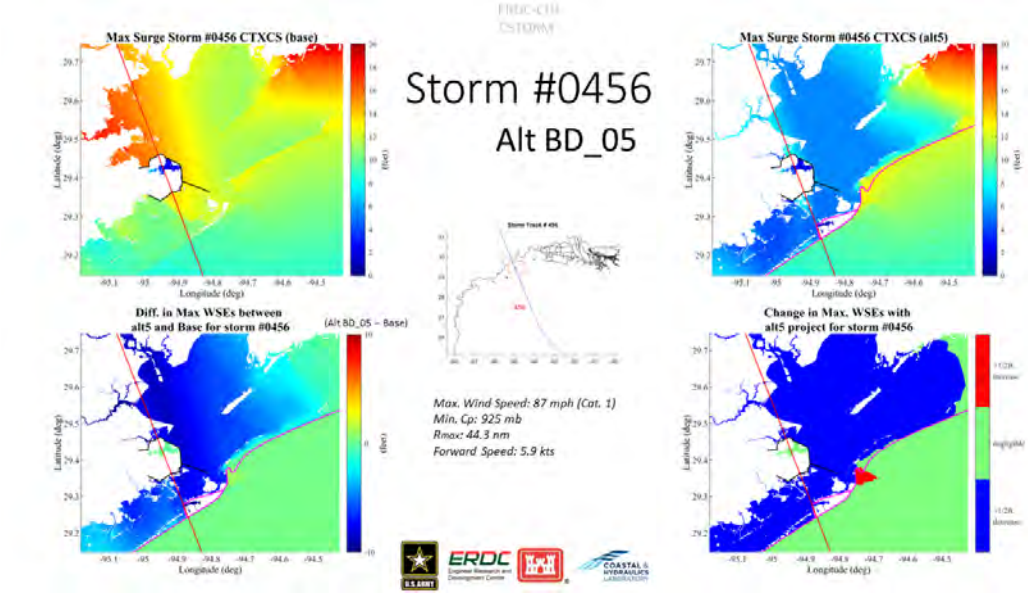

Figure D69. Comparison of maximum water surface elevations color contour plots from the CSTORM coupled ADCIRC+STWAVE simulations for storm 0461 under without-project and with-project BD_Alt5.

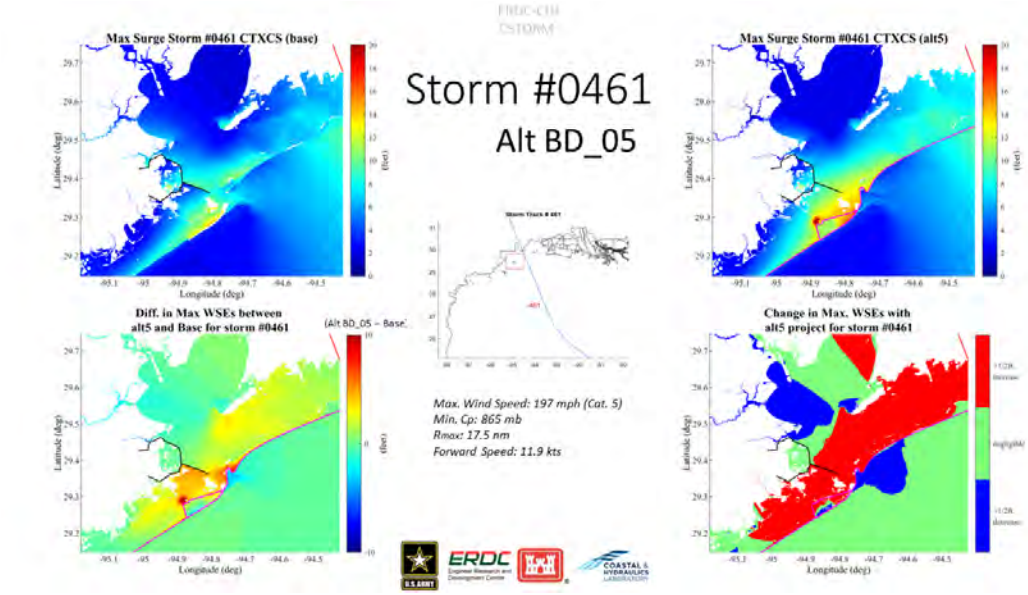

Figure D70. Comparison of maximum water surface elevations color contour plots from the CSTORM coupled ADCIRC+STWAVE simulations for storm 0529 under without-project and with-project BD_Alt5.

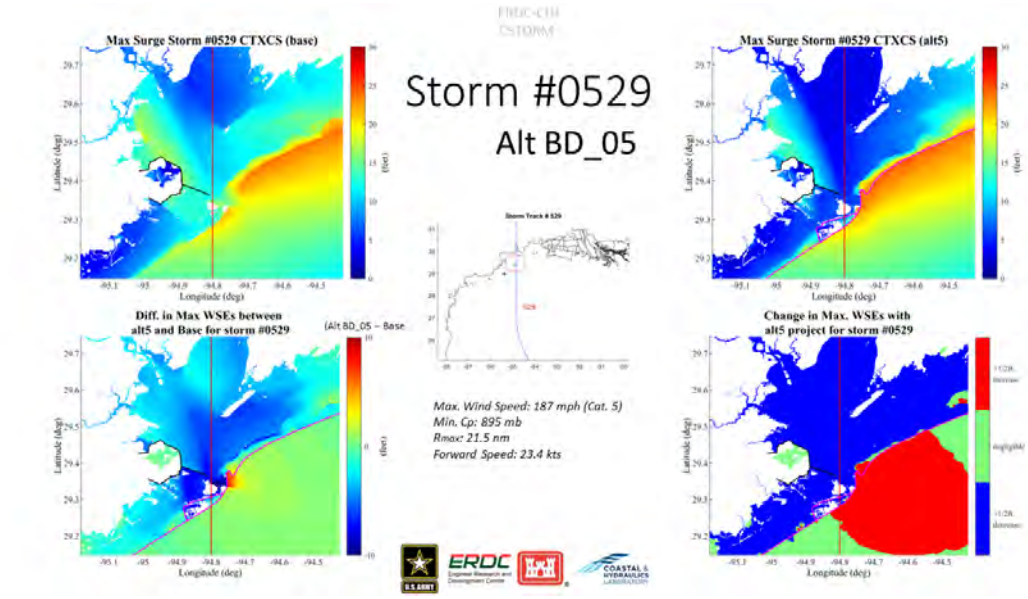

Figure D71. Comparison of maximum water surface elevations color contour plots from the CSTORM coupled ADCIRC+STWAVE simulations for storm 0578 under without-project and with-project BD_Alt5.

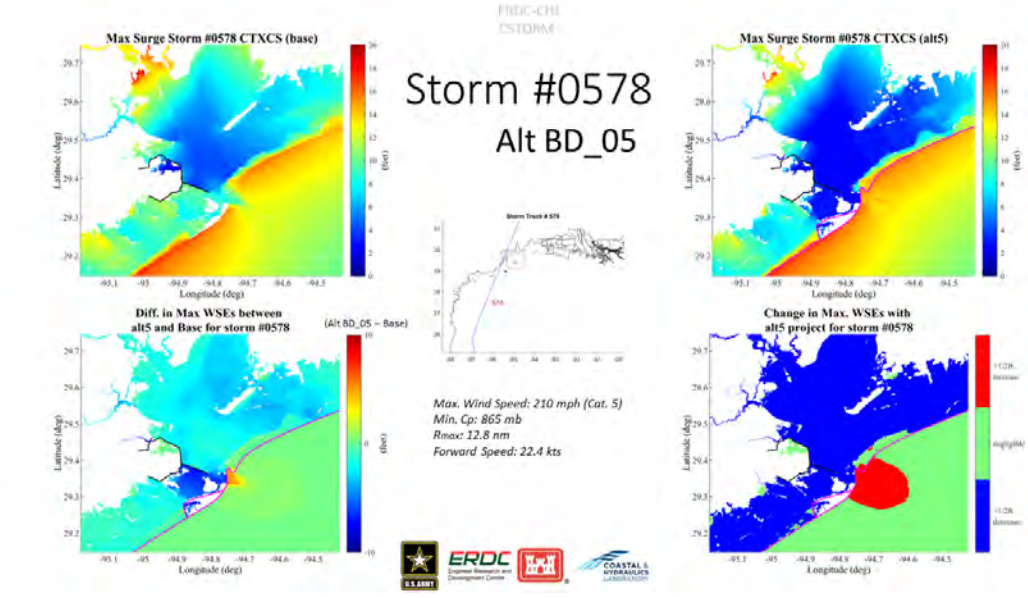

Figure D72. Comparison of maximum water surface elevations color contour plots from the CSTORM coupled ADCIRC+STWAVE simulations for storm 0595 under without-project and with-project BD_Alt5.

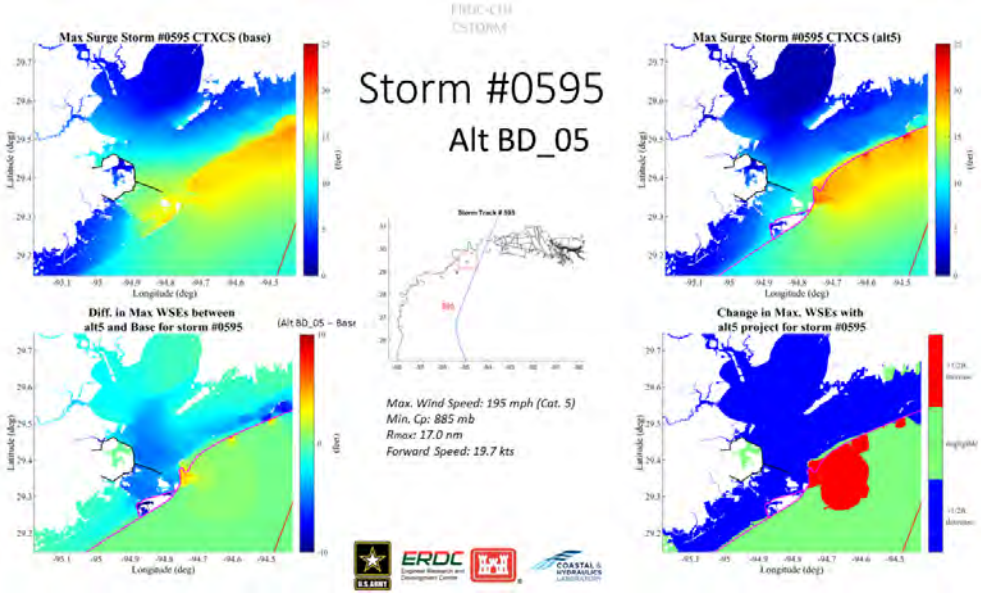

Figure D73. Comparison of maximum water surface elevations color contour plots from the CSTORM coupled ADCIRC+STWAVE simulations for storm 0633 under without-project and with-project BD_Alt5.

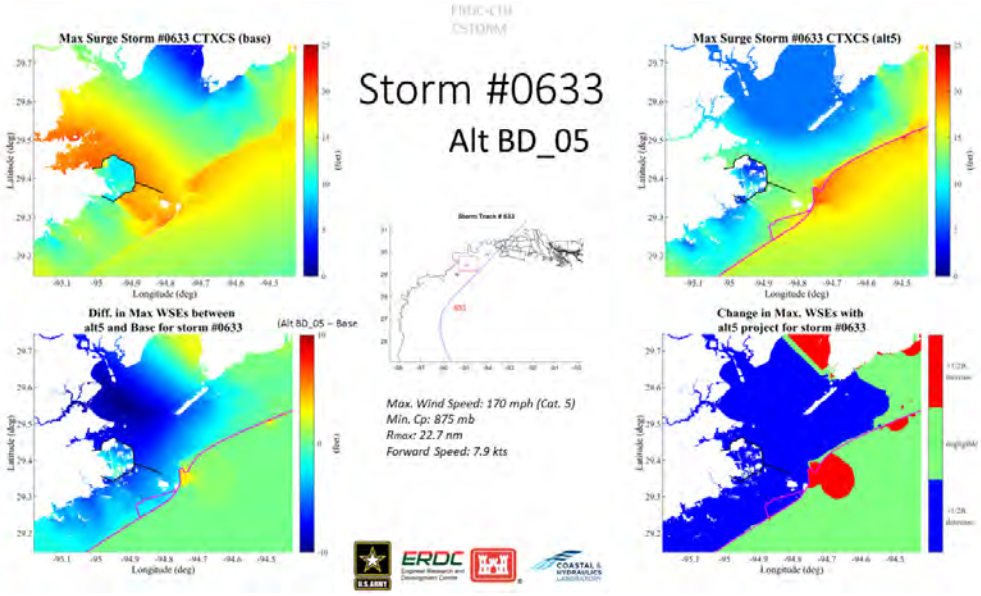

Appendix E. Storm Selection

Alex Taflanidis, PhD

University of Notre Dame

JPM-OS methods were adopted within the CTXCS to select the overall set of 660 tropical cyclones that spans the coast of Texas and neighboring regions that represent the Texas tropical storm hazard. This set was reduced to 170 using an optimization modeling approach. Consider an initial set of n_l storms with the l^{th} storm having frequency weight (mean annual rate) of y_j^l for save point (SP) j. A total of n_j SPs are considered in the geographic domain of interest. The hazard curve for each SP is represented by the annual exceedance rate $\lambda_j(b)$ that the surge will exceed threshold b (considering different values of b), and is calculated as

$$\lambda_j(b) = \frac{1}{n_l}\sum_{l=1}^{n_l} \lambda_j^l I[y_j^l > b] \tag{E.1}$$

where y_j^l denotes the surge at SP j for storm l and I is the indicator function corresponding to 1 if the quantity in the brackets is satisfied (else it is zero).

Consider now a subset of n_l' ($n_l' < n_l$) storms, with potentially adjusted rates $\lambda_j^{l'}$. The hazard curve is given by

$$\lambda_j'(b\,|\,\mathbf{s}) = \frac{1}{\sum_{l=1}^{n_l} s_l}\sum_{l=1}^{n_l} \lambda_j^{l'} I[y_j^l > b] s_l \tag{E.2}$$

where s_l is an indicator index denoting whether storm belongs (s_l=1) or not (s_l=0) in the considered subset, and **s** is the n_l dimensional vector (vector of 1's and 0's) with components corresponding to s_l. Vector **s** uniquely defines the reduced subset of storms. The discrepancy between the original and adjusted hazard curves over a partitioning of the hazard curve $\{b_i=1,\ldots,n_i\}$ is expressed as the weighted least squares

$$F(\mathbf{s}) = \sum_{j=1}^{n_j}\sum_{i=1}^{n_b} w_i(\lambda_j(b_i) - \lambda_j'(b_i\,|\,\mathbf{s}))^2 \tag{E.3}$$

where w_i is the weight for the discrepancy for threshold b_i, denoting the relative importance of the adjusted hazard curve matching the original one for that threshold. The partitioning of the hazard curve, i.e. selection of the threshold sequence $\{b_i=1,...,n_i\}$, is typically performed so that the sequence $\{b_i=i=1,...,n_i\}$ corresponds to specific rates of interest for the original hazard curve, that is, to specific values for $\lambda_j(b)$. The interior summation in Equation E.3 corresponds to calculation of the discrepancy of the hazard curves for each SP, considering the appropriate weights. The exterior summation corresponds to an averaging of this discrepancy over the desired SP.

The optimal selection of the storms to belong in the adjusted set is then given by the optimization

$$\begin{aligned} \mathbf{s}^* &= \arg\min_{\mathbf{s}\in[0,1]^{n_l}} F(\mathbf{s}) \\ &\text{such that } \sum_{l=1}^{n_l} s_l = n_l^{'} \end{aligned} \tag{E.4}$$

To address the computational challenges in Equation E.4 stemming from the fact that **s** includes binary variables (integer optimization), this problem is solved through genetic algorithms.

Hidden within the problem expressed through Equation E.4 is the subproblem of the selection of the adjusted rates $\lambda_j^{l\,'}$ and various implementations can be further distinguished based on the assumptions taken for that, ranging from (i) simply assigning the weights of the removed storms to the retained ones, maintaining proportionality of their relative likelihood, to (ii) explicitly optimizing the storm rates for a given **s**. Implementation (i) leads to

$$\lambda_j^{l\,'} = s_l \lambda_j^l \frac{\sum_{l=1}^{n_l} \lambda_j^l}{\sum_{l=1}^{n_l} \lambda_j^l s_l} \tag{E.5}$$

which guarantees that the total rate for the retained storms is the same as the original

$$\sum_{l=1}^{n_l} \lambda_j^{l\,'} = \sum_{l=1}^{n_l} \lambda_j^l \tag{E.6}$$

and that the relative likelihood of each of the retained storms is the same as in the original set. Implementation (ii) corresponds to the optimization problem

$$[\lambda_j^{l'}]^* = \arg\min_{[\lambda_j^{l'}]} \sum_{i=1}^{n_b} w_i (\lambda_j(b_i) - \lambda_j^{'}(b_i \mid \mathbf{s}))^2$$
$$\text{such that } \sum_{l=1}^{n_l} \lambda_j^{l'} = \sum_{l=1}^{n_l} \lambda_j^{l} \tag{E.7}$$

where $[\lambda_j^{l'}]$ denotes the vector composed of $\lambda_j^{l'}$ for the different storms.

Optimization of Equation E.7 identifies, for a given subset of storms, the optimal storm weights so that the hazard curve discrepancy is minimized for a specific SP. This implementation leads to a double loop optimization with the outer loop given by Equation E.4 and the inner loop, solved for every new **s** examined for the outer loop, given by Equation E.7. For this study, the optimization in Equation E.7 was employed using the genetic algorithm tool in Matlab.

Appendix F. Coastal Hazards

This appendix contains analysis of coastal hazards at specific locations across the reaches from offshore to just onshore and over the landform into the intercoastal waterway. Offshore locations were shown in the main report. The shape of the curves is generally well behaved. However, some curves have a stepped shape that is odd (e.g. SP 11232). These odd points are typically in shallow water in the surf zone and are usually in STWAVE or ADCIRC cells that are partially dry. Cells that straddle the wet-dry interface, tend to have unpredictable responses for multiple reasons. We typically avoid using these cells in engineering analysis. Hazard curves that cross the abscissa at lower AEPs occur for cells that are dry for high frequency storms (e.g. SP 1456).

Figure F1. Select cross-shore hazard locations on Galveston Island.

Figure F2. Hazard curves for select cross-shore hazard locations on west end of Galveston Island for Beach-Dune SLC0 alternative.

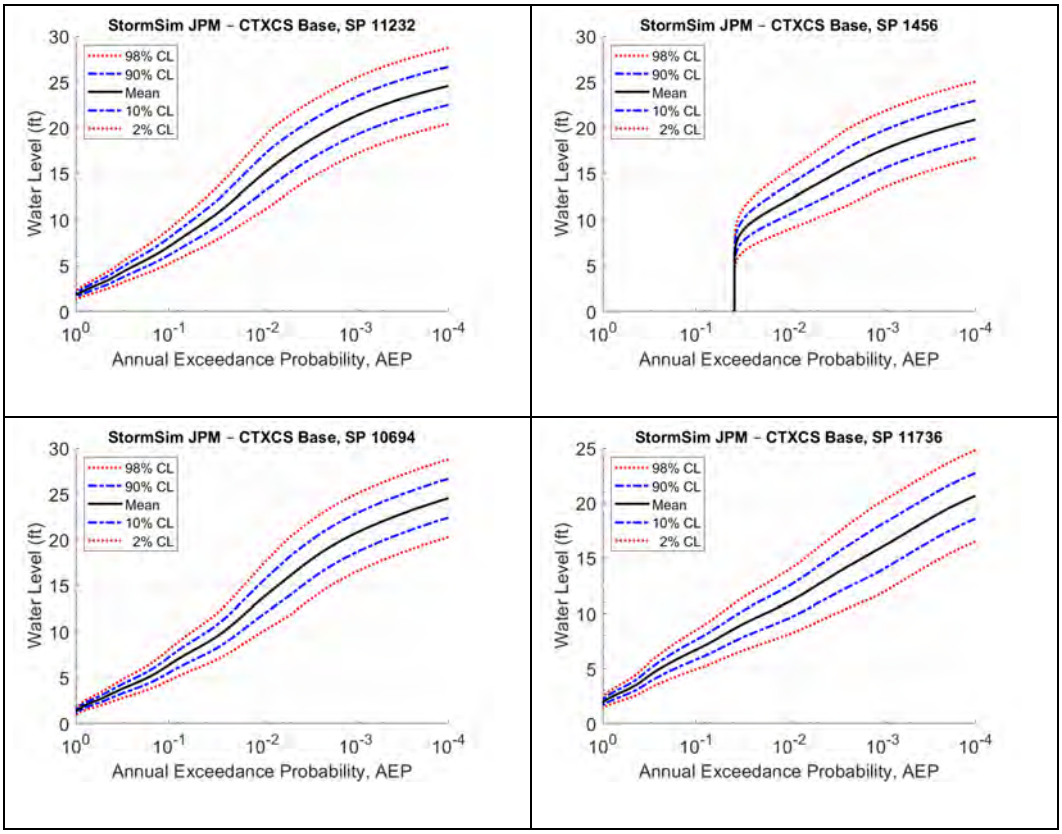

Figure F3. Hazard curves for select cross-shore hazard locations on west end of Galveston Island for Beach-Dune SLC1 alternative.

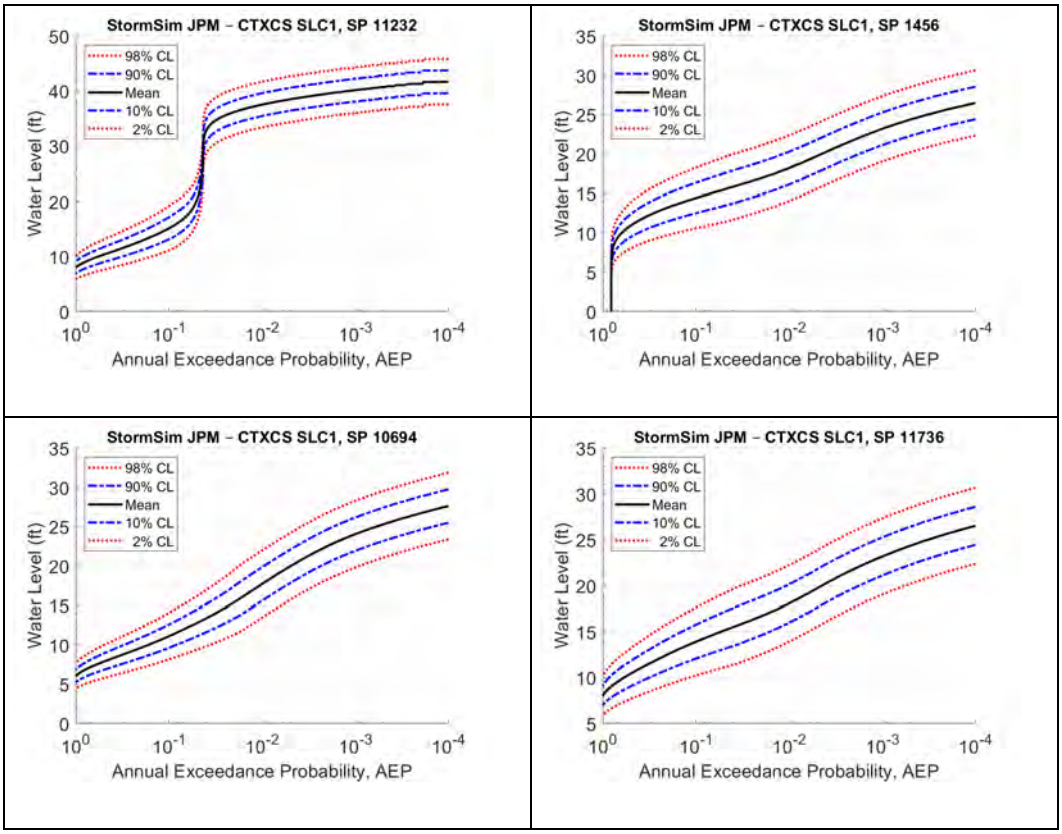

Figure F4. Hazard curves for select cross-shore hazard locations on west end of Galveston Island for Surge Barrier Only SLC0 alternative.

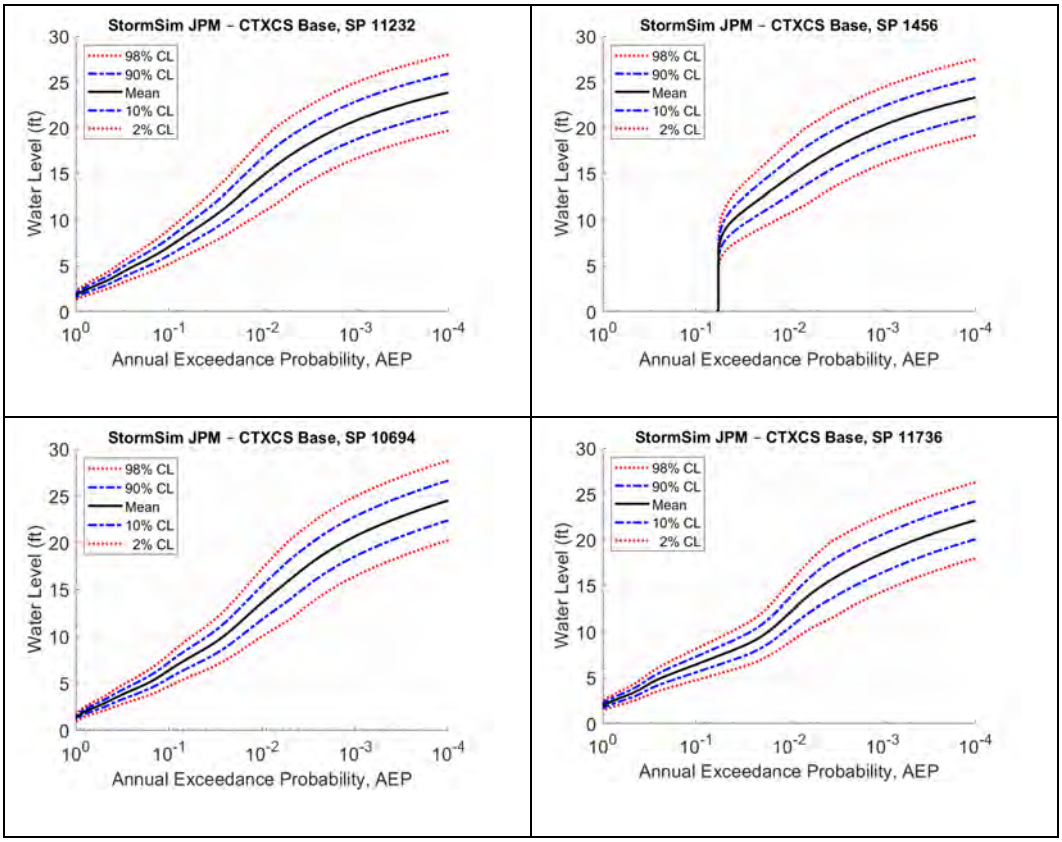

Figure F5. Hazard curves for select cross-shore hazard locations at Jamaica Beach on Galveston Island for Beach-Dune SLC0 alternative.

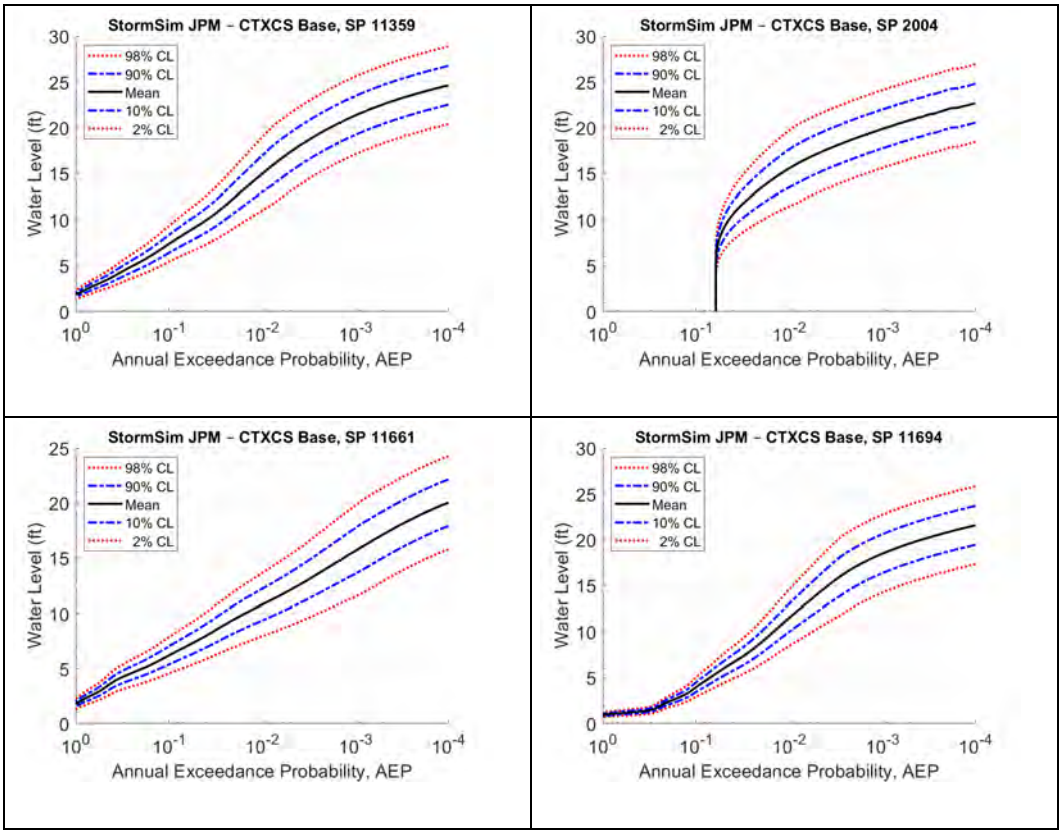

Figure F6. Hazard curves for select cross-shore hazard locations at Jamaica Beach on Galveston Island for Beach-Dune SLC1 alternative.

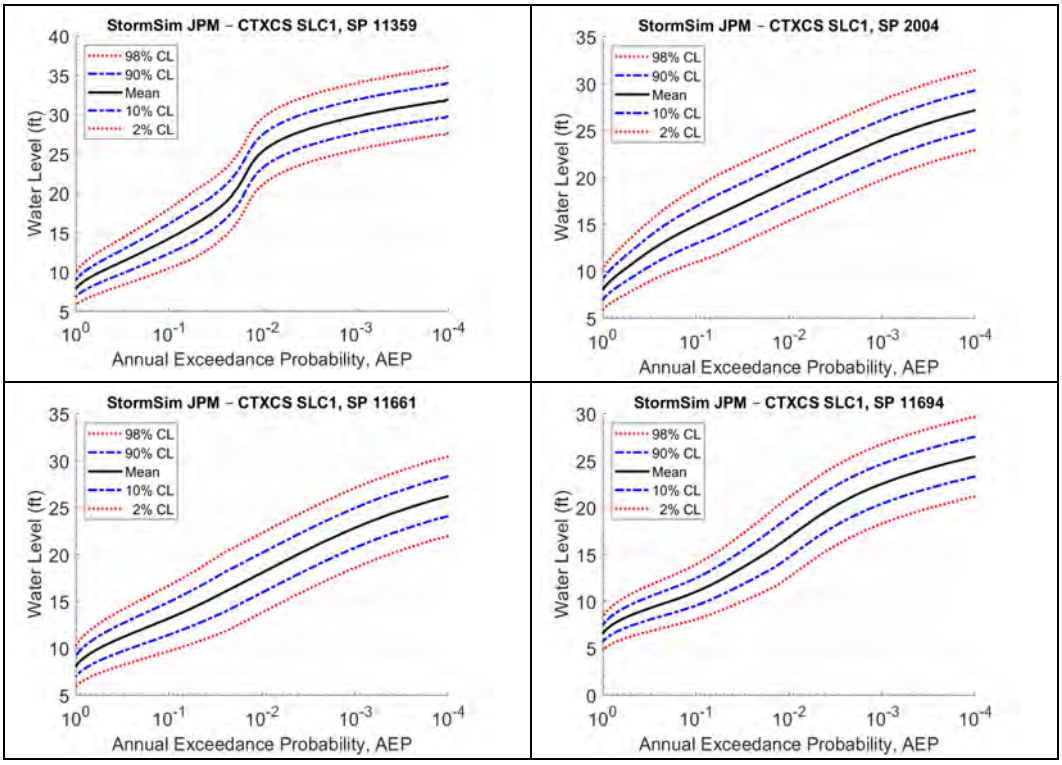

Figure F7. Hazard curves for select cross-shore hazard locations at Jamaica Beach on Galveston Island for surge Barrier Only SLC0 alternative.

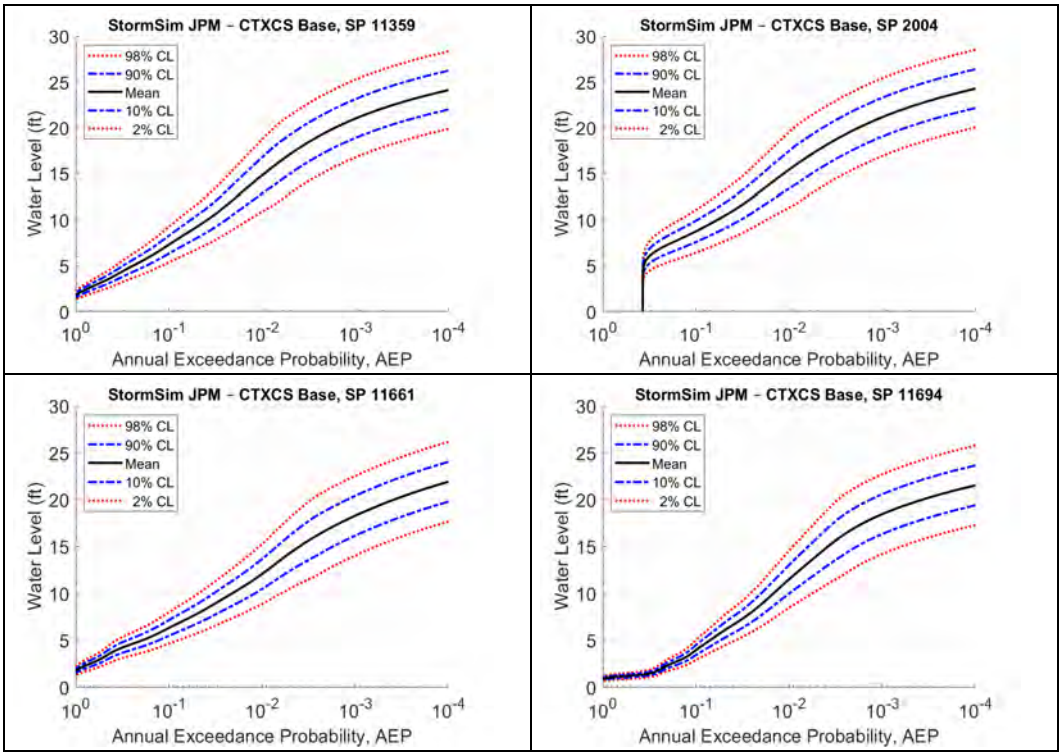

Figure F8. Select cross-shore hazard locations on west Bolivar Peninsula.

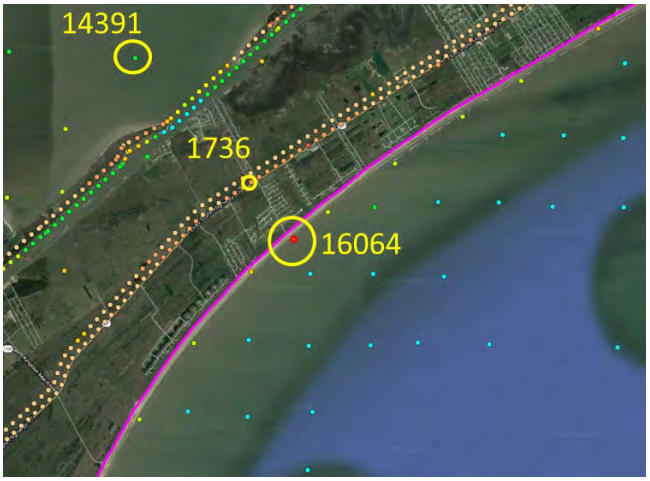

Figure F9. Hazard curves for select cross-shore hazard locations on west Bolivar Peninsula for Beach-Dune SLC0 alternative.

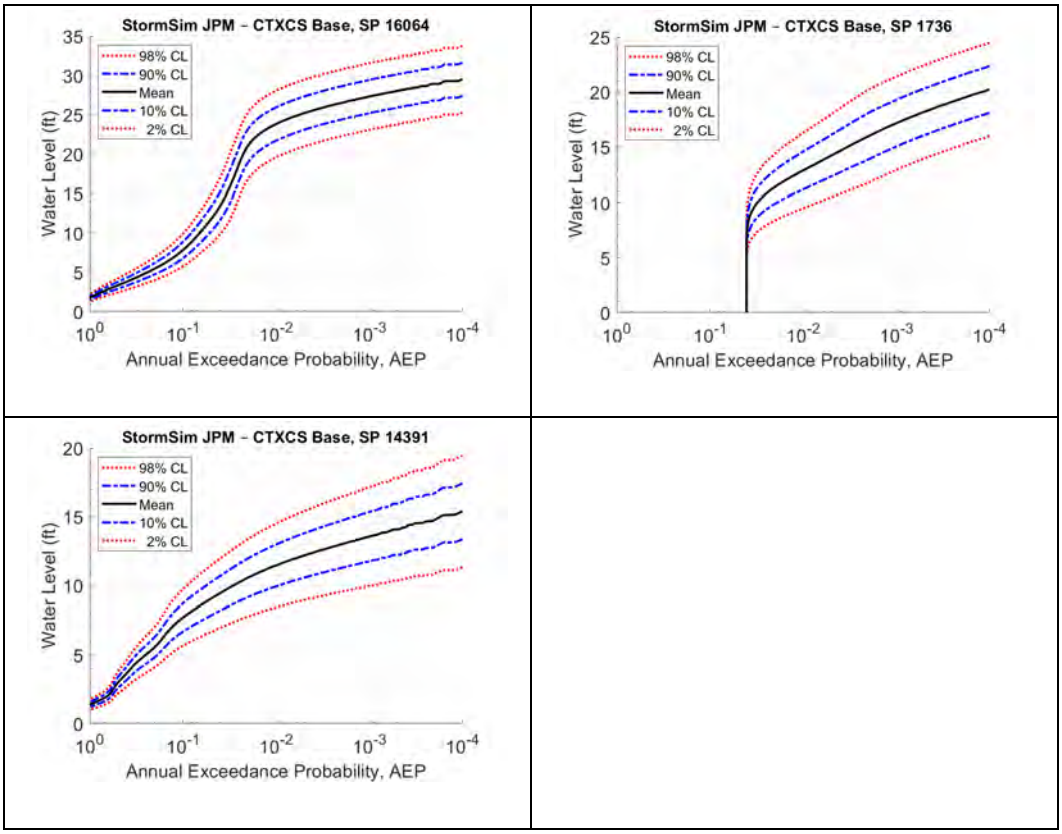

Figure F10. Hazard curves for select cross-shore hazard locations on west Bolivar Peninsula for Beach-Dune SLC1 alternative.

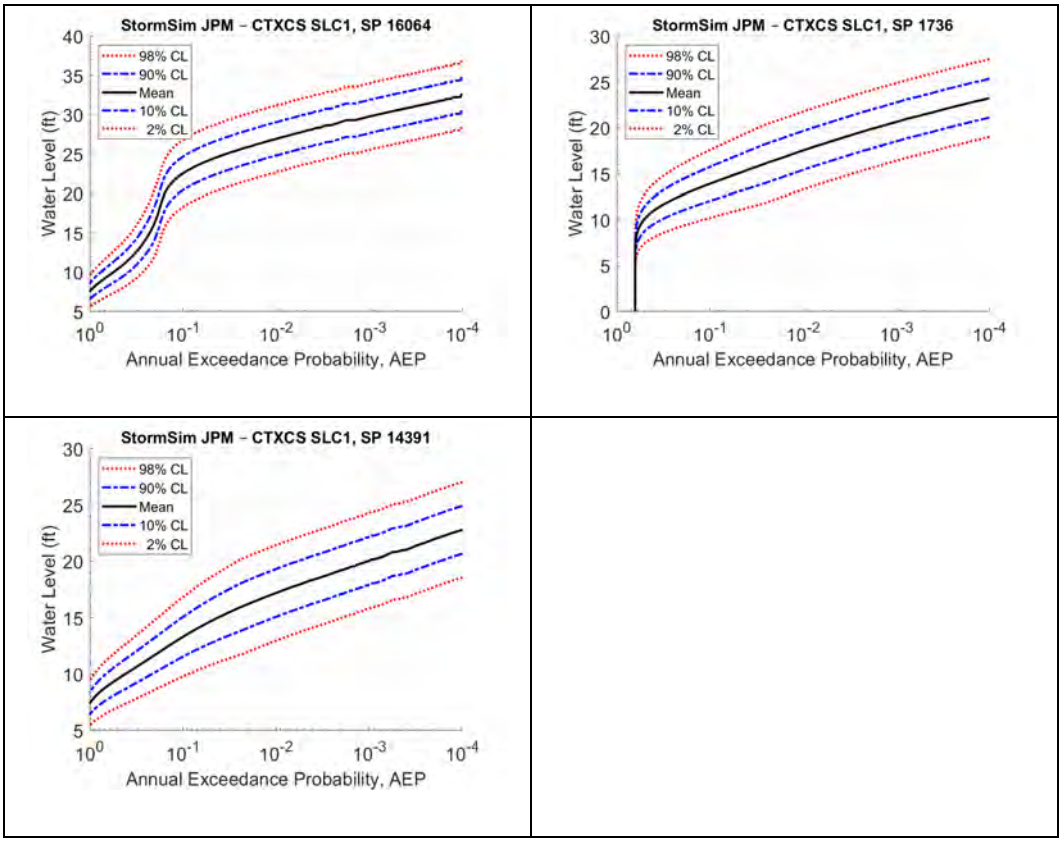

Figure F11. Hazard curves for select cross-shore hazard locations on west Bolivar Peninsula for Surge Barrier Only SLC0 alternative.

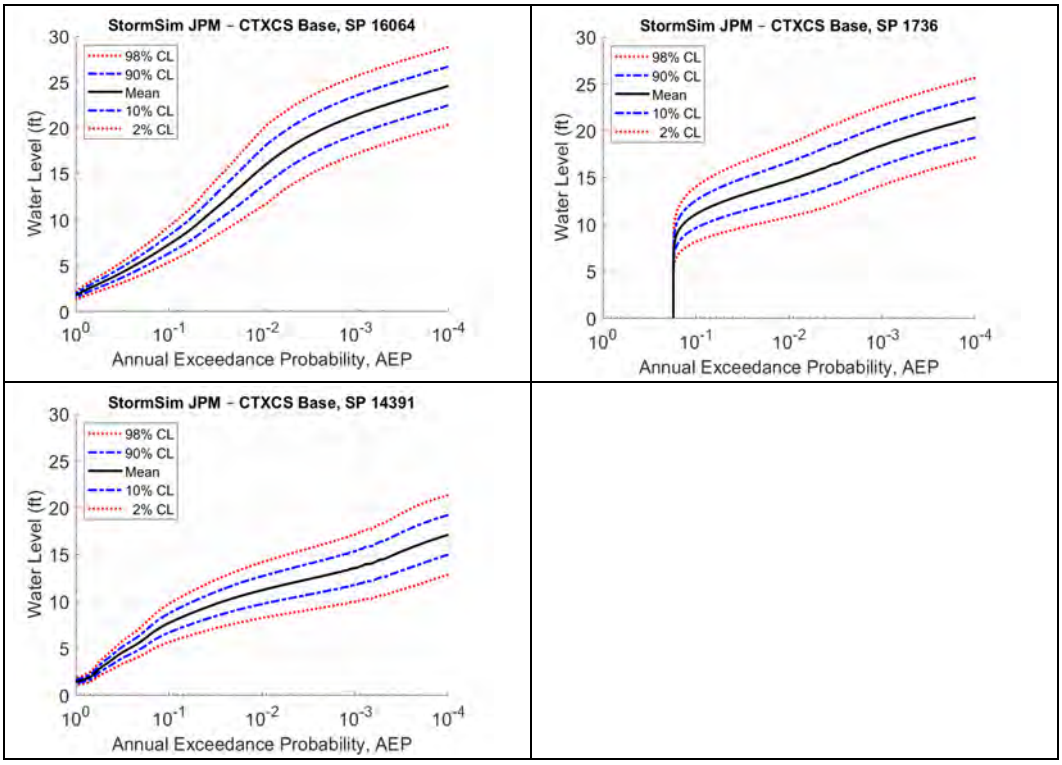

Figure F12. Select cross-shore hazard locations on in Crystal Beach area of Bolivar Peninsula.

Figure F13. Hazard curves for select cross-shore hazard locations in Crystal Beach area of Bolivar Peninsula (Part 1) for Beach-Dune SLC0 alternative.

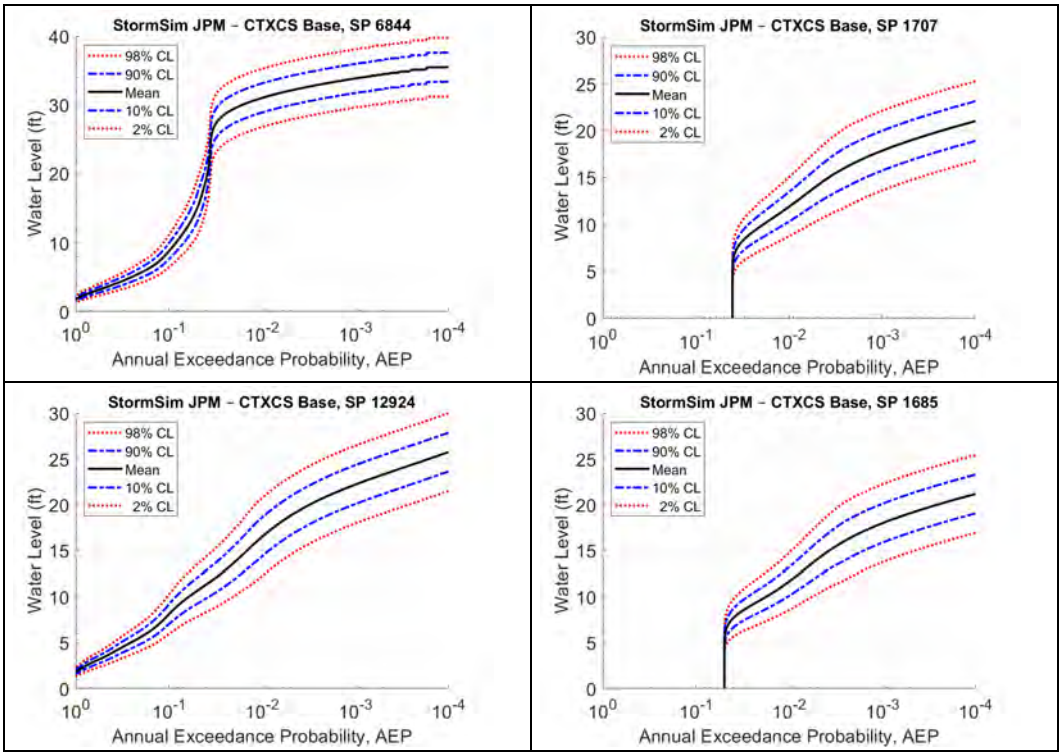

Figure F14. Hazard curves for select cross-shore hazard locations in Crystal Beach area of Bolivar Peninsula (Part 1) for Beach-Dune SLC1 alternative.

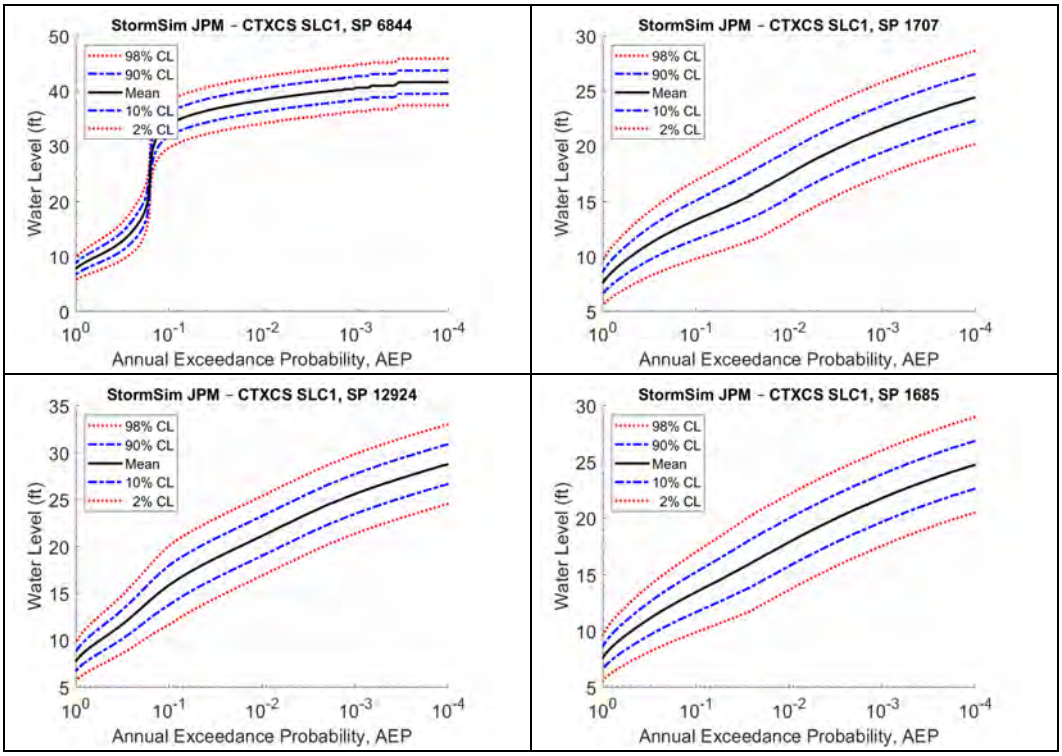

Figure F15. Hazard curves for select cross-shore hazard locations in Crystal Beach area of Bolivar Peninsula (Part 1) for Surge Barrier Only SLC0 alternative.

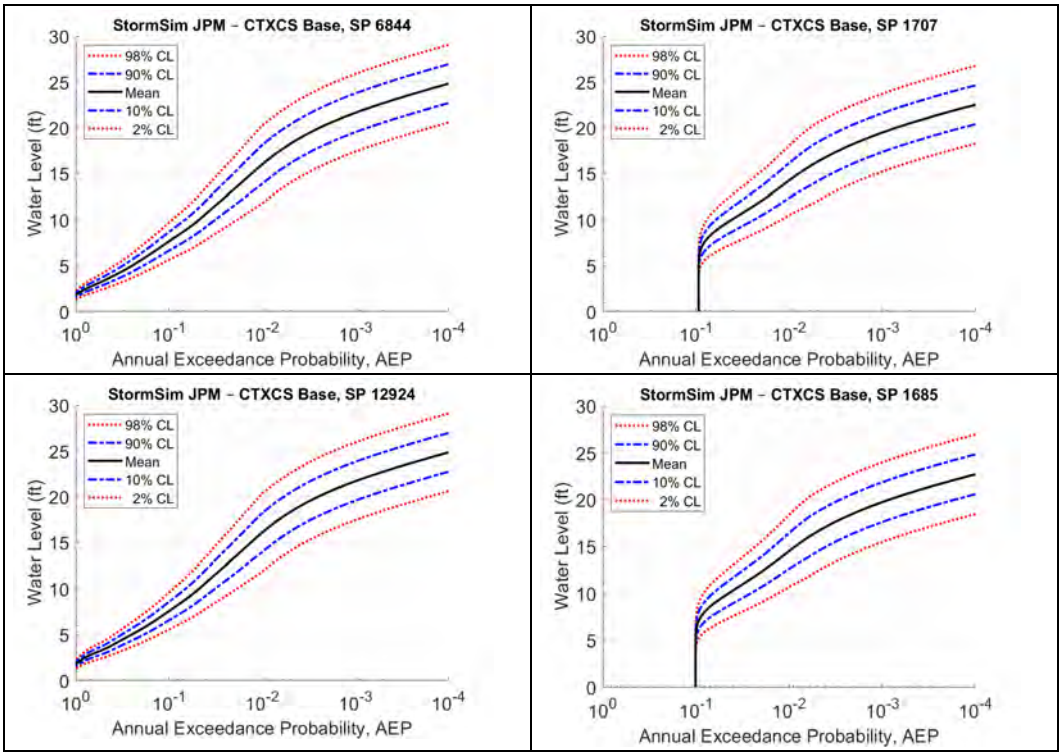

Figure F16. Hazard curves for select cross-shore hazard locations in Crystal Beach area of Bolivar Peninsula (Part 2) for Beach-Dune SLC0 alternative.

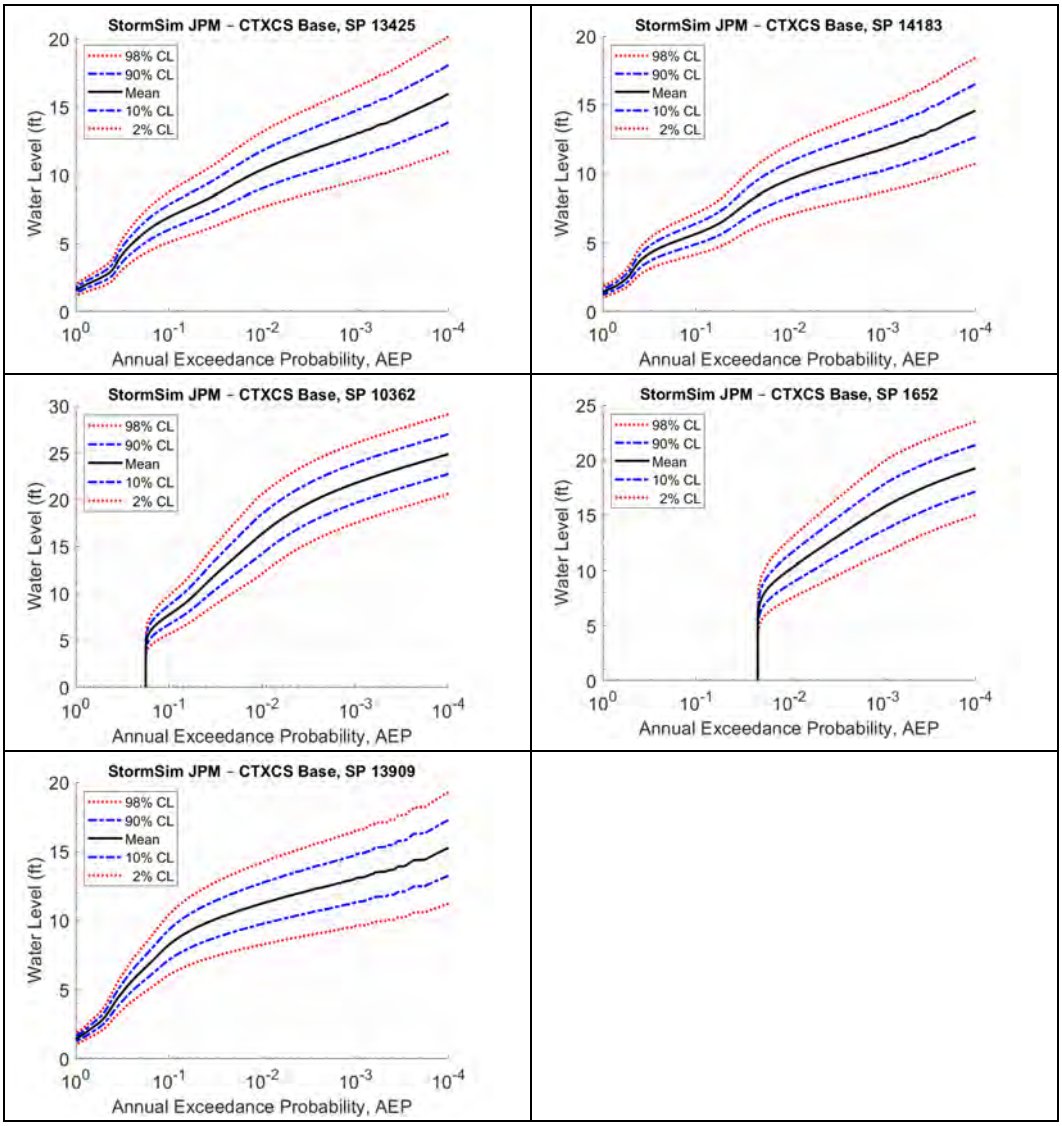

Figure F17. Hazard curves for select cross-shore hazard locations in Crystal Beach area of Bolivar Peninsula (Part 2) for Beach-Dune SLC1 alternative.

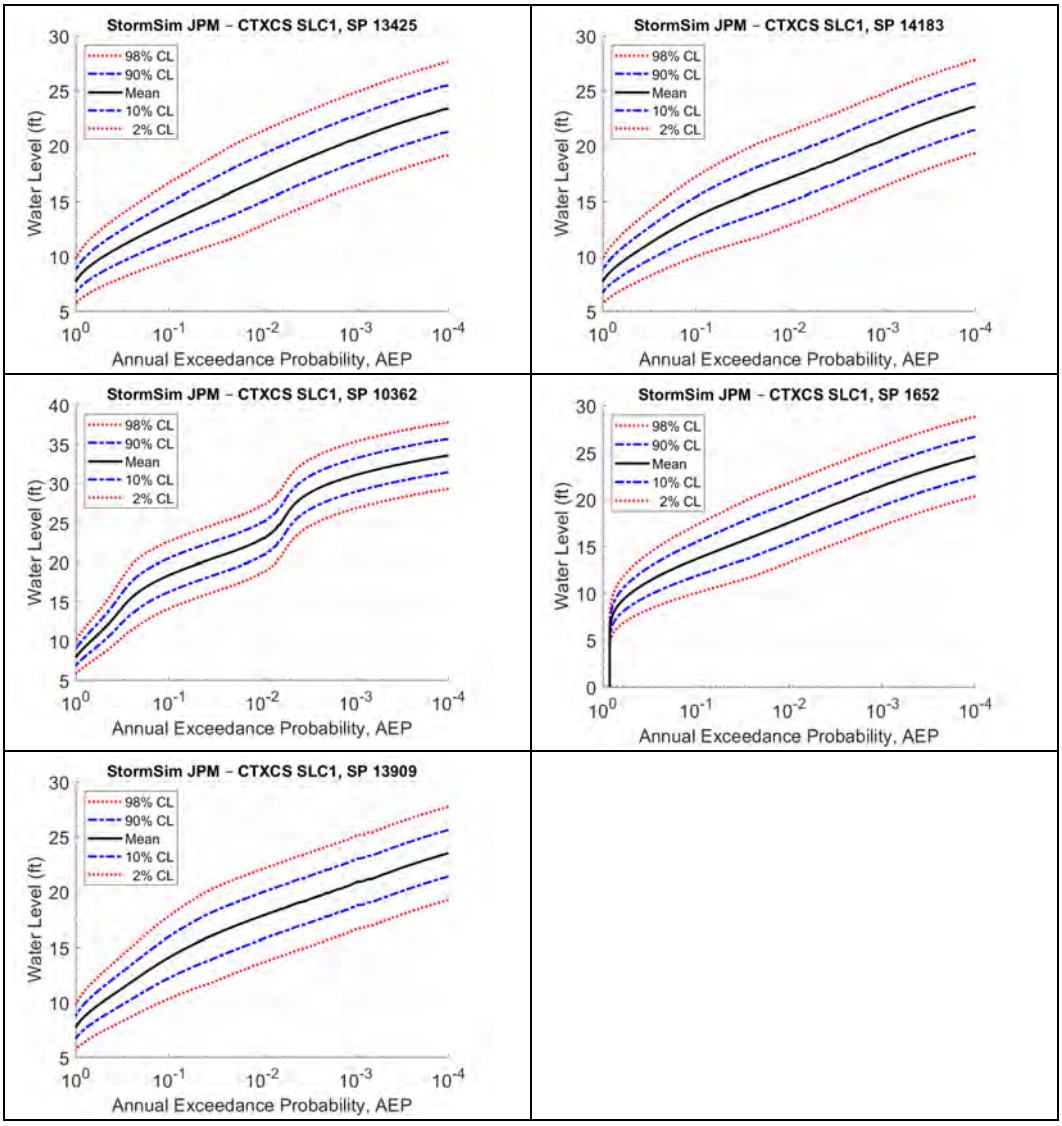

Figure F18. Hazard curves for select cross-shore hazard locations in Crystal Beach area of Bolivar Peninsula (Part 2) for Surge Barrier Only SLC0 alternative.

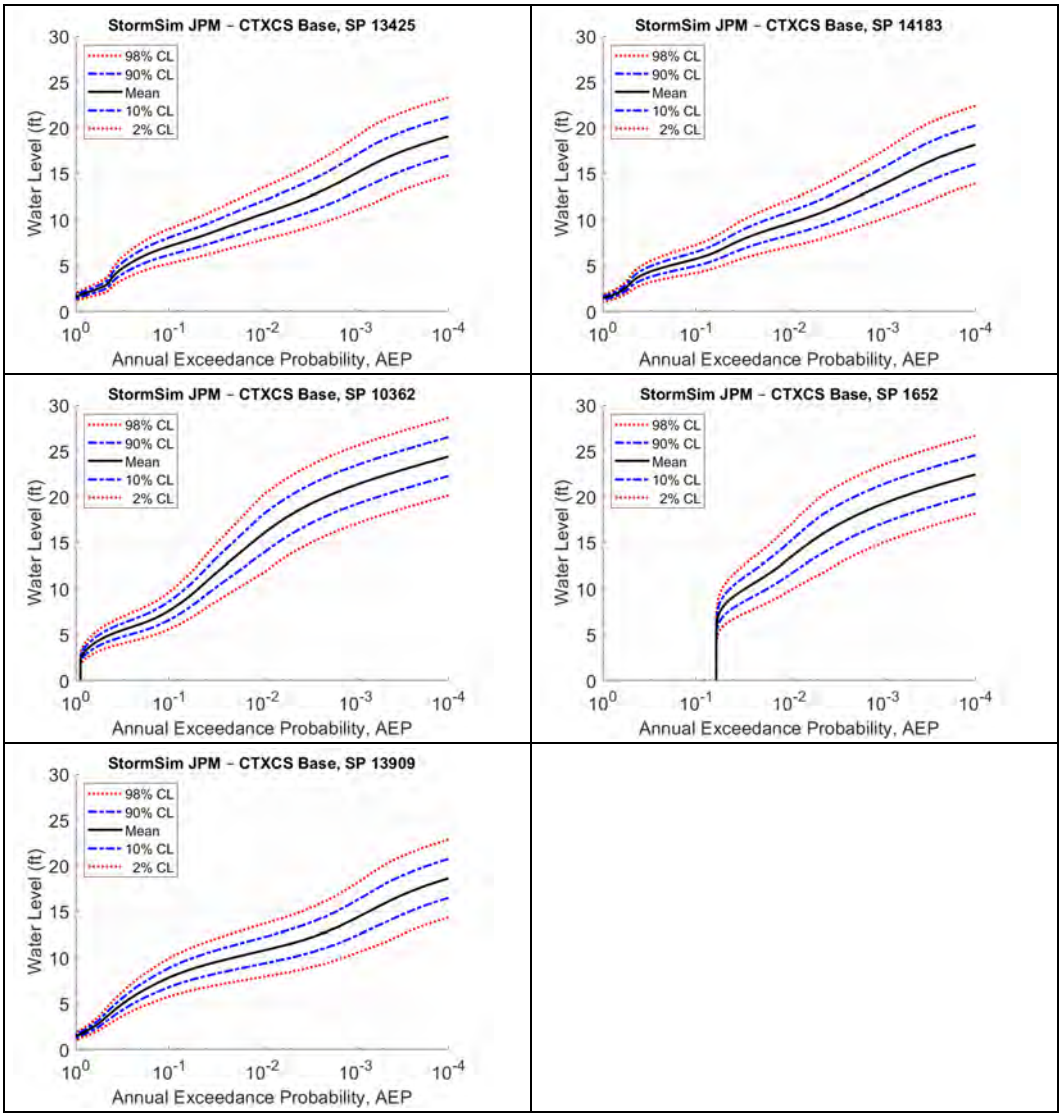

Figure F19. Select cross-shore hazard locations on in Caplen/Gilchrist area of Bolivar Peninsula.

Figure F20. Hazard curves for select cross-shore hazard locations in Caplen area of Bolivar Peninsula for Beach-Dune SLC0 alternative.

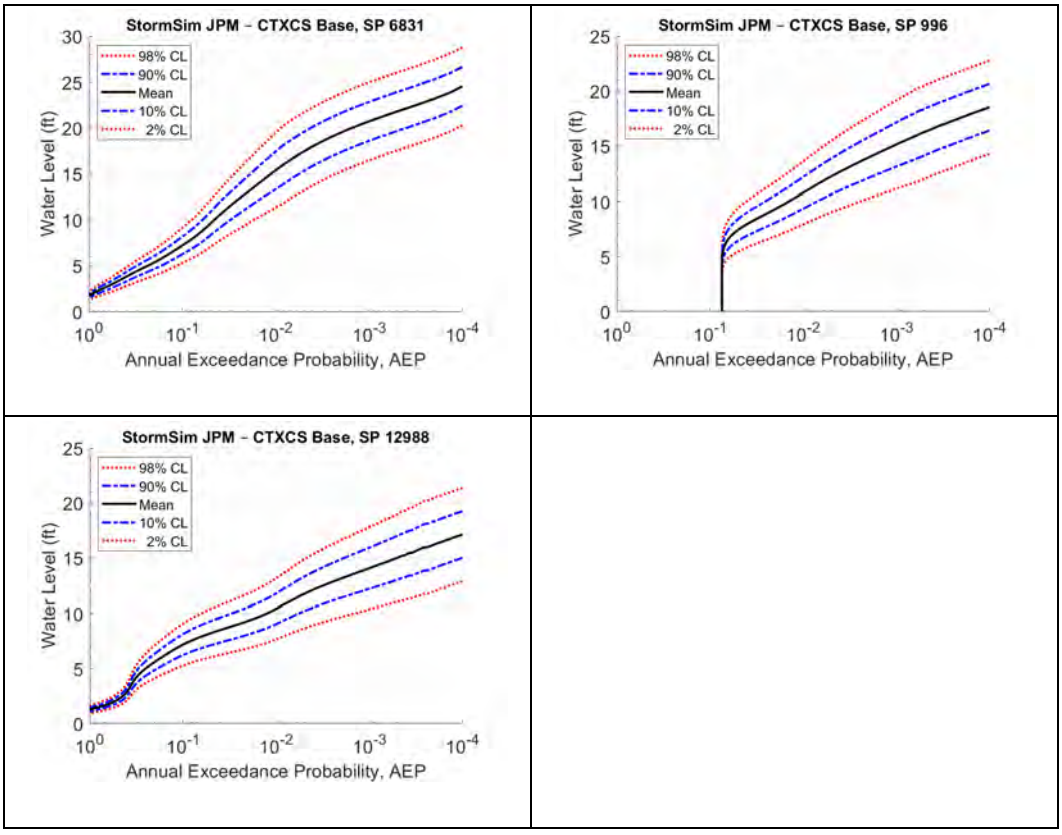

Figure F21. Hazard curves for select cross-shore hazard locations in Caplen area of Bolivar Peninsula for Beach-Dune SLC1 alternative.

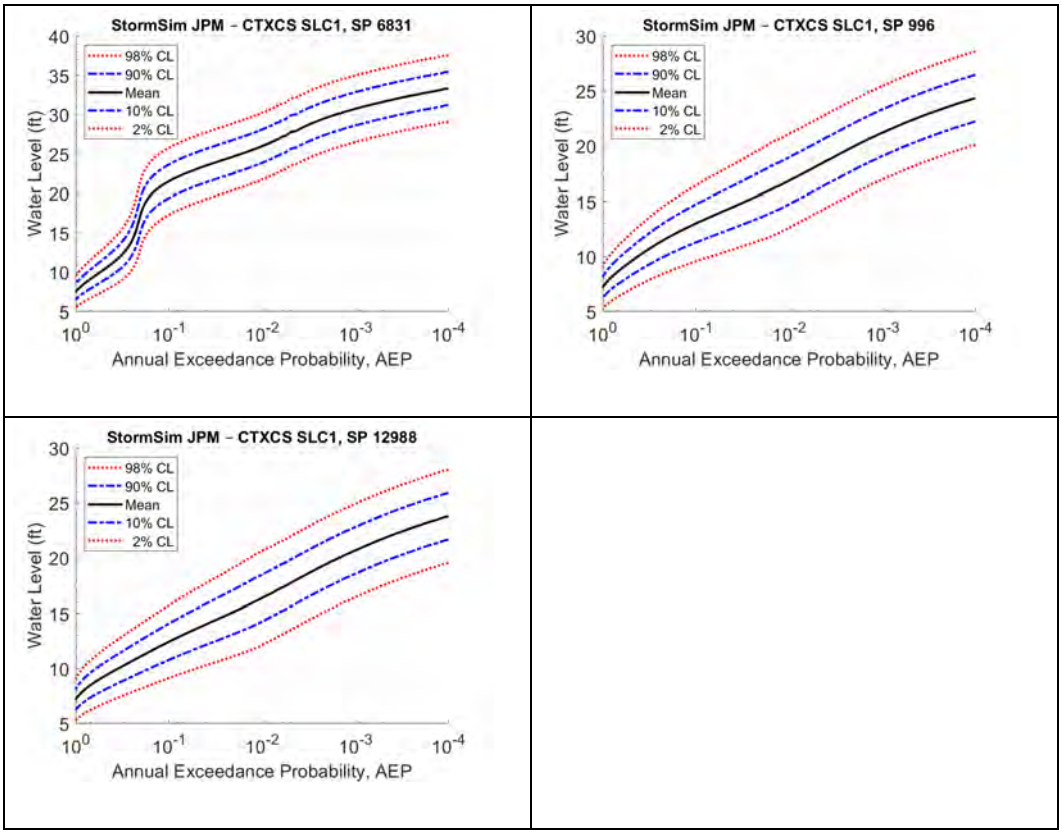

Figure F22. Hazard curves for select cross-shore hazard locations in Caplen area of Bolivar Peninsula for Surge Barrier Only SLC0 alternative.

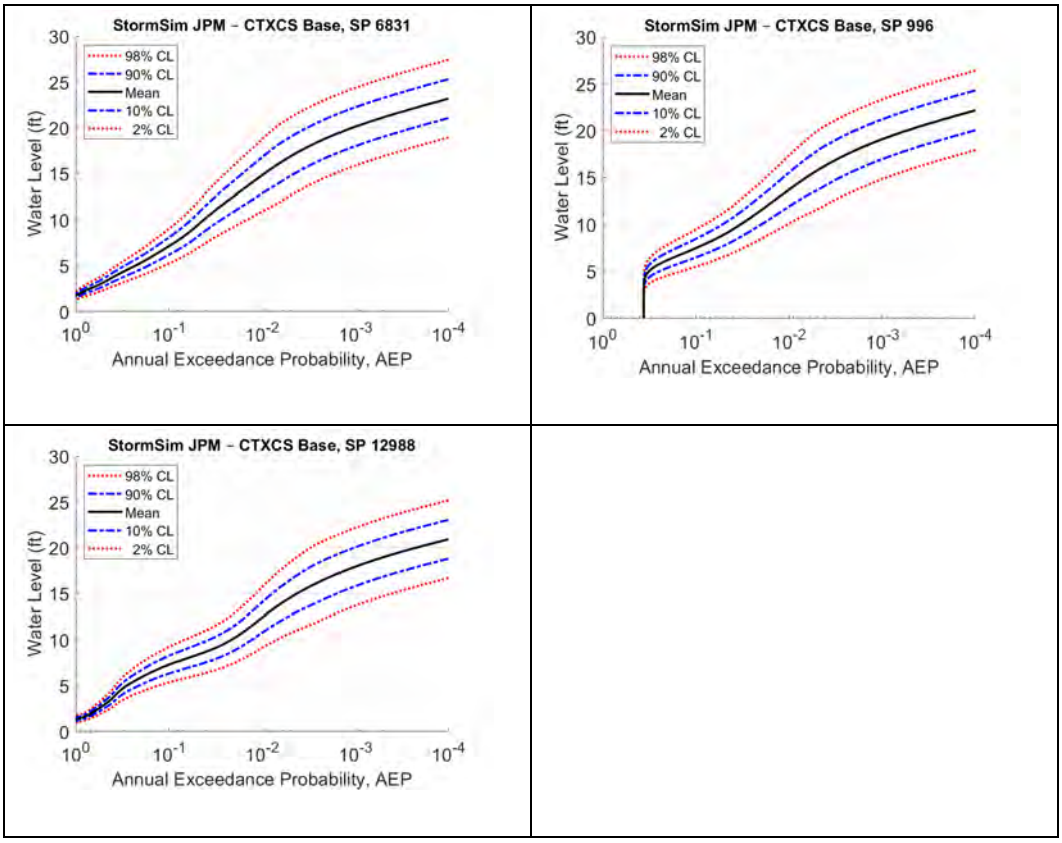

Figure F23. Hazard curves for select cross-shore hazard locations in Gilchrist area of Bolivar Peninsula for Beach-Dune SLC0 alternative.

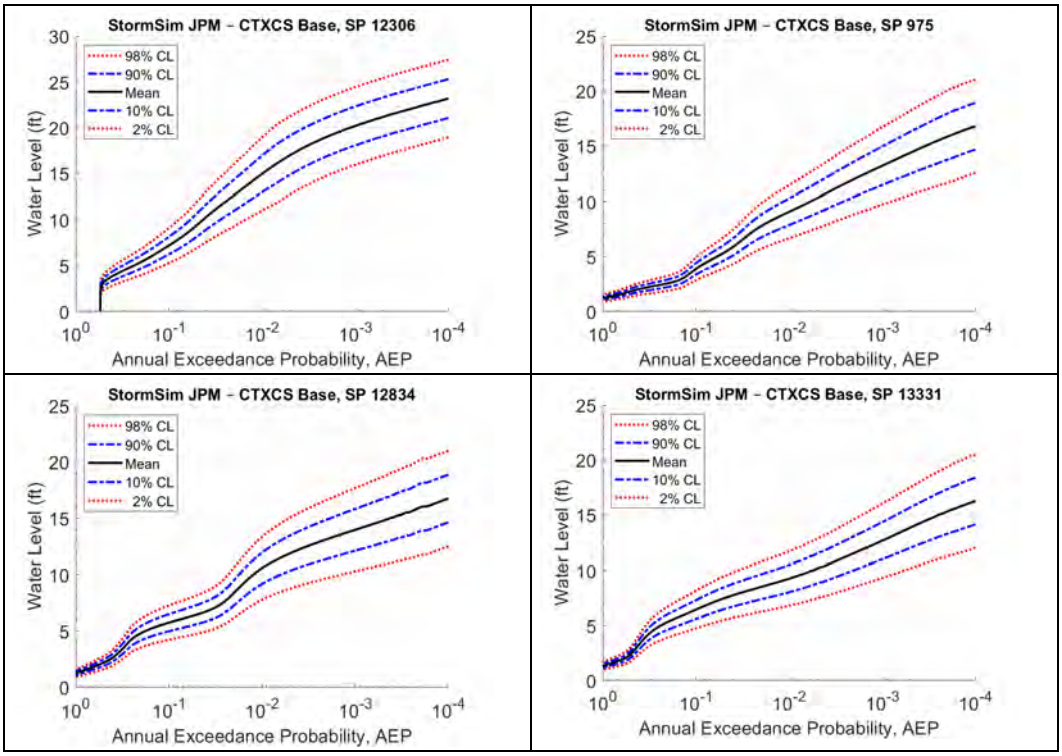

Figure F24. Hazard curves for select cross-shore hazard locations in Gilchrist area of Bolivar Peninsula for Beach-Dune SLC1 alternative.

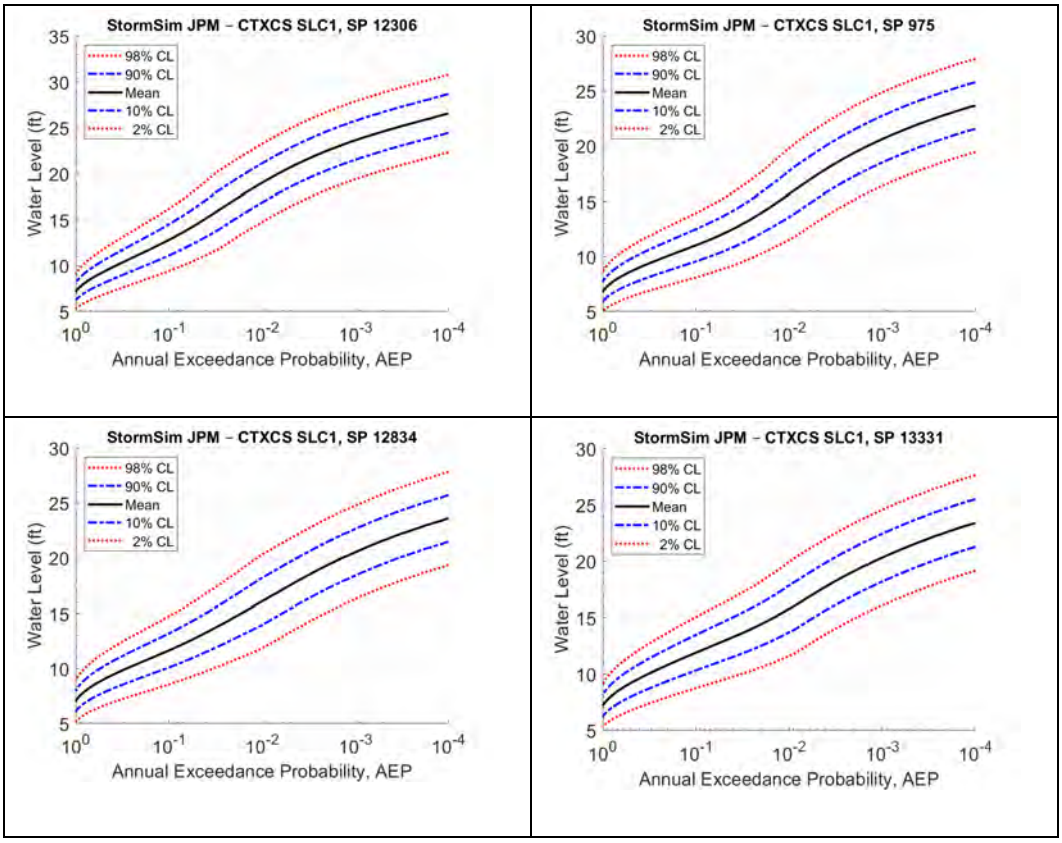

Figure F25. Hazard curves for select cross-shore hazard locations in Gilchrist area of Bolivar Peninsula for Surge Barrier Only SLC0 alternative.

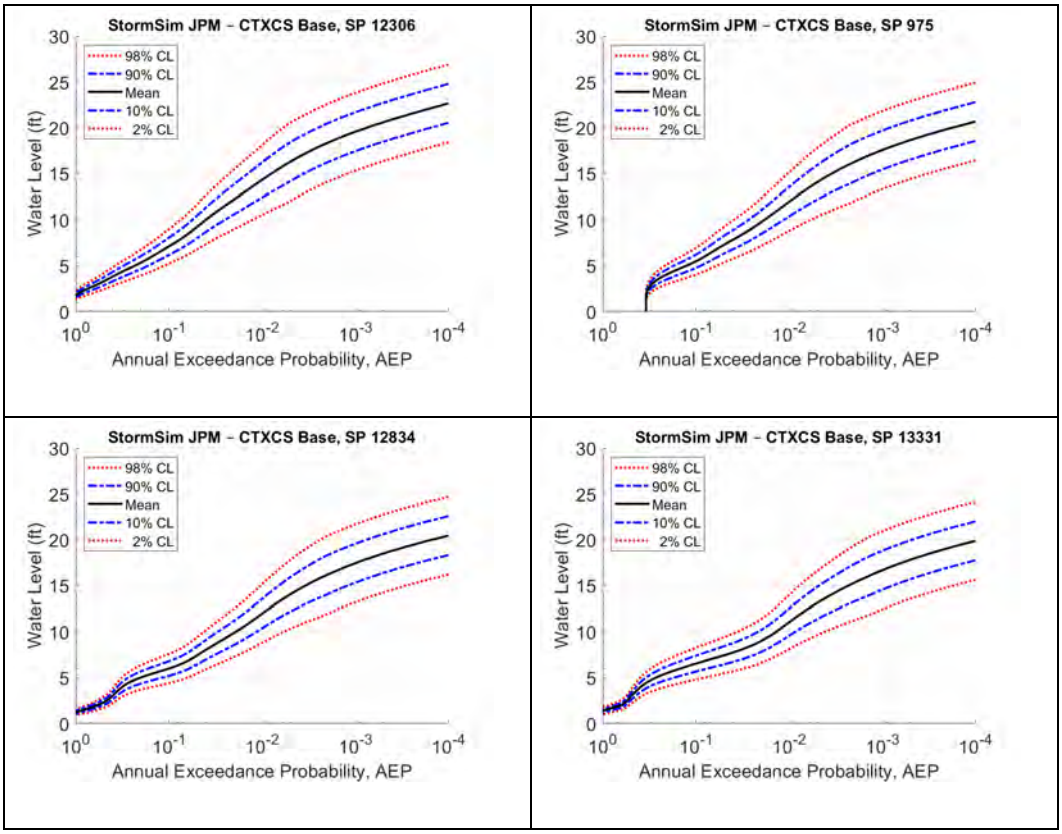

Appendix G. Alternative Response

The figures in this section provide additional examples of single life cycles. Alternative Bolivar XS1 single dune was shown in the main report and is not repeated here.

Figure G1. Time series of profile elevations at select locations for a single life cycle from Alternative Bolivar XS1, dual dune, low RSLC

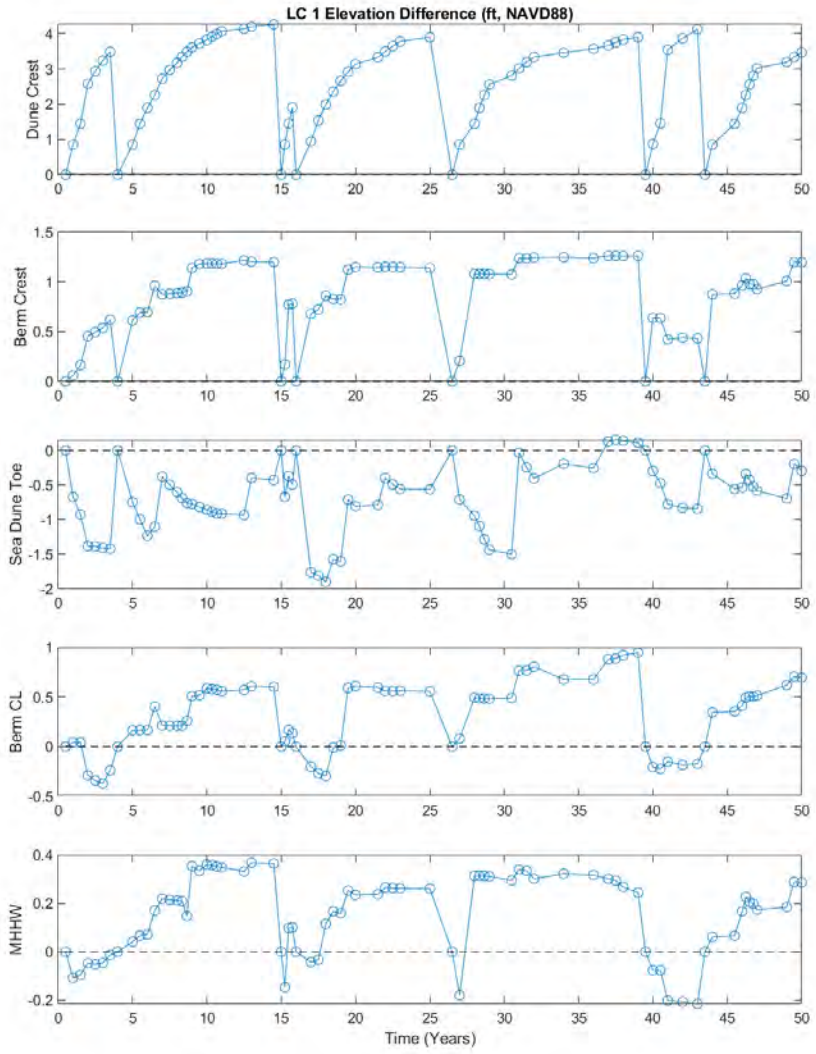

Figure G2. Profile elevations throughout a single life cycle from Alternative Bolivar XS1, dual dune, low RSLC

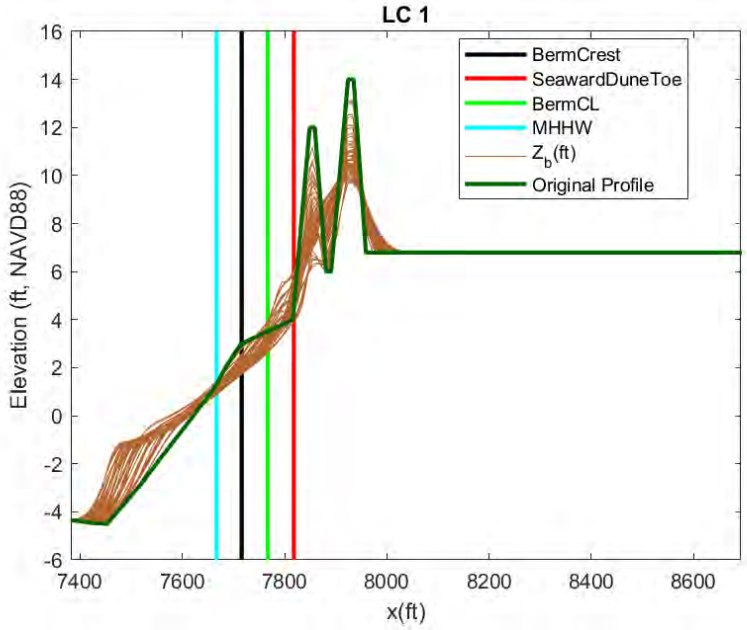

Figure G3. Time series of profile elevations at select locations for a single life cycle from Alternative Bolivar XS1, single dune, high RSLC

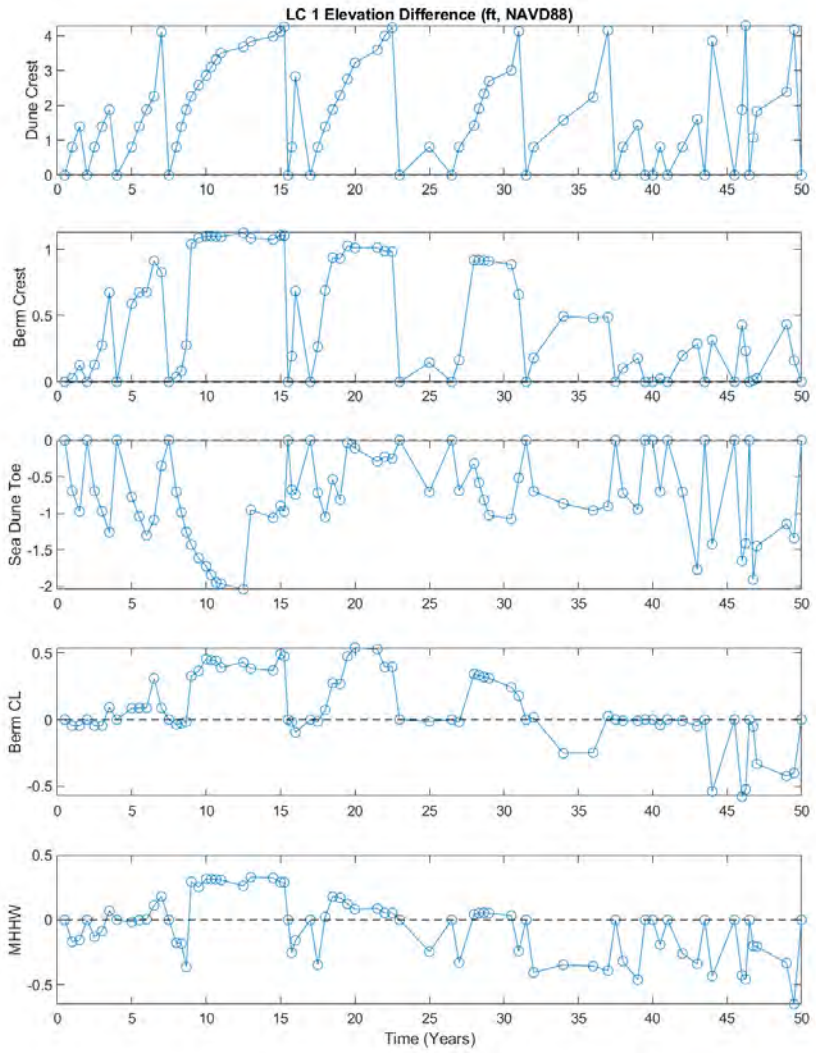

Figure G4. Profile elevations throughout a single life cycle from Alternative Bolivar XS1, single dune, high RSLC

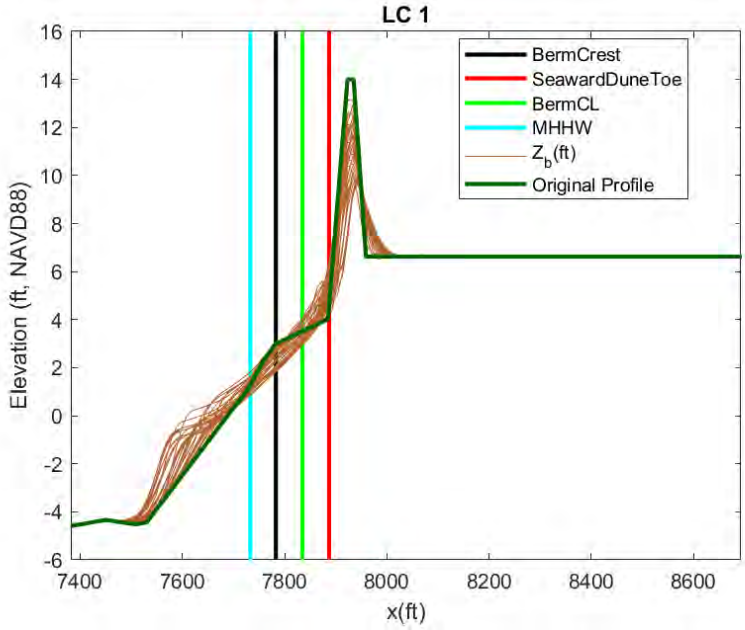

Figure G5. Time series of profile elevations at select locations for a single life cycle from Alternative Bolivar XS1, dual dune, high RSLC

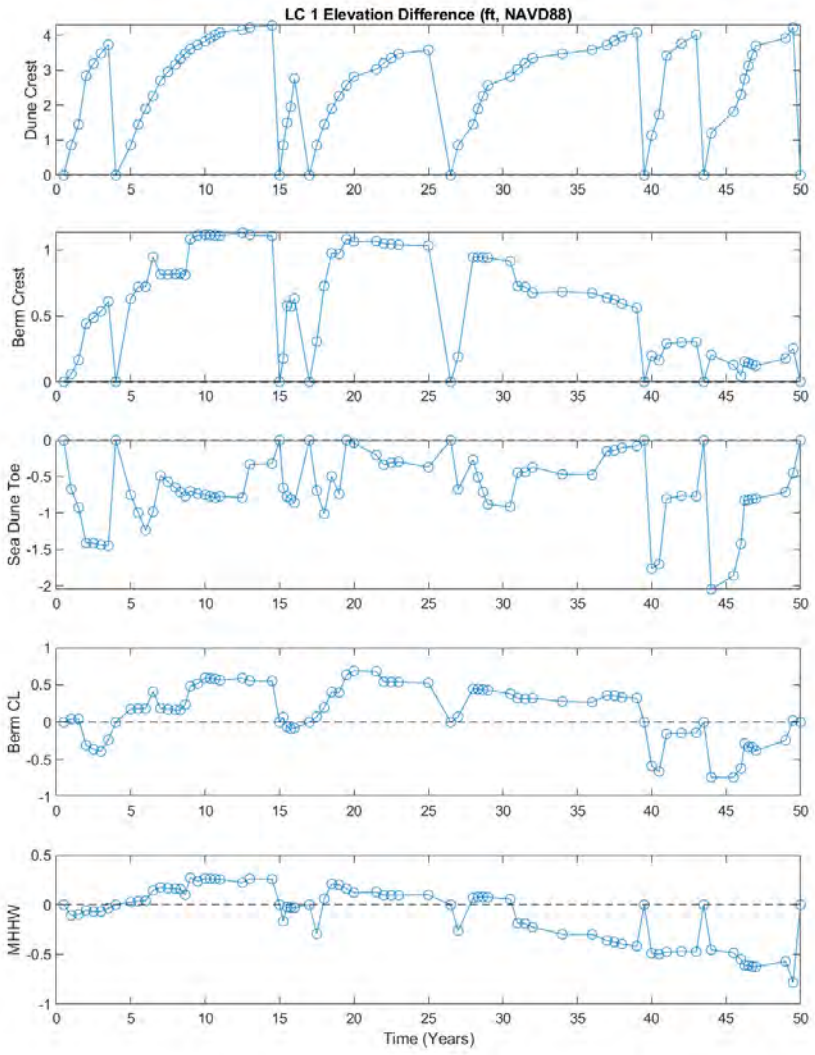

Figure G6. Profile elevations throughout a single life cycle from Alternative Bolivar XS1, dual dune, high RSLC

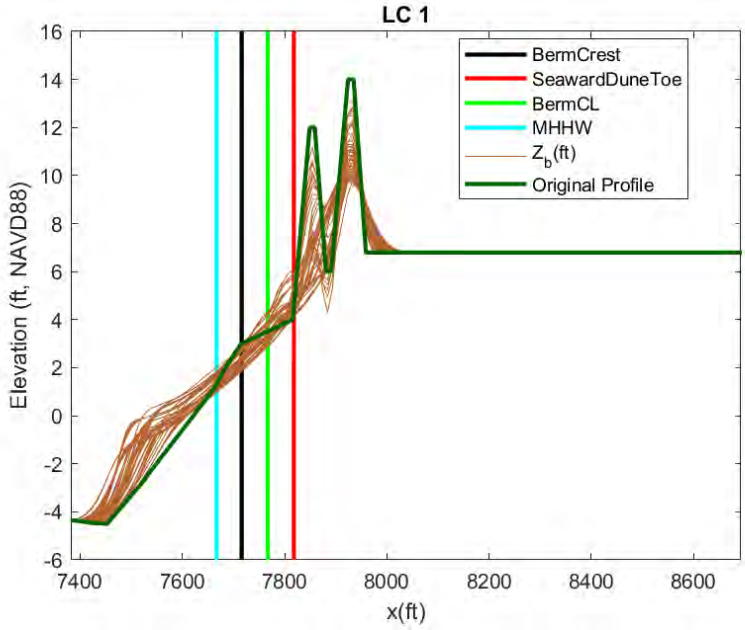

Figure G7. Time series of profile elevations at select locations for a single life cycle from Alternative Galveston XS1, single dune, low RSLC

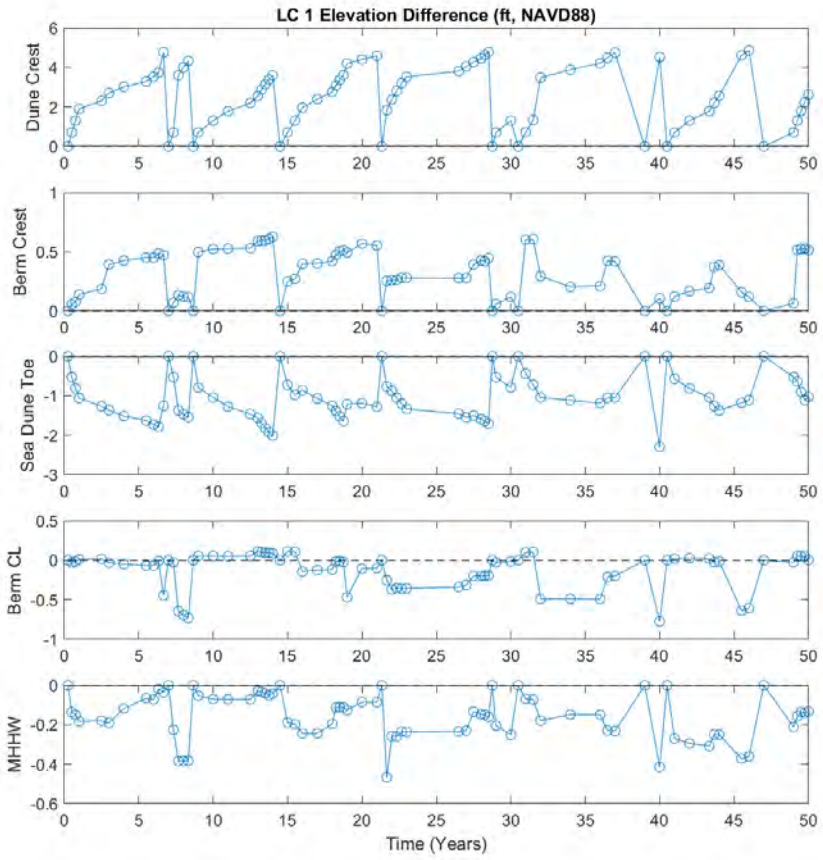

Figure G8. Profile elevations throughout a single life cycle from Alternative Galveston XS1, single dune, low RSLC

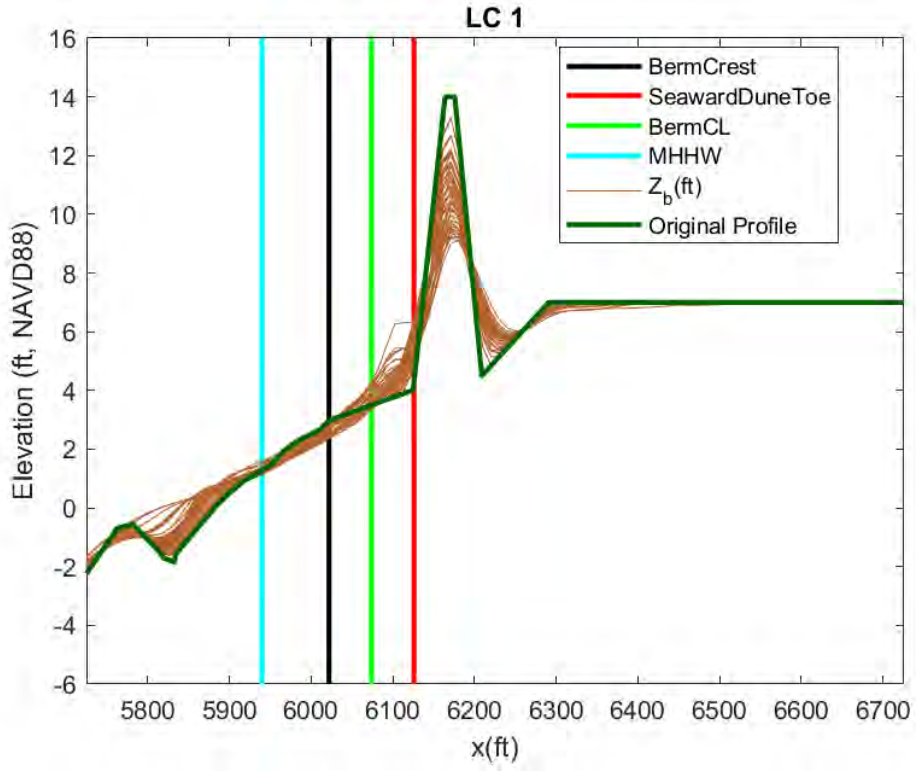

Figure G9. Time series of profile elevations at select locations for a single life cycle from Alternative Galveston XS1, dual dune, low RSLC

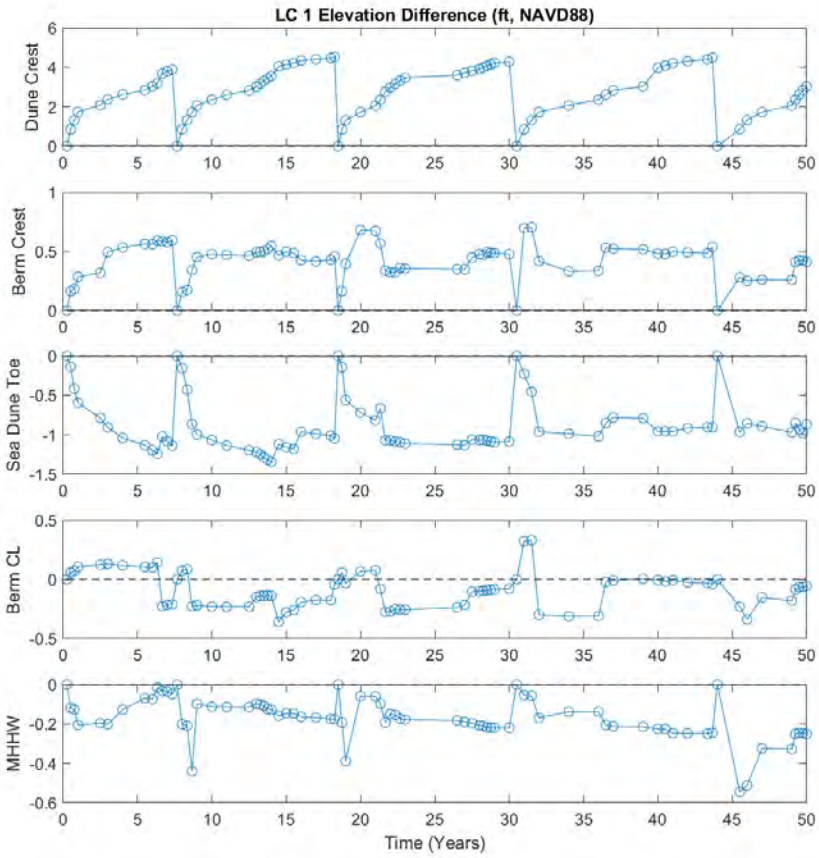

Figure G10. Profile elevations throughout a single life cycle from Alternative Galveston XS1, dual dune, low RSLC

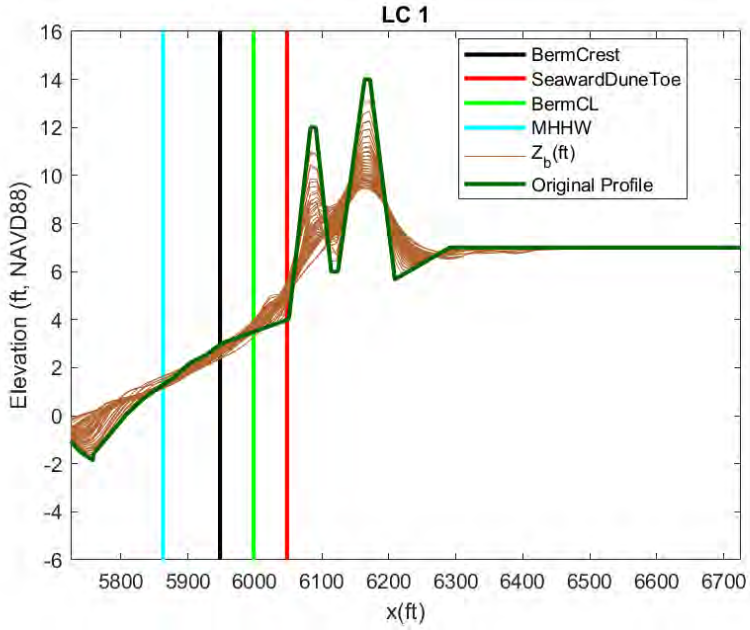

Figure G11. Time series of profile elevations at select locations for a single life cycle from Alternative Galveston XS1, single dune, high RSLC

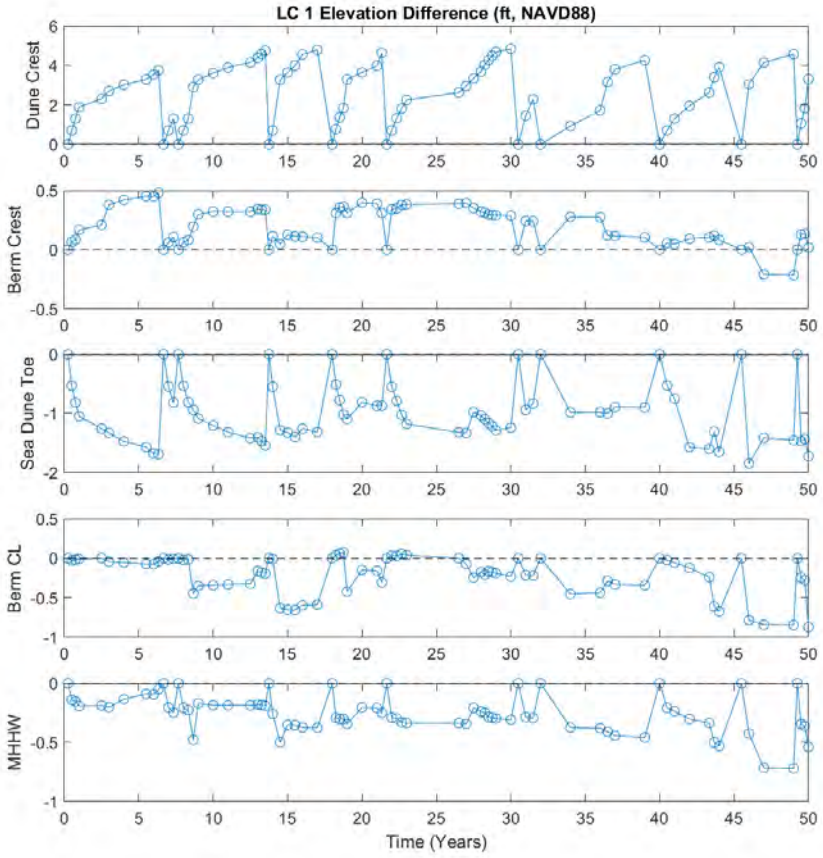

Figure G12. Profile elevations throughout a single life cycle from Alternative Galveston XS1, single dune, high RSLC

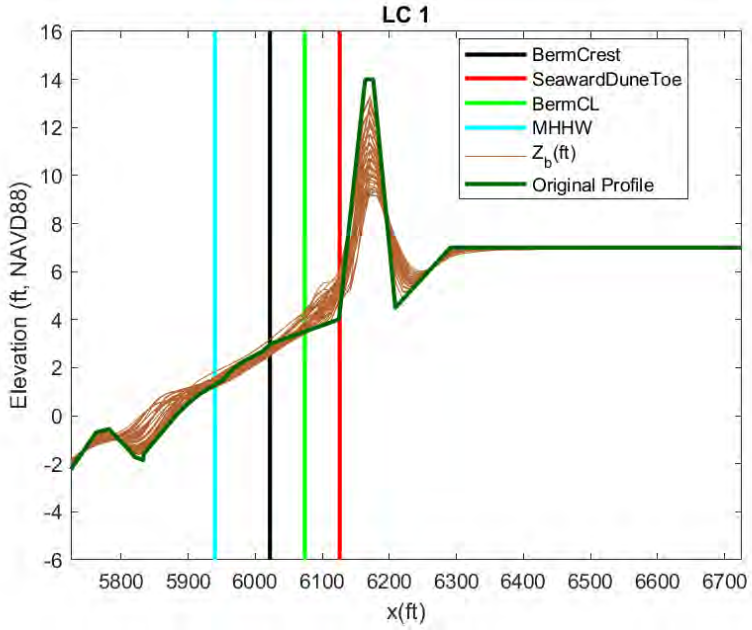

Figure G13. Time series of profile elevations at select locations for a single life cycle from Alternative Galveston XS1, dual dune, high RSLC

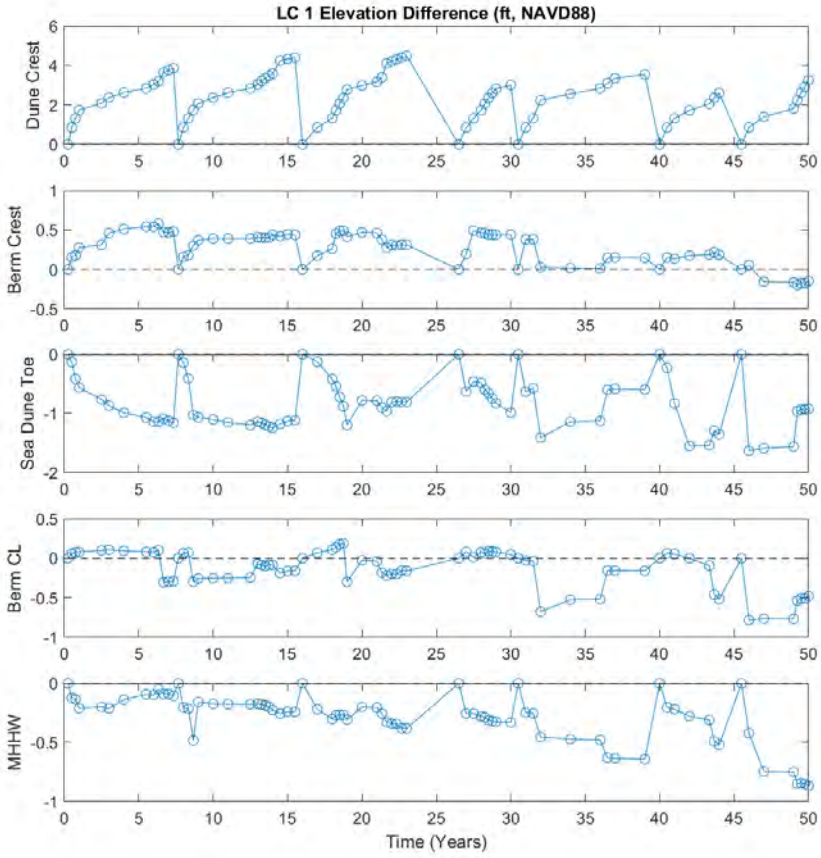

Figure G14. Profile elevations throughout a single life cycle from Alternative Galveston XS1, dual dune, high RSLC

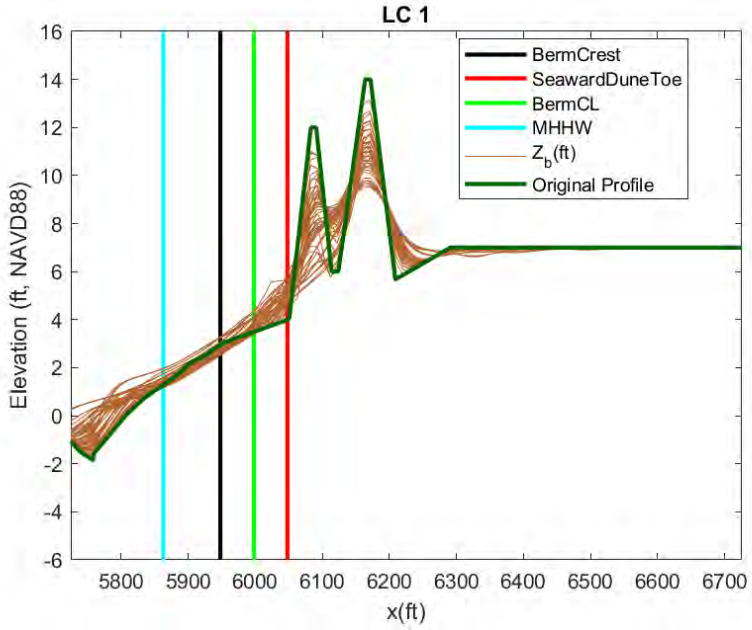

Acronyms and Abbreviations

ACE	Annual chance exceedance
AEP	Annual exceedance probability
ARI	Average recurrence interval
cfs	Cubic feet per second
CHS	Coastal Hazards System
CL	Confidence limit
CRL	Coastal Reference Location
CSRM	Coastal storm risk management
CTXCS	Coastal Texas Comprehensive Study
cy	cubic yards
deg	Degrees
DL	Damage level
DoC	Depth of Closure
FEMA	Federal Emergency Management Agency
FIS	Flood Information Study
ft	Feet or foot
GKF	Gaussian Kernel Function
GLCC	Global land cover characterization
GOM	Gulf of Mexico
GPM	Gaussian Process Metamodeling
HSDRRS	Hurricane Storm Damage Risk Reduction System
HURDAT2	HURricane DATa 2nd generation hurricane parameter database
ICWW	Intercoastal waterway
JPM	Joint probability method
JPM-OS	Joint probability method with optimal sampling
LACPR	Louisiana Coastal Protection and Restoration
LCLU	Land cover and land use
LiDAR	Light detection and ranging
Mcy	Million cubic yards
MGC	Multivariate Gaussian Copula

MHHW	Mean higher high water vertical datum
MRLC	Multi-Resolution Land Characteristics Consortium
MSL	Mean sea level vertical datum
MWD	Mean wave direction
NACCS	North Atlantic Coast Comprehensive Study
NAVD88	North American Vertical Datum of 1988
NFIP	National Flood Insurance Program
NLCD	National Land Cover Database
NOAA	National Oceanic and Atmospheric Administration
NRC	National Research Council
PED	Preconstruction-Engineering and Design phase of USACE project
PCHA	Probabilistic coastal hazard analysis
PBL	Planetary boundary layer
POT	Peaks over threshold storm censoring method
RANS	Reynolds averaged Navier-Stokes
RS	Response surface
RSLC	Relative sea level change
RWH	Runup wire height setting in CSHORE
s	Second
S2G	Sabine Pass to Galveston Bay
S2G2015	Sabine Pass to Galveston Bay Feasibility Study
SLC0	Sea level change corresponding to beginning of service life
SLC1	Sea level change corresponding to 50 yr service life, high curve
SLC2	Sea level change corresponding to 50 yr service life, intermediate curve
SLR	Sea level rise
SP	Save point
SRR	Storm recurrence rate
SD	Standard Deviation
SWG	United States Army Corps of Engineers Galveston District
SWL	Storm water level including wave setup but not wave runup
T1B, T2B	Transects XS1 and XS2 for Bolivar Penninsula
T1G, T2G	Transects XS1 and XS2 for Galveston Island

TC Tropical cyclone

TROP Data file containing time series of tropical cyclone climatological parameters

TX-LA STWAVE grid for Texas-Louisiana border region

TX-N STWAVE grid for North Texas region

TX-C STWAVE grid for Central Texas region

TX-S STWAVE grid for South Texas region

yr Year

USACE United States Army Corps of Engineers

USGS United States Geological Survey

WIS Wave Information Study

WNAT Western North Atlantic